
Path Integral Methods for Polarons in Real Materials

Bradley Andrew Alan Martin

SUBMITTED IN PARTIAL FULFILMENT OF THE
REQUIREMENTS FOR THE DEGREE OF DOCTOR
OF PHILOSOPHY OF IMPERIAL COLLEGE
LONDON AND THE DIPLOMA OF IMPERIAL
COLLEGE LONDON BY



IMPERIAL COLLEGE LONDON

DEPARTMENT OF PHYSICS

MARCH 2024

Some dedication.

– DECLARATION OF ORIGINALITY –

Write the declaration of originality here.

— COPYRIGHT STATEMENT —

The copyright of this thesis rests with the author. Unless otherwise indicated, its contents are licensed under a [Creative Commons Attribution-NonCommercial-NoDerivatives 4.0 International Licence](#) (CC BY-NC-ND 4.0).

Under this licence, you may copy and redistribute the material in any medium or format on the condition that; you credit the author, do not use it for commercial purposes and do not distribute modified versions of the work.

When reusing or sharing this work, ensure you make the licence terms clear to others by naming the licence and linking to the licence text.

Please seek permission from the copyright holder for uses of this work that are not included in this licence or permitted under UK Copyright Law.

– ABSTRACT –

Write abstract here.

– ACKNOWLEDGEMENTS –

Write acknowledgements here.

— CONTENTS —

List of Figures	10
List of Tables	16
List of Acronyms	17
List of Symbols	18
1 Introduction	19
1.1 The Polaron	19
1.2 Polaron Mobility	19
1.3 Relevance: Semiconductor Materials	19
2 Literature	21
2.1 Polaron Theories	21
2.1.1 A Brief History	21
2.1.2 Fröhlich's Large Polaron	25
2.1.3 Holstein's Small Polaron	33
2.2 The Feynman Path Integral & Variational Approach	33
2.2.1 Ground-State Polaron	34
2.2.2 Feynman-Jensen Variational Principle	38
2.2.3 Finite Temperature Polaron	49
2.3 Influence Functionals & Response Functions	56
2.3.1 Polaron DC Mobility	56
2.3.2 Optical Conductivity	67
2.3.3 Effective Multimode Mobility	72
2.4 Material Case Studies	82
2.4.1 Methylammonium Lead Halide Perovskite	82
2.4.2 Rubrene Organic Crystal	82
3 Generalising the Material Path Integral Model	83

3.1	Multiple Phonon Modes	83
3.1.1	Multiple Phonon Mode Path Integral	85
3.1.2	Multiple Phonon Mode Free Energy	87
3.2	Lattice Polarons	90
3.2.1	Discrete-Time Path Integral	90
3.2.2	Continuous-Time Path Integral	92
3.3	Beyond the Parabolic Approximation	96
3.3.1	Naïve effective-mass anisotropy	96
3.4	The General Polaron	96
3.4.1	General Phonon-Band Polarons	98
3.4.2	General Polaron Action	99
4	Improving the Trial Path Integral Model & Variational Solution	101
4.1	Multiple Fictitious Particles	101
4.1.1	Numerical Results	103
4.1.2	The additional parameters	104
4.1.3	Improving the Energy Bound	108
4.2	Lattice Polaron Variational Solution	108
4.2.1	Coupling Dependence	112
4.2.2	Holstein Polaron Temperature Dependence	116
4.3	The Optimal Functional Solution	120
4.3.1	Generalised Trial Action	120
4.3.2	Self-consistent Equations	123
4.3.3	General Memory Function	124
4.4	The Linear Polaron & Independent Boson Models	124
4.5	Cumulant Expansion Corrections	124
5	Computing Response Functions & Polaron Mobility	125
5.1	Polaron Mobility	125
5.1.1	The Fröhlich Model	127
5.1.2	Multiple Phonon Mode Mobility	130
5.1.3	Multiple Fictitious Particle Mobility	131
5.1.4	The Holstein Model	133
5.2	Frequency-Dependent Optical Conductivity	135
5.2.1	Holstein Model	135
5.3	The Optimal Self-Consistent Response Function	139
5.3.1	Statics = Dynamics	139
6	Application for Real Materials	140
6.1	Methylammonium Lead Halide Perovskites	140

6.1.1	Modelling terahertz spectroscopy unveiled polaron photoconductivity dynamics in Metal-Halide Perovskites	146
6.2	Rubrene & Organic Crystals	147
6.3	Cubic & Anisotropic Materials	152
6.4	High-Throughput Material Classification	153
7	Conclusion & Outlook	154
7.0.1	Predictions from FHIP and DSG for the complex mobility .	154
7.0.2	Comparison of the multiple phonon and effective frequency mobilities	155
7.0.3	Comparison of the multiple phonon mobility with THz photoconductivity data	156
7.0.4	Comparison of the variational and full perturbative approaches for modelling anisotropy	157
Bibliography		159
Appendices		166
A	First Appendix	166

– LIST OF FIGURES –

2.1 (left): Unitless values from Feynman's athermal 0K polaron theory, calculated for electron-phonon α couplings ranging from 1 to 12. Blue-solid is the negative of the best approximated ground-state energy F , orange-dashed is the polaron effective mass m_b , green-dotted is the v variational parameter and purple-dash-dotted is the w variational parameter. (right): The real conductivity (also the frequency-dependent mobility) of the polaron response obtained from the FHIP theory and calculated for α ranging from 1 to 12 and external field angular frequencies ranging from 0 ω_{LO} to 20 ω_{LO} multiples of the effective phonon angular frequency. The relative magnitudes of the curves for different values of α have been normalised and are not comparable.	48
2.2 Contour plots of (a) Ōsaka's polaron free energy, (b) Feynman's effective mass (log scale), (c) the v variational parameter (log scale) and (d) the w variational parameter (log scale), as a function of 'effective' temperature T/ω_{LO} and the Fröhlich α parameter.	56
2.3 Log contour plot of the DC mobility (arbitrary units).	67
2.4 Contours for the real (left) and imaginary (right) complex conductivity at different values of α . (a) Real conductivity at $\alpha = 3$. (b) Imaginary conductivity at $\alpha = 3$. (c) Real conductivity at $\alpha = 6$. (d) Imaginary conductivity at $\alpha = 6$. (e) Real conductivity at $\alpha = 9$. (f) Imaginary conductivity at $\alpha = 9$	70
2.5 Ridgeline plots for the real (left) and imaginary (right) complex conductivity at different values of α . (a) Real conductivity at $\alpha = 3$. (b) Imaginary conductivity at $\alpha = 3$. (c) Real conductivity at $\alpha = 6$. (d) Imaginary conductivity at $\alpha = 6$. (e) Real conductivity at $\alpha = 9$. (f) Imaginary conductivity at $\alpha = 9$	71

4.4 Polaron binding energy for the Fröhlich and Holstein models with respect to the electron-phonon dimensionless coupling parameter α . Left: Fröhlich model in 2D (solid blue) and 3D (dashed orange). Right: Holstein model in 1D (dashed orange), 2D (dot-dashed green) and 3D (dot-dot-dashed pink), and the 3D Fröhlich result scaled by 1/6 in energy and 1/3 in α to align with the Holstein weak-coupling ($\alpha < 1$). Co-plotted are DiagMC results for the Holstein model in 1D (blue diamonds), 2D (orange squares) and 3D (green circles).	114
4.5 Optimal values of the polaron variational parameters v and w for the Fröhlich and Holstein models with respect to the electron-phonon dimensionless coupling parameter α . Left: Fröhlich model in 2D (v solid blue and w dot-dash green) and 3D (v dashed orange and w dot-dot-dash pink). Right: Holstein model in 1D (v solid blue and w dot-dot-dash pink), 2D (v dashed orange and w solid yellow) and 3D (v dot-dashed green and w dashed turquoise).	115
4.6 Polaron binding energy for the Fröhlich model in 2D (dot-dash pink) and 3D (solid gold), and Holstein model in 1D (solid blue), 2D (dashed orange) and 3D (dotted green) with respect to temperature (in units of the phonon frequency ω_0), for values of the Fröhlich electron-phonon coupling $\alpha = 2.5, 4, 6, 8, 10, 12$ and $1/3$ of these values for the Holstein electron-phonon coupling. The Fröhlich free energy has been scaled down by 1/6 to better compare with the Holstein free energy. . . .	117
4.7 Temperature dependence (T , in units of phonon frequency ω_0) of the fictitious particle mass M from the trial system for the Fröhlich model in 2D (solid blue) and 3D (dashed orange), and for the Holstein model in 1D (dot-dashed green), 2D (dot-dot-dashed pink) and 3D (solid gold), for values of the Fröhlich electron-phonon coupling $\alpha = 2.5, 4, 6, 8, 10, 12$ and $1/3$ of these values for the Holstein electron-phonon coupling. This mass can be expressed in terms of the traditional v and w using $M = (v^2 - w^2)/w^2$. The Fröhlich results are un-scaled here. . . .	118
4.8 Temperature dependence (T , in units of phonon frequency ω_0) of the fictitious particle spring-constant κ from the trial system for the Fröhlich model in 2D (solid blue) and 3D (dashed orange), and for the Holstein model in 1D (dot-dashed green), 2D (dot-dot-dashed pink) and 3D (solid gold), for values of the Fröhlich electron-phonon coupling $\alpha = 2.5, 4, 6, 8, 10, 12$ and $1/3$ of these values for the Holstein electron-phonon coupling. This mass can be expressed in terms of the traditional v and w using $\kappa = (v^2 - w^2)$. The Fröhlich results are un-scaled here.	119

5.1	Temperature dependence of the polaron mobility. The Mott-Ioffe-Regel (MIR) threshold is given by the red dotted lines. Left: Mobility obtained from the thermal FHIP theory with v and w variational parameters calculated for each temperature, for Fröhlich alphas ranging from $\alpha = 1$ to 12. The temperature is given in units of the phonon frequency ω . Right: Mobility obtained by [40] using the diagrammatic Monte Carlo method for $\alpha = 6$. The temperature is in units of the phonon frequency Ω .	128
5.2	Polaron mobility for $\alpha = 6$. Left: Mobility obtained from the thermal FHIP theory with v and w variational parameters calculated for each temperature. The electric field frequency and temperature are given in units of the phonon frequency ω . Right: Mobility obtained by [40] using the diagrammatic Monte Carlo method. The electric field frequency and temperature are in units of the phonon frequency Ω .	129
5.3	Real component of the complex conductivity $\text{Re } \sigma(\Omega)$ for the Fröhlich model for increasing number N of fictitious particles in the trial model. Left: The frequency-dependence of the real conductivity at $\alpha = 6$ and $\beta\omega_0 = 12.375$. Here I are in the regime for the maximum potential improvement on the trial model with the additional of fictitious particles. Despite minor improvements on the free energy approximation, the corresponding prediction for the real conductivity changes drastically due to the sensitivity of analytic continuation of the trial model. Right: Dependence of the ground-state ($T = 0$ K) real conductivity with the dimensionless electron-phonon coupling α . The real conductivity converges quickly to its optimal solution as soon as $N = 3$ with the maximal improvement occurring around $\alpha = 6$.	132
5.4	Temperature dependence (T , in units of phonon frequency ω_0) of the polaron DC mobility μ for the Fröhlich model in 2D (solid blue) and 3D (dashed orange), and for the Holstein model in 1D (dot-dashed green), 2D (dot-dot-dashed pink) and 3D (solid gold), for values of the Fröhlich electron-phonon coupling $\alpha = 2.5, 4, 6, 8, 10, 12$ and $1/3$ of these values for the Holstein electron-phonon coupling.	134
5.5	Frequency dependence (Ω , in units of the phonon frequency ω_0) of the polaron memory function $\chi(\Omega)$ for the Fröhlich model in 3D (solid blue), and the Holstein model in 1D (dashed orange), 2D (dot-dashed green) and 3D (solid gold), for values of the Fröhlich electron-phonon coupling $\alpha = 1, 3, 5, 6, 7$ and $1/3$ of these values for the Holstein electron-phonon coupling. Here, I only consider the imaginary component to reduce graph clutter, but the real component was also evaluated.	136

5.6 Frequency dependence (Ω , in units of the phonon frequency ω_0) of the polaron complex conductivity $\sigma(\Omega)$ for the Fröhlich model in 2D (solid blue) and 3D (dashed orange), and for the Holstein model in 1D (dotted green), 2D (dot-dashed pink) and 3D (d pink), for values of the Fröhlich electron-phonon coupling $\alpha = 3, 5, 7$ and $1/3$ of these values for the Holstein electron-phonon coupling. Here, I only consider the imaginary component to reduce graph clutter, but the real component was also evaluated.	138
6.1 (left): The free energy of the Hellwarth and Biaggio effective mode A & B schemes and for the multiple phonon model between 1K and 400K. The two Hellwarth schemes agree almost exactly, except for a small deviation at low temperatures. The multiple phonon model gives a lower free energy estimate for temperatures above 100K. (right): The variational parameters v & w from the Hellwarth and Biaggio effective mode A & B schemes and the multiple phonon model. The effective mode schemes agree, whereas the multiple phonon model gives values larger than the Hellwarth schemes but approaches their values towards zero temperature.	142
6.2 Left: Multiple phonon scheme (a) real conductivity, (c) imaginary conductivity, (e) absolute conductivity. Right: Hellwarth 'B' scheme: (b) real conductivity, (d) imaginary conductivity, (f) absolute conductivity.	143
6.3 Left: Multiple phonon scheme (a) real conductivity, (c) imaginary conductivity, (e) absolute conductivity. Right: Hellwarth 'B' scheme: (b) real conductivity, (d) imaginary conductivity, (f) absolute conductivity. At lower temperatures, the conductivity has been cut off at 600 to enable us to see the main features.	144
6.4 (a) Multiple phonon real conductivity. (b) A scheme of real conductivity. (c) Multiple phonon imaginary conductivity. (d) A scheme of imaginary conductivity. (e) Multiple phonon absolute conductivity. (f) A scheme of absolute conductivity.	145
6.5 (left): The imaginary part of the multiple phonon mode memory function in Eq. (5.17) evaluated for MAPbI_3 . (right): The real part of the multiple phonon mode complex conductivity (i.e. mobility) in Eq. (5.20) evaluated for MAPbI_3 . These are calculated for the phonon modes listed in Table 1. The reduced thermodynamic beta $\beta_j = \hbar\omega_j / (k_B T)$ is evaluated for temperatures $T = 1$ K (black curves) to $T = 30$ K (yellow curves).	146

6.6	Terahertz photo-conductivity spectra obtained from a visible pump-IR push-THz probe measurement in [42]. The plot shows the complex conductivity's real (solid markers) and imaginary (hollow markers) parts in MAPbI_3 . The blue, black and green dashed lines show before, at and after the arrival of the push pulse, respectively.	147
6.7	Contour plots for (left): The imaginary part of the multiple phonon mode memory function (5.17) evaluated for MAPbI_3 . (right): The real part of the multiple phonon mode complex conductivity (5.20) evaluated for MAPbI_3 . Here the temperature axis is log-scaled and ranges from $T = 1 \text{ K}$ to $T = 400 \text{ K}$ and frequency zoomed in onto the range $\nu = 0 \text{ THz}$ to $\nu = 3.5 \text{ THz}$	148
6.8	Polaron properties of the variational Holstein model for a bulk 3D Rubrene organic crystal. Top-left: The polaron free energy F (meV) in Rubrene as a function of temperature (K). Top-right: Optimal variational parameters v and w ($\text{THz}^2\pi$) as a function of temperature (K). There appears to be some possible numerical artefact manifesting as the step-like increments. Bottom-left: The DC polaron mobility $\mu(T)$ ($\text{cm}^2 \text{ V}^{-1} \text{ s}^{-1}$) as a function of temperature T (K). Bottom-right: The real component of the conductivity $\text{Re } \sigma(\Omega)$ (mS) as a function of frequency Ω (THz) for temperatures $T = 0.1 \text{ K}, 0.8 \text{ K}, 6.3 \text{ K}$ and 50 K	149
6.9	Both figures are taken from [45]. (left): The relative differences between the ground-state energy of the polaron determined using perturbation theory (which fully accounts for any anisotropy) and the Feynman variational approach (using my approximate treatment of anisotropy). (right): The relative difference between the effective masses was determined using perturbation theory and the Feynman variational approach (again, only approximately accounting for anisotropy). $m_{P,iso}^*$ is the isotropic effective mass, $m_{P,\perp}^*$ and $m_{P,z}^*$ are the in-plane and out-of-plane polaron effective masses.	152

– LIST OF TABLES –

6.1	Infrared activity, ionic dielectric contribution and decomposed Fröhlich alpha values associated with each of the phonon modes in MAPbI ₃ taken from Ref [41]. The effective Fröhlich alpha $\alpha_{\text{eff}} = \sum_j \alpha_j$ is found to be 2.66 for MAPbI ₃	141
6.2	3D Rubrene Bulk crystal data. Here g is the Holstein hole-phonon coupling element, ω_0 is the single-mode effective phonon frequency, J is the electron transfer/hopping integral, a is the geometric-meaned crystal lattice constant, γ is the Holstein adiabaticity unitless parameter, m_b is the effective hole band-mass, $\lambda^2 = (g/\hbar\omega_0)^2$ is the unitless squared hole-phonon coupling element and $\alpha = \lambda^2\gamma/6$ is the 3D unitless Holstein electron-phonon parameter.	150
6.3	Ground-state polaron properties for a Rubrene Bulk crystal calculated using the variational Holstein and Fröhlich models.	150
6.4	Room temperature (300 K) polaron properties for a Rubrene Bulk crystal calculated using the variational Holstein and Fröhlich models. . .	150

– LIST OF ACRONYMS –

2D	Two-dimensional
3D	Three-dimensional
PhD	Doctor of Philosophy
FHIP	<i>Feynman-Hellwarth-Iddings-Platzman</i>
FVA	<i>Feynman Variational Approach</i>

— LIST OF SYMBOLS —

Subscripts

- _i imaginary part
- _r real part

Superscripts

- ̄ mean quantity

Greek symbols

- δ_{ij} Kronecker delta

Latin symbols

- f frequency
- t time coordinate

CHAPTER 1

INTRODUCTION

“The underlying physical laws necessary for the mathematical theory of a large part of physics and the whole of chemistry are thus completely known, and the difficulty is only that the exact application of these laws leads to equations much too complicated to be soluble. It, therefore, becomes desirable that approximate practical methods of applying quantum mechanics should be developed, which can lead to an explanation of the main features of complex atomic systems without too much computation.”

—Paul A. M. Dirac, *Quantum mechanics of many-electron systems*, 1929

This is the introduction paragraph.

1.1 The Polaron

1.2 Polaron Mobility

1.3 Relevance: Semiconductor Materials

Semiconductor materials have enormous technical applications ranging from photovoltaic cells and light-emitting diodes to field-effect transistors and solid-state lasers. A key phenomenological quantity that influences the performance of a semiconductor is the charge carrier mobility. The required mobility depends on the application; for example, a solid-state laser requires higher mobility than a photovoltaic cell. As a phenomenological quantity, mobility is not a direct ground-state property. Instead, mobility arises from competitive dynamic pro-

cesses within a material and can, on occasion, be strongly temperature-dependent. Most mobility theories tend to use semi-classical approximations for modelling the mobility, using an effective scattering time such as in Drude-like models, or neglecting electron-phonon interactions as in the adiabatic Born-Oppenheimer approximation. Otherwise, it is usually assumed that the electron-phonon coupling is either weak or strong, where approximate limits are taken. However, some semiconductors, such as halide perovskites, possess large dielectric electron-phonon interactions, leading to the formation of large polarons. These materials typically exhibit intermediate electron-phonon coupling strengths. Alternatively, one can use the path integral formulation of quantum mechanics to derive an inherently quantum theory of mobility ([1, 2]). Though based on a linear-response theory, this is non-perturbative and can provide a temperature-dependent model of mobility to all orders in the electron-phonon coupling strength.

CHAPTER 2

LITERATURE

“What I cannot create, I do not understand. Know how to solve every problem that has been solved.”

—Richard P. Feynman, *Feynman’s Last Chalkboard*, 1988

This is the introduction paragraph.

2.1 Polaron Theories

2.1.1 A Brief History

Landau and Pekar, 1933-1948

The self-localisation of an electron in a perfect crystal due to lattice deformations was investigated by [3]. He was concerned with the effect of lattice defects on materials such as sodium chloride. Later, the concept of a “polaron” was initially proposed and coined by Pekar [4, 5, 6] to describe the spontaneous trapping of an electron due to the induced polarisation of an atomic lattice in a strongly ionic material. Further developments on the exact definition of a polaron led to a joint paper by Pekar and Landau [7], where they calculated the effective mass of a large, strongly-coupled polaron. The polaron was established as a *quasiparticle* that consists of a charge carrier (such as an electron or hole) ‘dressed’ by a cloud of virtual phonon excitations that follow the charge carrier as it propagates through a polarisable medium. Suppose the polaron’s spatial delocalisation is large compared to the lattice parameter of a material. The material can be treated as a polarisable

continuum, and we have a *large* polaron. However, when the extent of the polaron is of the order of the lattice parameter, we have a *small* polaron, and lattice effects cannot be ignored.

Fröhlich & Holstein, 1950-1959

The theoretical groundwork for polaron theories was formally established by Fröhlich [8] and Holstein [9, 10]. Both Fröhlich and Holstein developed rigorous quantum-field Hamiltonians that describe large or small polarons respectively. The Fröhlich Hamiltonian represents a simplistic physical system composed of a single conduction-band electron linearly coupled to a polarisation field. This polarisation field, carried by longitudinal optical phonons, is represented by a set of quantum harmonic oscillators with no dispersion and oscillating at the same frequency. The strength of the electron-phonon coupling is characterised by a dimensionless coupling constant called the “Fröhlich alpha parameter” and can be determined from the properties of the material. Despite its simplistic representation, an exact solution to the Fröhlich Hamiltonian has evaded direct evaluation.

[Add Holstein summary.](#)

Feynman, 1955

[Add more introductory summary.](#)

Feynman [1], cast the Fröhlich Hamiltonian into a Lagrangian. Feynman did this by converting the electron and phonon creation and annihilation operators into the corresponding coordinates and momenta and by doing a Legendre transformation. After a Gaussian integration over the momenta, we obtain a Gaussian configuration path integral over the phonon coordinates, which can be calculated explicitly. The result is an exact ‘*model*’ action of the electron coupled by a non-local Coulomb potential to a second fictitious particle.

The path integral cannot be evaluated precisely because the remaining electron coordinates have a $1/r$ dependence; the path integral is non-Gaussian. So, Feynman proposed a ‘*trial*’ action that attempts to capture the main properties of the model action but is quadratic in the electron coordinates and leads to a solvable Gaussian path integral. This trial action represents a system of an electron coupled to a fictitious massive particle via a spring-like harmonic potential that decays exponentially in time. After passing the model and trial actions into imaginary time, we can obtain an expression for the quantum statistical partition function that is a convex functional, allowing for applying Jensen’s inequality. In the zero temperature limit, the result is a variational inequality that minimises the difference

between the trial and model action to give an approximate lower upper bound to polaron self-energy.

Feynman's variational inequality involves two variational parameters. The first, denoted by C , controls the strength of the harmonic coupling and the second, denoted by w , controls the decay rate of the coupling in time. Later in his paper, Feynman substituted C with the parameter v , which is the frequency of the harmonic coupling. Feynman used his polaron theory to evaluate the polaron's ground-state energy and effective mass for all coupling strengths.

Ōsaka, 1959-1961

Ōsaka [11, 12], generalised Feynman's path integral approach to nonzero temperatures. The result was a variational principle not just for the self-energy of the polaron but also a variational principle for the free energy. Ōsaka managed this by recognising that the equation of motion resulting from another more straightforward trial action produced the same equation of motion as Feynman proposed. Therefore, Ōsaka could use the solution of the path integral of this more tractable action instead to obtain the temperature-dependent density matrix for the polaron state. At zero temperature, Ōsaka's expression for the polaron free energy becomes identical to Feynman's expression for the polaron self-energy.

Feynman, Hellwarth, Iddings & Platzman, 1962

Mention influence functionals. Maybe Feynman-Vernon.

Feynman, Hellwarth, Iddings & Platzman [2] (commonly referred to as "FHIP") derived, from the path integral approach, an approximate expression for the impedance function of the polaron under the influence of a weakly alternating electric field. This impedance function is valid for all frequencies of an applied electric field, temperatures, and all electron-phonon coupling strengths. The impedance function is not variational, instead it is obtained from a second-order functional expansion around the quadratic trial action used by [1]. The critical step of this derivation is evaluating the "memory function". This memory function is obtained from the imaginary part of the dynamic structure factor, which is, in turn, obtained from the electron density-density correlation function and evaluated as a path integral. The memory function contains the dynamics of the polaron and depends on the values of the variational parameters that give the lowest estimate of the polaron-free energy. It was assumed that these values of the variational parameters provide the most accurate prediction of the dynamics. An explicit expression for the imaginary part of the memory function was given, from which

they obtained an expression for the DC mobility of the polaron and looked at the behaviour in the limit of zero, low and high temperatures.

Devreese, Sitter & Goovaerts, 1972

Starting from the approach used by [2], Devreese, Sitter & Goovaerts [13] (commonly referred to as “DSG”) showed how to calculate the optical absorption of Fröhlich polarons, for all coupling, temperature and frequency. It was demonstrated that three different kinds of polaron excitations appear in the spectra produced from their expression: scattering states where, for example, one real phonon is excited; relaxed excited states (RES); and Franck-Condon (FC) states. It was found that these spectral features only appear from an expansion of the impedance function obtained in FHIP and not from the corresponding conductivity function that is the reciprocal of the impedance. This was argued as justification for the choice in FHIP to expand the impedance to second-order instead of the conductivity, which is more commonly used when studying the linear response of a system. Additionally, they provided both the real and imaginary parts of the memory function explicitly as an infinite series of special functions (e.g. Bessel functions) and simplified forms of these series at zero temperature.

Hellwarth & Biaggio, 1997-8

Hellwarth & Biaggio [14], derived a Lagrangian that describes a free electron interacting with a polar lattice with multiple infrared-active optical-phonon modes, in the presence of an applied field. From this Lagrangian, they derive an effective model action comparative to Feynman’s model action, except that it has a summation over terms differing only in the phonon frequencies and the corresponding electron-phonon coupling strength for each phonon mode. Rather than use this effective action directly, they define a single effective phonon frequency and electron-phonon coupling (for which they provide two different schemes to obtain) and use Ōsaka’s free energy minimisation procedure instead. They used the mobility equation derived in FHIP and their own derived Lorentz-Lorenz relation to produce accurate predictions for the room-temperature electron mobility and reflectivity in $\text{Bi}_{12}\text{SiO}_{20}$.

Mishchenko, Prokof’ev, Sakamoto & Svistunov, 1998-2000

More DQMC papers? 2019 Mobility, 2016 Holstein, 2022 Stefano etc.

Prokof’ev & Svistunov [15], in addition to Mishchenko & Sakamoto [16], performed a detailed study on the Fröhlich polaron model using a diagrammatic

quantum Monte Carlo method (DQMC). They produced precise numerical data for the polaron binding energy, effective mass, general structure of the polaron cloud and spectral density of the polaron from intermediate to strong electron-phonon couplings. Their method uses a set of Green's functions of the polaron, which they simulate using a standard diagrammatic expansion-Matsubara technique at zero temperature and relate them to the polaron parameters. The results are considered the 'gold standard' for the Fröhlich model and are often used as a theoretical benchmark to compare newer model predictions against.

2.1.2 Fröhlich's Large Polaron

Fröhlich [8] studied a system whereby a charged particle in a dielectric medium polarises its surroundings. The resultant polarisation field interacts with the particle, and the particle then possesses self-energy in the field due to the changes it, in turn, causes in the field. A simple example is the motion of a free conduction band electron in an ionic crystal. This is a relevant model for physical materials and also theoretically interesting as it is a simple example of a non-relativistic quantum field theory of a fermion interacting with a bosonic quantum field. For a slow electron in the conduction band, the electronic dispersion relation ϵ_k is approximately quadratic in the momentum $\hbar\mathbf{k}$

$$\epsilon_k = \frac{\hbar^2 k^2}{2m_b}, \quad (2.1)$$

Where m_b is the effective band mass of the electron and is usually different to the electronic mass m_e , and \mathbf{k} is the wave vector of the electron. Eq. (2.1) is typically only valid near the extrema of the valence and conduction bands, such as for slow conduction electrons. This results from a typical Bloch electron plane wave moving through a rigid lattice.

Fröhlich improved Bloch's approximation by modelling an electron moving through a non-rigid isotropic polar lattice. The electron experiences an electrostatic potential generated by the displacement of ions from their lattice sites. For small ion displacements compared to the lattice spacing, this potential is one generated by an electric dipole. Since the lattice is polar, ion displacements that lead to electric polarisations interact more strongly with electrons than other types of displacements. Therefore, Fröhlich disregards the latter displacements. The electronic wave function varies slowly over many lattice spacings for sufficiently low-energy electrons. The lattice can be approximated by a continuum such that the electric

field, generated by the displacement of ions in the lattice, can be described by a macroscopic continuous polarisation field, $\mathbf{P}(\mathbf{r})$.

Classical field theory

From the usual definition of the electric displacement field $\mathbf{D}(\mathbf{r})$, the polarisation field is related to the total electric field intensity $\mathbf{E}(\mathbf{r})$ by (in Gaussian units **what are these units?**),

$$\mathbf{E}(\mathbf{r}) = \mathbf{D}(\mathbf{r}) - 4\pi\mathbf{P}(\mathbf{r}). \quad (2.2)$$

Therefore, $-4\pi\mathbf{P}(\mathbf{r})$ is the contribution made by the lattice to the total electric field intensity. Since the main force acting on the electron is the polarisation field $\mathbf{P}(\mathbf{r})$ from the ionic displacement, the classical equation of motion of the electron is

$$m_b \ddot{\mathbf{r}} = 4\pi e \mathbf{P}(\mathbf{r}). \quad (2.3)$$

For a single free electron with charge e and position \mathbf{r}_{el} , the electric displacement is

$$\mathbf{D}(\mathbf{r}, \mathbf{r}_{el}) = -e \nabla \left(\frac{1}{|\mathbf{r} - \mathbf{r}_{el}|} \right), \quad (2.4)$$

such that $\nabla \times \mathbf{D}(\mathbf{r}, \mathbf{r}_{el}) = 0$ and $\nabla \cdot \mathbf{D}(\mathbf{r}, \mathbf{r}_{el}) = 4\pi e \delta(\mathbf{r} - \mathbf{r}_{el})$. This electric displacement represents the ‘external’ electric fields that act on the electron in the crystal. Since the displacement field is longitudinal ($\nabla \times \mathbf{D}(\mathbf{r}, \mathbf{r}_{el}) = 0$), the polarisation field generated by the electron will be longitudinal too (assuming that magnetic fields can be neglected). Therefore, if $\mathbf{P}(\mathbf{r})$ is the electric polarisation at the position \mathbf{r} , then the rotational part of the field must be zero,

$$\nabla \times \mathbf{P}(\mathbf{r}) = 0. \quad (2.5)$$

The electric field generated by the polarisation $-4\pi\mathbf{P}$ can be expressed by an electric potential $\Phi(\mathbf{r})$ given by Poisson’s equation,

$$-\nabla \Phi(\mathbf{r}) = -4\pi \mathbf{P}(\mathbf{r}). \quad (2.6)$$

The energy of the interaction between the electron and the lattice displacements is then

$$\begin{aligned} E_{e-l} &= - \int \mathbf{D}(\mathbf{r}, \mathbf{r}_{el}) \mathbf{P}(\mathbf{r}) d^3 \mathbf{r}, \\ &= \frac{e}{4\pi} \int \nabla \left(\frac{1}{|\mathbf{r} - \mathbf{r}_{el}|} \right) \nabla \Phi(\mathbf{r}) d^3 \mathbf{r}, \\ &= e\Phi(\mathbf{r}_{el}). \end{aligned} \quad (2.7)$$

The longitudinal modes of the lattice that generate the polarisation field are either optical lattice modes (where two adjacent ions move in opposite directions) or acoustic modes (where adjacent ions move in the same direction). Only the optical modes produce dipole moments that add constructively for small lattice displacements, generating a considerably significant resultant polarisation. This is especially true of long-wavelength optical modes, which have the most significant interaction with the electron and are dispersion-less with constant vibrational frequency ω_{LO} . Fröhlich assumed that only these long-wavelength longitudinal optical (LO) modes had any considerable effect on the conduction electron and neglected all other lattice modes.

The total lattice polarisation has two contributions, one from high-frequency oscillations $\mathbf{P}_e(\mathbf{r})$ due to the deformation of the ions, and one from infrared oscillations due to ionic displacement $\mathbf{P}_i(\mathbf{r})$

$$\mathbf{P}(\mathbf{r}) = \mathbf{P}_e(\mathbf{r}) + \mathbf{P}_i(\mathbf{r}). \quad (2.8)$$

Under an external field $\mathbf{D}(\mathbf{r})$ the equations of motion for these two polarisations are driven harmonic oscillator equations

$$\ddot{\mathbf{P}}_i(\mathbf{r}) + \omega_i^2 \mathbf{P}_i(\mathbf{r}) = \mathbf{D}(\mathbf{r}, \mathbf{r}_{el}) / \gamma, \quad (2.9a)$$

$$\ddot{\mathbf{P}}_e(\mathbf{r}) + \omega_e^2 \mathbf{P}_e(\mathbf{r}) = \mathbf{D}(\mathbf{r}, \mathbf{r}_{el}) / \delta, \quad (2.9b)$$

where $\omega_e/2\pi$ and $\omega_i/2\pi$ are the frequencies corresponding to the optical absorption in the high- and infrared regions, respectively. γ and δ are constants related to energy associated with the respective displacements. To determine these constants, we go to the zero-frequency “static” case where $\dot{\mathbf{P}} = 0$ and $\mathbf{D} = \epsilon_0 \mathbf{E}$, with ϵ_0 the total zero-frequency dielectric constant. In the zero-frequency limit, the polarisation is

$$4\pi \mathbf{P}(\mathbf{r}) = (\epsilon_0 - 1) \mathbf{E}(\mathbf{r}) = (1 - \epsilon_0^{-1}) \mathbf{D}(\mathbf{r}). \quad (2.10)$$

In the high-frequency limit, the frequency Ω of the external field \mathbf{D} satisfies $\omega_e \gg \Omega \gg \omega_i$ such that the lattice polarisation is not excited. In the high-frequency limit, the polarisation is

$$4\pi \mathbf{P}(\mathbf{r}) = 4\pi \mathbf{P}_e(\mathbf{r}) = (1 - \epsilon_\infty^{-1}) \mathbf{D}(\mathbf{r}), \quad (2.11)$$

where ϵ_∞ is the high-frequency dielectric constant. In the high-frequency limit, the ions can no longer keep up $\mathbf{P}_i \approx 0$, whereas the electronic oscillators can follow nearly adiabatically. Therefore, the $\ddot{\mathbf{P}}_e$ term would be negligible compared

to $\omega_e^2 \mathbf{P}_e$, and so for a field \mathbf{D} of equal strength, \mathbf{P}_e would have roughly the same value in the static limit as in the high-frequency limit. Hence, we can combine the two expressions above to obtain the ionic polarisation

$$\mathbf{P}_i(\mathbf{r}) = \mathbf{P}(\mathbf{r}) - \mathbf{P}_e(\mathbf{r}) = \frac{1}{4\pi} \left(\frac{1}{\epsilon_\infty} - \frac{1}{\epsilon} \right) \mathbf{D}(\mathbf{r}), \quad (2.12)$$

where \mathbf{P}_e in either limit will cancel. Now, using the equations of motion in the static limit ($\ddot{\mathbf{P}}_e = \ddot{\mathbf{P}}_i = 0$) and our expressions for \mathbf{P}_i and \mathbf{P}_e we find

$$\frac{1}{\gamma} = \frac{\omega_{LO,i}^2}{4\pi} \left(\frac{1}{\epsilon_\infty} - \frac{1}{\epsilon_0} \right), \quad (2.13a)$$

$$\frac{1}{\delta} = \frac{\omega_{LO,e}^2}{4\pi} \left(1 - \frac{1}{\epsilon_\infty} \right). \quad (2.13b)$$

Combined with the equation of motion for the electron, all three equations of motion can be obtained from the overall Lagrangian

$$L = \frac{1}{2} m_b \dot{\mathbf{r}}_{el}^2 + \frac{1}{2} \gamma \int [\dot{\mathbf{P}}_i^2(\mathbf{r}) - \omega_i^2 \mathbf{P}_i^2(\mathbf{r})] d^3\mathbf{r} + \frac{1}{2} \delta \int [\dot{\mathbf{P}}_e^2(\mathbf{r}) - \omega_e^2 \mathbf{P}_e^2(\mathbf{r})] d^3\mathbf{r} + \int \mathbf{D}(\mathbf{r}, \mathbf{r}_{el}) [\mathbf{P}_e(\mathbf{r}) + \mathbf{P}_i(\mathbf{r})] d^3\mathbf{r} + E_{zp} \quad (2.14)$$

by using the standard method of extremising the corresponding action $\delta S = \int dt \delta L = 0$ with \mathbf{r}_{el} , $\mathbf{P}_e(\mathbf{r})$ and $\mathbf{P}_i(\mathbf{r})$ as variables. E_{zp} is an arbitrary constant representing the polarisation field's zero-point energy without the electron's interaction.

The corresponding Hamiltonian can be derived via a Legendre transformation by noting that the conjugate momenta (defined as $\partial L / \partial \dot{q}$ with the generalised coordinate $q \in \{\mathbf{r}_{el}, \mathbf{P}_e(\mathbf{r}), \mathbf{P}_i(\mathbf{r})\}$) are $\mathbf{p}_{el} = m_b \dot{\mathbf{r}}_{el}$, $\Pi_e(\mathbf{r}) = \gamma \dot{\mathbf{P}}_e(\mathbf{r})$ and $\Pi_i(\mathbf{r}) = \delta \dot{\mathbf{P}}_i(\mathbf{r})$. Hence, the Hamiltonian is

$$H = \sum_q \frac{\partial L}{\partial \dot{q}} \dot{q} - L = \frac{\mathbf{p}_{el}^2}{2m_b} + \frac{1}{2} \int [\Pi_i^2(\mathbf{r})/\gamma + \gamma \omega_{LO,i}^2 \mathbf{P}_i^2(\mathbf{r})] d^3\mathbf{r} + \frac{1}{2} \int [\Pi_e^2(\mathbf{r})/\delta + \delta \omega_{LO,e}^2 \mathbf{P}_e^2(\mathbf{r})] d^3\mathbf{r} - \int \mathbf{D}(\mathbf{r}, \mathbf{r}_{el}) [\mathbf{P}_e(\mathbf{r}) + \mathbf{P}_i(\mathbf{r})] d^3\mathbf{r} - E_{zp}. \quad (2.15)$$

The canonically conjugate variables all obey the classical Poisson's Brackets

$$\left\{ \mathbf{p}_{el,j}, \mathbf{r}_{el,j'} \right\} = \delta_{j,j'}, \quad (2.16a)$$

$$\left\{ \mathbf{P}_j(\mathbf{r}), \Pi_{j'}(\mathbf{r}') \right\} = \delta_{j,j'} \delta(\mathbf{r} - \mathbf{r}'). \quad (2.16b)$$

Classically, when the electron is at rest, the force acting on the electron must vanish, and so $\Phi(\mathbf{r})$ must be minimum at $\mathbf{r} = \mathbf{r}_{el}$. However, the above Hamiltonian diverges as $\mathbf{r} \rightarrow \mathbf{r}_{el}$. This happens because the lattice has been approximated as a continuum. This can be accounted for by representing the polarisation vectors as a Fourier series and excluding terms with wavelengths shorter than the lattice constant. With this cut-off, $\Phi(\mathbf{r})$ will now have a minimum at $\mathbf{r} = \mathbf{r}_{el}$ and $\mathbf{P}(\mathbf{r}_{el}) = 0$. Nonetheless, when the electron is moving slowly, $\mathbf{P}(\mathbf{r}_{el}) \neq 0$ due to the time-dependent terms in the equation of motion, but $\mathbf{P}_e(\mathbf{r}_{el}) \ll \mathbf{P}_i(\mathbf{r}_{el})$ because $\omega_e^2 \gg \omega_i^2$. This means that for a slow electron, the displacement of ions in the lattice is primarily due to the infrared polarisation field $\mathbf{P}_i(\mathbf{r})$. Therefore, for a slow electron, the $\mathbf{P}_e(\mathbf{r})$ terms remain mostly constant and can be disregarded from the lattice dynamics. This gives Fröhlich's Hamiltonian for a slow electron in an ionic lattice to be

$$H = \frac{\mathbf{p}_{el}^2}{2m_b} + \frac{1}{2} \int \left[\Pi_i^2(\mathbf{r})/\gamma + \gamma\omega_{LO,i}^2 \mathbf{P}_i^2(\mathbf{r}) \right] d^3\mathbf{r} - \int \mathbf{D}(\mathbf{r}, \mathbf{r}_{el}) \mathbf{P}_i(\mathbf{r}) d^3\mathbf{r} - E_{zp}. \quad (2.17)$$

Quantising Fröhlich's Hamiltonian

From now on, I will drop the ' i ' index for the infrared polarisation field, and $\mathbf{P}(\mathbf{r})$ will represent the infrared ionic displacement polarisation field, with frequency ω_{LO} . To prepare this Hamiltonian for quantisation, Fröhlich introduced an auxiliary complex vector field $\mathbf{B}(\mathbf{r})$ that is defined by

$$\mathbf{B}(\mathbf{r}) = \sqrt{\frac{\gamma\omega_{LO}}{2\hbar}} \left[\mathbf{P}(\mathbf{r}) + \frac{i}{\gamma\omega_{LO}} \boldsymbol{\Pi}(\mathbf{r}) \right], \quad (2.18a)$$

$$\mathbf{B}^*(\mathbf{r}) = \sqrt{\frac{\gamma\omega_{LO}}{2\hbar}} \left[\mathbf{P}(\mathbf{r}) - \frac{i}{\gamma\omega_{LO}} \boldsymbol{\Pi}(\mathbf{r}) \right], \quad (2.18b)$$

where $\nabla \times \mathbf{B}(\mathbf{r}) = \nabla \times \mathbf{B}^*(\mathbf{r}) = 0$. Equivalently, this can be written in terms of the infrared polarisation field,

$$\mathbf{P}(\mathbf{r}) = \sqrt{\frac{\hbar}{2\gamma\omega_{LO}}} [\mathbf{B}^*(\mathbf{r}) + \mathbf{B}(\mathbf{r})], \quad (2.19a)$$

$$\boldsymbol{\Pi}(\mathbf{r}) = i\sqrt{\frac{\gamma\hbar\omega_{LO}}{2}} [\mathbf{B}^*(\mathbf{r}) - \mathbf{B}(\mathbf{r})]. \quad (2.19b)$$

Substituting these into (??) gives the Hamiltonian

$$\begin{aligned} H = & \frac{\mathbf{p}_{el}^2}{2m_b} + \hbar\omega_{LO} \int \mathbf{B}^*(\mathbf{r}) \mathbf{B}(\mathbf{r}) d^3\mathbf{r} \\ & - \sqrt{\frac{\hbar}{2\gamma\omega_{LO}}} \int \mathbf{D}(\mathbf{r}, \mathbf{r}_{el}) [\mathbf{B}^*(\mathbf{r}) + \mathbf{B}(\mathbf{r})] d^3\mathbf{r} \\ & - E_{zp}. \end{aligned} \quad (2.20)$$

To quantise this Hamiltonian, $\mathbf{B}(\mathbf{r})$ is given a periodic boundary condition over a cube of volume $\Omega_0 = L^3$ and is expressed as a Fourier series,

$$\mathbf{B}(\mathbf{r}) = \frac{1}{\sqrt{\Omega_0}} \sum_{\mathbf{k}} \frac{\mathbf{k}}{|\mathbf{k}|} b_{\mathbf{k}} e^{i\mathbf{k}\cdot\mathbf{r}}, \quad (2.21a)$$

$$\mathbf{B}^*(\mathbf{r}) = \frac{1}{\sqrt{\Omega_0}} \sum_{\mathbf{k}} \frac{\mathbf{k}}{|\mathbf{k}|} b_{\mathbf{k}}^* e^{-i\mathbf{k}\cdot\mathbf{r}}. \quad (2.21b)$$

The Fourier coefficients are given by

$$b_{\mathbf{k}} = \frac{1}{\sqrt{\Omega_0}} \frac{\mathbf{k}}{|\mathbf{k}|} \cdot \int d^3\mathbf{r} \mathbf{B}(\mathbf{r}) e^{-i\mathbf{k}\cdot\mathbf{r}}, \quad (2.22a)$$

$$b_{\mathbf{k}} = \frac{1}{\sqrt{\Omega_0}} \frac{\mathbf{k}}{|\mathbf{k}|} \cdot \int d^3\mathbf{r} \mathbf{B}^*(\mathbf{r}) e^{i\mathbf{k}\cdot\mathbf{r}}, \quad (2.22b)$$

where the components k_j of the wave-vector \mathbf{k} satisfy

$$k_j = \frac{2\pi}{\Omega_0^{1/3}} n_j, \quad n_j = 0, \pm 1, \pm 2, \dots. \quad (2.23)$$

In the limit as the volume goes to infinity $\Omega_0 \rightarrow \infty$ the sum over \mathbf{k} becomes

$$\sum_{\mathbf{k}} \rightarrow \frac{\Omega_0}{(2\pi)^3} \int d^3\mathbf{k}. \quad (2.24)$$

The fact that $\mathbf{P}(\mathbf{r})$ and $\mathbf{\Pi}(\mathbf{r})$ are real functions imposes the following condition on the Fourier components $b_{\mathbf{k}}$ and $b_{\mathbf{k}}^*$,

$$b_{\mathbf{k}}^* = -b_{-\mathbf{k}}. \quad (2.25)$$

The infra-red polarisation field and its momenta conjugate can be written in terms of $b_{\mathbf{k}}$ and $b_{\mathbf{k}}^*$

$$\mathbf{P}(\mathbf{r}) = \sqrt{\frac{\hbar}{2\gamma\omega_{LO}\Omega_0}} \sum_{\mathbf{k}} \frac{\mathbf{k}}{|\mathbf{k}|} \left[b_{\mathbf{k}}^* e^{-i\mathbf{k}\cdot\mathbf{r}} + b_{\mathbf{k}} e^{i\mathbf{k}\cdot\mathbf{r}} \right], \quad (2.26a)$$

$$\boldsymbol{\Pi}(\mathbf{r}) = i\sqrt{\frac{\gamma\hbar\omega_{LO}}{2\Omega_0}} \sum_{\mathbf{k}} \frac{\mathbf{k}}{|\mathbf{k}|} \left[b_{\mathbf{k}}^* e^{-i\mathbf{k}\cdot\mathbf{r}} - b_{\mathbf{k}} e^{i\mathbf{k}\cdot\mathbf{r}} \right]. \quad (2.26b)$$

To derive the Poisson Bracket's for $b_{\mathbf{k}}$ and $b_{\mathbf{k}}^*$, note that $\mathbf{P}(\mathbf{r})$ and $\boldsymbol{\Pi}(\mathbf{r})$ are conjugate variables. This means that $\sqrt{\hbar/2\gamma\omega_{LO}}(b_{\mathbf{k}}^* + b_{\mathbf{k}})$ and $i\sqrt{\hbar\omega_{LO}/2\gamma}(b_{\mathbf{k}}^* - b_{\mathbf{k}})$ are conjugate too. Therefore, quantisation via Bose statistics gives

$$\{b_{\mathbf{k}}^* + b_{\mathbf{k}}, b_{\mathbf{k}'}^* - b_{\mathbf{k}'}\} = \frac{2}{i\hbar} \delta_{\mathbf{k},\mathbf{k}'}, \quad (2.27)$$

and since commutators involving the same operator but different \mathbf{k} 's vanish, the commutators are

$$\{b_{\mathbf{k}}, b_{\mathbf{k}'}^*\} = \frac{1}{i\hbar} \delta_{\mathbf{k},\mathbf{k}'}, \quad (2.28a)$$

$$\{b_{\mathbf{k}}, b_{\mathbf{k}'}\} = \{b_{\mathbf{k}}^*, b_{\mathbf{k}'}^*\} = 0. \quad (2.28b)$$

The interaction energy between the electron and the infrared polarisation field can now be defined in terms of $b_{\mathbf{k}}$ and $b_{\mathbf{k}}^*$,

$$\begin{aligned} e\Phi(\mathbf{r}_{el}) &= - \int \mathbf{D}(\mathbf{r}, \mathbf{r}_{el}) \mathbf{P}(\mathbf{r}) d^3\mathbf{r} \\ &= - \sqrt{\frac{\hbar}{2\gamma\omega_{LO}\Omega_0}} \int \mathbf{D}(\mathbf{r}, \mathbf{r}_{el}) \sum_{\mathbf{k}} \frac{\mathbf{k}}{|\mathbf{k}|} \left[b_{\mathbf{k}}^* e^{-i\mathbf{k}\cdot\mathbf{r}} + b_{\mathbf{k}} e^{i\mathbf{k}\cdot\mathbf{r}} \right] d^3\mathbf{r}, \end{aligned} \quad (2.29)$$

Where to proceed, one integrates by parts to give

$$\begin{aligned} e\Phi(\mathbf{r}_{el}) &= 4\pi i \sqrt{\frac{e^2\hbar}{2\gamma\omega_{LO}\Omega_0}} \int \delta(\mathbf{r} - \mathbf{r}_{el}) \sum_{\mathbf{k}} \frac{1}{|\mathbf{k}|} \left[b_{\mathbf{k}}^* e^{-i\mathbf{k}\cdot\mathbf{r}} - b_{\mathbf{k}} e^{i\mathbf{k}\cdot\mathbf{r}} \right] d^3\mathbf{r} \\ &= 4\pi i \left(\frac{e^2\hbar}{2\gamma\omega_{LO}\Omega_0} \right)^{1/2} \sum_{\mathbf{k}} \frac{1}{|\mathbf{k}|} \left[b_{\mathbf{k}}^* e^{-i\mathbf{k}\cdot\mathbf{r}_{el}} - b_{\mathbf{k}} e^{i\mathbf{k}\cdot\mathbf{r}_{el}} \right]. \end{aligned} \quad (2.30)$$

Hence, for the Hamiltonian (written in symmetrised form), we get

$$\begin{aligned} H = & \frac{\mathbf{p}_{el}^2}{2m_b} + \frac{\hbar\omega_{LO}}{2} \sum_{\mathbf{k}} [b_{\mathbf{k}}^* b_{\mathbf{k}} + b_{\mathbf{k}} b_{\mathbf{k}}^*] - E_{zp} \\ & + 4\pi ie \left(\frac{\hbar}{2\gamma\omega_{LO}\Omega_0} \right)^{1/2} \sum_{\mathbf{k}} \frac{1}{|\mathbf{k}|} [b_{\mathbf{k}}^* e^{-i\mathbf{k}\cdot\mathbf{r}_{el}} - b_{\mathbf{k}} e^{i\mathbf{k}\cdot\mathbf{r}_{el}}]. \end{aligned} \quad (2.31)$$

The result for $\Phi(\mathbf{r}_{el})$ in Eq. (2.30) only holds if $\mathbf{k} \neq 0$, and the summations must exclude the case for when $\mathbf{k} = 0$. This situation represents an electron in a neutral, rigid lattice and must not be subjected to periodic boundary conditions. Otherwise, the periodic boundary conditions would repeat this charge since the volume Ω_0 contains a charge e . This cannot happen as it leads to a diverging overlap of the many long-range repulsive Coulomb interactions. To avoid this, an opposite ‘‘mirror’’ charge $-e$ is distributed homogeneously over the volume Ω_0 , which compensates for the $\mathbf{k} = 0$ component of the electronic charge. So, the $\mathbf{k} = 0$ component does not contribute to the interaction energy. This is known as the homogeneous background charge.

To quantise, the electron momentum \mathbf{p}_{el} is replaced with the operator $i\hat{\nabla}_{\mathbf{r}}$, $b_{\mathbf{k}}$ and $b_{\mathbf{k}}^*$ by the operators $\hat{b}_{\mathbf{k}}$ and $\hat{b}_{\mathbf{k}}^\dagger$, and the Poisson Brackets by $i\hbar$ times the corresponding commutator

$$[b_{\mathbf{k}}, b_{\mathbf{k}'}^\dagger] = \delta_{\mathbf{k},\mathbf{k}'}, \quad (2.32a)$$

$$[b_{\mathbf{k}}, b_{\mathbf{k}}^\dagger] = [b_{\mathbf{k}'}, b_{\mathbf{k}'}^\dagger] = 0. \quad (2.32b)$$

The polarisation field can be viewed as a set of harmonic oscillators \mathbf{k} , all with the same frequency $\omega_{LO}/2\pi$. The operators $b_{\mathbf{k}}$ and $b_{\mathbf{k}}^\dagger$ then represent the creation and annihilation operators, respectively, of quanta of polarisation with different wave-numbers \mathbf{k} but all with the same energy $\hbar\omega_{LO}$. These quanta are usually referred to as *phonons*. Thus, $\hat{b}_{\mathbf{k}}$ and $\hat{b}_{\mathbf{k}}^\dagger$ possess ‘raising’ and ‘lowering’ properties when acting on a normalised eigenfunction $|n_{\mathbf{k}}\rangle$,

$$(\hat{b}_{\mathbf{k}}^\dagger)^n |0_{\mathbf{k}}\rangle = (n!)^{1/2} |n_{\mathbf{k}}\rangle \quad (2.33a)$$

$$(\hat{b}_{\mathbf{k}})^n |n_{\mathbf{k}}\rangle = (n!)^{1/2} |0_{\mathbf{k}}\rangle, \quad \hat{b}_{\mathbf{k}} |0_{\mathbf{k}}\rangle = 0. \quad (2.33b)$$

Fröhlich defined a single dimensionless parameter α that quantifies the strength of the electron-phonon interaction described by the last term in the Hamiltonian. This is defined by

$$\alpha = \frac{2\pi e^2}{\hbar \gamma \omega_{LO}^3} \sqrt{\frac{2m\omega_{LO}}{\hbar}} = \frac{1}{2} \left(\frac{1}{\epsilon_\infty} - \frac{1}{\epsilon_0} \right) \frac{e^2}{\hbar \omega_{LO}} \sqrt{\frac{2m\omega_{LO}}{\hbar}}. \quad (2.34)$$

Therefore, Fröhlich's Hamiltonian becomes

$$\hat{H} = -\frac{\hat{\nabla}_{\mathbf{r}_{el}}^2}{2m_b} + \frac{\hbar\omega_{LO}}{2} \sum_{\mathbf{k}} \left[\hat{b}_{\mathbf{k}}^\dagger \hat{b}_{\mathbf{k}} + \hat{b}_{\mathbf{k}} \hat{b}_{\mathbf{k}}^\dagger \right] - E_{zp} + \sum_{\mathbf{k}} (V_{\mathbf{k}} \hat{b}_{\mathbf{k}} e^{i\mathbf{k}\cdot\mathbf{r}_{el}} + V_{\mathbf{k}}^* \hat{b}_{\mathbf{k}}^\dagger e^{-i\mathbf{k}\cdot\mathbf{r}_{el}}), \quad (2.35)$$

with the interaction term

$$V_{\mathbf{k}} = i \frac{2\hbar\omega_{LO}}{k} \left(\sqrt{\frac{\hbar}{2m_b\omega_{LO}}} \frac{\alpha\pi}{\Omega_0} \right)^{1/2}. \quad (2.36)$$

The zero-point energy E_{zp} can be eliminated using the commutation relations where E_{zp} is given by

$$E_{zp} = \sum_{\mathbf{k}} \frac{\hbar\omega_{LO}}{2}. \quad (2.37)$$

This results in

$$\hat{H} = -\frac{\hat{\nabla}_{\mathbf{r}_{el}}^2}{2m_b} + \frac{\hbar\omega_{LO}}{2} \sum_{\mathbf{k}} \hat{b}_{\mathbf{k}} \hat{b}_{\mathbf{k}}^\dagger + \sum_{\mathbf{k}} (V_{\mathbf{k}} \hat{b}_{\mathbf{k}} e^{i\mathbf{k}\cdot\mathbf{r}_{el}} + V_{\mathbf{k}}^* \hat{b}_{\mathbf{k}}^\dagger e^{-i\mathbf{k}\cdot\mathbf{r}_{el}}). \quad (2.38)$$

The first term is the electron's band energy measured at the bottom of the conduction band. The second term gives the polarisation field's energy measured at the zero-point energy of the polarisation field. Finally, the third term is the electron's interaction energy when interacting with a long-wavelength longitudinal optical phonon.

2.1.3 Holstein's Small Polaron

2.2 The Feynman Path Integral & Variational Approach

Feynman developed a variational principle to find the lowest energy of a system described by a path integral. This variational principle was applied to the Fröhlich model of the polaron [8] and was the first method to accurately predict the ground-state energy and effective mass of the polaron for all values of the electron-phonon coupling constant. We start with Fröhlich's Hamiltonian for a slow electron as

given in Eq. (2.38) and cast the phonon creation and annihilation operators into their corresponding coordinates $q_{\mathbf{k}}$ and momenta $p_{\mathbf{k}}$

$$q_{\mathbf{k}} = \sqrt{\frac{\hbar}{2\omega_{LO}}} (b_{\mathbf{k}}^\dagger + b_{\mathbf{k}}), \quad p_{\mathbf{k}} = i\sqrt{\frac{\hbar\omega_{LO}}{2}} (b_{\mathbf{k}}^\dagger - b_{\mathbf{k}}), \quad (2.39)$$

or Fourier components

$$b_{\mathbf{k}} = \sqrt{\frac{1}{2\hbar\omega_{LO}}} (\omega_{LO}q_{\mathbf{k}} + ip_{\mathbf{k}}), \quad b_{\mathbf{k}}^\dagger = \sqrt{\frac{1}{2\hbar\omega_{LO}}} (\omega_{LO}q_{\mathbf{k}} - ip_{\mathbf{k}}), \quad (2.40)$$

which substituted into Eq. (2.38) gives

$$H = \frac{\mathbf{p}_{el}^2}{2m_b} + \frac{1}{2} \sum_{\mathbf{k}} (p_{\mathbf{k}}^2 + \omega_{LO}^2 q_{\mathbf{k}}^2) + \hbar\omega_{LO} \left(\frac{2\pi\alpha}{\Omega_0} \sqrt{\frac{2\hbar}{m_b\omega_{LO}}} \right)^{1/2} \sum_{\mathbf{k}} \frac{1}{k} q_{\mathbf{k}} e^{i\mathbf{k}\cdot\mathbf{r}_{el}}. \quad (2.41)$$

2.2.1 Ground-State Polaron

If the wavefunction $\psi(\mathbf{r}_i, q_i, t_i)$ corresponding to the polaron system is known at some initial time t_i , then the wavefunction at some later time t_f is given by

$$\psi(\mathbf{r}_f, q_f, t_f) = \int d^3\mathbf{r}_i \int dq_i K(\mathbf{r}_f, q_f, t_f; \mathbf{r}_i, q_i, t_i) \psi(\mathbf{r}_i, q_i, t_i), \quad (2.42)$$

where $\mathbf{r} \equiv \mathbf{r}_{el}$ and $q \equiv \{q_{\mathbf{k}}\}$ represents the set of all polarisation coordinate oscillators. $K(\mathbf{r}_f, q_f, t_f; \mathbf{r}_i, q_i, t_i)$ is commonly called the time-evolution “kernel” or “propagator” and gives the probability amplitude to go from the state of the system $\{\mathbf{r}_i, q_i\}$ at time t_i to the state of the system $\{\mathbf{r}_f, q_f\}$ at time t_f . It can be defined as

$$K(\mathbf{r}_f, q_f, t_f; \mathbf{r}_i, q_i, t_i) \equiv \langle \psi(\mathbf{r}_f, q_f) | e^{-i\hat{H}(t_f-t_i)} | \psi(\mathbf{r}_i, q_i) \rangle = \sum_n \psi_n(\mathbf{r}_f, q_f) \psi_n^*(\mathbf{r}_i, q_i) e^{-iE_n t_f}, \quad (2.43)$$

where ψ_n are a complete orthonormal set of the Fröhlich Hamiltonian eigenfunctions and E_n are the corresponding energy eigenvalues. The ground-state energy can be obtained by letting $\phi_0(q)$ be any function of the phonon coordinates q that is

not orthogonal to the exact ground-state wavefunction $\psi_0(\mathbf{r}, q)$. The inner product of the kernel concerning $\phi_0(q)$ gives the probability amplitude $G_{0,0}$ for the system in the ground state to return to the ground state

$$\begin{aligned} G_{0,0}(t_f) &= \left\langle \phi_0(q_f) \middle| K(\mathbf{r}_f, q_f, t_f; \mathbf{r}_i, q_i, t_i) \right| \phi_0(q_i) \rangle \\ &= \int \int dq_f dq_i \phi_0^*(q_f) K(\mathbf{r}_f, q_f, t_f; \mathbf{r}_i, q_i, t_i) \phi_0(q_i) \\ &= \sum_n a_{n,0}(\mathbf{r}_f) a_{n,0}^*(\mathbf{r}_i) e^{-iE_n t_f}, \end{aligned} \quad (2.44)$$

where

$$a_{n,0}(\mathbf{r}) = \int dq \phi_0^*(q) \psi_n(\mathbf{r}, q). \quad (2.45)$$

If we evaluate this for the electron to start and end at the same position (which we choose to be 0 for convenience), $\mathbf{r}_f = \mathbf{r}_i = 0$ from imaginary-time $i0$ to $-i\tau$ we obtain

$$\begin{aligned} G_{0,0}(-i\tau) &= \left\langle \phi_0(q_f) \middle| K(0, q_f, -i\tau; i0, q_i, 0) \right| \phi_0(q_i) \rangle \\ &= \int \int dq_f dq_i \phi_0^*(q_f) K(0, q_f, -i\tau; 0, q_i, i0) \phi_0(q_i) \\ &= \sum_n a_{n,0}(0) a_{n,0}^*(0) e^{-E_n \tau}, \end{aligned} \quad (2.46)$$

which in the limit as $\tau \rightarrow \infty$ picks out the ground-state of the system

$$\lim_{\tau \rightarrow \infty} \sum_n a_{n,0}(0) a_{n,0}^*(0) e^{-E_n \tau} \rightarrow a_{0,0}(0) a_{0,0}^*(0) e^{-E_0 \tau}. \quad (2.47)$$

Therefore we find that ground-state energy E_{gs}

$$E_{gs} = \lim_{\tau \rightarrow \infty} \left[-\frac{1}{\tau} \ln G_{0,0}(-i\tau) \right]. \quad (2.48)$$

If we identify $\tau = \hbar/(k_B T) = \hbar\beta$ (where β is the thermodynamic beta) then the kernel $K(\mathbf{r}_f, q_f, -i\beta; \mathbf{r}_i, q_i, 0)$ is the same as the statistical density matrix $\rho(\mathbf{r}_f, q_f, \hbar\beta; \mathbf{r}_i, q_i, 0)$, and $G_{0,0}(-i\hbar\beta)$ is the same as the statistical partition function Z where

$$Z(\beta) = \text{Tr} [\rho] = \int \int d\mathbf{r} dq \rho(\mathbf{r}, q, \mathbf{r}, q; \beta), \quad (2.49)$$

and is related to the Helmholtz free energy F by

$$Z(\beta) = e^{-\beta F} = \text{Tr} \left[e^{-\beta \hat{H}} \right] = \sum_n e^{-\beta E_n}. \quad (2.50)$$

Therefore, we can rewrite the expression for the ground-state energy as

$$E_{gs} = \lim_{\beta \rightarrow \infty} [F(\beta)] = \lim_{\beta \rightarrow \infty} \left[-\frac{1}{\beta} \ln Z(\beta) \right]. \quad (2.51)$$

Path Integral Expression

The kernel can be expressed explicitly as a path integral.

$$K(\mathbf{r}_f, q_f, t_f; \mathbf{r}_i, q_i, t_i) = \int_{\mathbf{r}_i, t_i}^{\mathbf{r}_f, t_f} \mathcal{D}\mathbf{r}(t) \int_{q_i, t_i}^{q_f, t_f} \mathcal{D}q(t) \exp \left\{ \frac{iS[\mathbf{r}(t), q(t)]}{\hbar} \right\}, \quad (2.52)$$

where the action $S[\mathbf{r}, q]$ is given by

$$\begin{aligned} S[\mathbf{r}(t), q(t)] &= \frac{m_b}{2} \int_{t_i}^{t_f} dt \dot{\mathbf{r}}_{el}^2 + \frac{1}{2} \int_{t_i}^{t_f} dt \sum_{\mathbf{k}} \left(\dot{q}_{\mathbf{k}}^2 - \omega_{LO}^2 q_{\mathbf{k}}^2 \right) \\ &\quad - \hbar \omega_{LO} \left(\frac{2\pi\alpha}{\Omega_0} \sqrt{\frac{2\hbar}{m_b \omega_{LO}}} \right)^{1/2} \int_{t_i}^{t_f} dt \left(\sum_{\mathbf{k}} \frac{1}{k} q_{\mathbf{k}} e^{i\mathbf{k} \cdot \mathbf{r}_{el}} \right). \end{aligned} \quad (2.53)$$

Since the phonon coordinates $q(t)$ appear quadratically in the action, the path integral over them can be made to be Gaussian and done explicitly to simplify $G_{0,0}$

$$G_{0,0}(t_f, t_i) = \prod_{\mathbf{k}} G_{\mathbf{k}}(t_f, t_i) \times \int_{0, t_i}^{0, t_f} \mathcal{D}\mathbf{r}(t) \exp \left\{ \frac{i}{\hbar} \frac{m_b}{2} \int_{t_i}^{t_f} dt \dot{\mathbf{r}}_{el}^2 \right\}, \quad (2.54)$$

where

$$\begin{aligned} G_{\mathbf{k}}(t_f, t_i) &= \int_{-\infty}^{\infty} dq_{\mathbf{k}, f} dq_{\mathbf{k}, i} \phi_0^*(q_{\mathbf{k}, f}) \\ &\times \left[\int_{q_{\mathbf{k}, i}, t_i}^{q_{\mathbf{k}, f}, t_f} \mathcal{D}q_{\mathbf{k}}(t) \exp \left\{ \frac{i}{\hbar} \int_{t_i}^{t_f} \frac{1}{2} \left(\dot{q}_{\mathbf{k}}^2 - \omega_{LO}^2 q_{\mathbf{k}}^2 \right) - \gamma_{\mathbf{k}}(t) q_{\mathbf{k}}(t) dt \right\} \right] \phi_0(q_{\mathbf{k}, i}), \end{aligned} \quad (2.55)$$

and where

$$\gamma_{\mathbf{k}}(t) = \hbar\omega_{LO} \left(\frac{2\pi\alpha}{\Omega_0} \sqrt{\frac{2\hbar}{m_b\omega_{LO}}} \right)^{1/2} \frac{e^{i\mathbf{k}\cdot\mathbf{r}_{el}}}{k} \quad (2.56)$$

It is the coupling function. To make the phonon path integral Gaussian, we can choose $\phi_0(q_{\mathbf{k}})$ to be the ground-state wavefunction of a simple harmonic oscillator.

$$\phi_0(q_{\mathbf{k}}) = \left(\frac{\omega_{LO}}{\pi\hbar} \right)^{1/4} \exp \left\{ -\frac{\omega_{LO}}{2\hbar} q_{\mathbf{k}}^2 \right\}. \quad (2.57)$$

Now $G_{\mathbf{k}}$ can be done analytically and gives

$$G_{\mathbf{k}}(t_f, t_i) = \exp \left\{ -\frac{1}{4\pi} \int_{t_i}^{t_f} \int_{t_i}^{t_f} dt ds \gamma_{\mathbf{k}}(t) \gamma_{-\mathbf{k}}(s) e^{-i|t-s|} \right\}. \quad (2.58)$$

This gives

$$G_{0,0}(t_f, t_i) = \int_{0, t_i}^{0, t_f} \mathcal{D}\mathbf{r}(t) \exp \left\{ \frac{i}{\hbar} \left[\frac{m_b}{2} \int_{t_i}^{t_f} dt \dot{\mathbf{r}}_{el}^2 - \frac{1}{4\pi} \int_{t_i}^{t_f} \int_{t_i}^{t_f} dt ds e^{-i|t-s|} \sum_{\mathbf{k}} \gamma_{\mathbf{k}}(t) \gamma_{-\mathbf{k}}(s) \right] \right\}. \quad (2.59)$$

The summation of \mathbf{k} gives

$$\begin{aligned} \sum_{\mathbf{k}} \gamma_{\mathbf{k}}(t) \gamma_{-\mathbf{k}}(s) &= \frac{4\pi(\hbar\omega_{LO})^{3/2}\alpha}{\sqrt{8m_b}\Omega_0} \int \frac{d^3\mathbf{k}}{(2\pi)^3/\Omega_0} \frac{e^{i\mathbf{k}\cdot(\mathbf{r}_{el}(t)-\mathbf{r}_{el}(s))}}{k^2} \\ &= \frac{4\pi\hbar(\hbar\omega_{LO})^{3/2}\alpha}{\sqrt{8m_b}} \frac{1}{|\mathbf{r}_{el}(t) - \mathbf{r}_{el}(s)|}. \end{aligned} \quad (2.60)$$

Substituting the result of this summation and setting $t_i = 0$ gives the final form of $G_{0,0}$ to be

$$G_{0,0}(t_f) = \int_{0,0}^{0, t_f} \mathcal{D}\mathbf{r}(t) \exp \left\{ \frac{i}{\hbar} S_{eff} [\mathbf{r}_{el}(t)] \right\}, \quad (2.61)$$

where the new effective action S_{eff} is given by

$$S_{eff}[\mathbf{r}_{el}(t)] = \frac{m_b}{2} \int_0^{t_f} dt \dot{\mathbf{r}}_{el}(t)^2 - \frac{(\hbar\omega_{LO})^{3/2}\alpha}{\sqrt{2m_b}} \int_0^{t_f} \int_0^{t_f} dt ds \frac{e^{-i|t-s|}}{|\mathbf{r}_{el}(t) - \mathbf{r}_{el}(s)|}. \quad (2.62)$$

This new effective *model* action represents an electron coupled by a non-local time-retarded Coulomb potential to itself from an earlier time. If we do a Wick rotation back into imaginary time, we obtain the density matrix as a path integral.

$$\rho(\mathbf{r}_f, \hbar\beta; \mathbf{r}_i, 0) = \int_{\mathbf{r}_i, 0}^{\mathbf{r}_f, \hbar\beta} \mathcal{D}\mathbf{r}(\tau) \exp \left\{ \left(-\frac{S[\mathbf{r}(\tau)]}{\hbar} \right) \right\}, \quad (2.63)$$

Where the model action becomes

$$S[\mathbf{r}(\tau)] = \frac{m_b}{2} \int_0^{\hbar\beta} d\tau \left(\frac{d\mathbf{r}(\tau)}{d\tau} \right)^2 - \frac{(\hbar\omega_{LO})^{3/2}\alpha}{\sqrt{8m_b}} \int_0^{\hbar\beta} d\tau \int_0^{\hbar\beta} d\sigma \frac{e^{-|\tau-\sigma|}}{|\mathbf{r}(\tau) - \mathbf{r}(\sigma)|}. \quad (2.64)$$

Therefore, we can find the exact ground-state energy of the polaron using

$$E_{gs} = \lim_{\beta \rightarrow \infty} \left\{ \frac{1}{\beta} \ln \int_{0, 0}^{0, \hbar\beta} \mathcal{D}\mathbf{r}(\tau) e^{-S[\mathbf{r}(\tau)]/\hbar} \right\}. \quad (2.65)$$

The power of this result is that the many-body problem involving an infinite number of phonons interacting with a single conduction electron has been reduced to a one-body problem with one integral to solve. The first term in the model action is the electron's kinetic energy, and the second term is a 'potential energy' term. This potential energy term represents an attractive Coulomb potential between the electron at an imaginary time τ and itself at an earlier imaginary time σ . The exponential term indicates that the self-interaction of the electron is more robust with a smaller time gap.

2.2.2 Feynman-Jensen Variational Principle

The model action cannot be solved exactly as a path integral since it is not quadratic in the electron coordinates. However, Feynman was able to obtain a variational upper-bound approximation of the ground-state energy of the polaron. Feynman noticed that he could use Jensen's inequality where for a set of real values f , the average of $\exp(f)$ exceeds the exponential of the average,

$$\langle \exp(f) \rangle \geq \exp(\langle f \rangle). \quad (2.66)$$

Therefore, if one can find another path-integrable trial action S_0 that closely approximates the model action S for the paths $\mathbf{r}(\tau)$ that most significantly contribute to the path integral, then Jensen's inequality can be used as so:

$$\begin{aligned} Z(\beta) &= \int_{0,0}^{0,\hbar\beta} \mathcal{D}\mathbf{r}(\tau) e^{-S[\mathbf{r}(\tau)]/\hbar} \\ &= \int_{0,0}^{0,\hbar\beta} \mathcal{D}\mathbf{r}(\tau) e^{-(S[\mathbf{r}(\tau)] - S_0[\mathbf{r}(\tau)])/\hbar} e^{-S_0[\mathbf{r}(\tau)]/\hbar} \\ &= \langle \exp([S - S_0]/\hbar) \rangle_{S_0} \cdot Z_0(\beta) \\ &\geq \exp(\langle S - S_0 \rangle_{S_0}/\hbar) \cdot Z_0(\beta), \end{aligned} \quad (2.67)$$

Where the average taken with positive weight S_0 is given by

$$\langle S - S_0 \rangle_{S_0} = [Z_0(\beta)]^{-1} \int_{0,0}^{0,\hbar\beta} \mathcal{D}\mathbf{r}(\tau) (S - S_0) e^{-S_0[\mathbf{r}]/\hbar} \quad (2.68)$$

and where

$$Z_0(\beta) = \int_{0,0}^{0,\hbar\beta} \mathcal{D}\mathbf{r}(\tau) e^{-S_0[\mathbf{r}(\tau)]/\hbar}, \quad (2.69)$$

Is the partition function for the system described by the trial action S_0 . Therefore, using the relation between the partition function and the ground-state energy, we obtain

$$\begin{aligned} E_{gs} &= \lim_{\beta \rightarrow \infty} \left[-\frac{1}{\beta} \ln Z(\beta) \right], \\ &\leq \lim_{\beta \rightarrow \infty} \left[\frac{1}{\beta} \ln Z_0(\beta) - \frac{1}{\beta} \langle S - S_0 \rangle_{S_0} \right], \\ &\leq E_{gs}^0 - \lim_{\beta \rightarrow \infty} \left[\frac{1}{\beta} \langle S - S_0 \rangle_{S_0} \right]. \end{aligned} \quad (2.70)$$

Here E_{gs}^0 is the ground-state energy of the trial system.

Next, we determine which trial action, S_0 , to use. Feynman proposed using an action with the same form as the model action S , except that a simpler attractive harmonic potential replaces the attractive Coulomb potential.

$$-\frac{\hbar(\hbar\omega_{LO})^{3/2}\alpha}{\sqrt{8m_b}} \frac{e^{-|\tau-\sigma|}}{|\mathbf{r}(\tau) - \mathbf{r}(\sigma)|} \longrightarrow \frac{C}{2} [\mathbf{r}(\tau) - \mathbf{r}(\sigma)]^2 e^{-w|\tau-\sigma|}, \quad (2.71)$$

Where C (a harmonic coupling term) and w (which controls the decay of the potential in imaginary time) are variational parameters, the trial action is then.

$$\begin{aligned} S_0[\mathbf{r}(\tau)] &= \frac{m_b}{2} \int_0^{\hbar\beta} d\tau \left(\frac{d\mathbf{r}(\tau)}{d\tau} \right)^2 \\ &\quad + \frac{C}{2} \int_0^{\hbar\beta} d\tau \int_0^{\hbar\beta} d\sigma [\mathbf{r}(\tau) - \mathbf{r}(\sigma)]^2 e^{-w|\tau-\sigma|}. \end{aligned} \quad (2.72)$$

Substituting the model action S and trial action S_0 into the variational inequality gives

$$E_{gs} \leq E_{gs}^0 - (A + B), \quad (2.73)$$

where

$$A = \lim_{\beta \rightarrow \infty} \frac{(\hbar\omega_{LO})^{3/2}\alpha}{\beta\sqrt{8m_b}} \int_0^{\hbar\beta} d\tau \int_0^{\hbar\beta} d\sigma e^{-|\tau-\sigma|} \langle |\mathbf{r}(\tau) - \mathbf{r}(\sigma)|^{-1} \rangle_{S_0}, \quad (2.74a)$$

$$B = \lim_{\beta \rightarrow \infty} \frac{C}{2\hbar\beta} \int_0^{\hbar\beta} d\tau \int_0^{\hbar\beta} d\sigma e^{-w|\tau-\sigma|} \langle [\mathbf{r}(\tau) - \mathbf{r}(\sigma)]^2 \rangle_{S_0}. \quad (2.74b)$$

To solve A and B we concentrate on the $|\mathbf{r}(\tau) - \mathbf{r}(\sigma)|^{-1}$ term in A and express it by a Fourier transform

$$\begin{aligned} |\mathbf{r}(\tau) - \mathbf{r}(\sigma)|^{-1} &= \int \frac{d^3\mathbf{k}}{2\pi^2|\mathbf{k}|^2} \exp \left(i\mathbf{k} \cdot [\mathbf{r}(\tau) - \mathbf{r}(\sigma)] \right) \\ &\equiv \int \frac{d^3\mathbf{k}}{2\pi^2|\mathbf{k}|^2} \exp \left(\int_0^{\hbar\beta} dt \mathbf{f}(\mathbf{k}, t, \tau, \sigma) \cdot \mathbf{r}(t) \right), \end{aligned} \quad (2.75)$$

where we have defined an ‘external force’ function $\mathbf{f}(\mathbf{k}, t, \tau, \sigma) = i\mathbf{k} [\delta(t - \tau) - \delta(t - \sigma)]$. Substituting this into A and B simplifies them into

$$A = \lim_{\beta \rightarrow \infty} \frac{(\hbar\omega_{LO})^{3/2}\alpha}{\beta\sqrt{8m_b}} \int_0^{\hbar\beta} d\tau \int_0^{\hbar\beta} d\sigma e^{-|\tau-\sigma|} \int \frac{d^3\mathbf{k}}{2\pi^2|\mathbf{k}|^2} \mathcal{Z}(\mathbf{k}, \tau, \sigma), \quad (2.76a)$$

$$B = \lim_{\beta \rightarrow \infty} \frac{C}{2\hbar\beta} \int_0^{\hbar\beta} d\tau \int_0^{\hbar\beta} d\sigma e^{-w|\tau-\sigma|} \left[-\nabla_{\mathbf{k}}^2 \mathcal{Z}(\mathbf{k}, \tau, \sigma) \Big|_{\mathbf{k}=0} \right], \quad (2.76b)$$

where

$$\mathcal{Z}(\mathbf{k}, \tau, \sigma) \equiv \left\langle \exp \left(\int_0^{\hbar\beta} dt \mathbf{f}(\mathbf{k}, t, \tau, \sigma) \cdot \mathbf{r}(t) \right) \right\rangle_{S_0}, \quad (2.77)$$

is the generating functional. The generating functional is also the intermediate scattering function, the temporal Fourier transform of the dynamical structure factor and is proportional to the two-point electron density-density correlation function.

We need the ground-state energy E_{gs}^0 associated with the trial system. We can avoid directly evaluating the path integral Z_0 by noting that

$$Z_0(\beta) = \exp(-\beta E_{gs}^0) = \lim_{\beta \rightarrow \infty} \int_{-\infty}^{\infty} d\mathbf{r} \int_{\mathbf{r}}^{\mathbf{r}'} \mathcal{D}\mathbf{r}'(\tau) \exp \left(-\frac{S_0[\mathbf{r}'(\tau)]}{\hbar} \right). \quad (2.78)$$

So, differentiating both sides concerning C ,

$$\left(\frac{\partial E_{gs}^0}{\partial C} \right)_{\alpha, w} = \frac{B}{C} \quad (2.79)$$

and then integrating both sides,

$$E_{gs}^0 = \int_0^C dC' \frac{B(C', w)}{C'} \propto \mathcal{Z}. \quad (2.80)$$

Since $E_{gs}^0 = 0$ when $C = 0$ (i.e. the free particle). Hence, solving for the upper-bound to the ground-state energy has been reduced to solving $\mathcal{Z}(\mathbf{k}, \tau, \sigma)$, which, written explicitly, is

$$\mathcal{Z}(\mathbf{k}, \tau, \sigma) = \frac{\int_{0,0}^{0,\hbar\beta} \mathcal{D}\mathbf{r}(\tau) \exp \left(-\frac{S_0}{\hbar} + \frac{1}{\hbar} \int_0^{\hbar\beta} dt \mathbf{f}(\mathbf{k}, t, \tau, \sigma) \cdot \mathbf{r}(t) \right)}{\int_{0,0}^{0,\hbar\beta} \mathcal{D}\mathbf{r}(\tau) \exp \left(-\frac{S_0}{\hbar} \right)}. \quad (2.81)$$

We can solve the path integral in the numerator by the usual method of changing the path-integration variable to $\mathbf{r}'(\tau) \equiv \mathbf{r}(\tau) - \bar{\mathbf{r}}(\tau)$ where $\bar{\mathbf{r}}(\tau)$ is the path that extremises the trial action S_0 and with the boundary conditions $\bar{\mathbf{r}}(0) = \bar{\mathbf{r}}(\hbar\beta) = 0$. Thus, $\bar{\mathbf{r}}(\tau)$ contributes most to the path integral and is the classical path, whereas $\mathbf{r}'(\tau)$ are the ‘quantum fluctuations’ about the classical path. The path integral now only contains $\bar{\mathbf{r}}(\tau)$ quadratically, which then separates off as a normalisation factor that excludes the force term \mathbf{f} and is equal to the denominator (i.e. the trial partition function $Z_0(\beta)$), so it cancels. $\bar{\mathbf{r}}(\tau)$ solves the classical equation of motion that is obtained by extremising the trial action S_0 and gives the following integral-differential equation of motion

$$\frac{d^2\bar{\mathbf{r}}(t)}{dt^2} = 2C \int_0^{\hbar\beta} ds [\bar{\mathbf{r}}(t) - \bar{\mathbf{r}}(s)] e^{-w|t-s|} - \mathbf{f}(\mathbf{k}, t, \tau, \sigma) \quad (2.82)$$

which can be used to simplify $\mathcal{Z}(\mathbf{k}, \tau, \sigma)$ by eliminating the classical action term $S_0[\bar{\mathbf{r}}]$ to leave

$$\mathcal{Z}(\mathbf{k}, \tau, \sigma) = \exp \left(\frac{1}{2} \int_0^{\hbar\beta} dt \mathbf{f}(\mathbf{k}, t, \tau, \sigma) \cdot \bar{\mathbf{r}}(t) \right). \quad (2.83)$$

Now, all that is left is to solve the equation of motion to find the classical path $\bar{\mathbf{r}}(t)$. This can be done by first defining

$$\mathbf{R}(t) \equiv \frac{w}{2} \int_0^{\hbar\beta} ds \bar{\mathbf{r}}(s) e^{-w|t-s|}. \quad (2.84)$$

Since $d|t-s|/dt = \text{sgn}(t-s)$ and $d \text{sgn}(t-s)/dt = 2\delta(t-s)$, we have

$$\frac{d^2\mathbf{R}(t)}{dt^2} = w^2 [\mathbf{R}(t) - \bar{\mathbf{r}}(t)], \quad (2.85)$$

and

$$\frac{d^2\bar{\mathbf{r}}(t)}{dt^2} = \frac{4C}{w} [\bar{\mathbf{r}}(t) - \mathbf{R}(t)] - \mathbf{f}(\mathbf{k}, t, \tau, \sigma), \quad (2.86)$$

where in the second equation and in the limit $\beta \rightarrow \infty$ we obtain the term

$$\int_0^\infty ds e^{-w|t-s|} = \frac{2}{w} - \frac{e^{-wt}}{w}, \quad t \in [0, \infty) \quad (2.87)$$

and we neglect the second transient term since it has a negligible contribution. These differential equations can be separated and solved to give the classical path as

$$\bar{\mathbf{r}}(t) = \int_0^{\hbar\beta} ds G(|t-s|) \mathbf{f}(\mathbf{k}, s, \tau, \sigma), \quad (2.88)$$

where

$$\begin{aligned} G(|t-s|) &= \frac{1}{2\pi} \oint dz \frac{z^2 + w^2}{z^2(z^2 + v^2)} \left(e^{-z|t-s|} - 1 \right) \\ &= i \left[\frac{1}{2} \text{Res}(z=0) + \text{Res}(z=iv) \right] \\ &= -\frac{1}{2v^2} \left[\frac{v^2 - w^2}{v} \left(1 - e^{-v|t-s|} \right) + w^2|t-s| \right], \end{aligned} \quad (2.89)$$

with $v^2 \equiv w^2 + 4C/w$. Substituting the solution for $\bar{\mathbf{r}}(t)$ into $\mathcal{Z}(\mathbf{k}, \tau, \sigma)$ then gives

$$\begin{aligned} \mathcal{Z}(\mathbf{k}, \tau, \sigma) &= \exp \left(\frac{1}{2} \int_0^{\hbar\beta} dt \int_0^{\hbar\beta} ds \mathbf{f}(\mathbf{k}, t, \tau, \sigma) \cdot G(|t-s|) \cdot \mathbf{f}(\mathbf{k}, s, \tau, \sigma) \right) \\ &= \exp \left(\mathbf{k}^2 G(|\tau - \sigma|) \right). \end{aligned} \quad (2.90)$$

Finally, we can use the solution for $\mathcal{Z}(\mathbf{k}, \tau, \sigma)$ to determine A

$$A = \alpha \hbar \omega_{LO} \sqrt{\frac{1}{\pi}} \int_0^\infty d\tau \frac{e^{-\tau \omega_{LO}}}{\sqrt{D(\tau)}}, \quad (2.91)$$

where

$$D(\tau) = -2G(\tau) = \frac{w^2}{v^2} \left[\tau \omega_{LO} + \frac{v^2 - w^2}{w^2 v \omega_{LO}} \left(1 - e^{-v\tau \omega_{LO}} \right) \right], \quad (2.92)$$

and also determine B and E_{gs}^0

$$B = \frac{3\hbar\omega_{LO}C}{vw} = \frac{3\hbar\omega_{LO}}{4} \frac{v^2 - w^2}{v}, \quad (2.93)$$

$$E_{gs}^0 = \frac{3\hbar\omega_{LO}}{2} (v - w). \quad (2.94)$$

I want to note that I have now explicitly shown the ω_{LO} factors that were originally hidden in the variational parameters v and w . Finally, we obtain the variational principle for the ground-state energy of the polaron,

$$E_{gs} \leq \hbar\omega_{LO} \frac{3}{4v} (v - w)^2 - \alpha \hbar\omega_{LO}^2 \sqrt{\frac{1}{\pi}} \int_0^\infty d\tau \frac{e^{-\tau\omega_{LO}}}{\sqrt{D(\tau)}}. \quad (2.95)$$

Here v and w are to be varied to find the lowest approximate upper-bound to the exact ground-state E_{gs} .

Weak- and strong- coupling limits

For extremal values of the coupling α , w smoothly approaches limits of 1 and 3. The energy minimum in the weak-coupling (small alpha) limit occurs when v is near w . Therefore, Feynman set $v = (1 + \varepsilon)w$ where ε is small and expanded the energy expression (RHS of Eq. (2.95)) w.r.t ε . Feynman then minimised the energy first w.r.t ε and then w.r.t w and found that in the weak-coupling limit, the energy is least when

$$\begin{aligned} \frac{w}{\omega_{LO}} &= 3, & \frac{v}{\omega_{LO}} &= 3 \left[1 + \frac{2\alpha}{3w} \left(1 - \frac{2}{w} [\sqrt{w-1} - 1] \right) \right], \\ \frac{E_{gs}}{\hbar\omega_{LO}} &\leq -\alpha - 1.23 \left(\frac{\alpha}{10} \right)^2. \end{aligned} \quad (2.96)$$

In the strong-coupling (large alpha) limit, v is large, and w approaches one, so $w/v \ll 1$. Therefore, Feynman expanded the energy expression w.r.t w/v and then minimised the energy w.r.t v and w and found that in the strong-coupling limit the energy is least when

$$\begin{aligned} \frac{w}{\omega_{LO}} &= 1, & \frac{v}{\omega_{LO}} &= \frac{4\alpha^2}{9\pi} - 4 \left(\log 2 + \frac{1}{2}\gamma \right) + 1, \\ \frac{E_{gs}}{\hbar\omega_{LO}} &\leq -\frac{\alpha^2}{2\pi} - \frac{3}{2}(2\log 2 + \gamma) - \frac{3}{4} + \mathcal{O} \left(\frac{1}{\alpha^2} \right). \end{aligned} \quad (2.97)$$

where $\gamma = 0.5772\dots$ is the Euler-Mascheroni constant.

Feynman's polaron effective mass and radius

Feynman found the effective polaron mass at zero temperature [1] by assuming that the electron moves with a small velocity \mathbf{u} from an initial coordinate $\mathbf{0}$ to a final coordinate $\mathbf{r}_f = \mathbf{u}\hbar\beta$ in an imaginary-time $\hbar\beta$. Feynman then sought the

total energy of the polaron and equated it to the form $E_0 + \frac{1}{2}m_p^*u^2$ by expanding the total energy expression to quadratic-order in the velocity \mathbf{u} . From the kinetic energy term, Feynman found the polaron effective mass:

$$m_p = m_b \left[1 + \frac{\alpha}{3\sqrt{\pi}} \left(\frac{v}{w} \right)^3 \int_0^\infty d\tau \frac{e^{-\tau} \tau^{1/2}}{[D(\tau)]^{3/2}} \right]. \quad (2.98)$$

Here, the variational parameter values minimise the polaron ground-state energy when $u = 0$ in Eq. (2.95). From the values in Eq. (2.96) Feynman obtained the weak-coupling expression

$$m_p = m_b \left[1 + \frac{1}{6}\alpha + 0.025\alpha^2 + \dots \right], \quad (2.99)$$

and from the values in Eq. (2.97) the strong-coupling expression

$$m_p = m_b \frac{160}{81} \left(\frac{\alpha}{\pi} \right)^4. \quad (2.100)$$

As an aside, at finite temperatures the effective polaron mass (as described by [17]) is proportional to the imaginary part of the complex impedance function $Z(\Omega, \beta)$ provided by [2] (Eqs. (35), (36) & (41)) in the zero frequency limit $\nu \rightarrow 0$:

$$m_p(\beta) = e m_b \lim_{\Omega \rightarrow 0} \left\{ \frac{\text{Im}Z(\Omega, \beta)}{\Omega} \right\}. \quad (2.101)$$

Schultz [18] estimated the polaron size by calculating the root mean square distance between the electron and the fictitious particle.

The reduced mass of their relative motion is:

$$\mu = \frac{m_b}{m_p} (m_p - m_b). \quad (2.102)$$

Schultz used the ‘zeroth-order’ effective mass m_0 ,

$$m_0 = m_b \left(\frac{v}{w} \right)^2 \quad (2.103)$$

which is obtained by approximating the model action S with the trial S_0 ; no higher-order expansion terms are included. Schultz then used the ground-state harmonic

oscillator wave function for the relative coordinate ρ between the electron and the fictitious mass,

$$\phi_0(\rho) = \left(\frac{\mu v \omega_{LO}}{\pi \hbar} \right)^{3/4} \exp \left(-\frac{\mu v \omega_{LO} \rho^2}{2 \hbar} \right), \quad (2.104)$$

to define a polaron radius as the root mean square distance between the electron and the fictitious mass:

$$r_P \equiv \langle \rho^2 \rangle^{1/2} = \frac{1}{2} \left(\frac{3}{\mu v \omega_{LO}} \right)^{1/2} = \frac{1}{2} \left(\frac{3v}{m_b(v^2 - w^2)\omega_{LO}} \right)^{1/2}. \quad (2.105)$$

In the weak-coupling limit, with v and w given in Eq. 2.96, this expression for the polaron radius reduces to

$$r_P \sim \frac{3}{4} \left(\frac{6\hbar}{\alpha m_b \omega_{LO}} \right)^{1/2}, \quad (2.106)$$

and in the strong-coupling limit (Eq. 2.97) the radius becomes

$$r_P \sim \frac{3}{2\alpha} \left(\frac{\pi \hbar}{m_b \omega_{LO}} \right)^{1/2}. \quad (2.107)$$

For small α , the variational minimum occurs when

$$w = 3, \\ v = 3 \left[1 + \frac{2\alpha}{3w} \left(1 - \frac{2}{w} [\sqrt{w-1} - 1] \right) \right] \quad (2.108)$$

to give the upper-bound

$$\frac{E_{gs}}{\hbar \omega_{LO}} \leq -\alpha - \left(\frac{\alpha}{9} \right)^2 + \dots \approx -\alpha - 0.0123\alpha^2 + \dots \quad (2.109)$$

The result agrees well with the perturbative result E_{gs}^w

$$\frac{E_{gs}^w}{\hbar \omega_{LO}} = -\alpha - 0.0159196220\alpha^2 - 0.000806070048\alpha^3 - \mathcal{O}(\alpha^4) \quad (2.110)$$

For large α , the variational minimum occurs when

$$\begin{aligned} w &= 1, \\ v &= \frac{4\alpha^2}{9\pi} - 4 \left(\log 2 + \frac{1}{2}\gamma \right) + 1 \end{aligned} \tag{2.111}$$

where $\gamma \approx 0.5773\dots$ is the Euler-Mascheroni constant. This gives the upper-bound

$$\frac{E_{gs}}{\hbar\omega_{LO}} \leq -\frac{\alpha^2}{3\pi} - 3 \left(\frac{1}{4} + \ln 2 \right) + \mathcal{O} \left(\frac{1}{\alpha^2} \right) \approx -0.1061\alpha - 2.8294 + \mathcal{O} \left(\frac{1}{\alpha^2} \right) \tag{2.112}$$

which is reasonable when compared to the result of the precise strong-coupling expansion E_{gs}^s

$$\frac{E_{gs}^s}{\hbar\omega_{LO}} = -0.108513\alpha^2 - 2.836 - \mathcal{O} \left(\frac{1}{\alpha^2} \right). \tag{2.113}$$

Feynman's polaron effective mass

By shifting the velocity of the polaron in the path integral, Feynman was able to calculate an effective mass for the polaron, m_p . The result is

$$m_p = m_b \left[1 + \frac{\alpha\omega_{LO}^3}{3\sqrt{\pi}} \left(\frac{v}{w} \right)^3 \int_0^\infty d\tau \frac{\tau^2 e^{-\tau\omega_{LO}}}{[D(\tau)]^{3/2}} \right]. \tag{2.114}$$

In the weak-coupling limit (small α) this gives the expansion

$$m_p = m_b \left[1 + \frac{\alpha}{6} + 2.469136 \left(\frac{\alpha}{10} \right)^2 + 3.566719 \left(\frac{\alpha}{10} \right)^3 + \dots \right] \tag{2.115}$$

and in the strong-coupling limit, it gives the expansion

$$\begin{aligned} m_p &\approx m_b \left[11.85579 - \frac{4}{3\pi}(1 + \ln 4)\alpha^2 + \frac{16}{81\pi^2}\alpha^4 \dots \right] \\ &\approx m_b \left[11.85579 - 1.012775\alpha^2 + 0.020141\alpha^4 + \dots \right]. \end{aligned} \tag{2.116}$$

For comparison, the exact expansion results are

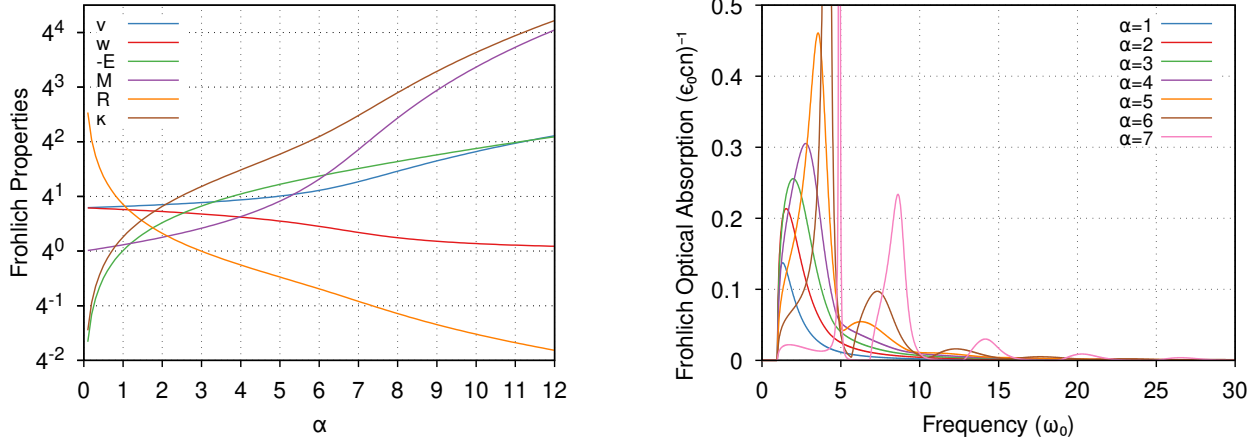


Figure 2.1: (left): Unitless values from Feynman's athermal 0K polaron theory, calculated for electron-phonon α couplings ranging from 1 to 12. Blue-solid is the negative of the best approximated ground-state energy F , orange-dashed is the polaron effective mass m_b , green-dotted is the v variational parameter and purple-dash-dotted is the w variational parameter. (right): The real conductivity (also the frequency-dependent mobility) of the polaron response obtained from the FHIP theory and calculated for α ranging from 1 to 12 and external field angular frequencies ranging from $0 \omega_{LO}$ to $20 \omega_{LO}$ multiples of the effective phonon angular frequency. The relative magnitudes of the curves for different values of α have been normalised and are not comparable.

$$m_p^w = m_b \left[1 + \frac{\alpha}{6} + 2.362763 \left(\frac{\alpha}{10} \right)^2 + \mathcal{O}(\alpha^4) \right] \quad (2.117)$$

and

$$m_p^s = m_b \left[0.0227019\alpha^4 + \mathcal{O}(\alpha^2) \right]. \quad (2.118)$$

Numerical Results

Feynman's original path integral theory ([1]) for the polaron produced a variational principle for the ground-state energy of the polaron. The variational v and w parameters that make the best lower upper bound to the ground-state energy are then used in expressions that Feynman derived for the polaron's effective mass and complex conductivity.

Figure 2.1a shows the values of the polaron ground-state energy $-E_{gs}$, effective mass m_p and the corresponding v and w , for values of the Fröhlich α parameter ranging from 1 to 12. These data are all presented in their 'polaron units' form for easier comparison to Feynman's original paper. The ground state demonstrates the linear weak-coupling behaviour at smaller α before it becomes exponentially

more negative as α increases (as the electron-phonon coupling strengthens). The effective mass starts roughly equal to the conduction electron band-mass $m_p = m_b$ at small α and then grows exponentially larger at stronger couplings. The v and w variational parameters start as approximately equal with $v \approx w \approx 3$ at weak couplings but diverge at strong couplings as w asymptotically approaches $w = 1$ and v increases exponentially at a similar rate to the ground-state energy.

Figure 2.1b shows the athermal real conductivity (which is equivalent to the frequency-dependent polaron mobility) for $0 \leq \alpha \leq 12$ and for an applied electric field with an angular frequency Ω ranging from 0 to 20 times that of the longitudinal optical phonon frequency ω_{LO} . At lower couplings $\alpha \leq 4$, all of the first peaks start at $\Omega = \omega_{LO}$ and for $\alpha \geq 5$ we see the appearance of additional peaks at $\Omega = \omega_{LO} + n\omega_{LO}v$, $n \in \mathbb{Z}^+$, with all of the peaks seemingly sharpening and blue-shifting to higher frequencies at stronger couplings $\alpha \geq 7$. However, for very strong couplings $\alpha \geq 10$, the initial peak at $\Omega = \omega_{LO}$ seems to appear again.

2.2.3 Finite Temperature Polaron

Osaka [11] extends Feynman's athermal path integral polaron model to the case at a finite temperature. This means that the variational principle of the self-energy of the polaron is replaced by the variation of the *free energy*. Osaka begins with the density matrix of the polaron system with the model action of the polaron at a finite temperature given by

$$S = \frac{m_b}{2} \int_0^\beta \dot{\mathbf{r}}^2(\tau) d\tau - \frac{2^{-3/2}\alpha e^\beta}{e^\beta - 1} \int_0^\beta \int_0^\beta \frac{e^{-|\tau-\sigma|}}{|\mathbf{r}(\tau) - \mathbf{r}(\sigma)|} d\tau d\sigma - \frac{2^{-3/2}\alpha}{e^\beta - 1} \int_0^\beta \int_0^\beta \frac{e^{|\tau-\sigma|}}{|\mathbf{r}(\tau) - \mathbf{r}(\sigma)|} d\tau d\sigma \quad (2.119)$$

which can be written more simply as (and now explicitly including m_b , \hbar and ω_{LO})

$$S = \frac{m_b}{2} \int_0^{\hbar\beta} d\tau \dot{\mathbf{r}}^2(\tau) - \frac{\alpha (\hbar\omega_{LO})^{3/2}}{2\sqrt{2m_b}} \int_0^{\hbar\beta} d\tau \int_0^{\hbar\beta} d\sigma \frac{G_{\omega_{LO}}(\tau - \sigma)}{|\mathbf{r}(\tau) - \mathbf{r}(\sigma)|} \quad (2.120)$$

where $G(\tau)$ is the dimensionless phonon Green's function

$$G_{\omega_{LO}}(\tau) = \frac{\cosh(\omega_{LO}(\hbar\beta/2 - |\tau|))}{\sinh(\hbar\omega_{LO}\beta/2)}. \quad (2.121)$$

Ōsaka then chose the trial action to be

$$S_0 = \frac{1}{2} \int_0^\beta \dot{\mathbf{r}}^2(\tau) d\tau + \frac{C}{2} \frac{e^{\beta w}}{e^{\beta w} - 1} \int_0^\beta \int_0^\beta \frac{e^{-w|\tau-\sigma|}}{|\mathbf{r}(\tau) - \mathbf{r}(\sigma)|^{-2}} d\tau d\sigma + \frac{C}{2} \frac{1}{e^{\beta w} - 1} \int_0^\beta \int_0^\beta \frac{e^{w|\tau-\sigma|}}{|\mathbf{r}(\tau) - \mathbf{r}(\sigma)|^{-2}} d\tau d\sigma \quad (2.122)$$

which can be written explicitly as

$$S_0 = \frac{m_b}{2} \int_0^{\hbar\beta} d\tau \dot{\mathbf{r}}^2(\tau) + \frac{C}{2} \int_0^{\hbar\beta} d\tau \int_0^{\hbar\beta} d\sigma G_w(\tau - \sigma) |\mathbf{r}(\tau) - \mathbf{r}(\sigma)|^2 \quad (2.123)$$

where $G_w(\tau)$ mimics the phonon Green's function

$$G_w(\tau) = \frac{\cosh(w(\hbar\beta/2 - |\tau|))}{\sinh(\hbar w\beta/2)}. \quad (2.124)$$

The model and trial density matrices are then

$$\rho(\mathbf{r}_f, \mathbf{r}_i; \hbar\beta) = \int_{\mathbf{r}(0)=\mathbf{r}_i}^{\mathbf{r}(\hbar\beta)=\mathbf{r}_f} \mathcal{D}\mathbf{r}(\tau) \exp\left(-\frac{S[\mathbf{r}(\tau)]}{\hbar}\right) \quad (2.125a)$$

$$\rho_{S_0}(\mathbf{r}_f, \mathbf{r}_i; \hbar\beta) = \int_{\mathbf{r}(0)=\mathbf{r}_i}^{\mathbf{r}(\hbar\beta)=\mathbf{r}_f} \mathcal{D}\mathbf{r}(\tau) \exp\left(-\frac{S_0[\mathbf{r}(\tau)]}{\hbar}\right). \quad (2.125b)$$

The variational principle for a finite temperature is then

$$\rho(\mathbf{r}_f, \mathbf{r}_i; \hbar\beta) \geq \rho_{S_0}(\mathbf{r}_f, \mathbf{r}_i; \hbar\beta) \exp\langle S - S_0 \rangle_{\mathbf{r}_i, \mathbf{r}_f} \quad (2.126)$$

where

$$\langle S - S_0 \rangle_{\mathbf{r}_i, \mathbf{r}_f} = \frac{\int_{\mathbf{r}(0)=\mathbf{r}_i}^{\mathbf{r}(\hbar\beta)=\mathbf{r}_f} \mathcal{D}\mathbf{r}(\tau) (S - S_0) \exp\left(-\frac{S_0[\mathbf{r}(\tau)]}{\hbar}\right)}{\rho_{S_0}(\mathbf{r}_f, \mathbf{r}_i; \hbar\beta)}. \quad (2.127)$$

The RHS of the variational equation then has to be calculated and minimised concerning the variational parameters v and C . The equation of motion obtained from the trial action S_0 is

$$\begin{aligned} m_b \ddot{\mathbf{r}}(\tau) &= 2C \left\{ \int_0^{\hbar\beta} d\sigma G_w(\tau - \sigma) [\mathbf{r}(\tau) - \mathbf{r}(\sigma)] \right\} \\ &= \frac{4C}{w} \mathbf{r}(\tau) - 2C \int_0^{\hbar\beta} d\sigma G_w(\tau - \sigma) \mathbf{r}(\sigma), \end{aligned} \quad (2.128)$$

which we can use with the boundary conditions $\mathbf{r}(\hbar\beta) = \mathbf{r}_f$ and $\mathbf{r}(0) = \mathbf{r}_i$ to give the trial density matrix to be

$$\rho_{S_0} (\mathbf{r}_i, \mathbf{r}_f; \hbar\beta) = \exp \left\{ -\frac{m_b}{2\hbar} (\mathbf{r}(\hbar\beta) \cdot \dot{\mathbf{r}}(\hbar\beta) - \mathbf{r}(0) \cdot \dot{\mathbf{r}}(0)) \right\}, \quad (2.129)$$

it has been approximated that the classical path dominates, and so is the only path evaluated.

Now, directly solving for $\mathbf{r}(\tau)$ from the equation of motion is difficult, so instead Ōsaka considered a system with a different Lagrangian L' ,

$$L' = \frac{1}{2} \left(m_b \dot{\mathbf{r}}^2 + M \dot{\mathbf{R}}^2 - \kappa (\mathbf{r} - \mathbf{R})^2 \right), \quad (2.130)$$

of a particle of mass m_b coupled by a harmonic spring with a force constant κ to a particle of mass M . After integrating over the \mathbf{R} coordinate, the density matrix ρ' of the Lagrangian L' is given by

$$\begin{aligned} \rho'(\mathbf{r}_i, \mathbf{r}_f; \hbar\beta) &= \left(2 \sinh \left(\frac{\hbar\beta w'}{2} \right) \right)^{-3} \int_{\mathbf{r}(0)=\mathbf{r}_i}^{\mathbf{r}(\hbar\beta)=\mathbf{r}_f} \exp \left[-\frac{m_b}{2\hbar} \int_0^{\hbar\beta} d\tau (\dot{\mathbf{r}}^2 + \kappa \mathbf{r}^2) \right. \\ &\quad \left. + \frac{M}{4\hbar} w'^3 \int_0^{\hbar\beta} d\tau \int_0^{\hbar\beta} d\sigma G_{w'}(\tau - \sigma) \mathbf{r}(\tau) \mathbf{r}(\sigma) \right] \mathcal{D}\mathbf{r}(\tau), \end{aligned} \quad (2.131)$$

where $w' = \sqrt{\kappa/M}$. This new action has the same equation of motion with the same form as the previous action

$$m_b \ddot{\mathbf{r}}(\tau) = \kappa \mathbf{r}(\tau) - \frac{M w'^3}{2} \int_0^{\hbar\beta} d\sigma G_{w'}(\tau - \sigma) \mathbf{r}(\sigma), \quad (2.132)$$

which, under the classical path approximation, gives the density matrix

$$\rho'(\mathbf{r}_i, \mathbf{r}_f; \hbar\beta) = \left(2 \sinh\left(\frac{\hbar\beta w'}{2}\right)\right)^{-3} \exp\left\{-\frac{m_b}{2\hbar} (\mathbf{r}(\hbar\beta) \cdot \dot{\mathbf{r}}(\hbar\beta) - \mathbf{r}(0) \cdot \dot{\mathbf{r}}(0))\right\}. \quad (2.133)$$

This means that the density matrix ρ' is the same as ρ , with the same equation of motion, if we put $w' = w$, $Mw'^3 = 4C$ and omit the unimportant normalisation factor $(2 \sinh(\hbar\beta w'/2))^{-3}$. Therefore, Ōsaka used the solution to the equation of motion in Eq. (2.132) to calculate the trial density matrix ρ_{S_0} where the trial action S_0 is replaced by the action corresponding to the Lagrangian L' .

The key to calculating $\langle S - S_0 \rangle_{\mathbf{r}_i, \mathbf{r}_f}$ is to evaluate the generating functional \mathcal{Z} in Eq. (2.81) using the same method Feynman used, except that Osaka replaced the trial action S_0 with that of L' and instead evaluated the path integral in the generating functional \mathcal{Z} using the Lagrangian

$$L = \frac{m_b}{2} \dot{\mathbf{r}}^2 + \frac{M}{2} \dot{\mathbf{R}}^2 - \frac{\kappa}{2} (\mathbf{r} - \mathbf{R})^2 + \mathbf{f}(\mathbf{k}, t, \tau, \sigma) \cdot \mathbf{r}, \quad (2.134)$$

where $\mathbf{f}(\mathbf{k}, t, \tau, \sigma) = i\mathbf{k} [\delta(t - \tau) - \delta(t - \sigma)]$ as before. This Lagrangian is evaluated by first doing a change of variables

$$\mathbf{R}' = \mathbf{r} - \mathbf{R}, \quad \mathbf{r}' = M\mathbf{R} + \frac{m_b}{M + m_b} \mathbf{r}, \quad (2.135)$$

to give

$$\begin{aligned} L = & \frac{M + m_b}{2} \dot{\mathbf{r}}'^2 + \frac{2Mm_b}{M + m_b} \dot{\mathbf{R}}'^2 - \frac{\kappa}{2} \mathbf{R}'^2 \\ & + \frac{Mm_b}{M + m_b} \mathbf{f}(\mathbf{k}, t, \tau, \sigma) \cdot \mathbf{R}' + m_b \mathbf{f}(\mathbf{k}, t, \tau, \sigma) \cdot \mathbf{r}'. \end{aligned} \quad (2.136)$$

This gives equations of motion for \mathbf{R}' and \mathbf{r}'

$$\ddot{\mathbf{R}}' = v\mathbf{R}' - \frac{1}{m_b} \mathbf{f}(\mathbf{k}, t, \tau, \sigma), \quad \ddot{\mathbf{r}}' = -\frac{1}{M + m_b} \mathbf{f}(\mathbf{k}, t, \tau, \sigma), \quad (2.137)$$

where $v^2 = \kappa(M + m_b)/(Mm_b) = 4C/w + w^2$ as defined by Feynman. Ōsaka gave the solution for \mathbf{R}' under the boundary conditions $\mathbf{R}'(0) = \mathbf{R}'_i$ and $\mathbf{R}'(\hbar\beta) = \mathbf{R}'_f$ to be

$$\begin{aligned}
 \mathbf{R}'(t) &= \frac{\mathbf{R}'_i \sinh(v[\hbar\beta - t]) + \mathbf{R}'_f \sinh(vt)}{v \sinh(v\hbar\beta)} \\
 &+ i\mathbf{k} \sinh(vt) \frac{\sinh(v[\hbar\beta - \tau]) - \sinh(v[\hbar\beta - \sigma])}{v \sinh(v\hbar\beta)} \\
 &- \frac{i\mathbf{k}}{v} \begin{cases} \sinh(v[t - \tau]) - \sinh(v[t - \sigma]) & t > \tau \\ -\sinh(v[t - \sigma]) & \sigma < t < \tau \\ 0 & t < \sigma, \end{cases} \tag{2.138}
 \end{aligned}$$

if $\tau > \sigma$, otherwise the conditional is

$$\begin{cases} \sinh(v[t - \tau]) - \sinh(v[t - \sigma]) & t > \sigma \\ \sinh(v[t - \sigma]) & \sigma < t < \tau \\ 0 & t < \sigma. \end{cases} \tag{2.139}$$

Under the boundary conditions $\mathbf{r}'(0) = \mathbf{r}'_i$ and $\mathbf{r}'(\hbar\beta) = \mathbf{r}'_f$ the solution for \mathbf{r}' is

$$\begin{aligned}
 \mathbf{r}'(t) &= \mathbf{r}'_i + \frac{v^2(\mathbf{r}'_f - \mathbf{r}'_i) - i\mathbf{k}w^2(\tau - \sigma)}{\hbar\beta v^2} \\
 &- i\mathbf{k} \frac{w^2}{v^2} \left[\left(\begin{cases} t - \tau & t > \tau \\ 0 & t < \tau \end{cases} \right) - \left(\begin{cases} t - \sigma & t > \sigma \\ 0 & t < \sigma. \end{cases} \right) \right]. \tag{2.140}
 \end{aligned}$$

Using the equations of motion, Ōsaka obtains the generating functional

$$\begin{aligned}
 \mathcal{Z}(\mathbf{k}, \tau, \sigma) &= \exp \left(-\frac{Mm_b}{2\hbar(M+m_b)} [\mathbf{R}'(\hbar\beta) \cdot \dot{\mathbf{R}}'(\hbar\beta) - \mathbf{R}'(0) \cdot \dot{\mathbf{R}}'(0)] \right. \\
 &- \frac{M+m_b}{2\hbar} [\mathbf{Q}(\hbar\beta) \cdot \dot{\mathbf{r}}'(\hbar\beta) - \mathbf{r}'(0) \cdot \dot{\mathbf{r}}'(0)] \\
 &+ \frac{Mm_b}{2\hbar(M+m_b)} \int_0^{\hbar\beta} dt \mathbf{f}(\mathbf{k}, t, \tau, \sigma) \cdot \mathbf{R}'(t) \\
 &\left. + \frac{m_b}{2\hbar} \int_0^{\hbar\beta} dt \mathbf{f}(\mathbf{k}, t, \tau, \sigma) \cdot \mathbf{r}'(t) \right). \tag{2.141}
 \end{aligned}$$

Ōsaka connects this to the original action S by identifying $\mathbf{r}'_{i,f}$ and $\mathbf{R}'_{i,f}$ to $\mathbf{r}_{i,f}$ and $\mathbf{R}_{i,f}$ respectively using the relations in Eq. (2.137) and then integrating over \mathbf{R}_i un-

der the boundary condition $\mathbf{R}_i = \mathbf{R}_f$. Using this, the fact that $\lim_{\mathbf{k} \rightarrow 0} \mathcal{Z}(\mathbf{k}, \tau, \sigma) = 1$ and that the kinetic energy terms in $\langle S - S_0 \rangle$ cancel, Ōsaka obtained $\langle S \rangle_{\mathbf{r}, \mathbf{r}}$ as

$$\begin{aligned}\langle S \rangle_{\mathbf{r}, \mathbf{r}} &= \frac{\alpha (\hbar\omega_{LO})^{3/2}}{2\sqrt{2m_b}} \int_0^{\hbar\beta} d\tau \int_0^{\hbar\beta} d\sigma G_{\omega_{LO}}(\tau - \sigma) \int \frac{d^3\mathbf{k}}{2\pi^2|\mathbf{k}|^2} \exp\left(-\frac{\hbar k^2}{2m_b} D(\tau)\right) \\ &= \frac{\alpha (\hbar\omega_{LO})^2}{\sqrt{\pi}} \frac{\beta e^{\hbar\omega_{LO}\beta}}{e^{\hbar\omega_{LO}\beta} - 1} \int_0^{\hbar\beta} d\tau e^{-\omega_{LO}\tau} [D(\tau)]^{-1/2}.\end{aligned}\quad (2.142)$$

Here $D(\tau)$ is now the finite temperature generalisation of (2.92) given by

$$D(\tau) = \frac{w^2}{v^2} \left[\frac{2 \sinh(|\tau|\omega_{LO}v/2) \sinh(v\omega_{LO}[\hbar\beta - |\tau|]/2)}{\sinh(\hbar\omega_{LO}\beta v/2)} + \omega_{LO}|\tau| \left(1 - \frac{|\tau|}{\hbar\beta}\right) \right].\quad (2.143)$$

$\langle S \rangle_{\mathbf{r}, \mathbf{r}}$ is independent of the boundary conditions so that we can write $\langle S \rangle$. $\langle S_0 \rangle$ is obtained as before from the power series of \mathbf{k} of $\mathcal{Z}(\mathbf{k}, \tau, \sigma)$ to give

$$\begin{aligned}\langle S_0 \rangle &= 3C\hbar\omega_{LO}\beta \int_0^{\hbar\beta} d\tau (\hbar\beta - \tau) G_w(\tau) D(\tau) \\ &= \frac{3C\hbar\omega_{LO}\beta}{vw} \left(\frac{2}{v\hbar\omega_{LO}\beta} - \coth\left(\frac{v\hbar\omega_{LO}\beta}{2}\right) \right).\end{aligned}\quad (2.144)$$

Ōsaka then obtained the partition function from the diagonal part of the density matrix

$$Z(\beta) = \rho(\mathbf{r}, \mathbf{r}; \hbar\beta) \geq \rho_{S_0}(\mathbf{r}, \mathbf{r}; \hbar\beta) \exp\langle S - S_0 \rangle = Z_{S_0}(\beta) \exp\langle S - S_0 \rangle,\quad (2.145)$$

giving the variational principle

$$F(\beta) \leq F_{S_0}(\beta) + \frac{1}{\beta} (\langle S \rangle - \langle S_0 \rangle). \quad (2.146)$$

Now, in a similar way to Feynman, Ōsaka obtained the trial free energy $F_{S_0}(\beta)$ using

$$\frac{\partial \log Z_{S_0}}{\partial C} = \frac{\langle S_0 \rangle}{C}, \quad (2.147)$$

and the fact that when $C = 0$, $Z_{S_0} = (2\pi\hbar\omega_{LO}\beta)^{-3/2}$. By integrating $\partial \log Z_{S_0}/\partial C$ with respect to C , Ōsaka obtained

$$\begin{aligned} F_{S_0}(\beta) &= -\frac{1}{\beta} \log Z_{S_0}(\beta) = \frac{3}{2\beta} \log(2\pi\hbar\omega_{LO}\beta) - \frac{1}{\beta} \int_0^C dC' \frac{\langle S_0 \rangle}{C'} \\ &= \frac{3}{2\beta} \log(2\pi\hbar\omega_{LO}\beta) + \hbar\omega_{LO} \frac{3C}{2vw} \int_w^v du \left(\coth\left(\frac{\hbar\omega_{LO}\beta u}{2}\right) - \frac{2}{\hbar\omega_{LO}\beta u} \right) \\ &= \frac{3}{2\beta} \log(2\pi\hbar\omega_{LO}\beta) + 3\hbar\omega_{LO} \log \left(\frac{w \sinh(\hbar\omega_{LO}\beta v/2)}{v \sinh(\hbar\omega_{LO}\beta w/2)} \right). \end{aligned} \quad (2.148)$$

If one finds the variational parameters v and w that give the lowest upper-bound to the free energy, then the average energy of the polaron state is given by

$$E = -\frac{\partial}{\partial \beta} (F_{S_0} + \langle S \rangle - \langle S_0 \rangle). \quad (2.149)$$

These results generalise Feynman's variational parameter for the polaron at zero temperature to finite temperatures parameterised by the thermodynamic beta parameter $\beta = 1/(k_B T)$. In this zero temperature limit, $\beta \rightarrow \infty$, Ōsaka's result reduces to Feynman's.

Numerical Results

Using Ōsaka's generalised variational principle, I was able to write codes that calculate the polaron free energy, effective mass and complex conductivity for temperatures T ranging from 1 to 10 multiples of ω_{LO} (here $\hbar = k_B = 1$) and for $1 \leq \alpha \leq 12$.

In Figure 2.2 are contour plots that show, as a function of temperature T/ω_{LO} and α , (a) the polaron free energy, (b) the polaron effective mass, (c) values of the v variational parameters and (d) values of the w variational parameter. The free energy shows similar behaviour at low temperatures $T \gtrsim \hbar\omega_{LO}/k_B$ to the ground-state energy. Still, it then seems to shift more negatively with an increasing negative gradient for $T \gtrsim \hbar\omega_{LO}/k_B$. The effective mass follows a similar pattern as it has roughly the same behaviour for $T \lesssim \hbar\omega_{LO}/k_B$ as it did for $T = 0$, but becomes exponentially more positive for temperatures $T \gtrsim \hbar\omega_{LO}/k_B$. The v and w parameters also show this pattern and increase exponentially with temperature beyond $T \gtrsim \hbar\omega_{LO}/k_B$. However, v grows faster than w , so their difference increases exponentially with temperature. The artefacts that appear in contour

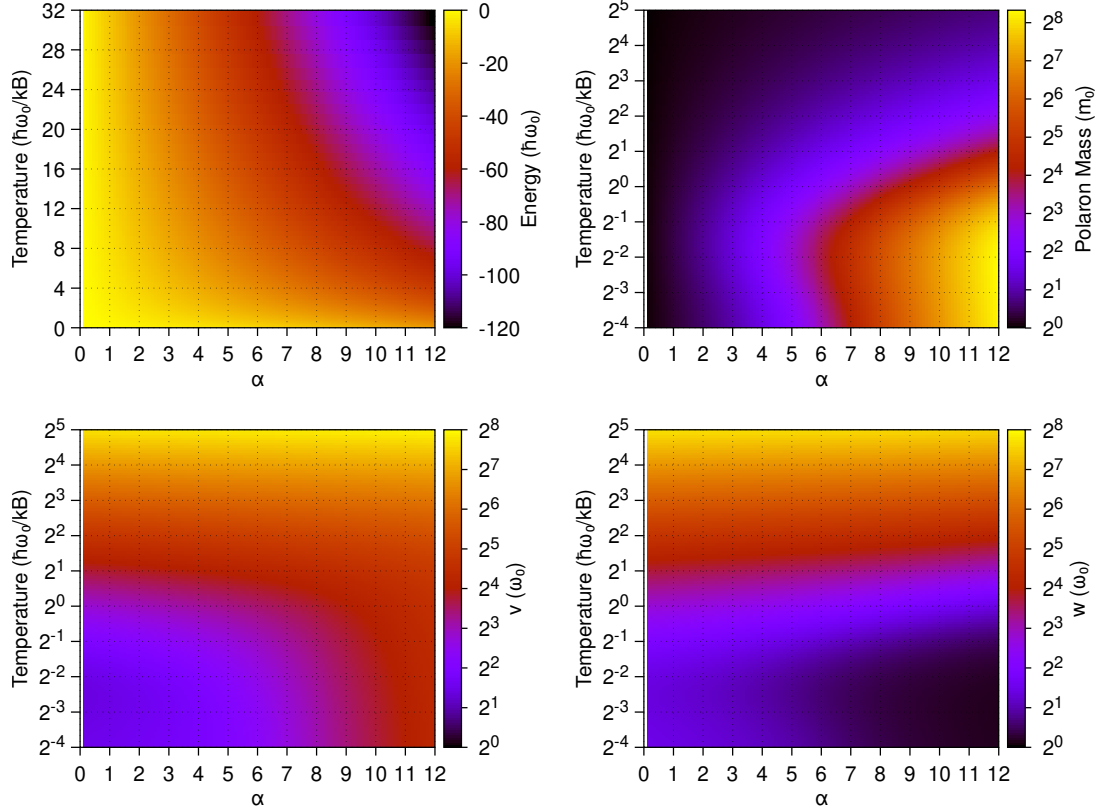


Figure 2.2: Contour plots of (a) Ōsaka’s polaron free energy, (b) Feynman’s effective mass (log scale), (c) the v variational parameter (log scale) and (d) the w variational parameter (log scale), as a function of ‘effective’ temperature T/ω_{LO} and the Fröhlich α parameter.

plots for the effective mass and variational parameters at lower α and high temperatures may be numerical errors due to difficulties in the optimisation process. The free energy seems to vary less with temperature at weak coupling, which may have made finding the global minima difficult, resulting in noise.

2.3 Influence Functionals & Response Functions

2.3.1 Polaron DC Mobility

FHIP [2] derive an expression for the response of the Feynman polaron to weak, spatially uniform, time-varying electric fields. The current induced by the motion of the electron under the influence of a weak alternating electric field $\mathbf{E} = E_0 \exp(i\Omega t)$ is generally

$$j(\Omega) = \frac{E(\Omega)}{z(\Omega)}, \quad (2.150)$$

where $z(\Omega)$ is the complex impedance function. It is assumed that the material is isotropic so that $j = \langle \dot{r} \rangle$, where $\langle r \rangle = E/(i\Omega z(\Omega))$ is the expectation of the electron displacement in the r direction. In the time domain, this is

$$\langle r(t) \rangle = -i \int_{-\infty}^{\infty} dt' G(t-t') E(t'), \quad (2.151)$$

$G(t)$ is the Green function corresponding to the *linear* electron displacement at a time t due to a delta function pulsed electric field at a time zero $t = 0$. The Fourier transform of $G(t)$ is

$$\int_{-\infty}^{\infty} dt G(t) e^{-i\Omega t} = G(\Omega) = \frac{1}{\Omega z(\Omega)}, \quad (2.152)$$

where $G(t) = 0$ for $t < 0$. Under the influence of the external electric field $E(t)$ the Föhlich Hamiltonian gains an additional term $-\mathbf{E} \cdot \mathbf{r}$. If ρ is the density matrix of the system, then the expected electron position at a time t is

$$\langle \mathbf{r}(t) \rangle = \text{Tr} \{ \mathbf{r} \rho(t) \}. \quad (2.153)$$

Furthermore, we assume that the system is initially in thermal equilibrium $\rho(t=0) = \exp(-\beta H)$, then the density matrix at any later time t is obtained from the time evolution equation

$$i\hbar \frac{\partial \rho}{\partial t} = [H, \rho]. \quad (2.154)$$

Therefore

$$\rho(t) = \exp \left\{ -\frac{i}{\hbar} \int_0^t [H(s) - \mathbf{r}(s) \cdot \mathbf{E}(s)] ds \right\} \rho(0) \exp \left\{ +\frac{i}{\hbar} \int_0^t [H'(s) - \mathbf{r}'(s) \cdot \mathbf{E}'(s)] ds \right\}, \quad (2.155)$$

where $\rho(0) \propto \exp(-\hbar\beta \sum_{\mathbf{k}} \omega_{\mathbf{k}} b_{\mathbf{k}}^\dagger b_{\mathbf{k}})$ such that only the phonon oscillators are initially in thermal equilibrium at temperature $(k_B\beta)^{-1}$. Due to the electron-phonon coupling, the entire polaron system will quickly return to thermal equilibrium as the electron is perturbed since the energy of the electron ($\sim 1/\text{volume}$) is infinitesimal relative to the heat bath of the system of phonon oscillators. As an aside, since \mathbf{E} is not an operator and the system is in thermodynamic equilibrium, then $\mathbf{E}'(s) = \mathbf{E}(s)$. Still, FHIP treats them separately as the more general case,

such as in a non-linear response system. We can write $\text{Tr } \rho(t)$ as the path integral generating functional

$$\begin{aligned} \text{Tr } \rho(t) &= \mathcal{Z}[\mathbf{E}, \mathbf{E}'] \\ &= \int \mathcal{D}\mathbf{r}(t) \mathcal{D}\mathbf{r}'(t) \exp \left(\frac{i}{\hbar} \Phi[\mathbf{r}(t), \mathbf{r}'(t)] - \frac{i}{\hbar} \int_{-\infty}^{\infty} dt [\mathbf{E}(t) \cdot \mathbf{r}(t) - \mathbf{E}'(t) \cdot \mathbf{r}'(t)] \right) \end{aligned} \quad (2.156)$$

where $\Phi[\mathbf{r}(t), \mathbf{r}'(t)]$ is given by

$$\begin{aligned} \Phi[\mathbf{r}(t), \mathbf{r}'(t)] &= \frac{m_b}{2} \int_{-\infty}^{\infty} dt [\dot{\mathbf{r}}(t)^2 - \dot{\mathbf{r}}'(t)^2] \\ &\quad + \frac{im_b}{2} \int \frac{d^3\mathbf{k}}{(2\pi)^3} |V_{\mathbf{k}}|^2 \int_{-\infty}^{\infty} dt \int_{-\infty}^{\infty} dt' \left(e^{i\mathbf{k} \cdot \mathbf{r}(t)} - e^{i\mathbf{k} \cdot \mathbf{r}'(t)} \right) [y(\omega_{\mathbf{k}}, t - t') \\ &\quad \times \left(e^{-i\mathbf{k} \cdot \mathbf{r}(t')} + e^{-i\mathbf{k} \cdot \mathbf{r}'(t')} \right) + ia(\omega_{\mathbf{k}}, t - t') \left(e^{-i\mathbf{k} \cdot \mathbf{r}(t')} - e^{-i\mathbf{k} \cdot \mathbf{r}'(t')} \right)] , \end{aligned} \quad (2.157)$$

where

$$\begin{aligned} y(\omega, t - t') &= \sin(\omega[t - t']) / \omega, & t > t' \\ &= 0, & t < t', \end{aligned} \quad (2.158)$$

and

$$a(\omega, t - t') = \frac{1}{2\omega} \cos(\omega[t - t']) \left[1 + \frac{2}{e^{\beta\omega} - 1} \right]. \quad (2.159)$$

For Fröhlich's Hamiltonian we set $\omega_{\mathbf{k}} = \omega_{LO}$ and the interaction term $V_{\mathbf{k}}$ is given by Eq. (2.36).

The double path integral $\mathcal{D}\mathbf{r}(t) \mathcal{D}\mathbf{r}'(t)$ is only over closed paths satisfying the boundary condition $\mathbf{r}(t) - \mathbf{r}'(t) = 0$ at times $t \rightarrow \pm\infty$. Since the electric field is weak, we can expand $\langle \mathbf{r}(t) \rangle$ to first-order and find the linear response Green's function for $\mathbf{r}(t)$, which can be obtained from the first functional derivative of the partition function concerning $\mathbf{E}(t) - \mathbf{E}'(t)$ as $t \rightarrow \infty$ when the steady state is reached. This gives

$$G(t - t') = -\frac{\hbar^2}{2} \frac{1}{Z} \frac{\delta^2 \mathcal{Z}[\mathbf{E}, \mathbf{E}']}{\delta \mathbf{E}(t, t') \delta \mathbf{E}'(t, t')} \Bigg|_{\mathbf{E}=\mathbf{E}'=0}, \quad (2.160)$$

where $Z = \mathcal{Z}[0, 0]$ is the partition function that acts as the normalisation constant. In FHIP, they set the electric field to a sum of two delta functions

$$\mathbf{E}(s) = [\epsilon\delta(s - t') + \eta\delta(s - t)] \mathbf{e}, \quad (2.161a)$$

$$\mathbf{E}'(s) = [\epsilon\delta(s - t') - \eta\delta(s - t)] \mathbf{e}, \quad (2.161b)$$

to give

$$G(t - t') = \frac{\hbar^2}{2Z} \frac{\partial^2 \mathcal{Z}(\epsilon, \eta)}{\partial \eta \partial \epsilon} \Big|_{\eta=\epsilon=0}. \quad (2.162)$$

Thus, the problem of finding the Green function $G(t - t')$ is reduced to that of finding the dependence of the generating function path integral $\mathcal{Z}[\mathbf{E}, \mathbf{E}']$ on the forcing functions $\mathbf{E}(t)$ and $\mathbf{E}'(t)$. The path integral in $\mathcal{Z}[\mathbf{E}, \mathbf{E}']$ depends on the functional $\Phi[\mathbf{r}(t), \mathbf{r}'(t)]$ which contains terms similar to the model action S (athermal expression in Eq. (2.64) or thermal expression in Eq. (2.120)), although I should note that this is now the real-time version of the model action (obtained from a Wick-rotation).

Approximating the polaron complex impedance

The path integral $\mathcal{Z}[\mathbf{E}, \mathbf{E}']$ cannot be evaluated exactly. However, it can be approximated by the trial influence functional $\Phi_0[\mathbf{r}(t), \mathbf{r}'(t)]$ (where $n(x) = [\exp(x) - 1]^{-1}$)

$$\begin{aligned} \Phi_0[\mathbf{r}(t), \mathbf{r}'(t)] &= \frac{m_b}{2} \int_{-\infty}^{\infty} dt \left[\dot{\mathbf{r}}(t)^2 - \dot{\mathbf{r}}'(t)^2 \right] \\ &+ \frac{C}{2} \int_{-\infty}^{\infty} dt \int_{-\infty}^{\infty} dt' \left\{ (\mathbf{r}(t) - \mathbf{r}(t'))^2 \left[e^{-iw|t-t'|} + 2n(\beta w) \cos(w(t - t')) \right] \right. \\ &\quad (\mathbf{r}'(t) - \mathbf{r}'(t'))^2 \left[e^{iw|t-t'|} + 2n(\beta w) \cos(w(t - t')) \right] \\ &\quad \left. - 2(\mathbf{r}'(t) - \mathbf{r}'(t'))^2 \left[e^{-iw(t-t')} + 2n(\beta w) \cos(w(t - t')) \right] \right\}. \end{aligned} \quad (2.163)$$

This contains terms similar to the trial action S_0 (such as the athermal trial action in Eq. (2.72) and thermal trial action in Eq. (2.123), but Wick-rotated from the imaginary-time variable to the real-time variable) in which the attractive Coulomb-like potential is roughly replaced by the simpler attractive parabolic potential

centred at the mean position of the electron in the past (weighted by an exponential decay with time where w is the decay factor). In FHIP, it is assumed that the Wick-rotation of the trial partition function Z_0 (the athermal partition function given by Eq. (2.78) and the thermal partition function by Eq. (2.148)), which gives the best approximation to the partition function of the actual model system via either Feynman's (athermal) or Osaka's (thermal) variational principle, can describe the dynamical behaviour of the polaron.

Therefore, in FHIP, they approximate the model generating functional $\mathcal{Z}[\mathbf{E}, \mathbf{E}']$ with the zeroth and first terms from the expansion of the path integral around the trial action

$$\begin{aligned}\mathcal{Z}[\mathbf{E}, \mathbf{E}'] &\approx \int \mathcal{D}\mathbf{r}(t) \mathcal{D}\mathbf{r}'(t) e^{\frac{i}{\hbar}(\Phi_0 + \int dt [\mathbf{E} \cdot \mathbf{r} - \mathbf{E}' \cdot \mathbf{r}'])} \\ &+ i \int \mathcal{D}\mathbf{r}(t) \mathcal{D}\mathbf{r}'(t) e^{\frac{i}{\hbar}(\Phi_0 + \int dt [\mathbf{E} \cdot \mathbf{r} - \mathbf{E}' \cdot \mathbf{r}'])} (\Phi - \Phi_0) \\ &\equiv \mathcal{Z}_0[\mathbf{E}, \mathbf{E}'] + \mathcal{Z}_1[\mathbf{E}, \mathbf{E}'].\end{aligned}\quad (2.164)$$

Calculating the zeroth term of the complex impedance

The zeroth term $\mathcal{Z}_0[\mathbf{E}, \mathbf{E}']$ is the classical response and is the same as the alternative model presented by Ōsaka of two masses coupled by a harmonic spring under the influence of a linear force \mathbf{f} (Eq. (2.134)), where $\mathbf{f} = \mathbf{E}$. This term is then reanalysed as the sum of two normal mode harmonic oscillators so that $\mathcal{Z}_0[\mathbf{E}, \mathbf{E}']$ is written as the product of two factors, one for each harmonic oscillator. The first oscillator has a mass $m_1 = M + m_b = m_b v^2 / w^2$ and frequency $\omega_1 = 0$ coupled by $\mathbf{f}_1(t) = \mathbf{E}(t)$, and the second oscillator has mass $m_2 = M m_b / (M + m_b)$, frequency $\omega_2 = v \omega_{LO}$ and coupling $\mathbf{f}_2(t) = -M m_b / (M + m_b) \mathbf{E}(t) = \mathbf{E}(t)(v^2 - w^2) / v^2$.

$\mathcal{Z}_0[\mathbf{E}, \mathbf{E}']$ is then given by

$$\begin{aligned}\mathcal{Z}_0[\mathbf{E}, \mathbf{E}'] &= \exp \left\{ \frac{i}{4\pi} \int_{-\infty}^{+\infty} d\Omega (\mathbf{E}(-\Omega) - \mathbf{E}'(\Omega)) \right. \\ &\times \left. \left[(\mathbf{E}(\Omega) + \mathbf{E}'(\Omega)) Y_0(\Omega) + i (\mathbf{E}(\Omega) - \mathbf{E}'(\Omega)) A_0(\Omega) \right] \right\},\end{aligned}\quad (2.165)$$

where

$$Y_0(\Omega) = \lim_{\varepsilon \rightarrow 0^+} \left\{ -\frac{\Omega^2 - w^2}{(\Omega - i\varepsilon)^2} [(\Omega - i\varepsilon)^2 - v^2] \right\} \quad (2.166)$$

and

$$A_0(\Omega) = \frac{\pi}{2} \lim_{\varepsilon \rightarrow 0^+} \left\{ \frac{2w^2}{v^2 \beta \varepsilon^2} [\delta(\Omega + \varepsilon) - \delta(\Omega - \varepsilon)] + \frac{v^2 - w^2}{v^3} \left[1 + \frac{2}{e^{\beta v} - 1} \right] [\delta(\Omega + v) + \delta(\Omega - v)] \right\} \quad (2.167)$$

where $\mathbf{E}(\Omega)$ is the Fourier transform of $\mathbf{E}(t)$. To obtain the classical Green's function $G_0(t - t')$, in FHIP they substitute

$$\mathbf{E}(\Omega) = (\epsilon e^{-i\Omega t'} + \eta e^{i\Omega t'}) \hat{\mathbf{k}} \quad (2.168a)$$

$$\mathbf{E}'(\Omega) = (\epsilon e^{-i\Omega t'} - \eta e^{i\Omega t'}) \hat{\mathbf{k}} \quad (2.168b)$$

into $\mathcal{Z}_0[\mathbf{E}, \mathbf{E}']$ and find the *linear term* of order $\epsilon\eta$. The zeroth order approximation to $G(t - t')$ is then

$$G_0(t - t') = \frac{i}{2\pi} \int_{-\infty}^{\infty} d\Omega Y_0(\Omega) e^{i\Omega(t-t')} \quad (2.169a)$$

$$G_0(\Omega) = +iY_0(\Omega) \quad (2.169b)$$

which is the classical response of the system.

Calculating the first correction term of the complex impedance

To include the first order of quantum corrections to the classical response of the electron, FHIP uses the $\mathcal{Z}_1[\mathbf{E}, \mathbf{E}']$ path integral to obtain the first order approximation $G_1(t - t')$ to $G(t - t')$. To evaluate $\mathcal{Z}_1[\mathbf{E}, \mathbf{E}']$ they first look at the $\Phi \exp(i\Phi_0/\hbar)$. Substituting the equation for Φ into $\Phi \exp(i\Phi_0/\hbar)$, the resulting expression contains terms \mathcal{T} that have the form

$$\begin{aligned} \mathcal{T} = & \int \mathcal{D}\mathbf{r}(t) \mathcal{D}\mathbf{r}'(t) e^{\frac{i}{\hbar}\Phi_0} \left\{ \int \frac{d^3\mathbf{k}}{(2\pi)^3} |V_{\mathbf{k}}|^2 \int_{-\infty}^{\infty} dt \int_{-\infty}^{\infty} dt' \right. \\ & \times e^{i\mathbf{k} \cdot (\mathbf{r}(t) - \mathbf{r}(t'))} [y(\omega_{\mathbf{k}}, t - t') + ia(\omega_{\mathbf{k}}, t - t')] \left. \right\}. \end{aligned} \quad (2.170)$$

The two other terms in $\Phi \exp(i\Phi_0/\hbar)$ come from the correlations between electron paths in the density matrix $\rho(\mathbf{r}, \mathbf{r}', t)$ (i.e. off-diagonal terms) and are similar to \mathcal{T} , but with different replacements of \mathbf{r} with \mathbf{r}' . To evaluate \mathcal{T} one has to evaluate the path integral

$$\begin{aligned}\mathcal{R}(\mathbf{k}, \tau, \sigma) &= \int_{\mathbf{r}=\mathbf{r}'} \mathcal{D}\mathbf{r}(t) \mathcal{D}\mathbf{r}'(t) \exp \left\{ i\mathbf{k} \cdot [\mathbf{r}(\tau) - \mathbf{r}(\sigma)] + \frac{i}{\hbar} \Phi_0 \right\} \\ &= Z_0 \langle e^{i\mathbf{k} \cdot [\mathbf{r}(\tau) - \mathbf{r}(\sigma)]} \rangle_{\Phi_0},\end{aligned}\quad (2.171)$$

where $Z_0 \equiv \mathcal{Z}_0[0, 0]$. This gives \mathcal{T} to be

$$\mathcal{T} = \int_{-\infty}^{\infty} d\tau \int_{-\infty}^{\infty} d\sigma [y(\tau - \sigma) + ia(\tau - \sigma)] \int \frac{d^3\mathbf{k}}{(2\pi)^3} |V_{\mathbf{k}}|^2 \langle e^{i\mathbf{k} \cdot [\mathbf{r}(\tau) - \mathbf{r}(\sigma)]} \rangle_{\Phi_0}. \quad (2.172)$$

The solution to $\mathcal{R}(\mathbf{k}, \tau, \sigma)$ is the same form as $\mathcal{Z}_0[\mathbf{E}, \mathbf{E}']$ in Eq. (2.165) except for the non-primed components

$$\mathbf{E}(\Omega) = (\epsilon e^{-i\Omega t'} + \eta e^{-i\Omega t}) \hat{\mathbf{k}} + \mathbf{k} (e^{-i\Omega\tau} - e^{-i\Omega\sigma}), \quad (2.173a)$$

$$\mathbf{E}'(\Omega) = (\epsilon e^{-i\Omega t'} - \eta e^{-i\Omega t}) \hat{\mathbf{k}}, \quad (2.173b)$$

to give

$$\begin{aligned}\mathcal{R}(\mathbf{k}, \tau, \sigma) &= \mathcal{Z}_0 \exp \left\{ \frac{i|\mathbf{k}|^2}{4\pi} \int_{-\infty}^{\infty} d\Omega \left| e^{i\Omega\tau} - e^{i\Omega\sigma} \right|^2 (Y_0 + iA_0) \right. \\ &\quad + \frac{i\mathbf{k}_r}{2\pi} \int_{-\infty}^{\infty} d\Omega (e^{i\Omega\tau} - e^{i\Omega\sigma}) (\epsilon Y_0 e^{-i\Omega t'} + i\eta A_0 e^{-i\Omega t}) \\ &\quad \left. + \frac{i\mathbf{k}_r}{2\pi} \int_{-\infty}^{\infty} d\Omega (e^{-i\Omega\tau} - e^{-i\Omega\sigma}) \eta e^{i\Omega t} (Y_0 + iA_0) \right\}\end{aligned}\quad (2.174)$$

where

$$\mathcal{Z}_0 = \exp \left[\frac{i}{\pi} \int_{-\infty}^{\infty} d\Omega \eta e^{i\Omega t} (\epsilon Y_0 e^{-i\Omega t'} + i\eta A_0 e^{-i\Omega t}) \right] \quad (2.175)$$

for $\mathbf{k} = 0$. Similarly, for the primed components,

$$\mathbf{E}(\Omega) = (\epsilon e^{-i\Omega t'} + \eta e^{-i\Omega t}) \hat{\mathbf{k}} - \mathbf{k} e^{-i\Omega\sigma}, \quad (2.176a)$$

$$\mathbf{E}'(\Omega) = \left(\epsilon e^{-i\Omega t'} - \eta e^{-i\Omega t} \right) \hat{\mathbf{k}} - \mathbf{k} e^{-i\Omega\tau}. \quad (2.176b)$$

To obtain $G_1(t - t')$ we need the first-order derivative of $\mathcal{R}(\mathbf{k}, \tau, \sigma)$ with respect to ϵ and η and then setting $\epsilon = \eta = 0$. The result is (including a 1/3 for averaging over the isotropic dimensions of \mathbf{k})

$$\begin{aligned} r(\mathbf{k}, \tau, \sigma) = & \left\{ \frac{i}{2\pi} \int_{-\infty}^{\infty} d\Omega Y_0 e^{i\Omega(t-t')} - \frac{k^2}{24\pi^2} \int_{-\infty}^{\infty} d\Omega \left(e^{i\Omega\tau} - e^{i\Omega\sigma} \right) Y_0 e^{-i\Omega t'} \right. \\ & \times \int_{-\infty}^{\infty} d\Lambda \left[\left(e^{i\Lambda\tau} - e^{i\Lambda\sigma} \right) iA_0(\Lambda) e^{-i\Lambda t} + \left(e^{i\Lambda\tau} - e^{i\Lambda\sigma} \right) e^{i\Lambda t} (Y_0(\Lambda) + iA_0(\Lambda)) \right] \Big\} \\ & \times \exp \left\{ \frac{ik^2}{4\pi} \int_{-\infty}^{\infty} d\Omega \left| e^{i\Omega\tau} - e^{i\Omega\sigma} \right|^2 (Y_0 + iA_0) \right\}. \end{aligned} \quad (2.177)$$

The first term is the classical response $G_0(t - t')$, and the later terms correspond to the trial path integral with no applied electric field $\epsilon = \eta = 0$. Hence, in total $r(\mathbf{k}, \tau, \sigma)$ is the \mathbf{k} -dependent term in $\langle S_0 - S'_0 \rangle_{S'_0, S_0}$, where the classical response G_0 has cancelled with the normalisation and does not contribute to the quantum corrections to the response, G_1 . We can do a change of variables $u = \tau - \sigma$ and perform the integral on σ in Eq. (2.172) to give

$$\begin{aligned} r(\mathbf{k}, u) = & -\frac{k^2}{6\pi^2} \int_{-\infty}^{\infty} d\Omega (1 - \cos(\Omega u)) Y_0(\Omega) (Y_0(\Omega) + 2iA_0(\Omega)) e^{i\Omega(t-t')} \\ & \times \exp \left\{ \frac{ik^2}{2\pi} \int_{-\infty}^{\infty} d\Omega' (1 - \cos(\Omega' u)) (Y_0(\Omega') + iA_0(\Omega')) \right\}, \end{aligned} \quad (2.178)$$

where $Y_0(-\Omega) = Y_0^*(\Omega)$ and $A_0(-\Omega) = A_0(\Omega)$. $r(\mathbf{k}, u)$ contributes to $G_1(u)$ and since it is already of the form of a Fourier transform, we can find the contribution $r(\mathbf{k}, \Omega)$ to $G_1(\Omega)$ by omitting the Fourier integral on Ω and the factor $e^{-\Omega(t-t')}$ to give:

$$\begin{aligned} r(\mathbf{k}, \Omega) = & -\frac{k^2}{6\pi^2} (1 - \cos(\Omega u)) Y_0(\Omega) (Y_0(\Omega) + 2iA_0(\Omega)) \\ & \times \exp \left\{ \frac{ik^2}{2\pi} \int_{-\infty}^{\infty} d\Omega' (1 - \cos(\Omega' u)) (Y_0(\Omega') + iA_0(\Omega')) \right\}. \end{aligned} \quad (2.179)$$

To obtain $\langle S - S_0 \rangle_{S'_0, S_0}$ we multiply $r(\mathbf{k}, u)$ by $y(u) + ia(u)$ and integrate on u . Feynman evaluated this integral by splitting the range of u from 0 to ∞ and from $-\infty$ to 0, where in the latter, he put $u \rightarrow -u$ to make all integrals on u positive. The integral in the exponent is $-k^2/2$ times $D(u)$

$$\begin{aligned} D(u) &= -\frac{i}{\pi} \int_{-\infty}^{\infty} d\Omega (1 - \cos(\Omega u)) [Y_0(\Omega) + iA_0(\Omega)] \\ &= \frac{i}{\pi} (\mathbf{Y}_0(u) + \mathbf{Y}_0(-u)) + 2(\mathbf{A}_0(0) - \mathbf{A}_0(u)) \\ &= 2 \frac{v^2 - w^2}{v^3} \frac{\sin(vu/2) \sin(v[u - i\hbar\omega_{LO}\beta]/2)}{\sinh(v\hbar\omega_{LO}\beta/2)} - i \frac{w^2}{v^2} u \left(1 - \frac{u}{i\hbar\omega_{LO}\beta}\right), \end{aligned} \quad (2.180)$$

where $u > 0$. $\mathbf{Y}_0(t)$ and $\mathbf{A}_0(t)$ are the inverse Fourier transforms of $Y_0(\Omega)$ and $A_0(\Omega)$ where we note that $\mathbf{Y}_0(u) = 0$ for $u < 0$. Therefore, overall for $r(k, u)$ is

$$\begin{aligned} r(k, u) &= \frac{-k^2}{3\pi} Y_0(\Omega) [Y_0(\Omega) + 2iA_0(\Omega)] \\ &\times \int_0^{\infty} du (1 - \cos(\Omega u)) [y(u) + y(-u) + 2ia(u)] e^{-\frac{1}{2}k^2D(u)} \end{aligned} \quad (2.181)$$

which contributes to G_1 . A similar calculation is also done to obtain the \mathcal{T} terms that come from the primed \mathbf{r}' components in $\Phi \exp(i\Phi_0/\hbar)$. Once all are obtained, they are summed together, and the k integral gives the first contribution to $G_1(\Omega)$ as

$$G_1^{(1)}(\Omega) = -iY_0^2(\Omega)\chi(\Omega) \quad (2.182)$$

where

$$\chi(\Omega) = \int_0^{\infty} dt [1 - e^{i\Omega t}] \text{Im}S(t) \quad (2.183)$$

with

$$S(t) = \frac{2}{3} \int \frac{d^3\mathbf{k}}{(2\pi)^3} |V_{\mathbf{k}}|^2 k^2 e^{-k^2D(t)/2} [e^{i\omega_{\mathbf{k}}t} + 2n(\beta\omega_{\mathbf{k}}) \cos(\omega_{\mathbf{k}}t)] \quad (2.184)$$

which for the Fröhlich Hamiltonian gives

$$S(t) = \frac{2\alpha}{3\sqrt{\pi}} \frac{\cos(t - i\hbar\omega_{LO}\beta/2)}{\sinh(\hbar\omega_{LO}\beta/2)} [D(t)]^{-3/2}. \quad (2.185)$$

Next, the second term is obtained analogously from Φ_0 and can be evaluated by differentiating \mathcal{R} (and thus on $r(k, u)$) twice concerning \mathbf{k} and then setting $\mathbf{k} = 0$ in the expression. This results in an integral on u

$$G_1^{(2)}(\Omega) = -i4Y_0^2(\Omega) \int_0^\infty du \left(1 - e^{i\Omega u}\right) S_0(u) = -i4Y_0^2(\Omega) \frac{C\Omega^2}{w(\Omega^2 - w^2)} \quad (2.186)$$

where

$$S_0(u) = C\text{Im} \left(e^{i\omega u} + 2n(\beta w) \cos(\omega u) \right) = C \sin(\omega u). \quad (2.187)$$

This gives the final result for the first-order change in G as

$$G_1(\Omega) = G_1^{(1)}(\Omega) + G_1^{(2)}(\Omega) = -iY_0^2(\Omega) \left[\chi(\Omega) + \frac{4C}{w} \frac{\Omega^2}{\Omega^2 - w^2} \right]. \quad (2.188)$$

Hence, FHIP find an approximate form for $G(\Omega)$ composed out of the zeroth and first-order terms of the Green's function

$$G(\Omega) = G_0(\Omega) + G_1(\Omega) \quad (2.189)$$

from which they find the impedance to first-order in $G_1(\Omega)$

$$\begin{aligned} \Omega z(\Omega) &= \frac{1}{G(\Omega)} \approx \frac{1}{G_0(\Omega) + G_1(\Omega)} \\ &\approx \frac{1}{G_0(\Omega)} - \frac{1}{G_0^2(\Omega)} G_1(\Omega). \end{aligned} \quad (2.190)$$

FHIP argue that this expanded form is more accurate than $z \sim (G_0 + G_1)^{-1}$ by considering a simple example of a free particle perturbed by a harmonic oscillator. The structure of the actual $G(\Omega)$ in this example includes a resonance at the oscillator frequency which is not present in $z \sim (G_0 + G_1)^{-1}$. This resonance is present if one expands $z(\Omega)$. Therefore, FHIP use this expanded form, which is written explicitly as

$$z(\Omega) \approx i \left(\Omega - \frac{\chi(\Omega)}{\Omega} \right). \quad (2.191)$$

The first term (Ω) on the right-hand side is a free-particle term, while $\chi(\Omega)$ contains the corrections from the electron-phonon interactions. All of the dependence on the trial influence functional Φ_0 is contained within $D(t)$, which appears in the exponential term in $S(t)$ (Eq. (2.185)). This exponential term describes the non-linear scattering of the electron due to its interaction with the phonon field oscillators. If the phonon oscillators are linearly coupled to the electron's coordinate, then Eq. (2.191) is exact regardless of the choice of Φ_0 . Otherwise, beyond a linear electron-phonon coupling approximation, Eq. (2.191) includes these higher-order interactions approximately by finding their effect for a trial influence functional Φ_0 that seeks to imitate the actual influence functional Φ . In FHIP, they expect Eq. (2.191) to be an excellent approximation to the actual impedance of the polaron.

Thornber investigated an extension beyond linear response [19], where they evaluate the steady-state response of the electron in a finite electric field of arbitrary strength.

Calculating the polaron mobility

To obtain a general expression for the dissipation, or equivalently the mobility, of the polaron in FHIP, they recognise that the dc mobility μ_{dc} for the polaron is

$$\mu_{dc}^{-1} = \lim_{\Omega \rightarrow 0} \frac{\text{Im}\chi(\Omega)}{\Omega}. \quad (2.192)$$

In FHIP, they rewrite $\text{Im}\chi(\Omega)$ into a more convenient form for calculation (which may have been true at the time due to their computational capabilities but is no longer necessarily true) by using contour integration. They recognise that since $S(u)$ is analytic between $u = \text{real}$ and $u = \text{real} + i\beta$, the contour of integration can be changed from along the real axis to one which goes first from 0 to $i\beta/2$ up the imaginary axis and then from $i\beta/2$ to $i\beta/2 + \infty$ parallel to the real axis. In the case of Fröhlich's Hamiltonian they obtain for $\text{Im}\chi(\Omega)$

$$\text{Im}\chi(\Omega) = -\frac{2\alpha}{3\sqrt{\pi}} \frac{\beta^{3/2} \sinh(\Omega\beta/2)}{\sinh(\beta/2)} \left(\frac{v}{w} \right)^3 \int_0^\infty \frac{\cos(\Omega x)\cos(x) dx}{[x^2 + a^2 - b \cos(vx)]^{3/2}} \quad (2.193)$$

where $a^2 \equiv \beta^2/4 + R\beta \coth(\beta v/2)$, $b \equiv R\beta/\sinh(\beta v/2)$ and $R \equiv (v^2 - w^2)/(w^2 v)$.

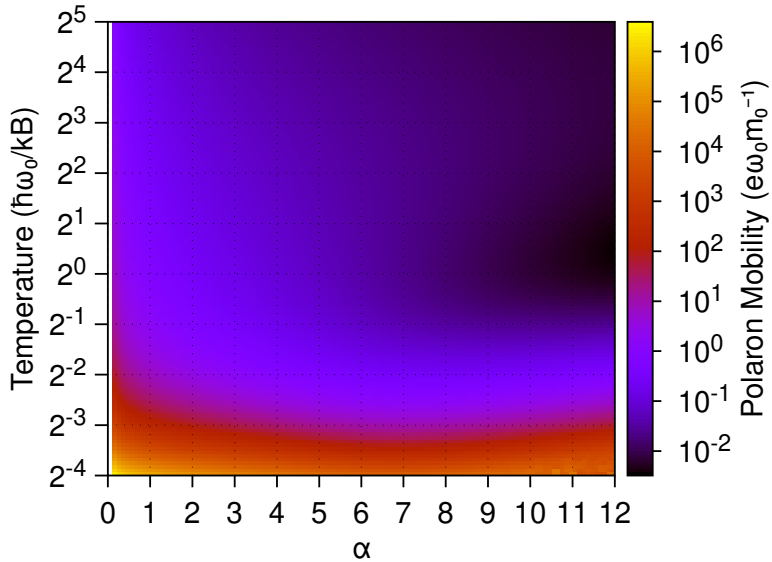


Figure 2.3: Log contour plot of the DC mobility (arbitrary units).

$\text{Im}\chi(\Omega)$ has maxima when Ω is equal to a frequency where absorption can happen to go to an excited polaron state, and the width of these maxima correspond to the state lifetimes for phonon emission. In FHIP, they compute $\text{Im}\chi(\Omega)$ by expanding Eq. (2.193) in an infinite power series of K modified Bessel functions of the second kind where only the first few terms are required for convergence in most cases.

In Appendix A, I have reproduced the contour integration for $\text{Im}\chi(\Omega)$ and also provided the contour integration for $\text{Re}\chi(\Omega)$ as well.

Numerical Results

Figure 2.3 shows a contour plot of the dc mobility derived in FHIP (note that this expression is unitless). For temperatures $T \lesssim \hbar\omega_{LO}/2k_B$, the DC mobility has a minimum around $\alpha \approx 7$, which shifts to larger values of α as the temperature increases. Similarly, for $\alpha \geq 7$, the mobility seems to be minimum around temperatures $T \approx \hbar\omega_{LO}/k_B$. Elsewhere, for $\alpha < 7$, the mobility seems to decrease rapidly as the temperature increases from 0K up until $T \approx \hbar\omega_{LO}/k_B$, then above this temperature, it decreases asymptotically towards zero.

2.3.2 Optical Conductivity

Devreese, Sitter and Gooverts [13] (otherwise referred to as “DSG”) expand upon the work done in FHIP by evaluating the optical absorption coefficient of the polaron. They note that $\text{Im}\chi(\Omega)$ is not this coefficient. To obtain this coefficient, they compare the expansion of the conductivity $\sigma(\Omega) = 1/z(\Omega)$ to the expansion of

the impedance (used by FHIP) $z(\Omega)$ and find further justification for the accuracy of the impedance function expansion. This, in turn, provides a more accurate expression for the frequency-dependent complex mobility $\mu(\Omega)$. To achieve this, they find an expression for the real component of the impedance function $\text{Re}\chi(\Omega)$. They then evaluate both $\text{Re}\chi(\Omega)$ and $\text{Im}\chi(\Omega)$ at zero temperature ($\beta = \infty$) by deriving involved analytical expressions.

DSG state the relation between the optical absorption coefficient $\Gamma(\Omega)$ and the impedance $z(\Omega)$ of polarons as

$$\Gamma(\Omega) = \frac{1}{c\epsilon_0 n} \text{Re} \left\{ \frac{1}{z(\Omega)} \right\} \quad (2.194)$$

where ϵ_0 is the dielectric constant of the vacuum, n is the index of refraction of the medium, and c is the speed of light. DSG find that for the expansion of $z(\Omega)$ at zero temperature, the optical absorption coefficient requires both the real $\text{Re}z(\Omega)$ and imaginary $\text{Im}z(\Omega)$ components of the impedance (or of $\chi(\Omega)$). They obtain the expression

$$\Gamma_z(\Omega) = \frac{1}{c\epsilon_0 n} \lim_{\beta \rightarrow \infty} \frac{\Omega \text{Im}\chi(\Omega)}{\Omega^4 - 2\Omega^2 \text{Re}\chi(\Omega) + |\chi(\Omega)|^2}. \quad (2.195)$$

If the expansion of the conductivity $1/z(\Omega)$ is used instead then they obtain

$$\Gamma_\sigma(\Omega) = \frac{\text{Im}\chi(\Omega)}{\Omega^3} \left(\frac{\Omega^2 - w^2}{\Omega^2 - v^2} \right)^2. \quad (2.196)$$

DSG take the zero temperature limit $\beta \rightarrow \infty$ rigorously. By taking the limit directly in the expression for $\chi(\Omega)$ in Eq. (2.183). The real and imaginary components at zero temperature ($\beta = \infty$) are

$$\text{Re}\chi(\Omega) = \text{Im} \int_0^\infty du \frac{[1 - \cos(\Omega u)] e^{iu}}{[R(1 - e^{ivu}) - iu]^{3/2}}, \quad (2.197a)$$

$$\text{Im}\chi(\Omega) = \text{Im} \int_0^\infty du \frac{\sin(\Omega u) e^{iu}}{[R(1 - e^{ivu}) - iu]^{3/2}}. \quad (2.197b)$$

By developing the denominator in the integrals, the expression for the two integrals become

$$\text{Re}\chi(\Omega) = \frac{2\alpha}{3} \frac{v^3}{w^3} \sum_{n=0}^{\infty} C_{-3/2}^n (-1)^n R^n \times \text{Im} \int_0^{\infty} du \frac{[1 - \cos(\Omega u)] e^{i(1+nv)u}}{[R - iu]^{3/2+n}}, \quad (2.198a)$$

$$\text{Im}\chi(\Omega) = \frac{2\alpha}{3} \frac{v^3}{w^3} \sum_{n=0}^{\infty} C_{-3/2}^n (-1)^n R^n \times \text{Im} \int_0^{\infty} du \frac{\sin(\Omega u) e^{i(1+nv)u}}{[R - iu]^{3/2+n}}, \quad (2.198b)$$

where C_r^n are the binomial coefficients. For $\text{Im}\chi(\Omega)$ at $\beta = \infty$ DSG find the expansion

$$\begin{aligned} \text{Im}\chi(\Omega) &= \frac{2\alpha}{3} \frac{v^3}{w^3} \sum_{n=0}^{\infty} C_{-3/2}^n (-1)^n \frac{(2R)^n}{(2n+1)!!} \\ &\times |\Omega - 1 - nv|^{n+1/2} e^{-|\Omega - 1 - nv|R} \frac{1 + \text{sgn}(\Omega - 1 - nv)}{2} \end{aligned} \quad (2.199)$$

where $(2n+1)!! = (2n+1)\dots5 \cdot 3 \cdot 1$ indicates the double factorial. In FHIP, they stated the first two terms of this expansion. FHIP find that following the same procedure for $\text{Re}\chi(\Omega)$ is far more complicated and has poor convergence properties. Therefore, DSG transform the integrals in Eq. (2.198b) to integrals with rapidly convergent integrands to give the result

$$\begin{aligned} \text{Re}\chi(\Omega) &= \frac{2\alpha}{3} \frac{v^3}{w^3} \sum_{n=0}^{\infty} -\frac{1}{\Gamma(n+3/2)} \\ &\times \int_0^{\infty} dx \left[\left(n + \frac{1}{2} \right) x^{n-1/2} e^{-Rx} - Rx^{n+1/2} e^{-Rx} \right] \\ &\times \ln \left| \frac{(1+nv+x)^2}{\Omega^2 - (1+nv+x)^2} \right|^{1/2}. \end{aligned} \quad (2.200)$$

From these expansions of $\text{Re}\chi(\Omega)$ and $\text{Im}\chi(\Omega)$ DSG evaluate the optical absorption coefficient.

In Appendices B and C, I have derived the expansions of $\text{Re}\chi(\Omega)$ and $\text{Im}\chi(\Omega)$ for finite temperatures in terms of hypergeometric functions.



Figure 2.4: Contours for the real (left) and imaginary (right) complex conductivity at different values of α . (a) Real conductivity at $\alpha = 3$. (b) Imaginary conductivity at $\alpha = 3$. (c) Real conductivity at $\alpha = 6$. (d) Imaginary conductivity at $\alpha = 6$. (e) Real conductivity at $\alpha = 9$. (f) Imaginary conductivity at $\alpha = 9$.

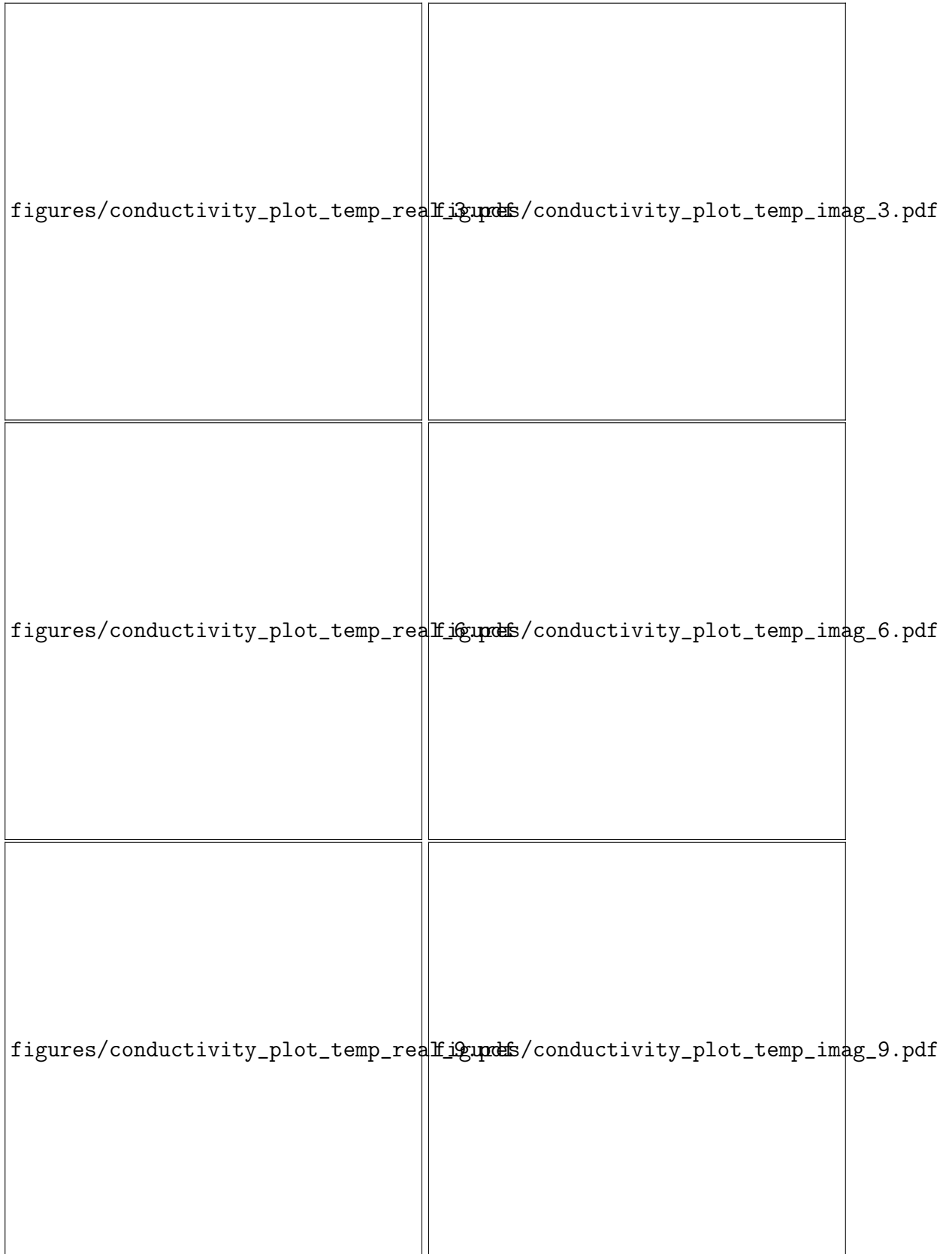


Figure 2.5: Ridgeline plots for the real (left) and imaginary (right) complex conductivity at different values of α . (a) Real conductivity at $\alpha = 3$. (b) Imaginary conductivity at $\alpha = 3$. (c) Real conductivity at $\alpha = 6$. (d) Imaginary conductivity at $\alpha = 6$. (e) Real conductivity at $\alpha = 9$. (f) Imaginary conductivity at $\alpha = 9$.

Numerical Results

I used the optical absorption expression obtained from [13] to extend the codes to calculate the complex conductivity of the polaron for different couplings $1 \leq \alpha \leq 12$, temperatures $0 \leq T/\omega_{LO} \leq 10$ and applied electric field frequencies $0 \leq \Omega/\omega_{LO} \leq 20$. I show the data obtained for $\alpha = 3, 6, 9$ where perturbation theory breaks down at $\alpha = 6$.

Figures 2.4 (contour plots) and 2.5 (ridge-line plots) show the real (left columns) and imaginary (right columns) of the complex conductivity for $\alpha = 3$ in the first rows, $\alpha = 6$ in the second rows and $\alpha = 9$ in the last rows. The figures are all log-scaled concerning the complex conductivity, and for the imaginary component, I have taken the absolute value to go to the log scale. This means that for the imaginary plots, any sharp ‘rifts’ indicate a change in sign as the imaginary component passes through zero. The imaginary component always starts negative at low temperature and frequency, so the first rift can be assumed to indicate a change to a positive sign. I chose $\alpha = 3, 6, 9$ to give some spread of coupling strength about $\alpha = 6$ where perturbation theory typically breaks down.

From Figures 2.4 and 2.5, we can see that firstly, at $\alpha = 3$, the complex conductivity starts with a single peak starting at $\Omega = \omega_{LO}$ for zero temperature, which broadens out and blue-shifts to higher frequencies as the temperature increases. This peak corresponds to a single phonon excitation. At $\alpha = 6$, the conductivity develops more peaks starting at $\Omega = \omega_{LO} + n\omega_{LO}v$, $n \in \mathbb{Z}^+$ at zero temperature, corresponding to further phonon excitations, which also broaden out and blue-shift to higher frequencies as the temperature increases. The first peak for $\alpha = 6$ now has more features, with an initial shoulder which leads into a far sharper peak than before and sharper, more structured peaks as α increases. Finally, for $\alpha = 9$, the landscape becomes much more erratic and complex. The first peak remains, however the trough that follows it has become so deep (reaching values close to zero) that the numerical results is noisy due to reaching float-point accuracy (working here with 64-bit floats). The second main peak (that I identify as regions now separated by the deep troughs) now seems to begin a little earlier than $\Omega = \omega_{LO} + v\omega_{LO}$ and appears to be composed of smaller, sharper peaks and shoulders.

2.3.3 Effective Multimode Mobility

Hellwarth and Biaggio [14] extended the Fröhlich model to where multiple phonon modes are present in a polar cubic material. They did this by deriving the full classical field Lagrangian that describes one conduction-band electron with charge $-e$,

isotropic band mass m_b and position $\mathbf{r}_{el}(t)$, which is coupled to a polar cubic lattice that possesses many infrared-active modes with varying strengths and frequencies. They derive an effective electron-phonon coupling constant that generalises Fröhlich's α parameter. Then, rather than explicitly incorporating the frequencies of multiple phonon modes into the Feynman path integral polaron model, they propose two different schemes for deriving an effective longitudinal optical phonon frequency. This enables them to directly use Ōsaka's finite-temhelpfulre variational principle for determining the temperature-dependent variational parameters v and w needed to evaluate the FHIP mobility.

As usual with Fröhlich polarons, they assume that the lattice unit cell is small compared to the electron wavelength such that the lattice polarisation density $\mathbf{P}(\mathbf{r}, t)$ can be treated as continuous. All other electrons are bound in fully occupied valence bands. The system is then perturbed by a homogeneous electric field $\mathbf{E}^{\text{ext}}(t)$. The polarisation density is composed of many independent terms $\mathbf{P}_j(\mathbf{r}, t)$ where $j = 1, \dots, m; m+1, \dots, m+M$ correspond to the m infrared (lattice) and M ultraviolet (bound electron) modes of the material such that

$$\mathbf{P}(\mathbf{r}, t) = \sum_{j=1}^{m+M} \mathbf{P}_j(\mathbf{r}, t) \quad (2.201)$$

where it will be useful to separate the transverse (divergence-less) $\mathbf{P}_j^{\text{Tr}}(\mathbf{r}, t)$ and longitudinal (curl-free) $\mathbf{P}_j^L(\mathbf{r}, t)$ parts of the polarisation fields.

Classical Lagrangian and action

Hellwarth's and Biaggio's Lagrangian are presented as

$$\begin{aligned} L = & \int d^3\mathbf{r} \left\{ \sum_{j=1}^{m+M} \frac{2\pi}{\mathcal{K}_j^2} \left[\left(\frac{\partial \mathbf{P}_j(\mathbf{r}, t)}{\partial t} \right)^2 - \mathcal{W}_j^2 \mathbf{P}_j^2(\mathbf{r}, t) \right] + \mathbf{P}^L(\mathbf{r}, t) \cdot \mathbf{D}^{el}(\mathbf{r}, t) \right. \\ & \left. \frac{1}{8\pi} \left[\left(\frac{\partial \mathbf{A}(\mathbf{r}, t)}{\partial t} \right)^2 - (\nabla \times \mathbf{A}(\mathbf{r}, t))^2 \right] + \frac{1}{c} \mathbf{A}(\mathbf{r}, t) \cdot \frac{\partial \mathbf{P}^{\text{Tr}}(\mathbf{r}, t)}{\partial t} \right\} \\ & \frac{1}{2} \int d^3\mathbf{r} \int d^3\mathbf{r}' \mathbf{P}(\mathbf{r}, t) \cdot \overleftrightarrow{\mathbf{G}}(\mathbf{r} - \mathbf{r}') \cdot \mathbf{P}(\mathbf{r}', t) \\ & + \frac{m_b}{2} \left(\frac{d\mathbf{r}_{el}(t)}{dt} \right)^2 + e\mathbf{r}_{el}(t) \cdot \mathbf{E}^{\text{ext}}(t) \end{aligned} \quad (2.202)$$

where $\mathbf{A}(\mathbf{r}, t)$ is the total electric vector potential (assumed purely transverse, i.e. Coulomb gauge), $\mathbf{D}^{el}(\mathbf{r}, t)$ is the longitudinal, un-shielded Coulomb field of the electron given by

$$\mathbf{D}^{el}(\mathbf{r}, t) = \nabla \frac{e}{|\mathbf{r} - \mathbf{r}_{el}(t)|}, \quad (2.203)$$

and finally $\overset{\leftrightarrow}{\mathbf{G}}(\mathbf{r} - \mathbf{r}')$ is the dipole-dipole kernel given by $-\nabla^2 |\mathbf{r} - \mathbf{r}'|^{-1}$. The first term in the Lagrangian describes the kinetic and potential energy of the lattice modes where \mathcal{W}_j and \mathcal{K}_j denote the frequencies and oscillator strengths of the isolated lattice modes. The dipole-dipole kernel $\overset{\leftrightarrow}{\mathbf{G}}(\mathbf{r})$ demonstrates a divergent self-interaction as $\mathbf{r} \rightarrow \mathbf{r}'$, so to remove this self-interaction and better imitate the finite size of a unit cell, Hellwarth and Biaggio introduce a cut-off distance $r_0 \sim$ inter-atomic distance. They choose $\overset{\leftrightarrow}{\mathbf{G}}(\mathbf{r})$ to be given by

$$G_{ab}(\mathbf{r}) = \begin{cases} \frac{3r_a r_b}{|\mathbf{r}|^5} - \frac{\delta_{ab}}{|\mathbf{r}|^3}, & |\mathbf{r}| > r_0 \\ 0, & |\mathbf{r}| \leq r_0. \end{cases} \quad (2.204)$$

so drops to zero at and below this cut-off.

Transforming the action to frequency and reciprocal space

The polarisation $\mathbf{P}_j(\mathbf{r}, t)$ and electric field $\mathbf{A}(\mathbf{r}, t)$ coordinates appear up to quadratically in the Lagrangian (Eq. (2.202)) but are coupled. Hellwarth and Biaggio seek to uncouple these coordinates by transforming them to normal coordinates by re-writing the action corresponding to Eq. (2.202) in terms of the Fourier transforms of the fields (denoted with a tilde)

$$\tilde{\mathbf{P}}_j^{\text{Tr} / \text{L}}(\mathbf{k}, \Omega) = \int dt \int d^3r \mathbf{P}_j^{\text{Tr} / \text{L}}(\mathbf{r}, t) e^{i\Omega t - i\mathbf{k} \cdot \mathbf{r}} \quad (2.205)$$

$$\tilde{\mathbf{A}}(\mathbf{k}, \Omega) = \int dt \int d^3r \mathbf{A}(\mathbf{r}, t) e^{i\Omega t - i\mathbf{k} \cdot \mathbf{r}} \quad (2.206)$$

$$\tilde{\mathbf{D}}^{el}(\mathbf{k}, \Omega) = \int dt \int d^3r \mathbf{D}^{el}(\mathbf{r}, t) e^{i\Omega t - i\mathbf{k} \cdot \mathbf{r}} \quad (2.207)$$

$$\tilde{\mathbf{G}}_{ab}(\mathbf{k}) = \int dt \int d^3r \mathbf{G}_{ab}(\mathbf{r}) e^{-i\mathbf{k} \cdot \mathbf{r}} \quad (2.208)$$

where $\tilde{\mathbf{P}}(\mathbf{k}, \Omega) = \tilde{\mathbf{P}}^L(\mathbf{k}, \Omega) + \tilde{\mathbf{P}}^{Tr}(\mathbf{k}, \Omega)$. Since the electron wave function is assumed larger than the cut-off distance r_0 , Hellwarth and Biaggio keep only the lowest-order terms of the dipole-dipole kernel and write

$$G_{ab}(\mathbf{k}) = \begin{cases} \frac{4\pi}{3} \left(\delta_{ab} - \frac{3k_a k_b}{|\mathbf{k}|} \right), & |\mathbf{k}| \ll \frac{1}{r_0} \\ 0, & \text{larger } |\mathbf{k}|. \end{cases} \quad (2.209)$$

Fourier transforming and assuming the absence of any terms where $|\mathbf{k}|$ is not $\ll r_0^{-1}$, Hellwarth and Biaggio obtain the frequency and wave-vector version of the action

$$\begin{aligned} S = & \frac{1}{(2\pi)^4} \int d\Omega \int d^3\mathbf{k} \left\{ \sum_{j=1}^{m+M} 2\pi \frac{\Omega^2 - \mathcal{W}_j^2}{\mathcal{K}_j^2} \left[|\tilde{\mathbf{P}}^{Tr}(\mathbf{k}, \Omega)|^2 + |\tilde{\mathbf{P}}^L(\mathbf{k}, \Omega)|^2 \right] \right. \\ & + \tilde{\mathbf{P}}^L(\mathbf{k}, \Omega)^* \cdot \tilde{\mathbf{D}}^{el}(\mathbf{k}, \Omega) \\ & + \frac{1}{8\pi} \left(\frac{\Omega^2}{c^2} - |\mathbf{k}|^2 \right) |\tilde{\mathbf{A}}(\mathbf{k}, \Omega)|^2 \\ & + i \frac{\Omega}{c} \tilde{\mathbf{A}}(\mathbf{k}, \Omega)^* \cdot \tilde{\mathbf{P}}^{Tr}(\mathbf{k}, \Omega) \\ & \left. + \frac{2\pi}{3} \left[|\tilde{\mathbf{P}}^{Tr}(\mathbf{k}, \Omega)|^2 - 2|\tilde{\mathbf{P}}^L(\mathbf{k}, \Omega)| \right] \right\} + S^{el} [\mathbf{r}_{el}(t)] \end{aligned} \quad (2.210)$$

where $S^{el} [\mathbf{r}_{el}(t)]$ is the action that depends on the electron coordinates $\mathbf{r}_{el}(t)$ (the last line of the Lagrangian in Eq. (2.202)).

Effective action for the electron-phonon interaction

Hellwarth and Biaggio follow the same procedure as [1] to evaluate the quantum-mechanical unitary transformation matrices $U(\mathbf{r}_{el,f}, \mathbf{P}_f, t_f; \mathbf{r}_{el,i}, \mathbf{P}_i, t_i)$ with path integrals over the polarisation fields $\mathbf{P}(\mathbf{r}, t)$ and electron position $\mathbf{r}_{el}(t)$

$$\begin{aligned} U(\mathbf{r}_{el,f}, \mathbf{P}_f, t_f; \mathbf{r}_{el,i}, \mathbf{P}_i, t_i) = & \int_{\mathbf{r}_{el,i}, t_i}^{\mathbf{r}_{el,f}, t_f} \mathcal{D}\mathbf{r}_{el}(t) \\ & \times \int_{\mathbf{P}_i, t_i}^{\mathbf{P}_f, t_f} \mathcal{D}\mathbf{P}(\mathbf{r}, t) \exp \left\{ \frac{iS[\mathbf{r}_{el}(t), \mathbf{P}(\mathbf{r}, t)]}{\hbar} \right\}, \end{aligned} \quad (2.211)$$

where $S[\mathbf{r}_{el}(t), \mathbf{P}(\mathbf{r}, t)]$ is the action functional corresponding to the Lagrangian in Eq. (2.202). The path integral over all trajectories of the polarisation coordinates $\mathbf{P}(\mathbf{r}, t)$ can be done precisely as before since they only appear up to quadratic order in the Lagrangian. Hellwarth and Biaggio evaluate the matrix element $\langle 0 | U(\mathbf{r}_{el,f}, \mathbf{P}_f, t_f; \mathbf{r}_{el,i}, \mathbf{P}_i, t_i) | 0 \rangle$ where the polarisation coordinate paths begin and end in the ground state for all unperturbed polarisation oscillators. The result is an effective model action akin to Feynman's (Eq. (2.64)) where the polarisation coordinates have been replaced by their classical solutions with no external field $\tilde{\mathbf{A}}(\mathbf{k}, \Omega) = 0$. For the transverse part of the polarisation density, the classical solution $\tilde{\mathbf{P}}_{C,j}^{\text{Tr}}(\mathbf{k}, \Omega)$ obeys the equation of motion

$$4\pi \frac{\Omega^2 - \mathcal{W}_j^2}{\mathcal{K}_j^2} \tilde{\mathbf{P}}_{C,j}^{\text{Tr}}(\mathbf{k}, \Omega) + \frac{4\pi}{3} \tilde{\mathbf{P}}_C^{\text{Tr}}(\mathbf{k}, \Omega) + i \frac{\Omega}{c} \tilde{\mathbf{A}}(\mathbf{k}, \Omega) = 0, \quad (2.212)$$

and the longitudinal part of the polarisation density, the classical solution $\tilde{\mathbf{P}}_{C,j}^L(\mathbf{k}, \Omega)$ obeys the equation of motion

$$4\pi \frac{\Omega^2 - \mathcal{W}_j^2}{\mathcal{K}_j^2} \tilde{\mathbf{P}}_{C,j}^L(\mathbf{k}, \Omega) - \frac{8\pi}{3} \tilde{\mathbf{P}}_C^L(\mathbf{k}, \Omega) + \tilde{\mathbf{D}}^{el}(\mathbf{k}, \Omega) = 0. \quad (2.213)$$

Hellwarth and Biaggio found the solution to these equations of motion to be

$$\tilde{\mathbf{P}}_C^{\text{Tr}}(\mathbf{k}, \Omega) = \sum_{j=1}^{m+M} \tilde{\mathbf{P}}_{C,j}^{\text{Tr}}(\mathbf{k}, \Omega) = -i \frac{\Omega}{c} \tilde{\mathbf{A}}(\mathbf{k}, \Omega) \frac{\alpha(\Omega)}{1 - (4\pi/3)\alpha(\Omega)} \quad (2.214)$$

and

$$\tilde{\mathbf{P}}_C^L(\mathbf{k}, \Omega) = \sum_{j=1}^{m+M} \tilde{\mathbf{P}}_{C,j}^L(\mathbf{k}, \Omega) = \frac{\alpha(\Omega)}{1 + (8\pi/3)\alpha(\Omega)} \tilde{\mathbf{D}}^{el}(\mathbf{k}, \Omega) \quad (2.215)$$

where

$$\alpha(\Omega) = \frac{1}{4\pi} \sum_{j=1}^{m+M} \frac{\mathcal{K}_j^2}{\mathcal{W}_j^2 - \Omega^2} \quad (2.216)$$

is the polarisability of a single-unit cell. Substituting $\tilde{\mathbf{P}}_C^{\text{Tr}}(\mathbf{k}, \Omega)$ and $\tilde{\mathbf{P}}_C^L(\mathbf{k}, \Omega)$ into the model action S gives the effective model action

$$S^{\text{eff}} = S^{el} [\mathbf{r}_{el}(t)] + S^{\text{int}} + S^{\text{norm}} \quad (2.217)$$

where S^{norm} is a normalisation term that cancels in the matrix element $\langle 0 | U | 0 \rangle$. S^{int} is an effective interaction term given by

$$S^{\text{int}} = \frac{1}{2(2\pi)^4} \int d\Omega \int d^3\mathbf{k} B(\Omega) \tilde{\mathbf{D}}^{el}(\mathbf{k}, \Omega)^* \cdot \tilde{\mathbf{D}}^{el}(\mathbf{k}, \Omega) \quad (2.218)$$

where $B(\Omega)$ was obtained from the relation $\tilde{\mathbf{P}}_C^L(\mathbf{k}, \Omega) = B(\Omega) \tilde{\mathbf{D}}^{el}(\mathbf{k}, \Omega)$ and is

$$B(\Omega) = \frac{1}{4\pi} \left(1 - \frac{1}{\epsilon(\Omega)} \right) = \frac{\alpha(\Omega)}{1 + (8\pi/3)\alpha(\Omega)} = \frac{1}{4\pi} \sum_{j=1}^{m+M} \frac{\kappa_j^2}{\omega_j^2 - \Omega^2}. \quad (2.219)$$

$B(\Omega)$ is the macroscopic polarisability, where each term in the sum of $B(\Omega)$ acts as a harmonic longitudinal lattice mode with a frequency ω_j and coupling constant κ_j that linearly coupled to the conduction electron field $\tilde{\mathbf{D}}^{el}$.

Hellwarth and Biaggio use the Born-Oppenheimer approximation just as in the original Fröhlich model by assuming that the bound-electrons (ultraviolet oscillators) response speed is near instantaneous. Therefore, the short-wavelength limit ϵ_∞ of the dielectric constant accounts for the electronic contribution when the ions are immobile. Otherwise, the contribution corresponding to ionic displacements is assumed to be described by the static dielectric constant ϵ_0 . Therefore, the ions slowly follow the harmonic movement of the electron with a time delay. Hellwarth and Biaggio separate $B(\Omega)$ into infrared and optical contributions where the latter is represented by ϵ_∞ so that

$$B(\Omega) = \tilde{B}(\Omega) + \frac{1}{4\pi} \left(1 - \frac{1}{\epsilon_\infty} \right) \quad (2.220)$$

where

$$\tilde{B}(\Omega) = \frac{1}{4\pi} \sum_{j=1}^m \frac{\kappa_j^2}{\omega_j^2 - \Omega^2}. \quad (2.221)$$

This $\tilde{B}(\Omega)$ is the infrared contributions of m polar infrared lattice modes and replaces $B(\Omega)$ when neglecting the ultraviolet contributions. Hence, since the zero frequency limit is represented by ϵ_0 , we can obtain the familiar Pekar factor

$$\sum_{j=1}^m \frac{\kappa_j^2}{\omega_j^2} = \frac{1}{\epsilon_\infty} - \frac{1}{\epsilon_0}. \quad (2.222)$$

Now it is assumed that the ultraviolet contributions are summarised by ϵ_∞ and an effective band mass m_b that replaces the electron mass m_e in the effective action S^{eff} . The space-time integral action is needed, so Hellwarth and Biaggio transform the effective action by evaluating the integrals over Ω and \mathbf{k} . The frequency integral in S^{int} corresponds to a Fourier-like transform

$$\int \frac{d\Omega}{2\pi} \frac{e^{-i\Omega t}}{\omega_j^2 - \Omega^2} = \frac{ie^{-i\omega_j|t|}}{2\omega_j}. \quad (2.223)$$

and the transform $\tilde{\mathbf{D}}^{el}(\mathbf{k}, \Omega)$ is calculated from Eq. (2.207) to give

$$\tilde{\mathbf{D}}^{el}(\mathbf{k}, \Omega) = 4\pi ie \int dt e^{i\Omega t} \frac{e^{-i\mathbf{k} \cdot \mathbf{r}_{el}(t)}}{|\mathbf{k}|}. \quad (2.224)$$

Substituting these into S^{int} gives

$$\begin{aligned} S^{\text{int}} &= \frac{ie^2}{(2\pi)^2} \int d^3\mathbf{k} \frac{1}{|\mathbf{k}|^2} \int dt \int dt' e^{i\mathbf{k} \cdot [\mathbf{r}_{el}(t) - \mathbf{r}_{el}(t')]} \sum_{j=1}^m \left(\frac{\kappa_j^2}{\omega_j} e^{-i\omega_j|t-t'|} \right) \\ &= i \frac{e^2}{4} \int dt \int dt' \frac{1}{|\mathbf{r}_{el}(t) - \mathbf{r}_{el}(t')|} \sum_{j=1}^m \left(\frac{\kappa_j^2}{\omega_j} e^{-i\omega_j|t-t'|} \right). \end{aligned} \quad (2.225)$$

Hellwarth and Biaggio find the final form of the effective action, akin to Feynman's, to be

$$\begin{aligned} S^p &= \frac{m_b}{2} \int dt \left(\frac{d\mathbf{r}_{el}(t)}{dt} \right)^2 + \int dt \mathbf{E}^{\text{ext}} \cdot \mathbf{r}_{el}(t) \\ &\quad + \frac{i\hbar\omega_p}{2\sqrt{2}} \sum_{j=1}^m \alpha_j \int dt \int dt' \frac{e^{-i\omega_j|t-t'|}}{|\mathbf{r}_{el}(t) - \mathbf{r}_{el}(t')|} \end{aligned} \quad (2.226)$$

where we have excluded the infinite normalisation term due to the phonon oscillators (this does not affect the electron coordinate $\mathbf{r}_{el}(t)$ and so can be ignored). The effective action is written in terms of "polaron units": frequencies are meas-

ured relative to a standard lattice frequency ω_p , time in units of ω_p^{-1} , energy $\hbar\omega_p$, lengths $\sqrt{\hbar/(m_b\omega_p)}$, temperature $\hbar\omega_p/k_B$ and mobility $e/(m_b\omega_p)$.

The dimensionless coupling constants α_j generalise the Fröhlich version to multiple phonon modes j and is given by

$$\alpha_j = \frac{\kappa_j^2}{\omega_p \omega_j} \frac{e^2}{\hbar} \left(\frac{m_b}{2\hbar\omega_p} \right)^{1/2}. \quad (2.227)$$

For a single phonon branch with frequency $\omega = \omega_p$ and strength κ then this coupling constant reduces to the familiar α

$$\alpha = \frac{\kappa^2}{\omega_p^2} \frac{e^2}{\hbar} \left(\frac{m_b}{2\hbar\omega_p} \right)^{1/2} = \left(\frac{1}{\epsilon_\infty} - \frac{1}{\epsilon_0} \right) \frac{e^2}{\hbar} \left(\frac{m_b}{2\hbar\omega_p} \right)^{1/2}. \quad (2.228)$$

The dielectric function

To compare to the experiment, Hellwarth and Biaggio seek an expression for the dielectric function $\epsilon(\Omega)$. They first obtain the classical solution for the magnetic vector potential $\tilde{\mathbf{A}}_C(\mathbf{k}, \Omega)$ and find that it obeys the equation of motion

$$\frac{1}{4\pi} \left(\frac{\Omega^2}{c^2} - |\mathbf{k}|^2 \right) \tilde{\mathbf{A}}_C(\mathbf{k}, \Omega) - i \frac{\Omega}{c} \tilde{\mathbf{P}}^{\text{Tr}}(\mathbf{k}, \Omega) = 0. \quad (2.229)$$

By substituting the classical solution for $\tilde{\mathbf{P}}_C^{\text{Tr}}(\mathbf{k}, \Omega)$ in Eq. (2.214) into the equation of motion for $\tilde{\mathbf{A}}_C(\mathbf{k}, \Omega)$ in Eq. (2.229) they find that the classical transverse solutions must also obey (for all \mathbf{k})

$$\left[\frac{1}{4\pi} \left(\frac{\Omega^2}{c^2} - |\mathbf{k}|^2 \right) + \frac{\Omega^2}{c^2} \frac{\alpha(\Omega)}{1 - (4\pi/3)\alpha(\Omega)} \right] \tilde{\mathbf{A}}_C(\mathbf{k}, \Omega) = 0, \quad (2.230)$$

from which they obtain the Lorentz-Lorenz relation for the dielectric function $\epsilon(\Omega)$,

$$\epsilon(\Omega) = n^2(\Omega) = \frac{1 + (8\pi/3)\alpha(\Omega)}{1 - (4\pi/3)\alpha(\Omega)}, \quad (2.231)$$

where $n(\Omega) = |\mathbf{k}|c/\Omega$ is the refractive index.

Obtaining a single effective phonon frequency

Hellwarth and Biaggio use the mobility result from FHIP combined with Ōsaka's temperature-dependent variational parameters. To do this, they reduce the many infrared longitudinal phonon mode frequencies to a single effective frequency. To do this, they first compare their athermal effective action in Eq. (2.226) to the thermal effective action derived by Ōsaka in Eq. (2.120). From this comparison, they see that the inclusion of multiple phonon modes converts the influence functional phase Φ^{int} (Eq. (2.157)) to a sum over terms differing only in the phonon frequencies ω_j and coupling constants α_j

$$\begin{aligned} \Phi^{\text{int}}[\mathbf{r}_{el}(t), \mathbf{r}'_{el}(t)] &\rightarrow \frac{(\hbar\omega_p)^{3/2}}{2\sqrt{2m_b}} \sum_{j=1}^m \frac{\alpha_j \omega_j^{-2}}{\sinh(\beta_j/2)} \int_0^{\beta_j} dt \int_0^{\beta_j} dt' \left\{ \frac{\cos(|t-t'| + i\beta_j/2)}{|\mathbf{r}_{el}(t) - \mathbf{r}_{el}(t')|} \right. \\ &\quad \left. + \frac{\cos(|t-t'| - i\beta_j/2)}{|\mathbf{r}'_{el}(t) - \mathbf{r}'_{el}(t')|} - \frac{2\cos(|t-t'| + i\beta_j/2)}{|\mathbf{r}'_{el}(t) - \mathbf{r}_{el}(t')|} \right\} \end{aligned} \quad (2.232)$$

where $\beta_j = \hbar\omega_j/k_B T$.

In [14], they propose two schemes, labelled 'A' and 'B', to reduce this expression to a single term with an effective frequency ω_{eff} and an effective coupling constant κ_{eff} . They then take the "polaron frequency" to be equal to this effective frequency $\omega_p = \omega_{\text{eff}}$.

In the first scheme, 'A', they seek an effective time kernel $H_{\text{eff}}(t)$ defined by

$$H_{\text{eff}}(t) \sim \alpha_{\text{eff}} \frac{\cos(\omega_{\text{eff}}|t-t'| \pm i\beta_{\text{eff}}/2)}{\sinh(\beta_{\text{eff}}/2)} \quad (2.233)$$

which has the properties

$$H_{\text{eff}}(0) = \sum_{j=1}^m H_j(0). \quad (2.234)$$

This is fulfilled by taking

$$\frac{\kappa_{\text{eff}}^2}{\omega_{\text{eff}}} \coth\left(\frac{\beta_{\text{eff}}}{2}\right) = \sum_{j=1}^m \frac{\kappa_j^2}{\omega_j} \coth\left(\frac{\beta_j}{2}\right), \quad (2.235)$$

and

$$\frac{dH_{\text{eff}}(t)}{dt} \Big|_{t=0} = \sum_{j=1}^m \frac{dH_j(t)}{dt} \Big|_{t=0}. \quad (2.236)$$

This requires

$$\kappa_{\text{eff}}^2 = \sum_{j=1}^m \kappa_j^2. \quad (2.237)$$

The second scheme, 'B', seeks to find the single effective frequency ω_{eff} and coupling constant κ_{eff} to match

$$\int_0^{\beta_{\text{eff}}} dt H_{\text{eff}}(it) = \sum_{j=1}^m \int_0^{\beta_j} dt H_j(it) \quad (2.238)$$

where they now used the imaginary-time kernel $H(it)$. They found that this expression is fulfilled by

$$\frac{\kappa_{\text{eff}}^2}{\omega_{\text{eff}}^2} = \sum_{j=1}^m \frac{\kappa_j^2}{\omega_j^2}. \quad (2.239)$$

The second scheme also requires that

$$\frac{dH_{\text{eff}}(it)}{dt} \Big|_{t=0} = \sum_{j=1}^m \frac{dH_j(it)}{dt} \Big|_{t=0} \quad (2.240)$$

which requires

$$\kappa_{\text{eff}}^2 = \sum_{j=1}^m \kappa_j^2. \quad (2.241)$$

Despite considering temperature dependence, the final result of the second 'B' scheme is independent of temperature as the temperature terms cancel.

Reformulation of Ōsaka's variational principle

Hellwarth and Biaggio used Ōsaka's variational principle in Eq. (2.146) to determine the variational parameters v and w to use within FHIP's mobility expression

in Eq. (2.192). However, they reformulated the result Ōsaka obtained for the upper-bound free energy expression to a form more straightforward to calculate

$$F(\beta)/(\hbar\omega_{\text{eff}}) \leq -(A(\beta) + B(\beta) + C(\beta)) \quad (2.242\text{a})$$

with

$$A(\beta) = -\frac{F_{S_0}(\beta)}{\hbar\omega_{\text{eff}}} = \frac{3}{\beta} \left[\ln\left(\frac{v}{w}\right) - \frac{1}{2} \ln(2\pi\beta) - \ln\left(\frac{\sinh(v\beta/2)}{\sinh(w\beta/2)}\right) \right] \quad (2.242\text{b})$$

and rewritten in a more symmetric form

$$B(\beta) = \frac{\langle S(\beta) \rangle}{\hbar\omega_{\text{eff}}} = \frac{\alpha v}{\sqrt{\pi}(e^\beta - 1)} \int_0^{\beta/2} dx \frac{e^{\beta-x} + e^x}{[w^2 x(1-x/\beta) + Y(x)(v^2 - w^2)/v]^{1/2}}, \quad (2.242\text{c})$$

where

$$Y(x) = \frac{1 + e^{-v\beta} - e^{-vx} - e^{v(x-\beta)}}{1e^{-v\beta}}, \quad (2.242\text{d})$$

and

$$C(\beta) = -\frac{\langle S_0(\beta) \rangle}{\hbar\omega_{\text{eff}}} = \frac{3}{4} \frac{v^2 - w^2}{v} \left(\coth\left(\frac{v\beta}{2}\right) - \frac{2}{v\beta} \right). \quad (2.242\text{e})$$

These equations are used to find the lowest upper-bound to the actual free energy of the polaron for a single effective phonon branch with frequency ω_{eff} and coupling constant κ_{eff} which determines an effective α_{eff} parameter.

2.4 Material Case Studies

2.4.1 Methylammonium Lead Halide Perovskite

2.4.2 Rubrene Organic Crystal

CHAPTER 3

GENERALISING THE MATERIAL PATH INTEGRAL MODEL

What is the meaning of life?

—John Doe, *Thoughts*, 1971

This is the introduction paragraph.

3.1 Multiple Phonon Modes

IN simple polar materials with two atoms in the basis, the single triply-degenerate optical phonon branch is split by dielectric coupling into the singly-degenerate longitudinal-optical mode and double-degenerate transverse-optical modes. Only the longitudinal-optical mode is infrared active and contributes to the Fröhlich dielectric electron-phonon interaction.

The infrared activity of this mode drives the formation of the polaron, and similarly, in a more complex material, the range of infrared active modes all contribute to the polaron stabilisation. This relationship is, however, slightly obscured by the algebra in Eq. (2.34), and instead, this electron-phonon coupling seems to emerge from bulk phenomenological quantities. The Pekar factor, $\frac{1}{\epsilon_\infty} - \frac{1}{\epsilon_0}$ being particularly opaque. Rearranging the Pekar factor as

$$\left(\frac{1}{\epsilon_\infty} - \frac{1}{\epsilon_0} \right) = \frac{\epsilon^{ionic}}{\epsilon_\infty \epsilon_0}, \quad (3.1)$$

we can now see that the Fröhlich α is proportional to the ionic dielectric contribution $\epsilon_j^{\text{ionic}}$, as would be expected from appreciating that this is the driving force for polaron formation.

The relative static dielectric constant is composed out of the high-frequency optical component (from the response of the electronic structure), and then the THz scale vibrational motion of the ions, $\epsilon_0 = \epsilon_\infty + \epsilon_j$. This vibrational contribution is typically calculated by summing the infrared activity of the individual harmonic modes as Lorentz oscillators [20]. This infrared activity can be obtained by projecting the Born effective charges along the dynamic matrix (harmonic phonon) eigenvectors. The overall dielectric function across the phonon frequency range can be written as

$$\epsilon_{\alpha\beta}^0(\omega) = \epsilon_{\alpha\beta}^\infty + \sum_j^{\text{modes}} \epsilon_{\alpha\beta j}^{\text{ionic}}(\omega) = \epsilon_{\alpha\beta}^\infty + \frac{4\pi e^2}{\Omega_0} \sum_{j\nu\mu} \frac{\sum_{\alpha'} Z_{\alpha\alpha'}^{*\mu} u_{\mu j}^{\alpha'} \sum_{\beta'} Z_{\beta\beta'}^{*\nu} u_{\nu j}^{\beta'}}{(\omega_j^2 - \omega^2)} \quad (3.2)$$

where e is the electron charge, Ω_0 the unit cell volume, $Z_{\alpha\beta}^{*\nu}$ is the Born effective charge tensor at atom ν , $u_{\mu j}^{\alpha}$ is the dynamic matrix eigenvector at atom μ for the j th phonon branch, ω_j is the dispersionless LO phonon frequency for the j th phonon branch and ω is the reduced frequency.

Considering the isotropic case (and therefore picking up a factor of $\frac{1}{3}$ for the averaged interaction with a dipole), and expressing the static (zero-frequency) dielectric contribution, in terms of the infrared activity of a mode, $\epsilon_j^{\text{ionic}}$ is

$$\epsilon^{\text{ionic}}(\hat{k}) = \sum_j^{\text{modes}} \epsilon_j^{\text{ionic}}(\hat{k}) = \frac{4\pi e^2}{\Omega_0} \sum_j^{\text{modes}} \frac{\left(\sum_{\nu\alpha\beta} k^\alpha Z_{\alpha\beta}^{*\nu} u_{\nu j}^\beta \right)^2}{k^2 \omega_j^2}. \quad (3.3)$$

This provides a clear route to defining α_j for individual phonon branches, with the simple constitutive relationship that $\alpha = \sum_j \alpha_j$:

$$|V_{\mathbf{k}}|^2 = \sum_j^{\text{modes}} \frac{4\pi\hbar(\hbar\omega_j)^{3/2}}{\sqrt{2m_b}\Omega_0 k^2} \alpha_j(\hat{k}) = \frac{2\pi\hbar}{\Omega_0 k^2} \sum_j^{\text{modes}} \frac{\omega_j \epsilon_j^{\text{ionic}}(\hat{k})}{\epsilon_\infty(\hat{k})\epsilon_0(\hat{k})} \quad (3.4)$$

where

$$\alpha_j = \frac{1}{4\pi\epsilon_0} \frac{\epsilon_j}{\epsilon_\infty\epsilon_0} \frac{e^2}{\hbar} \left(\frac{m_b}{2\hbar\omega_j} \right)^{\frac{1}{2}}. \quad (3.5)$$

This concept of decomposing α into constituent pieces associated with individual phonon modes is implicit in the effective mode scheme of Hellwarth and Biaggio (Eqs. (2.234) to (2.241)), and has also been used by Verdi, [21] and Devreese [22].

3.1.1 Multiple Phonon Mode Path Integral

Verbist [21] proposed an extended Fröhlich model Hamiltonian in Eq. (2.38) with a sum over multiple (m) phonon branches,

$$\hat{H} = \frac{p^2}{2m_b} + \sum_{\mathbf{k},j} \hbar\omega_j a_{\mathbf{k},j}^\dagger a_{\mathbf{k},j} + \sum_{\mathbf{k},j} (V_{\mathbf{k},j} a_{\mathbf{k},j} e^{i\mathbf{k}\cdot\mathbf{r}} + V_{\mathbf{k},j}^* a_{\mathbf{k},j}^\dagger e^{-i\mathbf{k}\cdot\mathbf{r}}). \quad (3.6)$$

Here, the index j indicates the j th phonon branch. The interaction coefficient is given by,

$$V_{\mathbf{k},j} = i \frac{2\hbar\omega_j}{\mathbf{k}} \left(\sqrt{\frac{\hbar}{2m_b\omega_j}} \frac{\alpha_j\pi}{\Omega_0} \right)^{1/2}, \quad (3.7)$$

with α_j as in Eq. (3.5). From this Hamiltonian, we get the following extended model action to use within the Feynman variational theory,

$$S_j[\mathbf{r}(\tau)] = \frac{m_b}{2} \int_0^{\beta_j} d\tau \left(\frac{d\mathbf{r}(\tau)}{d\tau} \right)^2 - \frac{\hbar^{3/2}}{2\sqrt{2m_b}} \alpha_j \omega_j^{3/2} \int_0^{\beta_j} d\tau \int_0^{\beta_j} d\sigma \frac{G_j(|\tau - \sigma|)}{|\mathbf{r}(\tau) - \mathbf{r}(\sigma)|}. \quad (3.8)$$

where I introduce the reduced thermodynamic temperature for the j th phonon branch $\beta_j = \hbar\omega_j / (k_B T)$. $G_j(x)$ is the phonon Green's function for a phonon with frequency ω_j ,

$$G_j(x) = \frac{\cosh(\beta_j/2 - x)}{\sinh(\beta_j/2)}. \quad (3.9)$$

This form of action is consistent with Hellwarth and Biaggio's deduction that multiple phonon branches result in the interaction term simply becoming a sum

over terms with phonon frequency ω_j and coupling constant α_j dependencies as shown in Eq. (2.232).

I now choose a suitable trial action to use with the action in Eq. (3.8). One option is to use Feynman's original trial action with two variational parameters, C and w , which physically represent a particle (the charge carrier) coupled harmonically to a single fictitious particle (the additional mass of the quasi-particle due to interaction with the phonon field) with a strength C and a frequency w .

Obviously, the dynamics of this model cannot be more complex than can be arrived at with the original Feynman theory, though the direct variational optimisation may get a better fit by using Hellwarth's and Biaggio's effective phonon mode approximation (Eqs. (2.234) to (2.241)). To build a model capable of expressing richer dynamics and more directly describing real materials with multiple phonon modes, I extend Feynman's trial action to represent a particle (the charge-carrier) coupled to n massive fictitious particles. This results in $2 \times n$ variational parameters (one for each fictitious particle's coupling strength and frequency per phonon branch).

I extend Feynman's trial action using equations (1.1), (3.11), and (3.16) by [23], which are given by:

A non-local harmonic action:

$$S = \frac{m}{2} \int_0^t d\tau \dot{\mathbf{r}}(\tau)^2 - \frac{1}{8} \sum_{p=1}^n \kappa_p \Omega_p \int_0^t d\tau \int_0^t d\sigma \frac{\cos(\Omega_p[t/2 - |\tau - \sigma|])}{\sin(\Omega_p t/2)} (\mathbf{r}(\tau) - \mathbf{r}(\sigma))^2 + \int_0^t d\tau \mathbf{F}(\tau) \cdot \mathbf{r}(\tau) \quad (1.1) \quad (3.10a)$$

a term corresponding to Hellwarth and Biaggio's C expression in Eq. (2.242e)

$$\frac{\partial}{\partial \kappa_p} \ln G(t) = \frac{3}{2} \sum_{q=1}^n \frac{h_q}{\omega_q} \frac{1}{\omega_q^2 - \Omega_p^2} \left(\frac{1}{\omega_q} - \frac{t}{2} \cot\left(\frac{\omega_q t}{2}\right) \right) \quad (3.11) \quad (3.10b)$$

where

$$\kappa_p = m \left(\omega_p^2 - \Omega_p^2 \right) \prod_{\substack{q=1 \\ q \neq p}}^n \frac{\omega_q^2 - \Omega_p^2}{\Omega_q^2 - \Omega_p^2}, \quad h_p = \frac{1}{m} \left(\omega_p^2 - \Omega_p^2 \right) \prod_{\substack{q=1 \\ q \neq p}}^n \frac{\Omega_q^2 - \omega_q^2}{\omega_q^2 - \Omega_p^2} \quad (3.10c)$$

and the path integral pre-factor $G(t)$ that corresponds to the trial partition function $Z_{S_0}(\beta) = \exp(-\beta F_{S_0})$ where $F_{S_0}(\beta) = A(\beta)$ is the trial free energy proportional to Hellwarth and Biaggio's A expression in Eq. (2.242b)

$$G(t) = \left(\frac{m}{2\pi i \hbar t} \right)^{3/2} \prod_{p=1}^n \left(\frac{\omega_p \sin(\Omega_p t/2)}{\Omega_p \sin(\omega_p t/2)} \right)^3. \quad (3.16)$$

I then perform a Wick-rotation and equate the total time-like variable elapsed (t in [23]) with $t \rightarrow -i\hbar\beta$. I recognise the parameters ω and Ω in [23] with Feynman's v and w respectively. This gives us a polaron trial action extended to a set n of variational parameters per phonon branch,

$$\begin{aligned} S_{0j}[\mathbf{r}(\tau)] &= \frac{m_b}{2} \int_0^{\beta_j} d\tau \left(\frac{d\mathbf{r}(\tau)}{d\tau} \right)^2 \\ &+ \frac{1}{8} \sum_{p=1}^n \kappa_p w_p \int_0^{\beta_j} d\tau \int_0^{\beta_j} d\sigma \frac{\cosh(w_p[\beta_j/2 - |\tau - \sigma|])}{\sinh(w_p\beta_j/2)} (\mathbf{r}(\tau) - \mathbf{r}(\sigma))^2. \end{aligned} \quad (3.11)$$

Here κ_p is the spring constant associated with the p th fictitious particle, and w_p is the corresponding oscillation frequency.

3.1.2 Multiple Phonon Mode Free Energy

I extend Hellwarth and Biaggio's A (2.242b) and C (2.242e) equations,

$$A_j = \frac{3}{\beta_j m} \left[\sum_{p=1}^n \left(\log \left(\frac{v_p \sinh(w_p \beta_j / 2)}{w_p \sinh(v_p \beta_j / 2)} \right) \right) - \frac{1}{2} \log(2\pi\beta_j) \right], \quad (3.12a)$$

$$C_j = \frac{3}{m} \sum_{p=1}^n \sum_{q=1}^n \frac{C_{pq}}{v_q w_p} \left(\coth \left(\frac{v_q \beta_j}{2} \right) - \frac{2}{v_q \beta_j} \right). \quad (3.12b)$$

With,

$$C_{pq} = \frac{w_p}{4} \frac{\kappa_p h_q}{v_q^2 - w_p^2}, \quad (3.13a)$$

$$\kappa_p = (v_p^2 - w_p^2) \prod_{\substack{q=1 \\ q \neq p}}^n \frac{v_q^2 - w_p^2}{w_q^2 - w_p^2}, \quad (3.13b)$$

$$h_p = (v_p^2 - w_p^2) \prod_{\substack{q=1 \\ q \neq p}}^n \frac{w_q^2 - v_p^2}{v_q^2 - v_p^2}. \quad (3.13c)$$

C_{pq} are the components of a generalised $(n \times n)$ matrix version of Feynman's C variational parameter. The cross (off-diagonal) terms give the coupling (interaction) between the fictitious particles.

Now I note that the $R(x)$ function appearing in Eq. (3.8) in [23]

$$R(x) = 2 \sum_{p=1}^n \frac{h_p}{\omega_p^3} \frac{\sin(\omega_p x/2) \sin(\omega_p [t-x]/2)}{\sin(\omega_p t/2)} + \frac{1}{mt} \left(1 - m \sum_{p=1}^n \frac{h_p}{\omega_p^2} \right) x(t-x) \quad (3.14)$$

is a generalisation of the $D(x)$ expression in FHIP given in Eq. (2.180), which is more familiar notation and again Wick-rotated to the form given in Eq. (2.92) gives

$$D_j(x) = 2 \sum_{p=1}^n \frac{h_p}{v_p^3} \frac{\sinh(v_p x/2) \sinh(v_p [\beta_j - x]/2)}{\sinh(v_p \beta_j/2)} + \left(1 - \sum_{p=1}^n \frac{h_p}{v_p^2} \right) x \left(1 - \frac{x}{\beta_j} \right). \quad (3.15)$$

When $n = 1$ (a single fictitious particle) with $x \rightarrow -iu$ and $t \rightarrow -i\hbar\beta$, $D_j(x)$ is the same form as $D(u)$ from Eq. (2.92) from Feynman's polaron theory.

Combining $D_j(x)$ in Eq. (4.4) and the multiple phonon action in Eq. (3.8), we arrive at a generalisation to Hellwarth and Biaggio's B expression, including multiple (m with index j) phonon branches, and multiple ($2n$ with index p) variational parameters v_p and w_p ,

$$B_j = \frac{\alpha_j}{\sqrt{\pi}} \int_0^{\frac{\beta_j}{2}} d\tau \frac{\cosh(\beta_j/2 - \tau)}{\sinh(\beta_j/2)} [D_j(\tau)]^{-\frac{1}{2}}. \quad (3.16)$$

Summing the trial free energy A_j in Eq. (4.2a), the trial-model interaction B_j in Eq. (4.5), and the trial action C_j in Eq. (4.2a), we obtain a generalised variational inequality for the contribution to the free energy of the polaron from the j th phonon branch with phonon frequency ω_j and coupling constant α_j , and $2n$ variational parameters v_p, w_p ,

$$\begin{aligned} F(\beta) &\leq - \sum_{j=1}^m \hbar\omega_j (A_j + B_j + C_j) \\ &= \sum_{j=1}^m \hbar\omega_j \left\{ \frac{3}{\beta_j m} \left[\sum_{p=1}^n \left(\log \left(\frac{v_p \sinh(w_p \beta_j/2)}{w_p \sinh(v_p \beta_j/2)} \right) \right) - \frac{1}{2} \log(2\pi\beta_j) \right] \right. \\ &\quad + \frac{3}{m} \sum_{p=1}^n \sum_{q=1}^n \frac{C_{pq}}{v_q w_p} \left(\coth \left(\frac{v_q \beta_j}{2} \right) - \frac{2}{v_q \beta_j} \right) \\ &\quad \left. + \frac{\alpha_j}{\sqrt{\pi}} \int_0^{\frac{\beta_j}{2}} d\tau \frac{\cosh(\beta_j/2 - \tau)}{\sinh(\beta_j/2)} \left[2 \sum_{p=1}^n \frac{h_p}{v_p^3} \frac{\sinh(v_p \tau/2) \sinh(v_p [\beta_j - \tau]/2)}{\sinh(v_p \beta_j/2)} \right. \right. \\ &\quad \left. \left. + \left(1 - \sum_{p=1}^n \frac{h_p}{v_p^2} \right) \tau \left(1 - \frac{\tau}{\beta_j} \right) \right]^{-\frac{1}{2}} \right\}. \end{aligned} \quad (3.17)$$

Here, I have written out the expression explicitly rather than using “polaron” units as used in the literature. Despite that each of the phonon branches j is independent, the RHS of Eq. (4.6) is minimised for total summation over each phonon branch to give the upper-bound for the total model free energy F .

I obtain vectors of length n for the variational parameters v_p and w_p that correspond to these minima, which will be used to evaluate the polaron mobility. When we consider only one phonon branch ($m = 1$) and only two variational parameters ($n = 1$), this simplifies to Hellwarth and Biaggio’s form of Ōsaka’s free energy in Eq. (2.242). Feynman’s original athermal version can then be obtained by taking the zero temperature limit ($\beta \rightarrow \infty$).

3.2 Lattice Polarons

Hans De Raedt and Ad Lagendijk [24, 25] derived the discrete path integral for a lattice polaron, which was then further developed by Pavel Kornilovitch [26, 27, 28, 29, 30, 31, 32]. Kornilovitch derived the continuous path integral limit of the lattice polaron and developed a Continuous-time Path Integral Monte Carlo method for calculating properties of small polarons, with a special focus on the Holstein model and a lattice version of the Fröhlich model (which allows for long-range electron-lattice interactions).

The topology of the phase-space for the continuum large polaron model is Euclidean, flat, and infinite plane. The topology of the lattice small polaron is that of a torus since both the position and the momentum space are periodic and discrete. If either one of the periodic boundary conditions (the thermodynamic limit of an infinite-size box or an infinite number of lattice points) or discreteness (going to the continuum limit) is removed, the topology changes to an infinitely long cylinder. Performing both limits gives back the infinite plane.

I have not found a way to extend Feynman's variational path integral approach to a case where we retain this topology of the electronic phase space. To explain the difficulties in trying this, I will first outline the key steps of deriving the exact lattice path integral for the Holstein model and use that to motivate the challenges the lattice small-polaron Path Integral presents for developing a variational method in analogy to that done for continuum large polarons.

3.2.1 Discrete-Time Path Integral

We begin with the Holstein Hamiltonian in a mixed representation:

$$\begin{aligned}
 H &= H_0 + H_1 + H_2, \\
 H_0 &= \frac{1}{2M} \sum_{i=1}^N p_i^2, \\
 H_1 &= \frac{M\omega_0^2}{2} \sum_{i=1}^N x_i^2 + \lambda \sum_{i=1}^N x_i c_i^\dagger c_i, \\
 H_2 &= -J \sum_{i=1}^N c_i^\dagger c_{i+1} + c_{i+1}^\dagger c_i,
 \end{aligned} \tag{3.18}$$

where the phonons are expressed in terms of their momenta p_i and positions x_i where i labels the corresponding lattice site. M is the mass of one lattice site (here, we assume all of them to have the same mass), and ω_0 is the dispersionless phonon

frequency where we assume to have only one mode (i.e. Einstein mode). The electron description remains in terms of the creation and annihilation operators c_i^\dagger, c_i on a lattice-site i .

In the derivation of the path integral, a system's quantum statistical partition function may be obtained by inserting successive resolutions of identity within the definition of a quantum trace. In the limit of an infinite number of insertions, the Trotter-Suzuki expression [33, 34] gives a direct equality between this discretised partition function Z_M and the full partition function Z :

$$\begin{aligned} Z &\equiv \text{Tr}\left\{e^{-\beta H}\right\} = \lim_{M \rightarrow \infty} Z_M, \\ Z_M &= \text{Tr}\left\{\left[e^{-\Delta\tau H_0} e^{-\Delta\tau H_1} e^{\Delta\tau H_2}\right]^M\right\}, \end{aligned} \quad (3.19)$$

where $\Delta\tau = \beta/M$ is the amount of imaginary-time between time-slices.

For the case of a lattice polaron, we have the time-discretised partition function,

$$Z_M = c_1 \Delta\tau^{-\frac{MN}{2}} \sum_{\{r_j\}} \int \left\{ \prod_{j=1}^M \prod_{n=1}^N dx_{n,j} \right\} e^{S_{ph}} \prod_{l=1}^M I_{\Delta r_l}(2\tau J), \quad (3.20)$$

where $\Delta r_l = r_{l+1} - r_l$ is the change in the electron position across one time-slice.

The discretised boson action is,

$$S_{ph} = \sum_{j=1}^M \sum_{n=1}^N \left(\frac{(\Delta x_{n,j})^2}{2\Delta\tau} + \frac{\Delta\tau\omega^2 x_{n,j}^2}{2} + \Delta\tau x_{n,j} \delta_{n,r_j} \right). \quad (3.21)$$

The kinetic portion of the discretised action for the fermion on a lattice is,

$$I_{\Delta r_l}(2\tau J) = \frac{1}{N} \sum_{n=1}^N \cos\left(\frac{2\pi n \Delta r_l}{N}\right) \exp\left(-z \cos\left(\frac{2\pi n}{N}\right)\right), \quad (3.22)$$

which is a discrete form of the modified Bessel function of the first-kind $I_m(z)$ [NIST:DLMF] where here we have $m = r_{j+1} - r_j$ and $z = 2\tau J$. This becomes the normal modified Bessel function in the thermodynamic limit $N \rightarrow \infty$.

The bosonic integrals are Gaussian and so have closed-form expressions. By expanding the bosonic coordinates in Fourier modes,

$$x_{n,j} = \frac{1}{\sqrt{M}} \sum_{k=0}^{M-1} v_{n,j} \exp\left(\frac{2\pi j k}{M}\right), \quad (3.23)$$

we can diagonalise the bosonic action,

$$S_{ph} = \sum_{n=1}^N \sum_{k=0}^{M-1} \left(\frac{|v_{n,j}|^2}{\Delta\tau D_k^{-1}} + \frac{\Delta\tau\lambda v_{n,k}}{\sqrt{M}} \sum_{j=1}^M \delta_{n,r_j} \exp\left(\frac{2\pi j k}{M}\right) \right), \quad (3.24)$$

where

$$D_k^{-1} = 1 - \cos\left(\frac{2\pi k}{M}\right) + \frac{\Delta\tau^2 \omega_0^2}{2}, \quad (3.25)$$

is the inverse of the free-phonon Green function. Integrating over $v_{n,k}$ gives.

$$\begin{aligned} Z_M &= c_2 Z_M^{ph} Z_M^{el}, \\ Z_M^{ph} &= \left(\prod_{k=0}^{M-1} D_k^{1/2} \right)^N, \\ Z_M^{el} &= \sum_{\{r_j\}} \left(\prod_{j=1}^M I_{\Delta r_j}(2\Delta\tau J) \right) \exp\left(\Delta\tau^2 \sum_{i=1}^M \sum_{j=1}^M F(i-j) \delta_{r_i, r_j}\right), \end{aligned} \quad (3.26)$$

where c_2 is just a collation of normalisation factors which will drop out of any expectation values and,

$$F(l) = \frac{\Delta\tau\lambda^2}{4M} \sum_{k=0}^{M-1} D_k \cos\left(\frac{2\pi k l}{M}\right), \quad (3.27)$$

is the memory function that fully encodes the electron-lattice interaction over all imaginary times.

3.2.2 Continuous-Time Path Integral

To obtain the continuous-time limit of the partition function, it is necessary to explicitly take out the summation over N lattice sites in the kinetic action. Doing so, we find that we have a product of this lattice-site summation for each time

slice,

$$Z_M^{el} = \frac{1}{(2N)^M} \sum_{\{r_j\}} \sum_{\{n_j\}} \exp \left\{ i \sum_{j=1}^M \frac{2\pi n_j}{N} \Delta r_j - z \sum_{j=1}^M \cos \left(\frac{2\pi n_j}{N} \right) \right\}, \quad (3.28)$$

since the cosine is even, we expanded it into phases and changed the limits of the n_j summations from $-N$ to N . It should be noted that the summations over n_j exclude $n_j = 0$. This is just a summation of all possible paths a particle can take on the lattice within M time-steps. From the kinetic action, we can also see that $2\pi n_j/N$ plays the role of a discrete lattice-momenta multiplying the changes in the electron's position Δr_j . The electronic partition function has become a discrete phase-space path integral. Therefore, in the continuous-time limit, the partition function may be written as,

$$Z = \mathcal{N} Z_B \sum_{r(\tau)} \sum_{n(\tau)} \exp\{S_{\text{eff}}\}, \quad (3.29)$$

where \mathcal{N} is just the accumulation of normalisation factors. The effective action is now given by,

$$\begin{aligned} S_{\text{eff}} &= K[n(\tau), r(\tau)] + V_{\text{eff}}[r(\tau)], \\ K &= 2J \int_0^{\hbar\beta} d\tau \cos \left(\frac{2\pi n(\tau)}{N} \right) + \frac{2\pi i}{N} \int_0^{\hbar\beta} d\tau n(\tau) \dot{r}(\tau), \\ V_{\text{eff}} &= \frac{\hbar\lambda^2}{4\omega M} \int_0^{\hbar\beta} \int_0^{\hbar\beta} d\tau d\tau' D_{\omega_0}(\tau - \tau') \delta_{r(\tau), r(\tau')}, \end{aligned} \quad (3.30)$$

where the summations of j have become imaginary-time integrals and $\lim_{\Delta\tau \rightarrow 0} \left\{ \Delta r_j / \Delta\tau \right\} \rightarrow dr(\tau) / d\tau$. Here $D_{\omega}(\tau)$ is the thermal (imaginary-time) phonon Green function and is given by,

$$D_{\omega}(\tau) = \coth \left(\frac{\hbar\beta\omega}{2} \right) \cosh(\omega\tau) - \sinh(\omega\tau). \quad (3.31)$$

In the thermodynamic limit, the summation over all discrete r and n paths become continuous and can be identified with the usual electron position $r(\tau)$ and electron quasi-momentum in the lattice $2\pi n(\tau)/N \rightarrow k(\tau)$. The discrete sums over r and n become continuous path integrals with position paths confined to the unit cell and quasi-momentum paths confined to the first Brillouin Zone,

$$Z = \mathcal{N} Z_B \int_{r \in V} \mathcal{D}r(\tau) \int_{k \in 1BZ} \mathcal{D}k(\tau) e^{S_{\text{eff}}}, \quad (3.32)$$

where the effective potential action is as above, but the kinetic action is now,

$$K = 2J \int_0^{\hbar\beta} d\tau \cos(ak(\tau)) + i \int_0^{\hbar\beta} d\tau k(\tau) \dot{r}(\tau), \quad (3.33)$$

where a is the lattice constant. This partition function is just the standard representation of the phase-space path integral,

$$Z = \int \mathcal{D}r(\tau) \int \mathcal{D}k(\tau) \exp \left[i \int_0^{\hbar\beta} d\tau k(\tau) \dot{r}(\tau) - \int_0^{\hbar\beta} d\tau H(r(\tau), k(\tau)) \right], \quad (3.34)$$

where the Hamiltonian is that of the tight-binding Hamiltonian with an additional non-local effective interaction term. In fact, we could have started with this phase-space path integral, substituted the Holstein Hamiltonian and performed the path integration over the lattice coordinates to arrive at the same result.

It is then clear how to generalise to higher dimensions by substituting the higher-dimensional variants of the tight-binding Hamiltonian. The effective interaction term will be similar but with a generalised Kronecker-Delta dependent on vector positions $r(\tau)$.

We still face difficulty when it comes to applying the variational method. The presence of the cosine in the kinetic action renders the overall action non-convex, even in imaginary time, so using Jensen's inequality would be invalid. To continue, we assume that the electron quasi-momentum is small $k \ll 1$, so we may make a parabolic effective-mass approximation. With $k \ll 1$, we can expand the cosine,

$$\cos(ak(\tau)) \approx 1 - \frac{a^2 [k(\tau)]^2}{2}, \quad (3.35)$$

so that the kinetic action is approximated by,

$$K = 2J\hbar\beta - \frac{m_b}{2} \int_0^{\hbar\beta} d\tau [k(\tau)]^2 + i \int_0^{\hbar\beta} d\tau k(\tau) \dot{r}(\tau), \quad (3.36)$$

where the band-mass is $m_b = \hbar^2/2Ja^2$. By making this approximation, the functional integral over $k(\tau)$ is the same Gaussian form as for a free particle and can be solved exactly. Overall, we get an effective Holstein action:

$$S_{\text{eff}}^{(H)} = \frac{m_b^{(H)}}{2} \int_0^{\hbar\beta} d\tau \dot{\mathbf{r}}^2 - \frac{\lambda^2}{4\omega M} \int_0^{\hbar\beta} \int_0^{\hbar\beta} d\tau d\tau' D(\tau - \tau') \delta_{\mathbf{r}(\tau), \mathbf{r}(\tau')} \cdot \quad (3.37)$$

It's important to reiterate the approximations made to arrive at this action. First, we went to the thermodynamic limit, which means we do not expect this model

to capture any finite-size effects. Secondly, we approximated the tight-binding-like band structure with a parabolic band centred at $\mathbf{k} = 0$. Whilst this may be a good approximation close to the band minimum, we have made a third approximation where we assumed that the electron momentum is unbounded as if it were free, albeit with an effective band mass. So, we can predict that this model will likely exclude any lattice effects concerning the electron, such as explicit hopping between lattice sites. Nonetheless, compared to the Fröhlich model, we have gained a different short-range electron-phonon coupling that is isolated to the currently occupied lattice site. Upon integrating out the phonons, this transforms into a non-local point-like interaction of the electron with itself through imaginary time, which is only non-zero when the electron crosses its prior path. The other feature gained is that since we have a Kronecker-delta-like interaction, the phonon momentum is bound to remain within the first Brillouin zone. This can be seen from the integral representation of the Kronecker delta:

$$\delta_{r,r'} = \frac{a}{2\pi} \int_0^{2\pi/a} dq e^{iq(r-r')}. \quad (3.38)$$

Therefore, as far as the phonons are concerned, we include a description of the lattice. We can generalise the Kronecker-delta to arbitrary dimensions n in Cartesian coordinates:

$$\delta_{\mathbf{r},\mathbf{r}'} = \frac{V_n}{(2\pi)^n} \int_0^{2\pi/a} d\mathbf{q} e^{i\mathbf{q}\cdot(\mathbf{r}-\mathbf{r}')}, \quad (3.39)$$

where for example for a cubic unitcell $V_3 = a^3$. However, to maintain a close analogy to the methodology used by Feynman for the Fröhlich Hamiltonian, we choose to use a Spherical coordinate representation of the Kronecker-delta in n -dimensions:

$$\delta_{\mathbf{r},\mathbf{r}'} = \frac{V_n |S^{n-1}|}{(2\pi)^n} \int_0^{\Lambda_n} dq q^{n-1} e^{iq(r-r')}, \quad (3.40)$$

where Λ_n is some momentum cutoff. We assume that the system has rotational invariance so that the angular components of $\mathbf{q} \cdot \mathbf{r}$ can be integrated over to give $|S^{n-1}| = 2\pi^{n/2}/\Gamma(n/2)$ the surface-“area” of an n -dimensional sphere where $\Gamma(x)$ is the Gamma function.

We now have everything we need to establish the general machinery for a variational method for polaron models.

3.3 Beyond the Parabolic Approximation

3.3.1 Naïve effective-mass anisotropy

In the degenerate anisotropic uni-axial case, I propose to naïvely incorporate the anisotropy into the Feynman approach (which is one-dimensional due to the underlying isotropy of the Fröhlich Hamiltonian) by treating the two directions independently with effective masses m_{\perp} and m_z .

I then use the variational principle separately in each direction to find the variational parameters $v_{\perp/z}$ and $w_{\perp/z}$ that give the lowest upper-bound to the ground-state energy $E_{\perp/z}$ for each direction.

The variational parameters can then be used to obtain the effective polaron masses $m_{P,\perp}^{*F}$ and $m_{P,z}^{*F}$ using Eq. (2.114) and polaron radii $r_{P\perp}$ and r_{Pz} using Eq. (2.105).

To make comparisons with the isotropic case, I define an effective ground-state energy by taking the arithmetic mean of the uniaxial components of the ground-state energy,

$$E = \frac{2E_{\perp} + E_z}{3}. \quad (3.41)$$

Similarly, I define an effective radius of the anisotropic polaron by finding the radius of a sphere with the same volume as the ellipsoidal anisotropic polaron. This means taking the geometric mean of the uni-axial components of the polaron radius,

$$r_P = \left(r_{P\perp}^2 r_{Pz} \right)^{1/3}. \quad (3.42)$$

The two averaging methods are justified as they are the only methods found to give a ground-state energy and polaron radius consistent with those evaluated by the original model, [1], when applied to an isotropic material.

3.4 The General Polaron

The Hamiltonian for a general polaron model [35] can be written in second-quantisation form and momentum-basis as,

$$H = \sum_{\mathbf{k}} \epsilon_{\mathbf{k}} c_{\mathbf{k}}^\dagger c_{\mathbf{k}} + \sum_{\mathbf{q}} \hbar \omega_{\mathbf{q}} b_{\mathbf{q}}^\dagger b_{\mathbf{q}} + \sum_{\mathbf{k},\mathbf{q}} V_{\mathbf{k},\mathbf{q}} c_{\mathbf{k}+\mathbf{q}}^\dagger c_{\mathbf{k}} (b_{-\mathbf{q}}^\dagger + b_{\mathbf{q}}) \quad (3.43)$$

where $\epsilon_{\mathbf{k}}$ is the electron band energy for momentum \mathbf{k} , $c_{\mathbf{k}}^\dagger$ and $c_{\mathbf{k}}$ are the electron creation and annihilation operators for an electron with momentum \mathbf{k} , $\omega_{\mathbf{q}}$ is the phonon frequency for momentum \mathbf{q} , $b_{\mathbf{q}}^\gamma$ and $b_{\mathbf{q}}$ are the phonon creation and annihilation operators for a phonon with momentum \mathbf{q} , $V_{\mathbf{k},\mathbf{q}}$ is the electron-phonon coupling matrix which describes the strength of the interaction.

For a model describing a parabolic band electron linearly coupled to harmonic phonons, the path integral over the phonon operators is Gaussian and can be evaluated analytically. The resultant electron action describes a temporally non-local self-interaction acting on the electron,

$$S_{\text{pol}}[\mathbf{r}(\tau)] = \frac{m_b}{2} \int_0^{\hbar\beta} d\tau \dot{\mathbf{r}}^2(\tau) - \frac{1}{4M\omega_0} \int_0^{\hbar\beta} d\tau \int_0^{\hbar\beta} d\tau' D_{\omega_0}(|\tau - \tau'|) \Phi [\mathbf{r}(\tau), \mathbf{r}(\tau')] , \quad (3.44)$$

where $D_{\omega_0}(\tau)$ is the imaginary-time thermal phonon propagator and self-interaction functional is:

$$\Phi [\mathbf{r}(\tau), \mathbf{r}(\tau')] = \sum_{\mathbf{q}} |V_{\mathbf{q}}|^2 \rho_{\mathbf{q}} [\mathbf{r}(\tau)] \rho_{-\mathbf{q}} [\mathbf{r}(\tau')] . \quad (3.45)$$

Here $\rho_{\mathbf{q}}[\mathbf{r}(\tau)] = e^{i\mathbf{q}\cdot\mathbf{r}(\tau)}$ is the density for the electron derived from corresponding first-quantisation density operator.

For the Fröhlich model, the self-interaction functional is,

$$\begin{aligned} \Phi^{(F)} [\mathbf{r}(\tau), \mathbf{r}(\tau')] &= \sum_{\mathbf{q}} \frac{g_F^2(n)}{V q^{n-1}} e^{i\mathbf{q}\cdot(\mathbf{r}(\tau)-\mathbf{r}(\tau'))}, \\ &= g_F^2(n) \int \frac{d^n q}{(2\pi)^n} \frac{e^{i\mathbf{q}\cdot(\mathbf{r}(\tau)-\mathbf{r}(\tau'))}}{q^{n-1}}, \\ &= \frac{g_F^2(n) |S^{n-1}|}{(2\pi)^n} \frac{1}{|\mathbf{r}(\tau) - \mathbf{r}(\tau')|}, \end{aligned} \quad (3.46)$$

where $|S^{n-1}| = 2\pi^{n/2}/\Gamma(n/2)$ is the hypervolume of the unit $(n-1)$ -sphere and the phonon momentum is unbounded, $0 \leq |\mathbf{q}| < \infty$. The Fröhlich model makes the continuum approximation of the lattice, $\lim_{V \rightarrow \infty} V^{-1} \sum_{\mathbf{q}} \sim \int d^n q / (2\pi)^n$, where V is the n -dimensional crystal volume.

For the Holstein model, the self-interaction functional is:

$$\begin{aligned}\Phi^{(H)} [\mathbf{r}(\tau), \mathbf{r}(\tau')] &= g_H^2(n) \sum_{\mathbf{q}} e^{i\mathbf{q} \cdot (\mathbf{r}(\tau) - \mathbf{r}(\tau'))}, \\ &= g_H^2(n) V \int \frac{d^n q}{(2\pi)^n} e^{i\mathbf{q} \cdot (\mathbf{r}(\tau) - \mathbf{r}(\tau'))}, \\ &= g_H^2(n) \delta_{\mathbf{r}(\tau), \mathbf{r}(\tau')}^n,\end{aligned}\quad (3.47)$$

where δ_{ij}^n is the n -dimensional Kronecker Delta function and $0 \leq |\mathbf{q}| \leq \Lambda_n$ where Λ_n is a momentum cutoff given by the radius of an n -ball with volume $\frac{(2\pi)^n}{V}$:

$$\Lambda = 2\sqrt{\pi} \left(V \Gamma \left(\frac{n}{2} + 1 \right) \right)^{1/n}. \quad (3.48)$$

We can now develop the variational path integral method for this generalised polaron action and specialise to a specific case by using an explicit expression for the electron-phonon coupling in the self-interaction functional as we have above for the Fröhlich and Holstein models. We will assume that we are only working with one parabolic-band electron so that the self-interaction functional contains depends on the electron position only through the term $e^{i\mathbf{q} \cdot (\mathbf{r}(\tau) - \mathbf{r}(\tau'))}$. If this is true, we can use Feynman's derivation of the variational path integral method.

3.4.1 General Phonon-Band Polarons

We now have general expressions for the free energy, complex conductivity and DC mobility for a whole class of polaron models. Before specialising in the Fröhlich and Holstein models, I'd like to discuss the potential for more ab initio numerical work.

The momentum integral can be evaluated numerically, either by substituting an explicit form for the electron-phonon matrix $|V_q|^2$ and phonon dispersion ω_q and then using a numerical integration algorithm like Gauss-Kronod. Many analytical forms are known for these as functions of q , such as for acoustic phonons, Bogoliubov-Fröhlich polaron, impurities, etc.

On the other hand, we could instead use other more 'ab initio' methods, such as Density Functional Theory (DFT), to obtain $|V_q|^2$ and ω_q . These would then enter the variational method as vectors of q -points evaluated at the electron/hole band-extremum (e.g. the gamma-point $\mathbf{k} = 0$). The above q -integrands would then become vector/matrix products that are then concatenated over all q -points.

3.4.2 General Polaron Action

Excluding spin and phonon branches, we may write the general polaron Hamiltonian:

$$H_{\text{polaron}} = \sum_{\mathbf{k}} \epsilon_{\mathbf{k}} c_{\mathbf{k}}^\dagger c_{\mathbf{k}} + \sum_{\mathbf{q}} \hbar \omega_{\mathbf{q}} b_{\mathbf{q}}^\dagger b_{\mathbf{q}} + \sum_{\mathbf{k}, \mathbf{q}} V_{\mathbf{k}, \mathbf{q}} c_{\mathbf{k}+\mathbf{q}}^\dagger c_{\mathbf{k}} (b_{-\mathbf{q}}^\dagger + b_{\mathbf{q}}) \quad (3.49)$$

Propose a trial Hamiltonian where we uncorrelated the electron and phonon momenta:

$$H_{\text{trial}} = \sum_{\mathbf{k}} \epsilon_{\mathbf{k}} c_{\mathbf{k}}^\dagger c_{\mathbf{k}} + \sum_{\mathbf{q}} \hbar \Omega_{\mathbf{q}} b_{\mathbf{q}}^\dagger b_{\mathbf{q}} + \sum_{\mathbf{k}, \mathbf{q}} M_{\mathbf{k}, \mathbf{q}} c_{\mathbf{k}}^\dagger c_{\mathbf{k}} (b_{-\mathbf{q}}^\dagger + b_{\mathbf{q}}) \quad (3.50)$$

where $\Omega_{\mathbf{q}}$ and $M_{\mathbf{k}, \mathbf{q}}$ will be variational parameters.

The coherent state path integral for the polaron Hamiltonian H_{polaron} :

$$Z_{\text{polaron}} = \int D[\bar{c}, c] \int D[\bar{b}, b] e^{-S_{\text{el}}[\bar{c}, c] - S_{\text{ph}}[\bar{b}, b] - S_{\text{el-ph}}[\bar{c}, c, \bar{b}, b]} \quad (3.51)$$

with the free-electron action:

$$S_{\text{el}} [\bar{c}, c] = \sum_{\mathbf{k}} \int_0^{\hbar \beta} d\tau \bar{c}_{\mathbf{k}}(\tau) [\partial_\tau - \epsilon_{\mathbf{k}} - \mu] c_{\mathbf{k}}(\tau) \quad (3.52)$$

the free-phonon action:

$$S_{\text{ph}} [\bar{b}, b] = \sum_{\mathbf{q}} \int_0^{\hbar \beta} d\tau \bar{b}_{\mathbf{q}}(\tau) [\partial_\tau - \omega_{\mathbf{q}}] b_{\mathbf{q}}(\tau) \quad (3.53)$$

and the electron-phonon interaction action:

$$\begin{aligned} S_{\text{el-ph}} [\bar{c}, c, \bar{b}, b] &= \sum_{\mathbf{k}, \mathbf{q}} V_{\mathbf{k}, \mathbf{q}} \int_0^{\hbar \beta} d\tau \bar{c}_{\mathbf{k}+\mathbf{q}}(\tau) c_{\mathbf{k}}(\tau) b_{\mathbf{q}}(\tau) \\ &\quad + \sum_{\mathbf{k}, \mathbf{q}} V_{\mathbf{k}, \mathbf{q}} \int_0^{\hbar \beta} d\tau \bar{b}_{-\mathbf{q}}(\tau) \bar{c}_{\mathbf{k}+\mathbf{q}}(\tau) c_{\mathbf{k}}(\tau) \end{aligned} \quad (3.54)$$

The phonon contribution to the action is quadratic and may be integrated to give:

$$Z_{\text{ph}}^0 \exp \left\{ \frac{1}{2} \sum_{\mathbf{q}, \mathbf{k}, \mathbf{k}'} V_{\mathbf{k}, \mathbf{q}} V_{\mathbf{k}', \mathbf{q}}^* \int_0^{\hbar\beta} \int_0^{\hbar\beta} d\tau d\tau' \bar{c}_{\mathbf{k}}(\tau) c_{\mathbf{k}-\mathbf{q}}(\tau) D_{\omega_{\mathbf{q}}}^0(\tau - \tau') \bar{c}_{\mathbf{k}'-\mathbf{q}}(\tau') c_{\mathbf{k}'}(\tau') \right\} \quad (3.55)$$

where $D_{\omega_{\mathbf{q}}}^0(\tau)$ is the bare phonon kernel for a harmonic oscillator and $Z_{\text{ph}}^0 = \det \{D^0\}^{-1/2}$ is the non-interacting phonon partition function.

The coherent state path integral for the polaron Hamiltonian H_{polaron} :

$$Z_{\text{polaron}} = \int D\bar{c} Dc \exp \left\{ -S_{\text{polaron}} [\bar{c}(\tau), c(\tau)] \right\} \quad (3.56)$$

with action:

$$\begin{aligned} S_{\text{polaron}} [\bar{c}(\tau), c(\tau)] &= \sum_{\mathbf{k}} \int_0^{\hbar\beta} d\tau \bar{c}_{\mathbf{k}}(\tau) [\partial_{\tau} - \epsilon_{\mathbf{k}} - \mu] c_{\mathbf{k}}(\tau) \\ &- \sum_{\mathbf{k}, \mathbf{q}} \frac{|V_{\mathbf{k}, \mathbf{q}}|^2}{2} \int_0^{\hbar\beta} \int_0^{\hbar\beta} d\tau d\tau' \bar{c}_{\mathbf{k}}(\tau) c_{\mathbf{k}+\mathbf{q}}(\tau) D_{\omega_{\mathbf{q}}}^0(\tau - \tau') \bar{c}_{\mathbf{k}+\mathbf{q}}(\tau') c_{\mathbf{k}}(\tau') \end{aligned} \quad (3.57)$$

CHAPTER 4

IMPROVING THE TRIAL PATH INTEGRAL MODEL & VARIATIONAL SOLUTION

What is the meaning of life?

—John Doe, *Thoughts*, 1971

This is the introduction paragraph.

4.1 Multiple Fictitious Particles

The first way to improve the trial action is to couple the electron to more than one fictitious particle, each with their respective mass and spring-constant that enter as multiple pairs of variational parameters in the model. This has been done before for one additional fictitious mass [36].

I have extended Feynman's trial action to represent a particle (the charge-carrier) coupled to n massive fictitious particles. This results in $2 \times n$ variational parameters (one for the coupling strength and one for the coupling frequency of each fictitious particle).

The generalised polaron trial action is,

$$S_0[\mathbf{r}(\tau)] = \frac{m_b}{2} \int_0^{\hbar\beta} d\tau \left(\frac{d\mathbf{r}(\tau)}{d\tau} \right)^2 + \frac{1}{8} \sum_{p=1}^n \kappa_p w_p \int_0^{\hbar\beta} d\tau \int_0^{\hbar\beta} d\sigma D_{w_p}(|\tau - \sigma|) (\mathbf{r}(\tau) - \mathbf{r}(\sigma))^2. \quad (4.1)$$

Here κ_p is the spring constant associated with the p th fictitious particle, and w_p is the corresponding oscillation frequency. The solution to the partition function for this action was evaluated in [23].

Following Feynman, I extend Hellwarth and Biaggio's A and C equations (Eqs. (62b) and (62e) in Ref. [14]), which are symmetrised (for ease of computation) versions of the finite temperature polaron actions of Ōsaka [11],

$$A = \frac{3}{\hbar\beta m} \left[\sum_{p=1}^n \log \left(\frac{v_p \sinh(w_p \hbar\beta/2)}{w_p \sinh(v_p \hbar\beta/2)} \right) + \frac{1}{2} \log(2\pi\hbar\beta) \right], \quad (4.2a)$$

$$C = \frac{3}{m} \sum_{p,q=1}^n \frac{C_{pq}}{v_q w_p} \left(\coth\left(\frac{v_q \hbar\beta}{2}\right) - \frac{2}{v_q \hbar\beta} \right). \quad (4.2b)$$

With,

$$C_{pq} = \frac{w_p}{4} \frac{\kappa_p h_q}{v_q^2 - w_p^2}, \quad (4.3a)$$

$$\kappa_p = (v_p^2 - w_p^2) \prod_{\substack{q=1 \\ q \neq p}}^n \frac{v_q^2 - w_p^2}{w_q^2 - w_p^2}, \quad (4.3b)$$

$$h_p = (v_p^2 - w_p^2) \prod_{\substack{q=1 \\ q \neq p}}^n \frac{w_q^2 - v_p^2}{v_q^2 - v_p^2}. \quad (4.3c)$$

C_{pq} are the components of a generalised ($n \times n$) matrix version of Feynman's C variational parameter. The cross (off-diagonal) terms give the coupling (interaction) between the fictitious particles.

A generalisation of the expression in the denominator of Hellwarth and Biaggio's B equation (Eqn. (62c) in [14]) is,

$$G(\tau) = \tau \left(1 - \frac{\tau}{\hbar\beta} \right) + \sum_{p=1}^n \frac{h_p}{v_p^3} \left(D_{v_p}(0) - D_{v_p}(\tau) - v_p \tau \left(1 - \frac{\tau}{\hbar\beta} \right) \right). \quad (4.4)$$

When $n = 1$ (a single fictitious particle) and $x \rightarrow iu$, $G(\tau)$ is the same as $D(u)$ from Eqn. (35c) in the FHIP [2] mobility theory.

From this trial Green function $G(\tau)$ we arrive at a generalisation to Hellwarth and Biaggio's B expression with multiple (n with index p) variational parameters v_p and w_p ,

$$B = \frac{\alpha\omega_0}{\sqrt{\pi}} \int_0^{\frac{\hbar\beta}{2}} d\tau D_{\omega_0}(\tau) [G(\tau)]^{-\frac{1}{2}}. \quad (4.5)$$

Summing the trial free energy A in Eqn. (4.2a), the trial-model interaction B in Eqn. (4.5), and the trial action C in Eqn. (4.2b), we obtain a generalised variational inequality for the contribution to the free energy of the polaron from $2n$ variational parameters v_p, w_p ,

$$F(\beta) \leq -\hbar\omega_0(A + C + B). \quad (4.6)$$

Here, I have written out the expression explicitly rather than using 'polaron' units.

We obtain vectors of length n for the variational parameters v_p and w_p that correspond to these minima, which will be used in evaluating the polaron mobility. Considering only two variational parameters ($n = 1$) simplifies Hellwarth and Biaggio's form of Ōsaka's free energy. Feynman's original athermal version can then be obtained by taking the zero-temperature limit ($\beta \rightarrow \infty$).

Our derivation supports a set of normal modes for the polaron quasi-particle model (multiple v_p and w_p parameters).

4.1.1 Numerical Results

In this section, I present my numerical investigations into the result of the trial model generalised to multiple fictitious particles in the case of the Fröhlich polaron model. Adding more fictitious particles adds two more variational parameters per particle to the trial model, representing the mass and frequency (or alternatively the spring constant) of each new particle coupled to the electron. These can be transformed into corresponding v_p and w_p parameters where p labels each fictitious particle. The ordering of these parameters can be fixed such that $v_1 > w_1 > v_2 > w_2 > \dots$. Due to the additional computational difficulty in converging the variational solution, I only present the results up to $N = 4$ additional fictitious particles. I found that converging these results became increasingly difficult as my initial guess had to be reasonably close to the actual optimal result otherwise, the optimisation easily converged instead to other local

minima or forced one or more of the fictitious particles to become infinite massive by collapsing the variational parameters $w \rightarrow 0, v \rightarrow \infty$. Likewise, the size of the optimisation box grew exponentially, making it harder to constrain the optimisation.

It is known that the Feynman variational result cannot obtain the true weak-coupling perturbative result. At small alpha α , Feynman's one fictitious mass model gives the weak coupling expansion for the polaron energy:

$$\frac{E}{\hbar\omega_0} = -\alpha - 0.0123\alpha^2. \quad (4.7)$$

It is known that using a general memory function in the trial model and finding its optimal form results in a α^2 coefficient 0.0125978 [37]. The true perturbative weak coupling result is 0.01592. So we can see that the gains in the free energy bound, at least for the Fröhlich model, will be small. As a side note, the Feynman variational method can be improved by including higher-order corrections in the form of higher-order cumulants in the difference between the polaron and trial actions. This has been found to bring it much closer to the true solution at the cost of significantly more computation. Despite small improvements in the energy bound of the variational method, we will see that the corresponding dynamical theory sees significant changes, likely due to the high sensitivity of analytic continuation on the optimal result obtained.

4.1.2 The additional parameters

In Figs. (4.1) is the coupling-dependence of the optimal v and w parameters for the Fröhlich model, an increasing number of fictitious particles in the trial model from $N = 1$ to $N = 5$. In the top-right figure ($N = 2$), I have also co-plotted the results obtained by Abe for the two-particle model in Ref. [36].

Notably, the first fictitious particle seems to follow a different trend for w , which asymptotes to $w = \omega_0$ at strong coupling, compared to any other additional particles where w follows a similar coupling dependence as the v parameter. As we add more particles, the v and w corresponding to each additional particle become exponentially larger, whilst the previous v and w parameters decrease slightly. The gap between v and w for each additional particle becomes significantly smaller until it is unperceivable in the plots. This suggests that each successive particle becomes exponentially lighter but with a larger spring constant. When we look at the energy, we will see that each additional particle contributes diminishingly to the system's free energy.

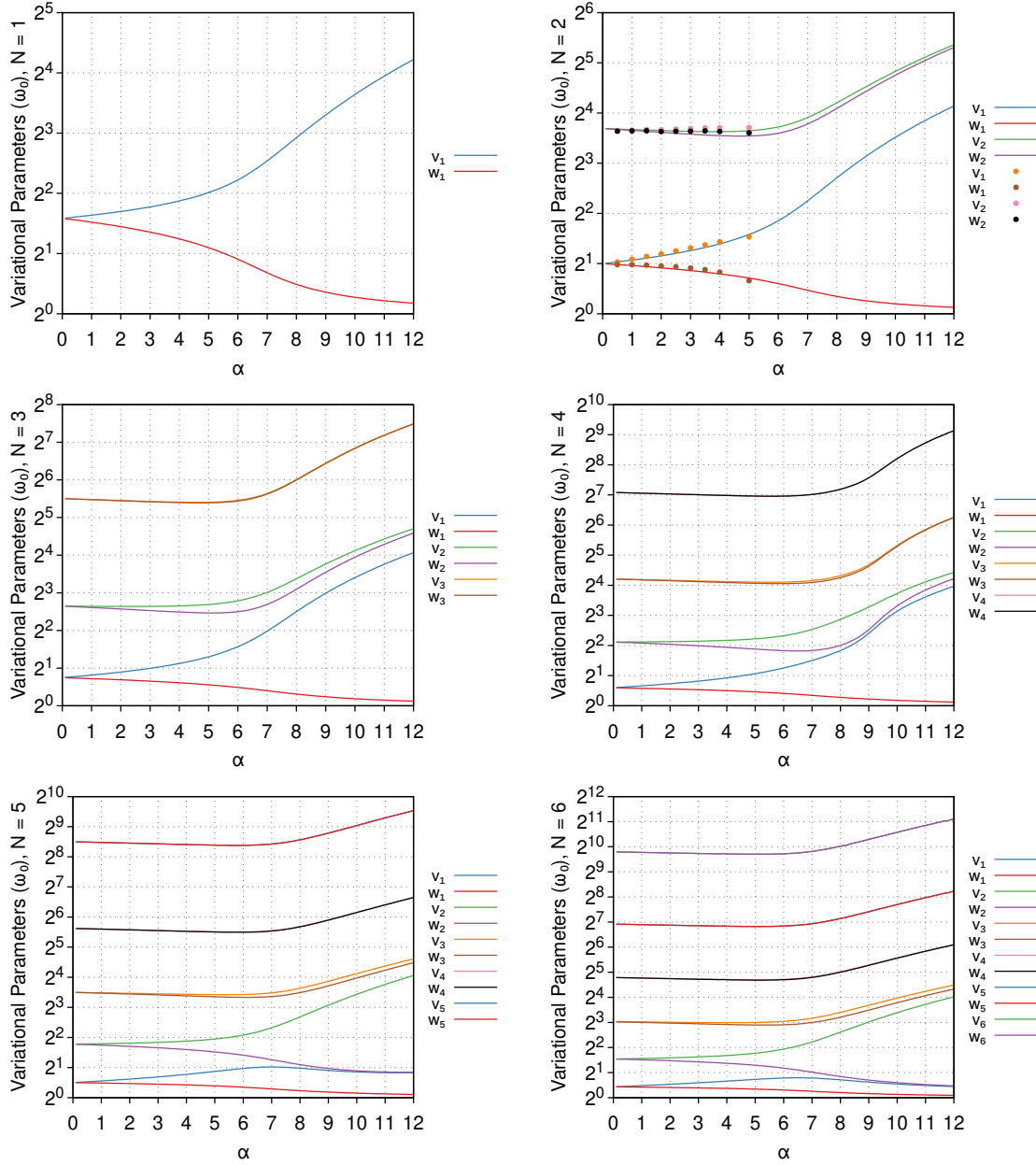


Figure 4.1: Successive optimal values of pairs of variational parameters v_i and w_i for the Fröhlich model, corresponding to additional fictitious particles in the trial model for a range of dimensionless electron-phonon $\alpha \in [0, 12]$. The first figure (**top-left**) is Feynman's original variational solution $N = 1$. The next generalisation to $N = 2$ fictitious particles (**top-right**) sees a shift down in the original v_1 and w_1 with the addition of two more v_2 and w_2 which follow a similar dependence on α as v_1 . I compare this result to those obtained for a specific $N = 2$ trial model used in Ref. [36]. The result for additional fictitious particles are shown in **middle-left** ($N = 3$), **middle-right** ($N = 4$) and **bottom** ($N = 5$). Each additional particle $N > 1$ is lighter than the last, whereas the corresponding spring constant increases conversely.

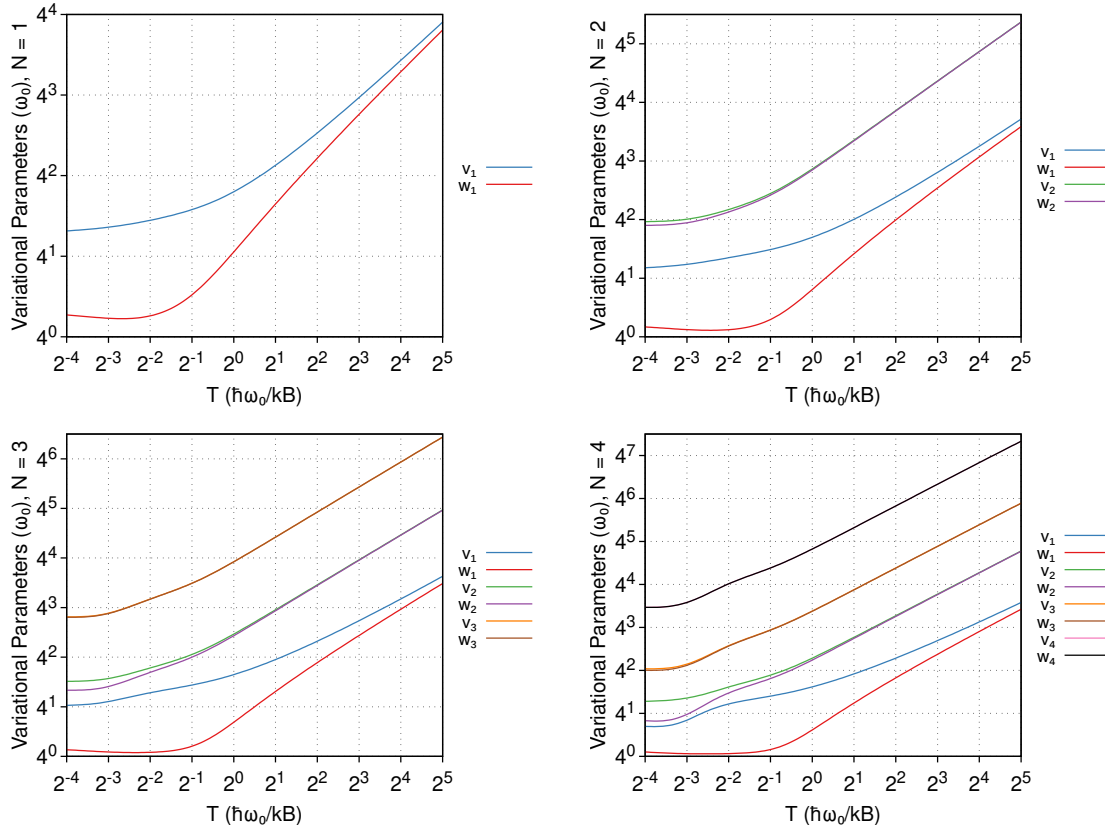


Figure 4.2: Successive optimal values of pairs of variational parameters v_i and w_i for the Fröhlich model, corresponding to additional fictitious particles in the trial model for coupling $\alpha = 6$ and a range of temperature $1/T \in [0.125\omega_0, 0.5\omega_0, 2.0\omega_0, 8.0\omega_0, 32.0\omega_0, 128.0\omega_0]$. The first figure (**top-left**) is Feynman's original variational solution $N = 1$. The result for additional fictitious particles are shown in **top-right** ($N = 2$), **bottom-left** ($N = 3$) and **bottom-right** ($N = 4$). Each v_i appears to reach a low plateau for $\beta\omega_0 > 8$ whereas each w_i appears to have a minimum around $\beta\omega_0 \approx \alpha = 6$.

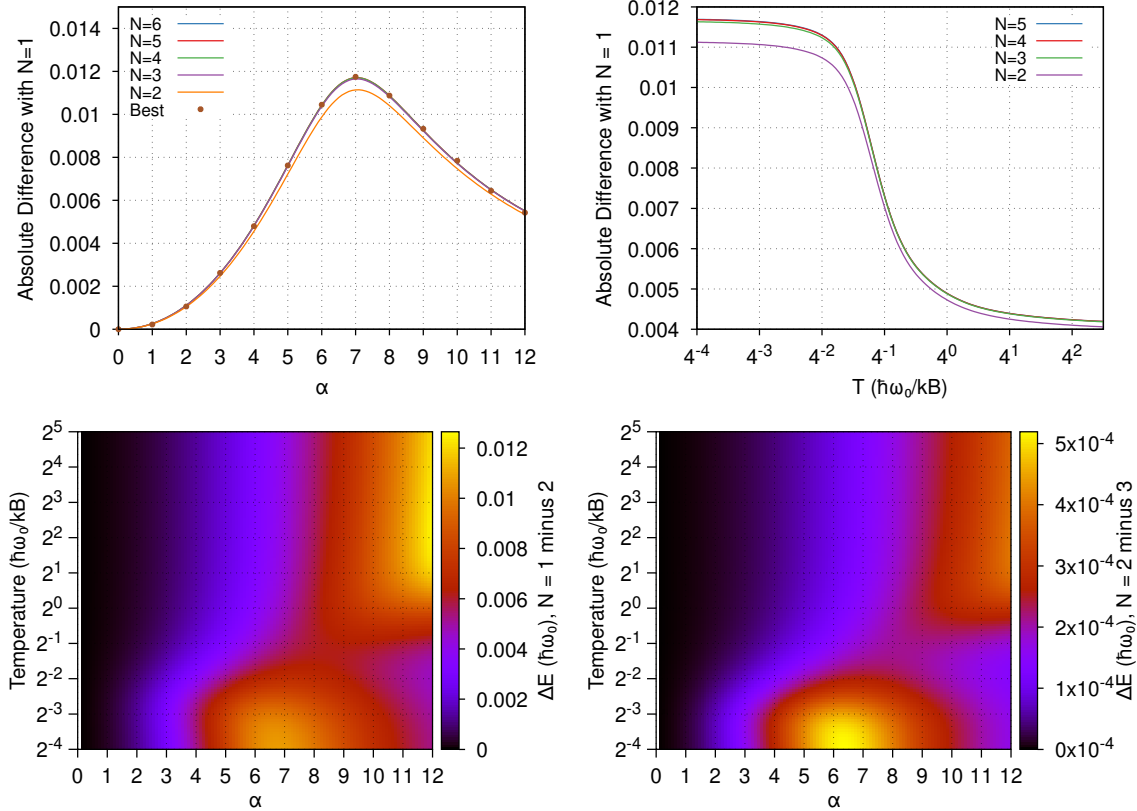


Figure 4.3: Polaron free energy for the Fröhlich model for increasing number N of fictitious particles in the trial model. **Top-left** Absolute change in the free energy for $N > 1$ compared to the free energy result for $N = 1$. The generalised trial models quickly converge to the optimal free-energy bound, with the greatest improvement on Feynman's original trial model seen around $\alpha = 7$. **Top-right** A complementary result to the first figure obtained in Ref by using a general spectral function corresponding to the $N \rightarrow \infty$ limit. By comparison, I can see that only a few fictitious particles are needed to converge to the best possible variational solution. **Bottom-left:** The temperature-dependence of the percentage improvement of additional fictitious particles compared to just one. The most improvement appears around $\beta\omega_0 \approx 8$ of 0.16%, after which the improvement plateaus. **Bottom-right:** Similar to the previous figure, the percentage improvement is relative to the previous number of fictitious particles (e.g. $N = 3$ compared to $N = 2$). Any improvements peak at $\beta\omega_0 \geq 8$ and exponentially decrease with the addition of more particles, showing a rapid convergence to the optimal trial solution.

In Figs. (4.2) is the temperature-dependence of the optimal v and w parameters for the Fröhlich model, an increasing number of fictitious particles in the trial model from $N = 1$ to $N = 4$. Each v_p and $w_{p>2}$ appears to reach a low plateau for $\beta\omega_0 > 8$ whereas the first w_1 appears to have a minimum around $\beta\omega_0 \approx \alpha = 6$ before increasing to a plateau. This suggests that the trial model eventually becomes insensitive to changes in temperature below some critical temperature.

4.1.3 Improving the Energy Bound

In Figs. (4.3) the top-left figure shows the relative shift in the free energy for $N > 1$ compared to the free energy result for $N = 1$ as a function of the electron-phonon coupling from $\alpha = 1$ to $\alpha = 12$. Two key observations are: firstly, the largest improvement to the free energy bound can be seen at intermediate coupling around $\alpha \approx 7$. Secondly, there is rapid convergence to the optimal free energy bound with no discernible difference between the results for $N = 3$, $N = 4$ and $N = 5$ fictitious particles. The two asymptotes are given by $3 \times 10^{-4}\alpha^2$ at lower coupling and $0.81\alpha^{-2}$ at higher coupling. The top-right figure is borrowed from Fig. 3 in [38] in which Dries Sels obtained the optimal result for the Feynman polaron model by using a general bath spectrum in the trial action, which corresponds to the $N \rightarrow \infty$ limit of our many fictitious particle trial action. Comparison with our results shows that we have obtained the correct optimal trial solution and that only $N = 3$ fictitious particles are required to do so, which is computationally tractable compared to more particles or a self-consistent approach with a general bath spectrum.

The lower figures in Figs.!(4.3) show the temperature dependence of the percentage improvement of additional fictitious particles compared to just one. The bottom-left figure shows that the maximum improvement to the free energy bound is obtained around $\beta\omega_0 = 8$, which is the temperature when w_1 takes its minimum value. At lower temperatures, the improvement slightly decreases before plateauing. The bottom-right figure shows the percentage improvement relative to the previous number of fictitious particles (e.g., $N = 3$ compared to $N = 2$). Here, we can see that the relative improvement in the free energy bound is exponentially decreasing with each additional particle with a maximum improvement of $N = 3$ over $N = 2$ at just 0.01%.

4.2 Lattice Polaron Variational Solution

We face two key difficulties in extending the Feynman Variational Method to lattice polarons. The first is that, unlike the path integral for the Fröhlich model, the path integral for the Holstein model is constrained. The position paths are confined to the unit cell of the lattice with periodic boundary conditions. Likewise, the quasi-momentum paths are confined to the first Brillouin zone.

Secondly, for the Fröhlich model, the kinetic part of the trial action was chosen to be identical to that of the model action. The two kinetic actions then cancel so that the final variational inequality for the polaron-free energy is independent of

the kinetic action. This is no longer possible for the Holstein model because by choosing the trial kinetic action to be the same as in the Holstein model, the trial path integral is no longer evaluable; it is no longer a Gaussian integral.

To circumnavigate these issues in pursuit of tangible results, I instead chose to approximate the Holstein kinetic action with an approximate parabolic form with an effective band mass, much like the Fröhlich model. I then allow the electron paths to be unconstrained such that the momentum integrals for the electron are unbounded and can be evaluated to give the standard Gaussian kinetic action. I could keep the momentum integrals bounded to the first Brillouin zone and still have a closed-form expression for the kinetic action; however, in addition to the standard Gaussian form, there are error functions that make it unclear how the resulting path integral could be evaluated - if it is even possible. By making these approximations, it is possible to follow the usual variational procedure with the same trial action as for the Fröhlich model. I should note that the Holstein electron-phonon interaction is still treated properly, and the phonon quasi-momenta is still confined to the first Brillouin zone.

Thus far, I have been unsuccessful in generalising the variational principle to incorporate these path constraints and non-quadratic kinetic action, but I have some ideas for how it may be approached.

The first idea is to maintain the usual trial action and obtain an additional term in the variational inequality for the polaron free energy accounting for the difference in the tight-binding-like Holstein model kinetic action and the approximate parabolic trial kinetic action. Here, the ‘electron’ mass in the trial action would be entered as a variational parameter in addition to the usual v and w parameters. The difficulty with this approach comes with calculating this additional expectation value as it is the expectation of a Modified Bessel function of the first kind with respect to the trial system. It is not clear to me if this has a closed-form expression.

The second idea is to use an entirely different representation for the path integral in terms of coherent states. Coherent state path integrals are commonly used in many-body condensed matter theory. I think the variational approximation may be derived from these coherent state path integrals, and it may allow for a more sophisticated approximation for general Hamiltonians, provided that Jensen’s inequality can still be applied.

By following the standard procedure as done for the Fröhlich model, we may derive an approximate variational inequality for the lattice polaron free energy that

fully accounts for the lattice electron-phonon integral despite allowing the electron not to be confined to individual lattice sites. Despite the latter approximation, this model still captures many of the typical features of small lattice polaron.

The variational method for the polaron developed by Feynman gives a lower upper-bound to the polaron-free energy,

$$\begin{aligned} F &\leq F_0(\beta) - \frac{1}{\hbar\beta} \langle S_{\text{pol}} - S_0 \rangle_0, \\ &\leq F_0(\beta) - \frac{1}{4\hbar\omega_0\beta M} \int_0^{\hbar\beta} d\tau \int_0^{\hbar\beta} d\tau' D_{\omega_0}(|\tau - \tau'|) \langle \Phi_{\text{pol}} - \Phi_0 \rangle_0, \end{aligned} \quad (4.8)$$

where the expectation $\langle \mathcal{O} \rangle_0$ is defined as,

$$\langle \mathcal{O} \rangle_0 \equiv \frac{\int \mathcal{D}^3 r(\tau) \mathcal{O} e^{-S_0[\mathbf{r}(\tau)]}}{\int \mathcal{D}^3 r(\tau) e^{-S_0[\mathbf{r}(\tau)]}}, \quad (4.9)$$

and $S_0[\mathbf{r}(\tau)]$ is a trial action that is chosen to approximate best the polaron model action $S_{\text{pol}}[\mathbf{r}(\tau)]$ and where the path integral for S_0 can be analytically evaluated. The trial action is typically chosen to be quadratic in the electron coordinate $\mathbf{r}(\tau)$ for this reason. We use the standard quasi-particle ‘trial action’ for the electron-phonon lattice model,

$$S_0[\mathbf{r}(\tau)] = \frac{m_b}{2} \int_0^{\hbar\beta} d\tau \dot{\mathbf{r}}^2(\tau) + \frac{w}{8\kappa} \int_0^{\hbar\beta} d\tau \int_0^{\hbar\beta} d\tau' D_w(|\tau - \tau'|) \Phi_0 [\mathbf{r}(\tau), \mathbf{r}(\tau')], \quad (4.10)$$

where κ and w are variational parameters, respectively, representing the spring constant and oscillation frequency of Feynman’s fictitious spring-mass trial model. The trial model is often reparameterised in terms of v and w variational parameters where $\kappa = m_b(v^2 - w^2)$. The trial self-interaction functional is quadratic,

$$\Phi_0[\mathbf{r}(\tau), \mathbf{r}(\tau')] = \kappa^2 [\mathbf{r}(\tau) - \mathbf{r}(\tau')]^2. \quad (4.11)$$

All the expectation values in the variational expression can be evaluated from $\langle e^{i\mathbf{q} \cdot (\mathbf{r}(\tau) - \mathbf{r}(\tau'))} \rangle_0$ which for the trial model has a closed-form expression:

$$\langle e^{i\mathbf{q} \cdot (\mathbf{r}(\tau) - \mathbf{r}(\tau'))} \rangle_0 := \exp \left[-q^2 r_p^2 G(|\tau - \tau'|) \right], \quad (4.12)$$

where the imaginary-time thermal polaron Green function $G(\tau)$ is given by

$$G(\tau) = \tau \left(1 - \frac{\tau}{\hbar\beta} \right) + \frac{v^2 - w^2}{v^3} \left[D_v(0) - D_v(\tau) - v\tau \left(1 - \frac{\tau}{\hbar\beta} \right) \right]. \quad (4.13)$$

Generally, we can transform the q -space summation into a spherical integral over the n -ball,

$$\begin{aligned}\langle \Phi_{\text{pol}} \rangle_0 &= \sum_{\mathbf{q}} |V_{\mathbf{q}}|^2 e^{-q^2 r_p^2 G(\tau)/2}, \\ &= \frac{V|S^{n-1}|}{(2\pi)^n} \int_0^R dq |V_q|^2 q^{n-1} e^{-q^2 r_p^2 G(\tau)},\end{aligned}\quad (4.14)$$

where $|S^{n-1}| = 2\pi^{n/2}/\Gamma(n/2)$ is the hypervolume of the unit $(n-1)$ -sphere and R is the radius of the ball. In n -dimensions, we have

$$\begin{aligned}F &\leq F_0(\beta) + \frac{1}{\beta} \langle S_0 \rangle_0 - \frac{1}{2\omega_0} \sum_{\mathbf{q}} |V_{\mathbf{q}}|^2 \int_0^{\hbar\beta} d\tau D_{\omega_0}(\tau) e^{-q^2 r_p^2 G(\tau)}, \\ &\leq F_0(\beta) + \frac{1}{\beta} \langle S_0 \rangle_0 - \frac{V|S^{n-1}|}{2(2\pi)^n \omega_0} \int_0^{\hbar\beta} d\tau D_{\omega_0}(\tau) \int_0^R dq |V_q|^2 q^{n-1} e^{-q^2 r_p^2 G(\tau)},\end{aligned}\quad (4.15)$$

where I have used,

$$\int_0^{\hbar\beta} d\tau \int_0^{\hbar\beta} d\tau' f(|\tau - \tau'|) \sim 2\hbar\beta \int_0^{\hbar\beta} d\tau f(\tau), \quad (4.16)$$

which is valid when the Hamiltonian for the system is time-translation invariant.

Specialising in the Holstein model for the self-interaction functional we have,

$$\begin{aligned}\langle \Phi^{(H)} \rangle_0 &= \frac{g_H^2(n)|S^{n-1}|}{(2\pi)^n} \int_0^\Lambda dq q^{n-1} e^{-q^2 r_p^2 G(\tau)}, \\ &= \frac{g_H^2(n)|S^{n-1}|}{(2\pi)^n} \frac{\Lambda^n}{2} \left(\Lambda^2 r_p^2 G(\tau) \right)^{-\frac{n}{2}} \left[\Gamma\left(\frac{n}{2}\right) - \Gamma\left(\frac{n}{2}, \frac{\Lambda^2 r_p^2}{2} G(\tau)\right) \right], \\ &= \frac{g_H^2(n)}{(4\pi r_p^2 G(\tau))^{n/2}} \left[1 - \frac{\Gamma\left(\frac{n}{2}, \Lambda^2 r_p^2 G(\tau)\right)}{\Gamma(\frac{n}{2})} \right],\end{aligned}\quad (4.17)$$

where $\Gamma(s, x)$ is the upper incomplete Gamma function. Since $\lim_{x \rightarrow \infty} \Gamma(s, x) \rightarrow 0$ the continuum approximation where $\Lambda \rightarrow \infty$ gives:

$$\langle \Phi^{(H)} \rangle_0^C = \frac{2nJ\hbar\omega_0\alpha_H}{(4\pi r_p^2 G(\tau))^{n/2}}. \quad (4.18)$$

However, the addition integral over the imaginary time variable diverges with this expression.

For the Fröhlich self-interaction functional we have

$$\begin{aligned}\langle \Phi^{(F)} \rangle_0 &= \frac{g_F^2(n) |S^{n-1}|}{(2\pi)^n} \int_0^\infty dq e^{-q^2 r_p^2 G(\tau)}, \\ &= \alpha_F \frac{\Gamma(\frac{n-1}{2})}{2\Gamma(\frac{n}{2})} \frac{1}{\sqrt{G(\tau)}}.\end{aligned}\quad (4.19)$$

One difference between the Holstein and Fröhlich model is in the domain of the radial reciprocal-space integral. Whereas the domain of the radial integral for the Fröhlich model is over all of reciprocal-space, it is bounded to the first Brillouin Zone for the Holstein model, keeping the total reciprocal-space integral within a sphere with volume equal to the Brillouin zone volume. Physically, this is a manifestation of an ultraviolet momentum cutoff due to the discrete lattice. In the continuum Fröhlich model, the integral is convergent for all $n > 1$ – the Fröhlich model diverges in 1D.

The variational inequality for the Holstein model is:

$$F^{(H)} \leq F_0(\beta) + \frac{1}{\beta} \langle S_0 \rangle_0 - \frac{g_H^2(n)}{2M\omega_0} \frac{V}{N} \int_0^{\hbar\beta} d\tau \frac{D_{\omega_0}(\tau)}{G(\tau)^{n/2}} \left[1 - \frac{\Gamma(n/2, \Lambda^2 r_p^2 G(\tau))}{\Gamma(n/2)} \right]. \quad (4.20)$$

and the variational inequality for the Fröhlich model is:

$$F^{(F)} \leq F_0(\beta) - \frac{1}{\beta} \langle S_0 \rangle_0 - \alpha_F \frac{\Gamma(\frac{n-1}{2})}{2\Gamma(\frac{n}{2})} \int_0^{\hbar\beta} d\tau \frac{D_{\omega_0}(\tau)}{\sqrt{G(\tau)}}, \quad (4.21)$$

The expectation value of the trial action $\langle S_0 \rangle_0$ and the free energy of the trial system $F_0(\beta)$ are the same for both models and are as given by Ōsaka [Osaka1959],

$$\langle S_0 \rangle_0 = \frac{n\hbar\beta}{4} \frac{v^2 - w^2}{v} \left(\frac{2}{v\hbar\beta} - \coth \left(\frac{v\hbar\beta}{2} \right) \right), \quad (4.22)$$

and the trial free energy is,

$$F_0(\beta) = \frac{n}{2\beta} \log(2\pi\hbar\beta) + \frac{n}{\beta} \log \left(\frac{w \sinh(\hbar\beta v/2)}{v \sinh(\hbar\beta w/2)} \right). \quad (4.23)$$

4.2.1 Coupling Dependence

The main weak-to-strong polaron transition occurs around $\alpha^H \approx 2$ for the Holstein model when using Ragni's convention. Elsewhere in the literature, this

happens at $\alpha^{(H)} \approx 1$ or at some other value. Ultimately, this is just a matter of rescaling the Holstein alpha parameter. I have assumed that this polaron transition is similar in nature to the $\alpha = 6$ transition present in the Fröhlich model - where perturbation theory diverges. Therefore, whenever I am comparing the Holstein polaron results to the Fröhlich polaron, I will scale the Fröhlich alpha according to a rough expression

$$\alpha^{(F)} \approx 3\alpha^{(H)} \quad (4.24)$$

This expression has only been deduced by eye and is not mathematically derived, but it will allow us better to compare the Fröhlich and Holstein models and differentiate their underlying physics. I choose to scale the Fröhlich model so that direct comparison with diagMC results is maintained and to avoid any possible unforeseen complications on the Holstein variational solution.

Polaron Ground-state Energy

The first numerical result in Fig. (4.4) is the dependence on the Holstein free energy on the unitless alpha parameter α . On the left, we have the Fröhlich free energy for 2D and 3D, and on the right, we have the Holstein free energy compared to diagMC data in 1D, 2D and 3D. The predictions made by this new variational theory agree fairly well with the diagMC, especially before the transition point at $\alpha = 2$, which is characterised by a distinctive kink in the free energy. After $\alpha = 2$, the variational theory *underestimates* the true free energy. Now, this begs an important question: is this theory variational? From its construction, it should *only* ever provide an **upper-bound** to the polaron free energy, so, at first sight, it goes below the diagMC data is concerning. However, it should be recognised that to apply the variational approximation, we have to approximate the Holstein model electron band as an unbounded parabola. Therefore, the variational method inevitably overestimates the kinetic energy in the model, which should be asymptotic to zero at large coupling. However, in our model, it continues to grow rough as $KE \sim \sqrt{\alpha}$. So, I argue that the variational bound is preserved; we are just not solving for the Holstein model exactly due to the approximations made along the way. Nonetheless, the variational approximation seems to capture the same small polaron transition at $\alpha = 2$ well, having the correct dependence and scaling with the number of spatial dimensions.

On another note, the Holstein model has a free energy that is significantly smaller than the large Fröhlich polaron. On the right, we have co-plotted the 3D Fröhlich free energy result in pink, scaled down by a factor of 6 to bring it inline with the weak-coupling prediction of the Holstein model. This suggests that polaronic

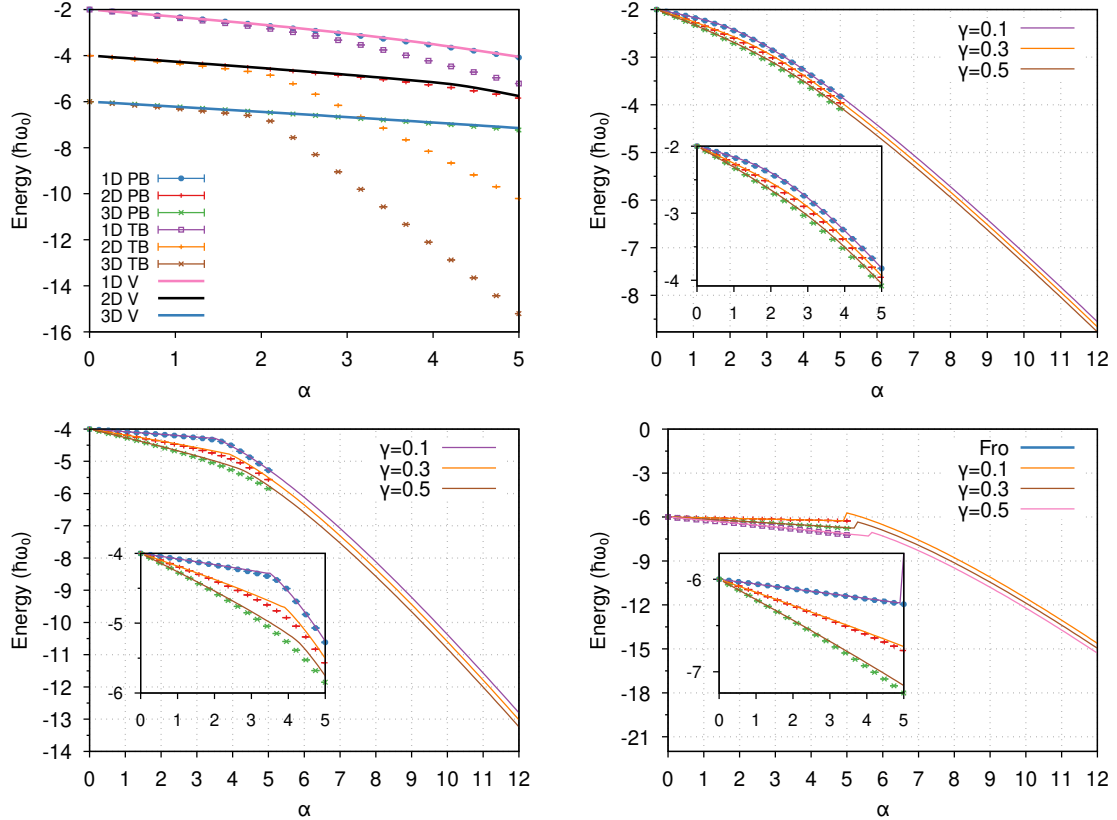


Figure 4.4: Polaron binding energy for the Fröhlich and Holstein models with respect to the electron-phonon dimensionless coupling parameter α . **Left:** Fröhlich model in 2D (solid blue) and 3D (dashed orange). **Right:** Holstein model in 1D (dashed orange), 2D (dot-dashed green) and 3D (dot-dot-dashed pink), and the 3D Fröhlich result scaled by 1/6 in energy and 1/3 in α to align with the Holstein weak-coupling ($\alpha < 1$). Co-plotted are DiagMC results for the Holstein model in 1D (blue diamonds), 2D (orange squares) and 3D (green circles).

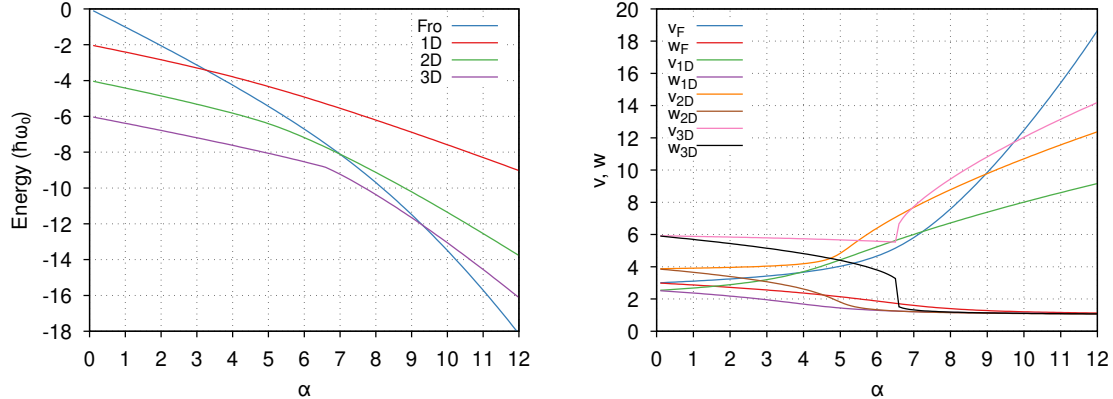


Figure 4.5: Optimal values of the polaron variational parameters v and w for the Fröhlich and Holstein models with respect to the electron-phonon dimensionless coupling parameter α . **Left:** Fröhlich model in 2D (v solid blue and w dot-dash green) and 3D (v dashed orange and w dot-dot-dash pink). **Right:** Holstein model in 1D (v solid blue and w dot-dot-dash pink), 2D (v dashed orange and w solid yellow) and 3D (v dot-dashed green and w dashed turquoise).

effects are stronger in materials that can form large polarons. Conceptually, this is logical as the Holstein electron-phonon interaction is purely local and isolated to individual lattice sites. In contrast, in the Fröhlich model, it is a long-range interaction and thus more strongly bounding.

Polaron Variational Parameters

Next are the results for the v and w variational parameters for the Holstein model (Fig. (4.5)). We have the Fröhlich results in 2D and 3D on the left. On the right are the Holstein results in 1D, 2D and 3D. We assume that the alpha ranges used produce similar physical regimes within either model for point of comparison, as mentioned above.

Immediately, the Holstein model noticeably has a very different variational solution to the Fröhlich model, with a distinctive discontinuity around $\alpha = 2$, which causes a suddenly more rapid increase in the polaron binding energy. This is attributed to transitioning into a small polaron state. Both models have $w \rightarrow 1\omega_0$ at large coupling, albeit more abruptly in the Holstein model. Also, the v parameters appear to have a different strong coupling dependency on α . In the Fröhlich model at large α , $v^{(F)} \sim \alpha^2$ whereas in the Holstein model $v^{(H)} \sim \sqrt{\alpha}$. Another noticeable difference is in the $\alpha \rightarrow 0$ limits where regardless of the number of spatial dimensions, the Fröhlich model parameters asymptote to $v = w = 3$, but in the Holstein model, the zero-coupling limit depends on the number of spatial dimensions. Finally, the polaron transition seems to be dimensionally dependent in the Fröhlich model, occurring at $\alpha = \approx 3$ in 2D and $\alpha \approx 6$ in 3D. Meanwhile,

the transition in the Holstein model seems to be independent of dimensionality. It should be noted, however, that the alpha unitless coupling is often *defined* this way.

4.2.2 Holstein Polaron Temperature Dependence

In this section, we look at how the Holstein model varies with temperature. Notably, its free energy, variational parameters and DC mobility. As the v and w parameter scale to large values with temperature, I have opted to represent them in terms of the trial model fictitious particle mass $M = v^2/w^2 - 1$ and spring-constant $\kappa = v^2 - w^2$ instead as they produce more readable and digestible plots. The temperature range looked at is $T = 0.125\omega_0$ to $T = 32\omega_0$. For clearer context, in the Fröhlich model, $T = \omega_0$ is roughly $T \approx 48\text{K}$, and in the Holstein model, it is roughly $T \approx 11.6\text{K}$ up to a multiple of the phonon frequency in units of THz 2π . We also look at these temperatures over a range of couplings $\alpha^{(F)} = 2.5, 4, 6, 8, 10, 12$ and $\alpha^{(H)} \approx \alpha^{(F)}/3 = 0.83, 1.33, 2, 2.67, 3.33, 4$.

Holstein Polaron Free Energy

In Figs. (4.6) we have many plots showing how the temperature dependence of the Holstein polaron in 1D, 2D and 3D, and the Fröhlich polaron in 2D and 3D, changes as the electron-phonon coupling increases. Note that the Fröhlich free energy has been scaled down by 1/6 to better compare trends with the Holstein free energy. A few trends can be noticed. First and foremost, at weaker coupling ($\alpha^{(F)} = 2.5, \alpha^{(H)} = 0.83$), the Holstein polaron energy grows more rapidly with increasing temperature than the Fröhlich polaron, but this difference fades with increasing coupling until they seem to have a similar dependence on temperature. Secondly, the different dimensional Holstein polarons have a similar temperature dependence at all coupling, aside from a seemingly constant multiplicative factor where the 1D and 2D Holstein polaron energies are roughly 1/3 and 2/3 respectively of the 3D Holstein polaron.

Polaron Mass and Spring Constant

In Figs. (4.7) we have the temperature dependence of the fictitious particle mass for the Holstein polaron with varying electron-phonon coupling. At smaller coupling, both the Holstein and Fröhlich models show a maximum at intermediate temperatures and show similar dependence on temperature up until some critical transition temperature where the Holstein polaron mass abruptly stops decreasing with temperature and starts to become heavier, unlike the Fröhlich polaron

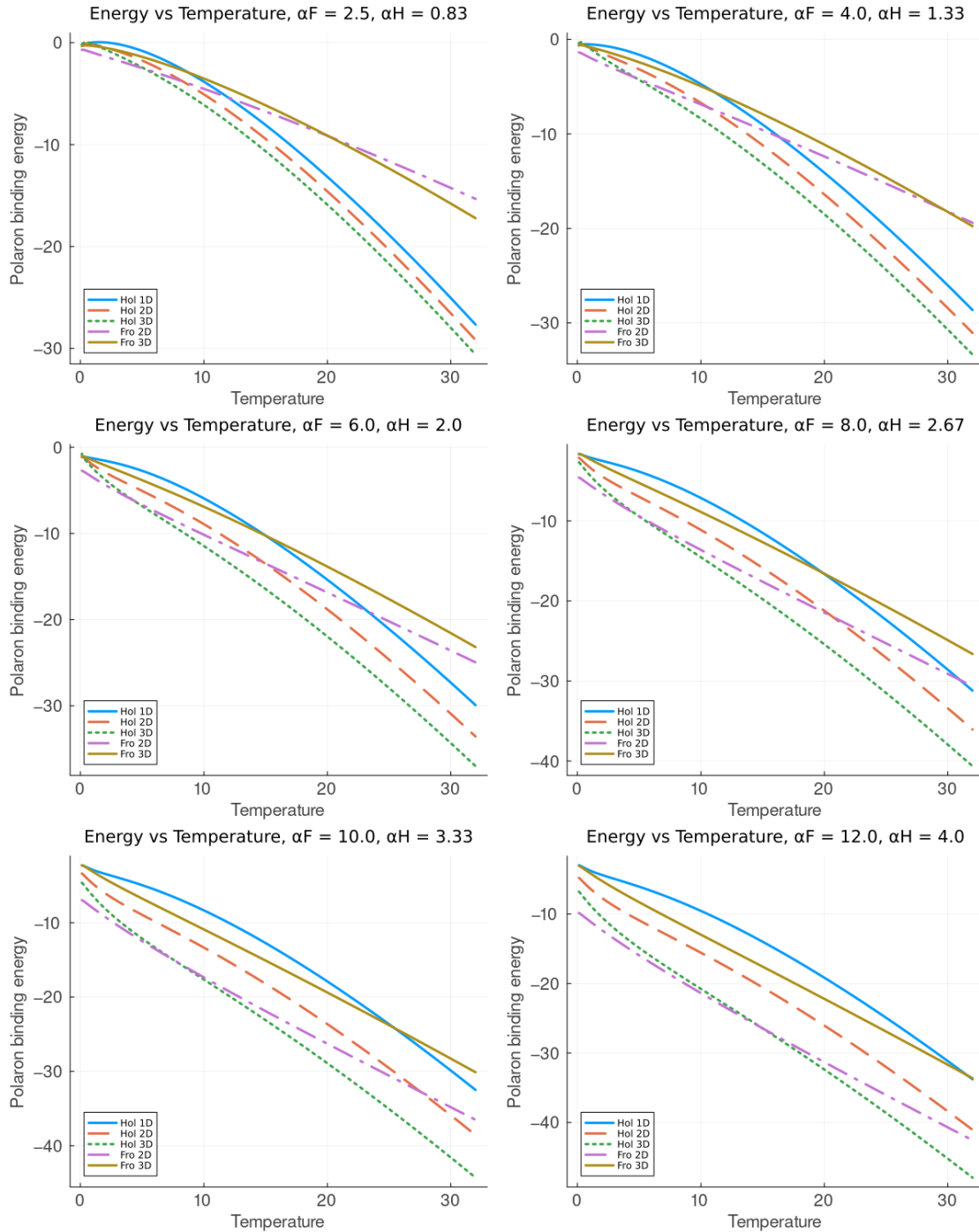


Figure 4.6: Polaron binding energy for the Fröhlich model in 2D (dot-dash pink) and 3D (solid gold), and Holstein model in 1D (solid blue), 2D (dashed orange) and 3D (dotted green) with respect to temperature (in units of the phonon frequency ω_0), for values of the Fröhlich electron-phonon coupling $\alpha = 2.5, 4, 6, 8, 10, 12$ and $1/3$ of these values for the Holstein electron-phonon coupling. The Fröhlich free energy has been scaled down by $1/6$ to better compare with the Holstein free energy.

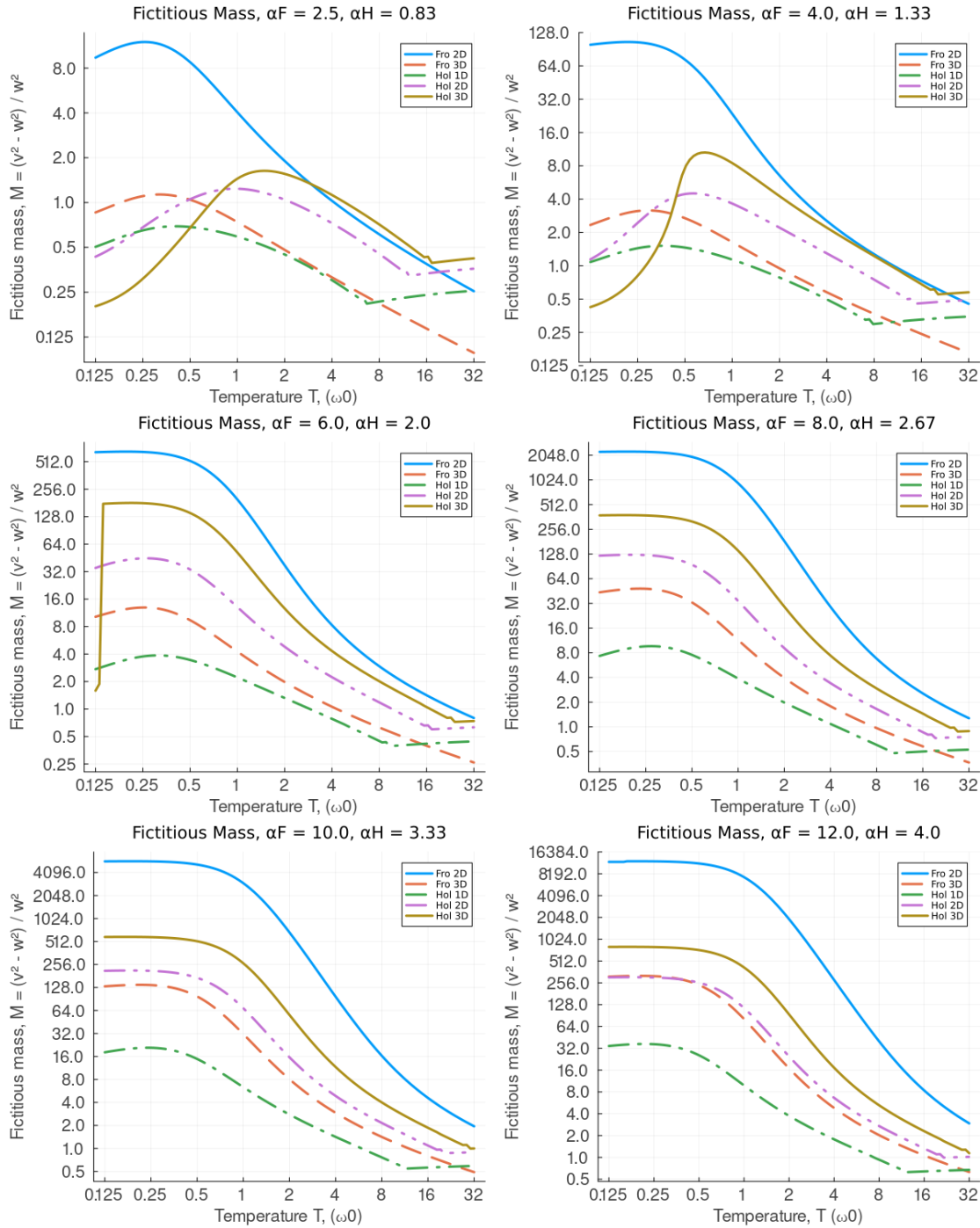


Figure 4.7: Temperature dependence (T , in units of phonon frequency ω_0) of the fictitious particle mass M from the trial system for the Fröhlich model in 2D (solid blue) and 3D (dashed orange), and for the Holstein model in 1D (dot-dashed green), 2D (dot-dot-dashed pink) and 3D (solid gold), for values of the Fröhlich electron-phonon coupling $\alpha = 2.5, 4, 6, 8, 10, 12$ and $1/3$ of these values for the Holstein electron-phonon coupling. This mass can be expressed in terms of the traditional v and w using $M = (v^2 - w^2)/w^2$. The Fröhlich results are un-scaled here.

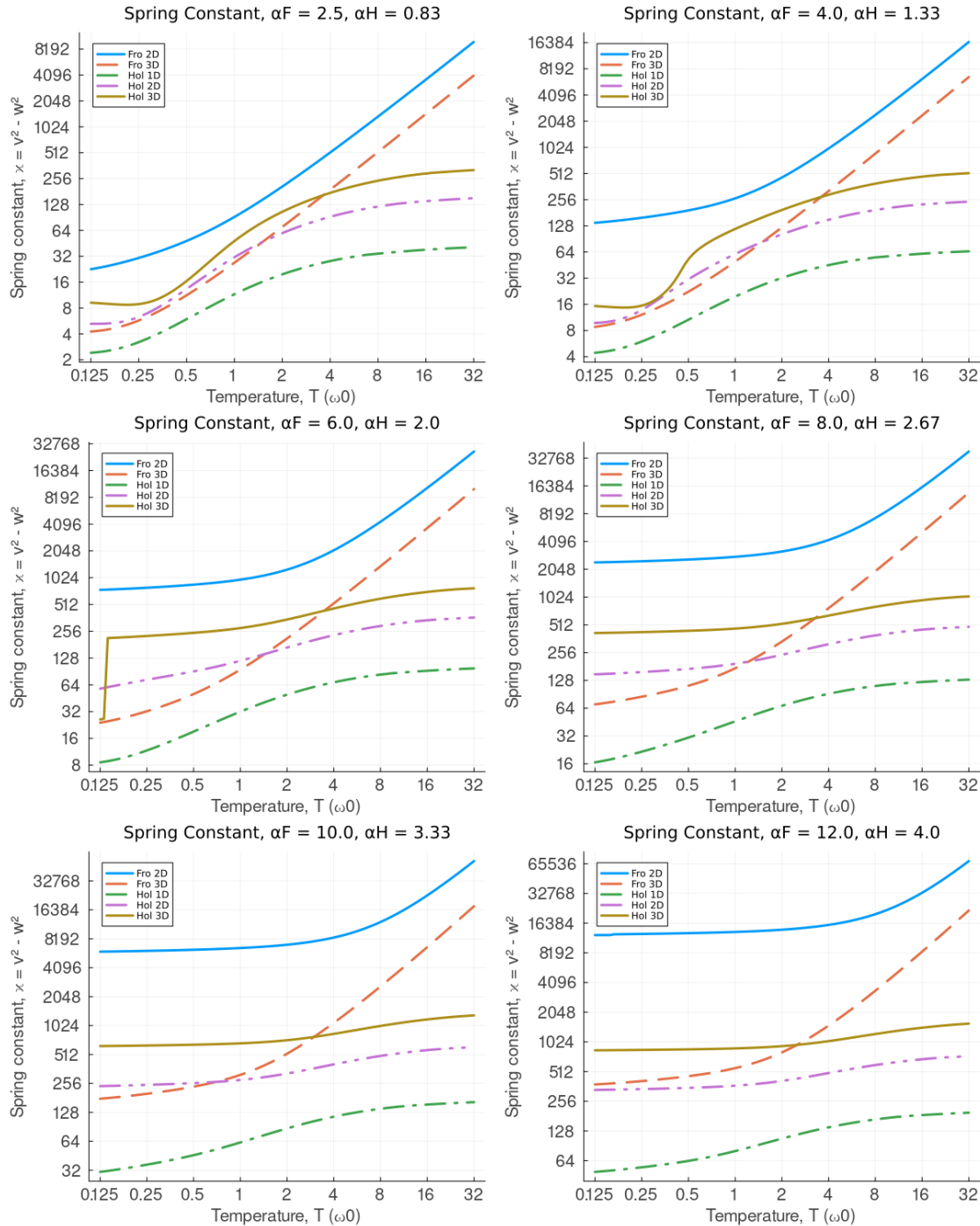


Figure 4.8: Temperature dependence (T , in units of phonon frequency ω_0) of the fictitious particle spring-constant κ from the trial system for the Fröhlich model in 2D (solid blue) and 3D (dashed orange), and for the Holstein model in 1D (dot-dashed green), 2D (dot-dot-dashed pink) and 3D (solid gold), for values of the Fröhlich electron-phonon coupling $\alpha = 2.5, 4, 6, 8, 10, 12$ and $1/3$ of these values for the Holstein electron-phonon coupling. This mass can be expressed in terms of the traditional v and w using $\kappa = (v^2 - w^2)$. The Fröhlich results are un-scaled here.

mass which continues to get lighter with increasing temperatures until reducing to the electron band-mass at infinite temperature. At stronger coupling, the maximum mass at intermediate temperatures is replaced with a plateaued maximum that exists for all temperatures $T < \omega_0$. The critical transition temperature at higher temperatures still exists for the Holstein polaron mass.

The plateau less than the phonon energy $T < \omega_0$ arises due to the lack of excited phonons whose random motion decreases the effective electron-phonon interaction, resulting in a decreasing phonon contribution to the effective electron mass. For the Holstein model, the polaron mass increases at a critical temperature equal to the natural frequency of the electron-phonon interaction v . Phonons then begin to transfer energy back into the effective electron-phonon interaction and increase the phonon contribution to the effective electron mass.

In Figs. (4.8) we have the temperature dependence of the fictitious particle spring constant for the Holstein polaron with varying electron-phonon coupling. An interesting difference here is that the spring constant for the Fröhlich polaron keeps increasing linearly with temperature, whereas the spring constant for the Holstein polaron seems to plateau to some value at higher temperatures. This is most noticeable in weaker couplings. Similar to the polaron mass, as we go to stronger coupling, both kinds of polarons reach a constant spring constant for temperatures lower than the phonon energy.

One final overall observation is that the 2D Holstein polaron and the 3D Fröhlich polaron seem to be most similar. This isn't all that surprising since it only for two dimensions that the self-interaction functional (Eqn. 4.14)) in the Holstein model has the same phonon-momentum dependence as in the Fröhlich model - which does not change with dimensionality unlike for the Holstein polaron.

4.3 The Optimal Functional Solution

4.3.1 Generalised Trial Action

The central quantity for the generalisation is the trial action functional,

$$S_0 = \frac{m_b}{2} \int_0^{\hbar\beta} \dot{\mathbf{r}}(\tau)^2 - \frac{m_b}{2} \int_0^{\hbar\beta} \int_0^{\hbar\beta} d\tau d\tau' \Sigma(\tau - \tau') \mathbf{r}(\tau) \cdot \mathbf{r}(\tau'), \quad (4.25)$$

where $\Sigma(\tau - \tau')$ is a general memory kernel and is a real, continuous function defined for $|\tau| \leq \hbar\beta$ and can be assumed to be symmetric $\Sigma(-\tau) = \Sigma(\tau)$. This is the most general quadratic, isotropic, two-time action. We can restrict the memory

kernel to be β -periodic and also assume a sum-rule,

$$\int_0^{\hbar\beta} \Sigma(\tau - \tau') d\tau' = 0 \quad \forall \tau \in [0, \hbar\beta], \quad (4.26a)$$

$$\Sigma(\tau - \hbar\beta) = \Sigma(\tau) \quad \forall \tau \in [0, \hbar\beta]. \quad (4.26b)$$

The first assumption is required for a translation invariant system, but the second assumption can be relaxed if required.

The goal is now to find the optimal memory function $\tilde{\Sigma}(\tau)$ that minimises the upper bound to the free energy. Therefore, the free energy becomes a functional of the memory function,

$$F \leq F_{\text{trial}}[\Sigma] = F_{\text{ph}} + F_{S_0[\Sigma]} + \frac{1}{\beta} \langle S - S_0[\Sigma] \rangle_{S_0[\Sigma]}. \quad (4.27)$$

To evaluate this functional, we need to evaluate the density-density correlation function,

$$\langle \rho^\dagger(\tau) \rho(\tau') \rangle = \langle e^{i\mathbf{q} \cdot [\mathbf{r}(\tau) - \mathbf{r}(\tau')]} \rangle_{S_0}. \quad (4.28)$$

To evaluate the density-density correlation function, we introduce the generating functional,

$$Z[J] = \left\langle \exp \left\{ \int_0^{\hbar\beta} d\tau J(\tau) \cdot \mathbf{r}(\tau) \right\} \right\rangle_{S_0}, \quad (4.29)$$

where $J(\tau)$ is an arbitrary source term. If we can evaluate this field integral, we can derive all correlation functions, and subsequently, we can calculate both $\langle S - S_0 \rangle_{S_0}$ and F_{S_0} . We recognise that the expectation $\langle \cdot \rangle_{S_0}$ indicates averaging with respect to an isotropic Gaussian stochastic process $\mathbf{r}(\tau)$ with zero mean and so is uniquely characterised by its covariance $\langle \mathbf{r}(\tau) \cdot \mathbf{r}(\tau') \rangle_{S_0}$,

$$Z[J] = \exp \left\{ \frac{m_b}{2n\hbar\beta} \int_0^{\hbar\beta} \int_0^{\hbar\beta} d\tau d\tau' \langle \mathbf{r}(\tau) \cdot \mathbf{r}(\tau') \rangle_{S_0} J(\tau) \cdot J(\tau') \right\}, \quad (4.30)$$

where n is the dimensionality. The covariance is also often referred to in this context as the single-particle Green's function $G(\tau, \tau') \equiv \langle \mathbf{r}(\tau) \cdot \mathbf{r}(\tau') \rangle$ and can be determined as an appropriate inverse of the integral kernel of the trial action,

$$S_0 = \frac{m_b}{2} \int_0^{\hbar\beta} \int_0^{\hbar\beta} d\tau d\tau' \mathbf{r}(\tau) \left[\frac{\partial}{\partial \tau} \delta(\tau - \tau') - \Sigma(\tau - \tau') \right] \mathbf{r}(\tau'), \quad (4.31)$$

where the integral kernel is $G^{-1}(\tau - \tau') = G_0(\tau - \tau') - \Sigma(\tau - \tau')$ with $G_0(\tau - \tau') = \partial_\tau \delta(\tau - \tau')$ the bare free particle Green's function. Under the assumption

of translation invariance and,

$$\int_0^{\hbar\beta} \Sigma(\tau) d\tau \neq 0, \quad (4.32)$$

the equation of motion of the polaron quasiparticle Green's function is,

$$\int_0^{\hbar\beta} d\tau'' G(\tau - \tau'') G^{-1}(\tau' - \tau'') = n\delta(\tau - \tau'), \quad (4.33)$$

where $\delta(\tau)$ is a periodic delta function and has the Fourier representation,

$$\delta(\tau) = \sum_{n=-\infty}^{\infty} e^{i\omega_n \tau}, \quad (4.34)$$

where $\omega_n = 2\pi n / \hbar\beta$ are the “even” Matsubara frequencies. The polaron Green's function is then given in Fourier representation as,

$$G(\tau - \tau') = \frac{1}{\hbar\beta} \sum_{n=-\infty}^{\infty} \frac{e^{i\omega_n(\tau-\tau')}}{\omega_n^2 - \Sigma_n}, \quad (4.35)$$

where we can identify the Fourier coefficients as $G_n = (\omega_n^2 - \Sigma_n)^{-1}$ where Σ_n is the n-th Fourier coefficient of the memory function,

$$\Sigma_n = \frac{1}{\hbar\beta} \int_0^{\hbar\beta} \Sigma(\tau) e^{-i\omega_n \tau} d\tau = \Sigma_{-n}. \quad (4.36)$$

If $\Sigma_0 = 0$ and we are in a translation-invariant system, the equation of motion for the Green function is still valid because we omit the term at $n = 0$.

Now equipped with the polaron quasiparticle Green's function and the generating functional, we can compute all the averages required in the free energy inequality. Setting the source term to be,

$$\mathbf{J}(\tau) = i\mathbf{q} [\delta(\tau - \sigma) - \delta(\tau - \sigma')] \equiv \mathbf{J}_{\mathbf{q},\sigma,\sigma'}(\tau). \quad (4.37)$$

Within $\langle S \rangle_0$ we have to evaluate the density-density correlation,

$$\langle e^{i\mathbf{q} \cdot [\mathbf{r}(\tau) - \mathbf{r}(0)]} \rangle_0 = \exp \left(-q^2 r_p^2 [G(0) - G(\tau)] \right). \quad (4.38)$$

For the Fröhlich polaron model, we have to evaluate the expectation of the two-time Coulomb interaction, which we do in the Fourier representation where we

use the result from the density-density correlation,

$$\begin{aligned} \left\langle \frac{1}{|\mathbf{r}(\sigma) - \mathbf{r}(\sigma')|} \right\rangle_{S_0} &= \frac{|S^{n-1}|}{(2\pi)^n} \int d^n q q^{-2} Z \left[\mathbf{J}_{\mathbf{q}, \sigma, \sigma'} \right], \\ &= \left(\frac{2n}{\pi \left\langle |\mathbf{r}(\sigma) - \mathbf{r}(\sigma')|^2 \right\rangle_{S_0}} \right)^{1/2}. \end{aligned} \quad (4.39)$$

We can evaluate the trial system free energy by using the “coupling constant” integration trick in which we extract a constant λ from the memory function $\Sigma \rightarrow \lambda \Sigma$. For a translation-invariant system, we can evaluate the free energy from,

$$F_{S_0}(\lambda) = F_{S_0}(0) + \int_0^\lambda d\lambda' \frac{\partial F_{S_0}(\lambda)}{\partial \lambda}. \quad (4.40)$$

The partial derivative is then,

$$\frac{\partial F_{S_0}(\lambda)}{\partial \lambda} = \frac{1}{\hbar\beta} \int_0^{\hbar\beta} \int_0^{\hbar\beta} d\tau d\tau' \Sigma(\tau - \tau') G(\tau - \tau'), \quad (4.41)$$

which implies,

$$F_{S_0}(0) = -\frac{1}{\beta} \ln \left\{ V \left(\frac{m_b}{2\pi\hbar^2\beta} \right)^{n/2} \right\} = F_{el}, \quad (4.42)$$

which is just the free energy for the free electron.

4.3.2 Self-consistent Equations

Overall, we have,

$$F \leq F_{ph} + F_{el} + \text{Tr} \ln \left(GG_0^{-1} \right) + \text{Tr} (\Sigma G) + \Phi[G], \quad (4.43)$$

where,

$$\begin{aligned} \Phi[G] &= \sum_{\mathbf{q}} |V_{\mathbf{q}}|^2 \int_0^{\hbar\beta} \int_0^{\hbar\beta} d\tau d\tau' D_{\omega_{\mathbf{q}}}(\tau - \tau') \exp \left(-q^2 r_p^2 G(\tau - \tau') \right), \\ &= 2 \sum_{\mathbf{q}} |V_{\mathbf{q}}|^2 \int_0^{\hbar\beta} d\tau (\hbar\beta - \tau) D_{\omega_{\mathbf{q}}}(\tau) \exp \left(-q^2 r_p^2 G(\tau) \right), \end{aligned} \quad (4.44)$$

where we have used that,

$$\int_0^{\hbar\beta} d\tau \int_0^{\hbar\beta} d\tau' f(|\tau - \tau'|) = 2 \int_0^{\hbar\beta} d\tau (\hbar\beta - \tau) f(\tau). \quad (4.45)$$

For the Fröhlich model, this becomes

$$\Phi^{(F)}[G] = |V_0|^2 \int_0^{\hbar\beta} d\tau \left(\frac{\tau}{\hbar\beta} - 1 \right) D_{\omega_0}(\tau) [G(\tau)]^{-1/2}. \quad (4.46)$$

Note that the free-electron energy is $F_{el} = \ln\{\det G_0^{-1}\} = \text{Tr} \ln G_0^{-1}$ and so the free-energy inequality is,

$$F \leq \frac{1}{2} \text{Tr} \ln (D_0) + \text{Tr} \ln (-G) + \text{Tr} (\Sigma G) + \Phi[G], \quad (4.47)$$

where we have used that for bosonic phonons $F_{ph} = \frac{1}{2} \text{Tr} \ln (D_0)$ where D_0 is the free phonon Green's function. We note that this takes on a similar form to the expression for the grand potential obtained by Luttinger and Ward [39] where $\Phi[G]$ is an approximation to the Luttinger-Ward functional; the sum of all closed, bold, two-particle irreducible diagrams. Other approximations to this functional include GW-theory where it is truncated to include just ring-diagrams $\Phi[G] \approx GUG + GUGGUG + \dots$, and Density Mean-Field Theory (DMFT) where only local-diagrams are accounted for.

4.3.3 General Memory Function

Feynman's original trial action has been proven successful in imitating the Fröhlich model, yet it has been demonstrated that this is not a universal result [38, 37]. Even for the Fröhlich model, the trial solution can be improved by finding the optimal "memory function" that reduces the upper-bound of the polaron free energy.

4.4 The Linear Polaron & Independent Boson Models

4.5 Cumulant Expansion Corrections

CHAPTER 5

COMPUTING RESPONSE FUNCTIONS & POLARON MOBILITY

What is the meaning of life?

—John Doe, *Thoughts*, 1971

This is the introduction paragraph.

5.1 Polaron Mobility

The polaron DC mobility may be obtained in the same way as was done for the Fröhlich model from real components of the frequency- and temperature-dependent impedance function,

$$\mu_{dc} = \lim_{\Omega \rightarrow 0} \operatorname{Re} \left\{ \frac{1}{z(\Omega)} \right\}, \quad (5.1)$$

where the impedance function is expressed in terms of the memory function $\Sigma(\Omega)$,

$$z(\Omega) = i (\Omega - \Sigma(\Omega)). \quad (5.2)$$

More specifically, we can express the inverse DC mobility just in terms of the memory function,

$$\mu_{dc}^{-1} = \lim_{\Omega \rightarrow 0} \operatorname{Im} \{ \Sigma(\Omega) \}. \quad (5.3)$$

We start from an expression for the dynamical memory function for a general polaron and specialise in the Holstein case. The general memory function can be written as,

$$\Sigma(\Omega) = \frac{4}{nm_b\hbar\Omega} \int_0^\infty dt \left(1 - e^{i\Omega t}\right) \text{Im} \left\{ \sum_{\mathbf{q}} |V_{\mathbf{q}}|^2 q^2 D_{\omega_{\mathbf{q}}}(t) \langle e^{i\mathbf{q} \cdot [\mathbf{r}(t) - \mathbf{r}(0)]} \rangle \right\}, \quad (5.4)$$

where we assume the system to be rotationally invariant. Here $D_{\omega}(t)$ is the *real-time thermal and dynamical* phonon Green function,

$$D_{\omega}(t) = \coth\left(\frac{\hbar\beta\omega}{2}\right) \cos(\omega t) - i \sin(\omega t), \quad (5.5)$$

and can be obtained from substituting $\tau \rightarrow it$ into Eqn. (3.31).

The key term to evaluate is the density-density correlation function or dynamical structure factor,

$$S_{\mathbf{q}}(t) = \langle \rho_{\mathbf{q}}(t) \rho_{\mathbf{q}}^*(0) \rangle = \langle e^{i\mathbf{q} \cdot [\mathbf{r}(t) - \mathbf{r}(0)]} \rangle. \quad (5.6)$$

As done earlier, the expectation value can be expressed as a path integral. However, even the full Fröhlich model cannot be evaluated exactly. We approximate this by evaluating this expectation value with respect to the Feynman polaron model,

$$\langle \rho_{\mathbf{q}}(t) \rho_{\mathbf{q}}^*(0) \rangle_0 = e^{-q^2 r_p^2 G(t)}, \quad (5.7)$$

where $G(t)$ is the polaron Green function evaluated in real-time (i.e. substitute $\tau \rightarrow it$ into Eqn. (4.13)),

$$G(t) = it \left(1 - \frac{it}{\hbar\beta}\right) + \frac{v^2 - w^2}{v^3} \left[D_v(0) - D_v(t) - ivt \left(1 - \frac{it}{\hbar\beta}\right) \right]. \quad (5.8)$$

In n -dimensions, we need to evaluate the reciprocal-space integral,

$$\begin{aligned} I(n) &= V \int \frac{d^n q}{(2\pi)^n} |V_{\mathbf{q}}|^2 q^2 D_{\omega_{\mathbf{q}}}(t) e^{-q^2 r_p^2 G(t)}, \\ &= \frac{V |S^{n-1}|}{(2\pi)^n} \int_0^R dq q^{n+1} |V_q|^2 D_{\omega_q}(t) e^{-q^2 r_p^2 G(t)}, \end{aligned} \quad (5.9)$$

where we have used that the system is rotation-invariant. For a general polaron model, we then have the memory function,

$$\Sigma(\Omega) = \frac{4}{nm_b\hbar\Omega} \frac{V|S^{n-1}|}{(2\pi)^n} \int_0^\infty dt \left(1 - e^{i\Omega t}\right) \int_0^\Lambda dq \left|V_q\right|^2 q^{n+1} \text{Im}\left\{D_{\omega_q}(t)e^{-q^2 r_p^2 G(t)}\right\}. \quad (5.10)$$

In the zero frequency limit, we have,

$$\lim_{\Omega \rightarrow 0} \frac{\left(1 - e^{i\Omega t}\right)}{\Omega} \rightarrow -it, \quad (5.11)$$

so for the general polaron DC mobility, we get,

$$\mu_{dc}^{-1} = -\frac{4e^2}{nm_b\hbar} \frac{V|S^{n-1}|}{(2\pi)^n} \int_0^\infty dt t \int_0^\Lambda dq q^{n+1} \left|V_q\right|^2 \text{Im}\left\{D_{\omega_q}(t)e^{-q^2 r_p^2 G(t)}\right\}. \quad (5.12)$$

5.1.1 The Fröhlich Model

Now equipped with the general polaron variational equations for the free energy and the corresponding memory function, we can specialise in the Fröhlich model by substituting

$$\left|V_q\right|^2 = g_F^2(n)/Vq^{n-1}, \quad (5.13a)$$

$$\omega_q = \omega_0, \quad (5.13b)$$

$$\Lambda \rightarrow \infty. \quad (5.13c)$$

The q -space integral is evaluated,

$$\begin{aligned} I^{(F)}(n) &= \frac{g_F^2(n)|S^{n-1}|}{(2\pi)^n} D_{\omega_0}(t) \int_0^\infty dq q^2 e^{-q^2 r_p^2 G(t)}, \\ &= \frac{g_F^2(n)|S^{n-1}| \sqrt{\pi}}{(2\pi)^n 4r_p^3} \frac{D_{\omega_0}(t)}{G(t)^{\frac{3}{2}}}, \\ &= \alpha^{(F)} \frac{\sqrt{\pi}}{2r_p^3} \frac{(2\sqrt{\pi})^{-n}}{\Gamma(\frac{n}{2})} \frac{D_{\omega_0}(t)}{G(t)^{\frac{3}{2}}}. \end{aligned} \quad (5.14)$$

The memory function for the Fröhlich model is then,

$$\Sigma^{(F)}(\Omega) = \frac{1}{m_b\hbar\Omega r_p^3} \frac{\pi\sqrt{2\pi}\alpha^{(F)}}{\Gamma(\frac{n}{2} + 1)} \frac{(2\sqrt{\pi})^n}{\left[2\sqrt{\pi}\right]^n} \int_0^\infty dt \left(1 - e^{i\Omega t}\right) \frac{D_{\omega_0}(t)}{\left[G(t)\right]^{3/2}}. \quad (5.15)$$

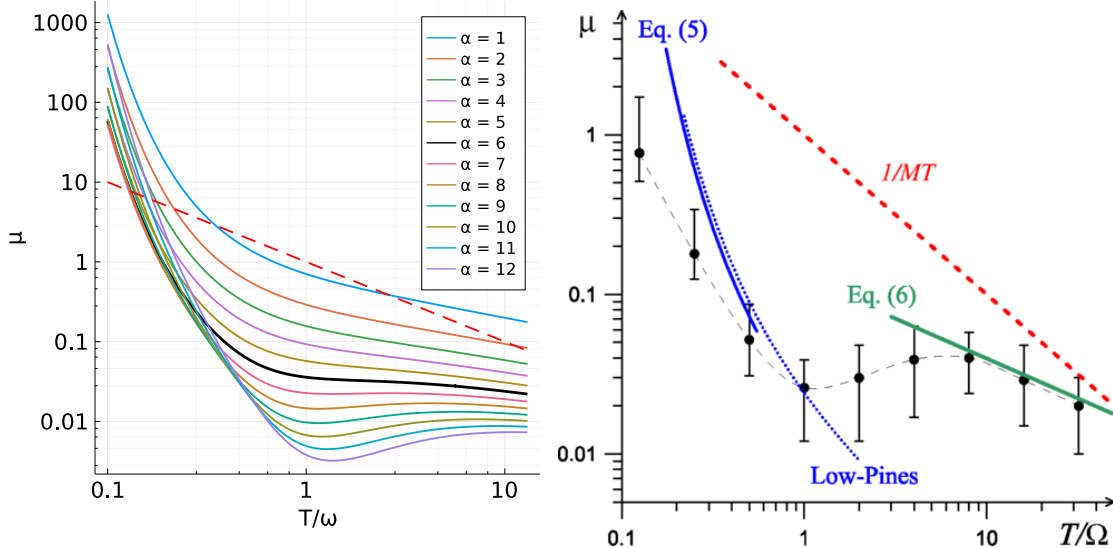


Figure 5.1: Temperature dependence of the polaron mobility. The Mott-Ioffe-Regel (MIR) threshold is given by the red dotted lines. Left: Mobility obtained from the thermal FHIP theory with v and w variational parameters calculated for each temperature, for Fröhlich alphas ranging from $\alpha = 1$ to 12. The temperature is given in units of the phonon frequency ω . Right: Mobility obtained by [40] using the diagrammatic Monte Carlo method for $\alpha = 6$. The temperature is in units of the phonon frequency Ω .

and the inverse Fröhlich DC mobility is,

$$\mu_{dc}^{-1} = -\frac{e^2}{m_b \hbar r_p^3} \frac{\pi \sqrt{2\pi} \alpha^{(F)}}{\Gamma(\frac{n}{2} + 1) (2\sqrt{\pi})^n} \int_0^\infty dt \frac{t D_{\omega_0}(t)}{[G(t)]^{3/2}}. \quad (5.16)$$

Comparison to Diagrammatic Monte Carlo

Mishchenko et al. [40] use the diagrammatic Monte Carlo (DiagMC) method to study the mobility of a Fröhlich polaron in the “Beyond Quasiparticle” regime. In this regime, the inelastic scattering rate exceeds the thermal energy of quasiparticles. This can be restated as the regime where the mean free path of the particle exceeds its de Broglie wavelength. This form coincides with the Mott-Ioffe-Regel (MIR) criterion, which is where the motion of quasiparticles is ill-defined.

In Figure 5.1 are comparisons between the temperature dependence of the polaron mobility evaluated using the [2] method (right) compared to the [40] DiagMC method (left). The key features of the DiagMC plot (right) are the non-monotonic behaviour of the mobility and the evaluation of the mobility near and below the MIR threshold (given by the red dotted line). These two features are also seen in FHIP mobility. The main difference between the two results is that, whilst the mobility minimum arises from the DiagMC method at $\alpha = 6$, the minimum arises from the FHIP method at $\alpha \geq 7$ and is less prominent. The mobility eval-

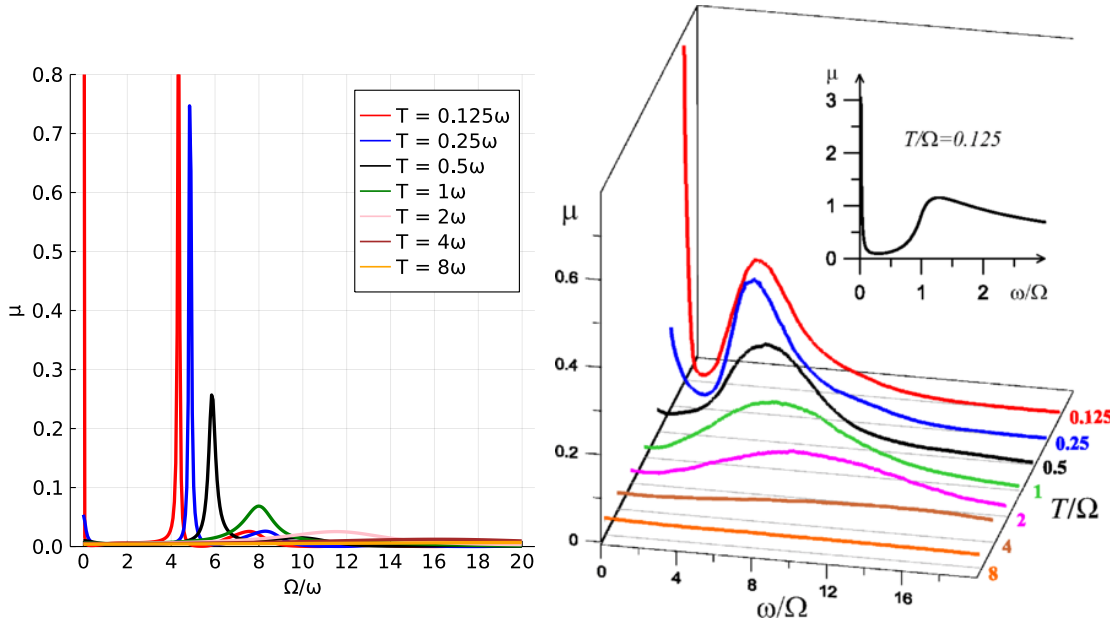


Figure 5.2: Polaron mobility for $\alpha = 6$. Left: Mobility obtained from the thermal FHIP theory with v and w variational parameters calculated for each temperature. The electric field frequency and temperature are given in units of the phonon frequency ω . Right: Mobility obtained by [40] using the diagrammatic Monte Carlo method. The electric field frequency and temperature are in units of the phonon frequency Ω .

uated below the MIR threshold is stated in [40] to be “beyond the quasiparticle” regime. However, the model from [2] can also reliably evaluate the mobility in this regime despite being a quasiparticle model of two fictitious masses coupled by a spring-like potential. Additionally, the FHIP can reproduce the mobility minimum, too. [40] suggest that the minimum emerges from the competition between the decreasing number of thermal excitations (which dominates at $T \ll \omega$) and a strong mass renormalisation (which is prominent for $T > \omega$).

Figure 5.2 compares the polaron mobility evaluated for a Fröhlich alpha $\alpha = 6$. The left figure shows the polaron mobility obtained from the thermal Feynman polaron theory (evaluated with (Eq. 2.192) for the dc polaron mobility). The right figure shows the polaron mobility obtained from [40]’s DiagMC method. The position of the peaks between the two methods align for each temperature ($0.125, 0.25, 0.5, 1, 2, 4 \& 8 K/\omega$, where ω is the single phonon mode frequency). The main difference between the two methods is that the peaks evaluated from the Feynman polaron method are taller and sharper, whereas the peaks evaluated from [40]’s DiagMC method are broader and shallower.

The difference in peak widths between the two methods is likely due to the two-mass spring model approximation made in the Feynman method within the trial action in Eq. (2.123). This fixes the dynamical behaviour of Feynman’s model

a priori since it only contains two harmonic degrees of freedom. The translation invariance of the Fröhlich Hamiltonian then fixes one eigenmode at zero frequency. The frequency of the other mode and the relative spectral weight of the peaks are then the free parameters. This spectrum differs greatly from the true spectrum of the polaron and means that the FHIP polaron mobility may only contain a very crude approximation of the true dissipation of the polaron. The dynamical properties of the FHIP approximation are investigated more by [38].

5.1.2 Multiple Phonon Mode Mobility

To generalise the frequency-dependent mobility in Eq. (5.20), I follow the same procedure as FHIP but use our generalised polaron action S in Eq. (3.8) and trial action S_0 in Eq. (4.1). The result is a memory function akin to Eq. (2.183) that is inclusive of multiple (m) phonon branches j and multiple ($2n$) variational parameters v_p and w_p ,

$$\chi(\Omega) = \sum_{j=1}^m \frac{2\alpha_j}{3\sqrt{\pi}} \int_0^\infty dt \left[1 - e^{i\Omega t/\omega_j} \right] \text{Im}S_j(t) \quad (5.17)$$

where

$$S_j(\Omega) = \frac{\cos(t - i\beta_j/2)}{\sinh(\beta_j/2)} [D_j(t)]^{-3/2} \quad (5.18)$$

where $D(t)$ is just $D_j(it)$ from Eq. (4.4) rotated back to real-time to give a generalised version of $D(u)$ in Eq. (2.180) from FHIP,

$$D_j(t) \equiv D_j(it) = 2 \sum_{p=1}^n \frac{h_p}{v_p^3} \frac{\sin(v_p t/2) \sin(v_p [t - i\beta_j]/2)}{\sinh(v_p \beta_j/2)} - i \left(1 - \sum_{p=1}^n \frac{h_p}{v_p^2} \right) t \left(1 - \frac{t}{i\beta_j} \right). \quad (5.19)$$

The new multiple-phonon frequency-dependent mobility $\mu(\Omega)$ is then obtained from the real and imaginary parts of the generalised χ using Eq. (5.20). The frequency-dependent mobility $\mu(\Omega)$ is obtained from the impedance using

$$\mu(\Omega)^{-1} = \frac{m_b}{e} \sum_j^m \omega_j \text{Re} \{ z_j(\Omega) \} = \frac{m_b}{e} \sum_j^m \omega_j \frac{\Omega^4 - 2\Omega^2 \text{Re}\chi_j(\Omega) + |\chi_j(\Omega)|^2}{\Omega \text{Im}\chi_j(\Omega)} \quad (5.20)$$

where $\chi_j(\Omega)$ is just the j th component of $\chi(\Omega)$. The limit that the frequency $\Omega \rightarrow 0$ gives the FHIP dc-mobility extended to multiple phonon modes,

$$\mu_{dc}^{-1} = \frac{m_b}{e} \lim_{\Omega \rightarrow 0} \sum_{j=1}^m \omega_j \frac{\text{Im}\chi_j(\Omega)}{\Omega} \quad (5.21)$$

since $\text{Re}\chi(\Omega = 0) = 0$.

Numerical integration of the memory function $\chi(\Omega)$

In FHIP [2], and DSG [13], they first convert the integral in the complex memory function $\chi(\Omega)$ (Eq. (2.183)) to a contour integral (Eq. (2.193)) (I provide more details in Appendix A). The contour integral is then evaluated by expanding it as an infinite power series in terms of K and Bessel functions with an imaginary argument.

5.1.3 Multiple Fictitious Particle Mobility

To generalise the frequency-dependent mobility in Eqn. (5.1), we follow the same procedure as FHIP but use our generalised polaron trial action S_0 in Eqn. (4.1). The result is a memory function akin to FHIP's χ (Eqn. (35) in [Feynman1962]), but includes multiple ($2n$) variational parameters v_p and w_p ,

$$\chi(\Omega) = \frac{\alpha\omega_0^2}{3\sqrt{\pi}} \int_0^\infty dt \left[1 - e^{i\Omega t} \right] \text{Im}S(t). \quad (5.22)$$

Here,

$$S(t) = D_{\omega_0}(t)[G(t)]^{-3/2}, \quad (5.23)$$

where $G(t)$ is $G(\tau = it)$ from Eqn. (4.4) rotated back to real-time to give a generalised version of $D(u)$ in Eqn. (35c) in FHIP,

$$G(t) = it \left(1 - \frac{it}{\hbar\beta} \right) + \sum_{p=1}^n \frac{h_p}{v_p^3} \left(D_{v_p}(0) - D_{v_p}(\tau) - iv_p t \left(1 - \frac{it}{\hbar\beta} \right) \right). \quad (5.24)$$

The new frequency-dependent mobility $\mu(\Omega)$ is then obtained from the real and imaginary parts of the generalised $\chi(\Omega)$ using Eqn. (5.1).

The Effect on Dynamics

Given that the multiple fictitious particle trial model rapidly converges to the optimal bound on the polaron-free energy, it is constructive to investigate how

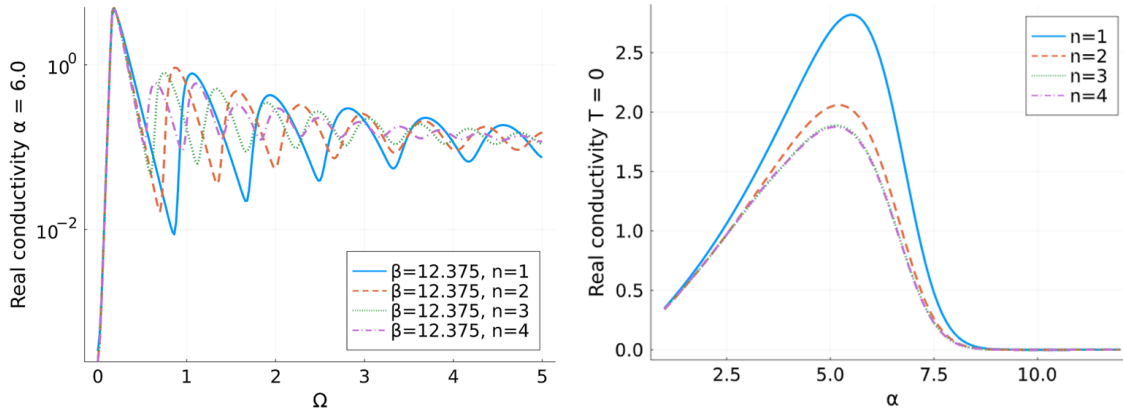


Figure 5.3: Real component of the complex conductivity $\text{Re } \sigma(\Omega)$ for the Fröhlich model for increasing number N of fictitious particles in the trial model. **Left:** The frequency-dependence of the real conductivity at $\alpha = 6$ and $\beta\omega_0 = 12.375$. Here I are in the regime for the maximum potential improvement on the trial model with the additional of fictitious particles. Despite minor improvements on the free energy approximation, the corresponding prediction for the real conductivity changes drastically due to the sensitivity of analytic continuation of the trial model. **Right:** Dependence of the ground-state ($T = 0$ K) real conductivity with the dimensionless electron-phonon coupling α . The real conductivity converges quickly to its optimal solution as soon as $N = 3$ with the maximal improvement occurring around $\alpha = 6$.

the dynamics of the trial system are altered. In Figs. (5.3) the left figure shows the frequency-dependent conductivity at $\alpha = 6$ and thermodynamic temperature $\beta = 12.375\omega_0$ for a number of fictitious particles coupled to the electron $N = 1, 2, 3$ and 4. This is a regime where, from our previous observations, we expect to be close to the maximum potential improvement to the trial model by adding more fictitious particles. All four trial models agree at low frequencies below the phonon frequency. However, upon reaching the phonon frequency and beyond, we see that each trial model produces a conductivity with different oscillation periods and amplitudes. The frequency of this oscillation is smallest for the $N = 1$ trial model and increases with each additional particle. Meanwhile, the amplitude of the oscillation decreases with more particles. The right figure shows the coupling dependence of the conductivity at zero temperature for $N = 1, 2, 3$ and 4. This figure shows that the maximum improvement in the zero-temperature conductivity is around $\alpha = 6$ with little discernible difference between $N = 3$ and 4. Despite the apparent convergence of the conductivity for $N = 3$ and $N = 4$, the frequency dependence shows a significant difference, suggesting that far more fictitious particles may be required to reach a truly converged optimal solution in the frequency response of the trial system.

5.1.4 The Holstein Model

We can specialise in the Holstein model by substituting,

$$|V_{\mathbf{q}}|^2 = g_H^2(n)/N, \quad (5.25a)$$

$$\omega_{\mathbf{q}} = \omega_0, \quad (5.25b)$$

$$\Lambda = 2\sqrt{\pi} \left(V \Gamma \left(\frac{n}{2} + 1 \right) \right)^{1/n} \equiv \Lambda_n. \quad (5.25c)$$

The q -space integral is evaluated,

$$\begin{aligned} I^{(H)}(n) &= \frac{g_H^2(n)V|S^{n-1}|}{N(2\pi)^n} D_{\omega_0}(t) \int_0^{\Lambda_n} dq q^{n+1} e^{-q^2 r_p^2 G(t)}, \\ &= \frac{g_H^2(n)|S^{n-1}|}{2(2\pi)^n r_p^{n+2}} \frac{V}{N} \frac{D_{\omega_0}(t)}{G(t)^{\frac{n}{2}+1}} \left[\Gamma \left(\frac{n}{2} + 1 \right) - \Gamma \left(\frac{n}{2} + 1, r_p^2 \Lambda_n^2 G(t) \right) \right], \\ &= \frac{1}{2r_p^2} \frac{V}{N} \frac{ng_H^2(n)}{(2r_p \sqrt{\pi})^n} \frac{D_{\omega_0}(t)}{G(t)^{\frac{n}{2}+1}} \left[1 - \frac{\Gamma \left(\frac{n}{2} + 1, r_p^2 \Lambda_n^2 G(t) \right)}{\Gamma \left(\frac{n}{2} + 1 \right)} \right]. \end{aligned} \quad (5.26)$$

The memory function for the Holstein model is then:

$$\Sigma^{(H)}(\Omega) = \frac{\rho}{m_b \hbar \Omega \gamma r_p^{n+2}} \frac{4n\alpha^{(H)}}{(2\sqrt{\pi})^n} \int_0^\infty dt \left(1 - e^{i\Omega t} \right) \frac{D_{\omega_0}(t)}{G(t)^{\frac{n}{2}+1}} \left[1 - \frac{\Gamma \left(\frac{n}{2} + 1, r_p^2 \Lambda_n^2 G(t) \right)}{\Gamma \left(\frac{n}{2} + 1 \right)} \right], \quad (5.27)$$

and where $\rho = V/N$ is the particle density and $\gamma = \hbar\omega_0/J$ is the adiabaticity. The inverse Holstein DC mobility is then,

$$\mu_{dc}^{-1} = \frac{\rho e^2}{m_b \hbar \gamma r_p^{n+2}} \frac{4n\alpha^{(H)}}{(2\sqrt{\pi})^n} \int_0^\infty dt t \frac{D_{\omega_0}(t)}{G(t)^{\frac{n}{2}+1}} \left[1 - \frac{\Gamma \left(\frac{n}{2} + 1, r_p^2 \Lambda_n^2 G(t) \right)}{\Gamma \left(\frac{n}{2} + 1 \right)} \right]. \quad (5.28)$$

Polaron Mobility

In Figs. (5.4) we have the temperature dependence of the polaron mobility for the Holstein polaron with varying electron-phonon coupling. At weaker coupling, mobility shows the typical exponentially decreasing band-like transport at temperatures below the phonon energy level. Above the phonon energy, the temperature dependence transitions to a power-law relationship T^{-x} where x is some number

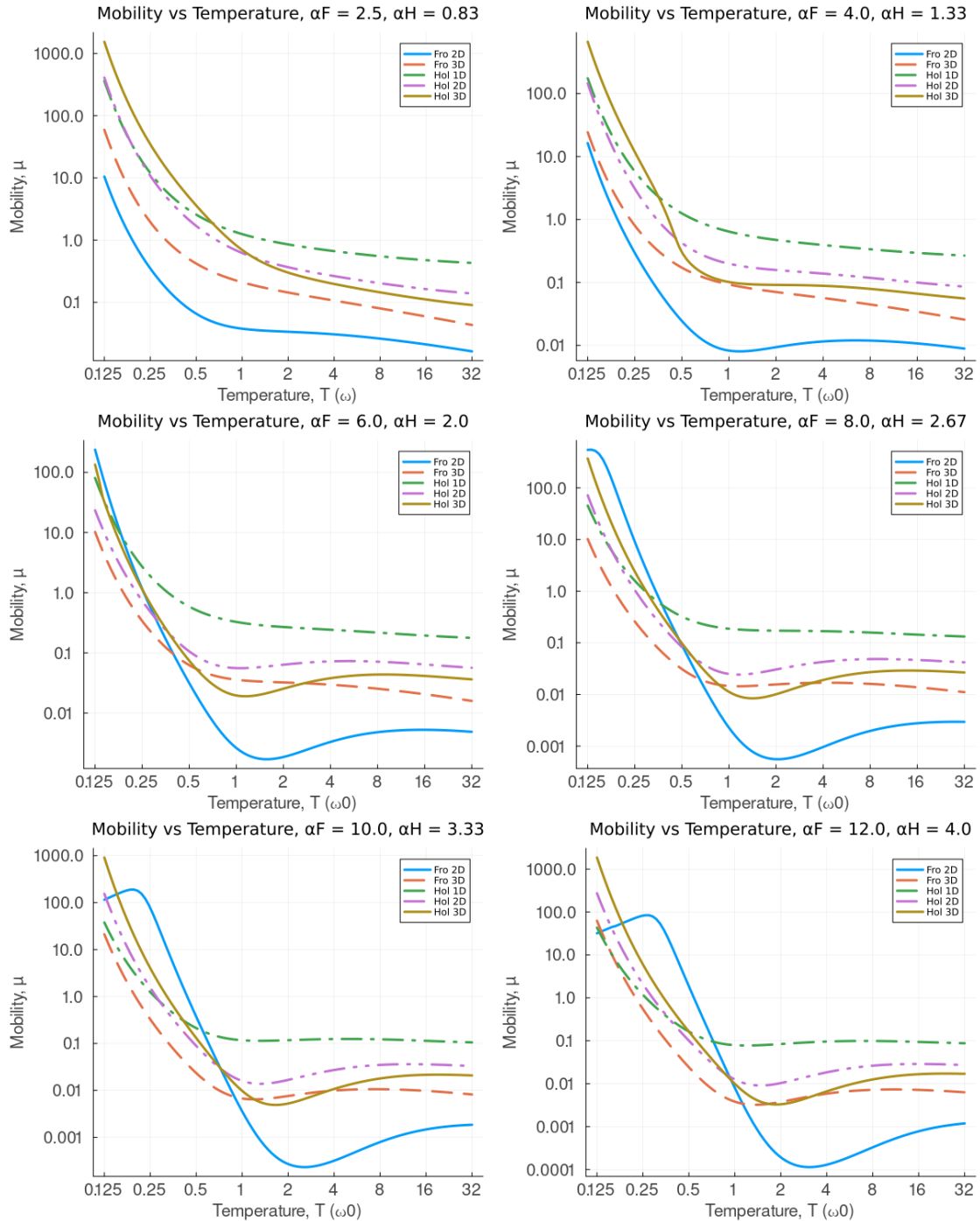


Figure 5.4: Temperature dependence (T , in units of phonon frequency ω_0) of the polaron DC mobility μ for the Fröhlich model in 2D (solid blue) and 3D (dashed orange), and for the Holstein model in 1D (dot-dashed green), 2D (dot-dot-dashed pink) and 3D (solid gold), for values of the Fröhlich electron-phonon coupling $\alpha = 2.5, 4, 6, 8, 10, 12$ and $1/3$ of these values for the Holstein electron-phonon coupling.

that is typically used to determine the dominant scattering mechanism within a material. For example, this index is typically $x = 3/2$ for acoustic phonons.

Again, as we saw previously, 2D Holstein and 3D Fröhlich appear to be most alike. As the electron-phonon coupling increases, we begin to see the onset of the ski-slope feature where the mobility takes on a local minimum at the phonon energy $T = \omega_0$ before increasing to a local maximum at the polaron quasiparticle frequency v and then transitioning back into a power-law relationship at higher temperatures. Each of the different dimensions of both polaron models seems to have a different dependence on the strength of the electron-phonon coupling when it comes to mobility. For the Fröhlich polaron, the ski-slope appears sooner for the 2D model than the 3D model. For the Holstein polaron, the opposite trend seems to be true, with the higher dimension model exhibiting the ski-slope. The 2D Fröhlich polaron also seems to manifest a low-temperature maximum at larger electron-phonon couplings, which transitions in a linear decrease to some finite value in mobility as the temperature goes to zero.

At high temperatures, the Fröhlich polaron mobility follows the temperature power-law $\mu^{(H)} \sim T^{-1/2}$, which is consistent with mobility derived from the electron scattering with optical phonons. However, the Holstein polaron mobility becomes constant at high temperatures, independent of temperature. This may be attributed to the phonon-induced electron hopping between lattice sites along which the electron motion is coherent in the direction of that particular energy band. Likewise, at low temperatures, the mobility increases abruptly below the Debye temperature due to the increasing contribution of the electron transfer without phonon participation.

5.2 Frequency-Dependent Optical Conductivity

5.2.1 Holstein Model

In this section, we look at how the Holstein model varies with an external, perturbing, and varying electric field frequency. Specifically, the polaron memory function, which we compare to the Fröhlich polaron results of FHIP [2], and the optical conductivity, which we compare to the Fröhlich polaron results of DSG [13]. For the memory function we look at frequencies Ω/ω_0 from 0 to 28 and $\alpha^{(F)} = 3, 5, 7$ or $\alpha^{(H)} = 1, 1.67, 2.33$. For the optical conductivity we look at frequencies Ω/ω_0 from 0 to 11 for $\alpha^{(F)} = 1, 3, 5, 6$ or $\alpha^{(H)} = 0.33, 1, 1.67, 2$ and frequencies Ω/ω_0 from 0 to 22 for $\alpha^{(F)} = 7$ or $\alpha^{(H)} = 2.33$.

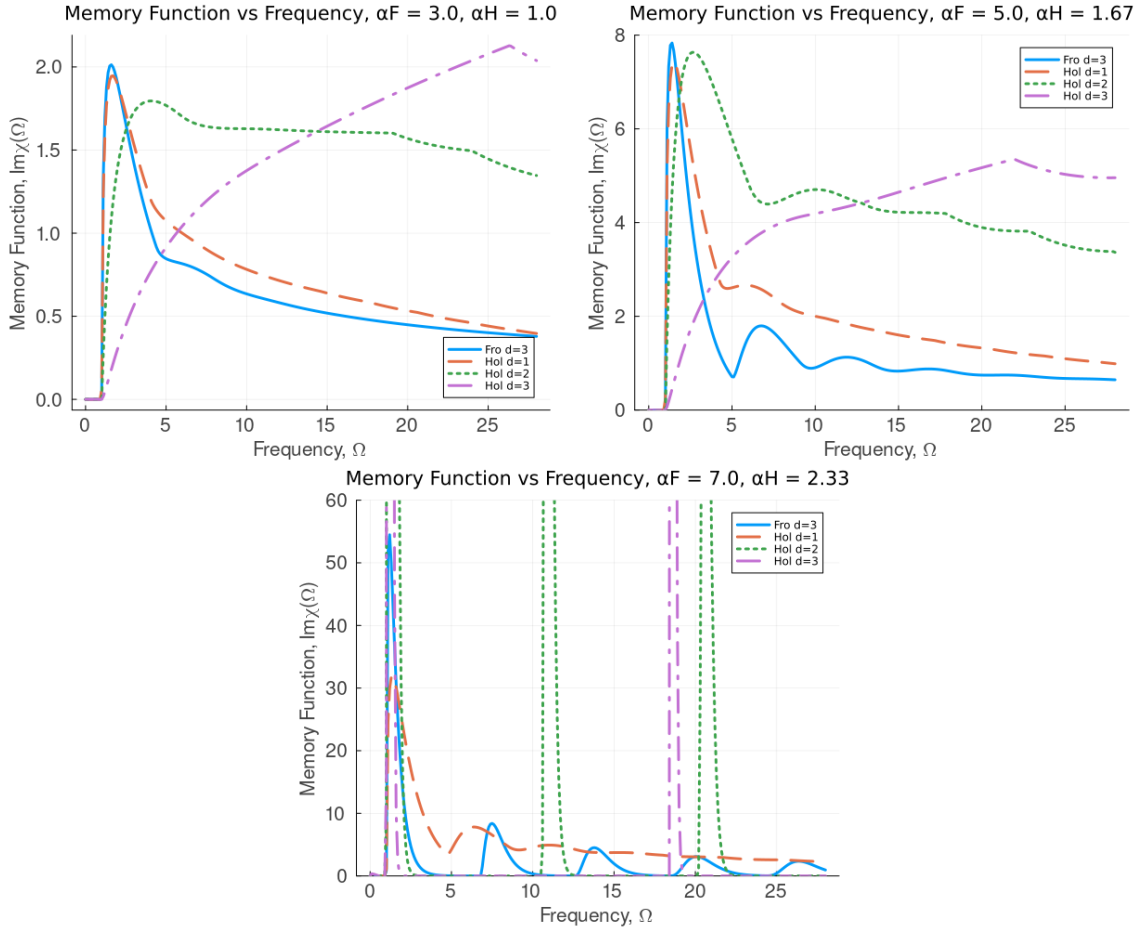


Figure 5.5: Frequency dependence (Ω , in units of the phonon frequency ω_0) of the polaron memory function $\chi(\Omega)$ for the Fröhlich model in 3D (solid blue), and the Holstein model in 1D (dashed orange), 2D (dot-dashed green) and 3D (solid gold), for values of the Fröhlich electron-phonon coupling $\alpha = 1, 3, 5, 6, 7$ and $1/3$ of these values for the Holstein electron-phonon coupling. Here, I only consider the imaginary component to reduce graph clutter, but the real component was also evaluated.

Polaron Memory Function

In Figs. (5.5) is the frequency-dependent imaginary component of the memory function for the Holstein and Fröhlich polarons for a range of electron-phonon coupling strengths. I chose these specific alpha values $\alpha^{(F)} = 3, 5, 7$ for direct comparison to figures (1-3) in FHIP [2]. Note that here we use Devreese and Peeter's definition of the memory function $\Sigma(\Omega)$ [17], which is related to the FHIP memory function $\chi(\Omega)$ by the expression $\Sigma(\Omega) = \chi(\Omega)/\Omega$. I have excluded the 2D Fröhlich result as even at 'weak' coupling, it behaves like the 3D Fröhlich result at strong coupling and is difficult to compare with.

The first most noticeable observation is that the 1D Holstein memory function seems to most closely relate to the 3D Fröhlich memory function. This also is not surprising because the q -space integral in the memory function $\Sigma(\Omega)$ is the

same for the 3D Fröhlich and 1D Holstein polarons. Additionally, the imaginary component of the memory function is zero for frequencies below the phonon frequency, and the first peak corresponds to one phonon excitation.

As the electron-phonon coupling strength increases, more oscillations manifest at multiples of the polaron quasiparticle frequency $\Omega_{\text{peaks}} = 1 + nv, n \in \mathbf{N}$ which correspond to two- three- four etc phonon excitations. These peaks are significantly stronger in the Holstein polaron.

The 2D and 3D Holstein memory functions take very different forms from what is seen for the 1D Holstein and 3D Fröhlich polarons. At lower coupling, there seems to be more of a background lattice response that obscures the underlying phonon excitations until the small polaron state is formed at $\alpha^{(H)} > 2$.

Polaron Optical Conductivity

In Figs. (5.6) is the frequency-dependent real component of the complex conductivity (otherwise known as the optical conductivity) for the Holstein and Fröhlich polarons for a range of electron-phonon coupling strengths. I chose these specific alpha values $\alpha^{(F)} = 1, 3, 5, 6, 7$ for direct comparison to Figs. (1-5) in DSG [13].

Starting at weak coupling $\alpha^{(F)} = 1, \alpha^{(H)} = 0.33$, both models in all the presented spatial dimensions show the same form of a one-phonon excitation peak that decays away at higher frequencies. At intermediate coupling, we begin to see more structure. Firstly, the 2D Fröhlich polaron shows many peaks and side bands that are only made apparent in the 3D Fröhlich polaron at strong coupling. At $\alpha^{(F)} = 3$, we already see a very intense relaxed excited state (RES) transition occurs for Fröhlich 2D followed by a prominent Frank-Condon (FC) excitation peak. Conversely, the other Fröhlich 3D and Holstein 1D, 2D and 3D only exhibit the initial one-phonon peak with no apparent RES transitions or FC peaks. At $\alpha^{(F)} = 5, \alpha^{(H)} = 1.67$, the features of the 2D Fröhlich polaron are pushed to very high frequencies far beyond the other polarons. However, the 3D Fröhlich polaron only just begins to develop a RES transition peak around $\Omega = v$ with the shoulder on the low-frequency side representing the original one-phonon peak and the additional peak on the high-frequency side representing a FC band. The Holstein polaron still only possesses the one-phonon peak for 1D, 2D and 3D. This pattern continues until we exceed $\alpha^{(H)} = 2$. Unlike the Fröhlich polaron, which developed RES and FC peaks before its polaron transition, the Holstein polaron does not develop these features until the coupling increases beyond $\alpha^{(H)} = 2$ where a small polaron state is formed, at which point the onset of strong RES and FC states is far more rapid than for the Fröhlich polaron.

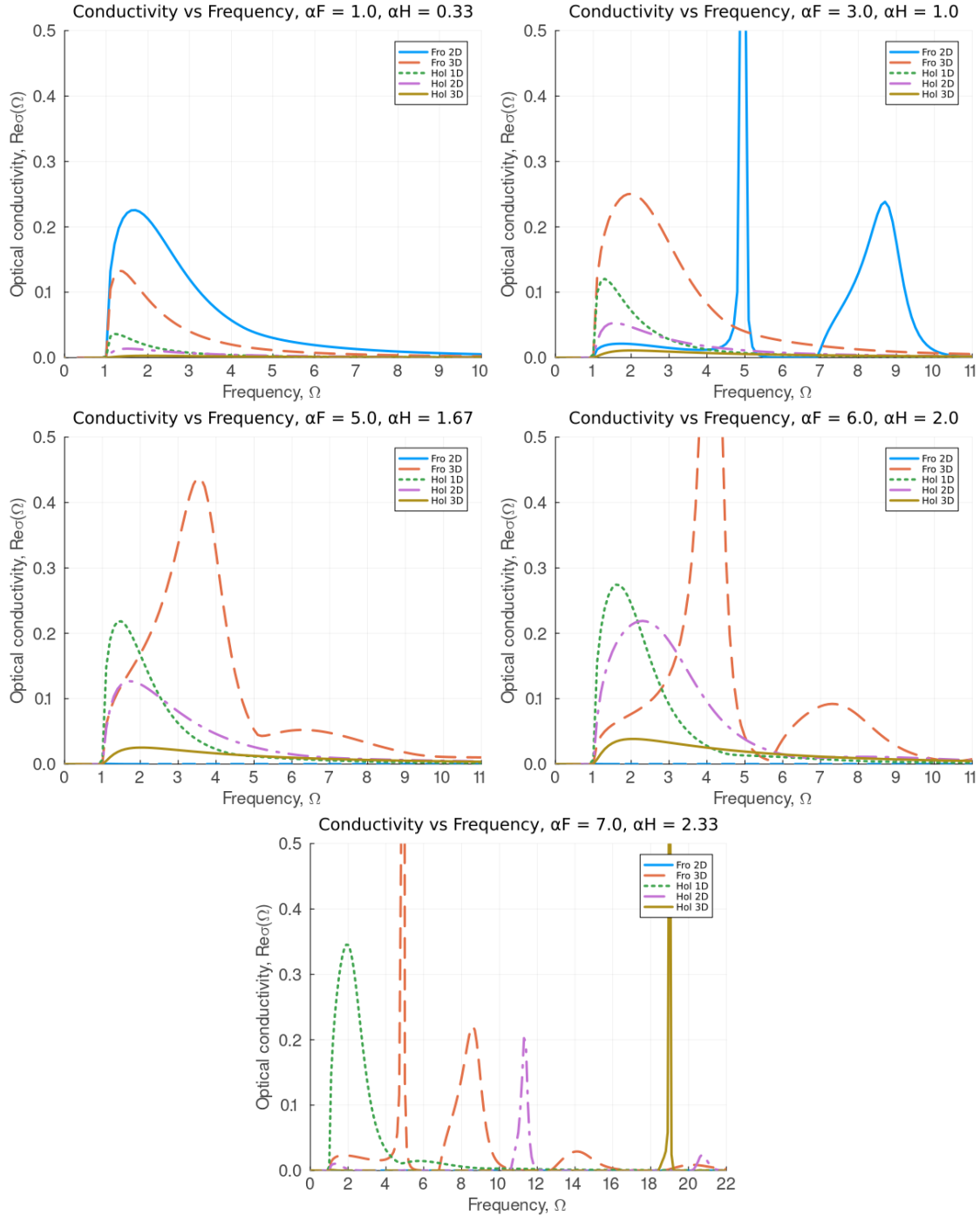


Figure 5.6: Frequency dependence (Ω , in units of the phonon frequency ω_0) of the polaron complex conductivity $\sigma(\Omega)$ for the Fröhlich model in 2D (solid blue) and 3D (dashed orange), and for the Holstein model in 1D (dotted green), 2D (dot-dashed pink) and 3D (d pink), for values of the Fröhlich electron-phonon coupling $\alpha = 3, 5, 7$ and $1/3$ of these values for the Holstein electron-phonon coupling. Here, I only consider the imaginary component to reduce graph clutter, but the real component was also evaluated.

5.3 The Optimal Self-Consistent Response Function

5.3.1 Statics = Dynamics

The function $\Sigma(\Omega)$, which gives the lowest energy in the variational principal at zero temperature, satisfies the integral equation,

$$\Sigma(\Omega) = \frac{2}{n} \sum_{\mathbf{q}} |V_{\mathbf{q}}|^2 q^2 \int_0^\infty d\tau (1 - \cos(\Omega\tau)) e^{-\omega_{\mathbf{q}}\tau} e^{-q^2 r_p^2 [G(0) - G(\tau)]}, \quad (5.29)$$

where,

$$G(\tau) = \int_{-\infty}^\infty \frac{d\omega}{2\pi} \frac{e^{i\omega\tau}}{m\omega^2 - \Sigma(\omega)}. \quad (5.30)$$

The polaron Green's function $G(\tau)$ that minimises the polaron free energy at arbitrary temperature without applied electric and magnetic fields also produces the optimal impedance function $z(\Omega)$.

Generalising the variational equations to a general polaron system, we obtain,

$$F \leq \frac{n}{\beta} \sum_{l=1}^{\infty} \ln \left(\frac{Z(\omega_l)}{m\omega_l^2} \right) - \frac{n}{\beta} \sum_{l=1}^{\infty} \frac{1 - m\omega_l^2}{Z(\omega_l)} - \int_0^{\frac{\hbar\beta}{2}} d\tau \sum_{\mathbf{q},j} |V_{\mathbf{q},j}|^2 D_{\mathbf{q},j}(\tau) e^{-q^2 r_p^2 [G(0) - G(\tau)]}, \quad (5.31)$$

where,

$$\Sigma(\tau) = \frac{2}{\beta} \sum_{l=1}^{\infty} \frac{1 - \cos(\omega_l \tau)}{Z(\omega_l)}, \quad (5.32)$$

and,

$$Z(\omega_l) = m\omega_l^2 + 4 \int_{-\infty}^{\infty} d\Omega \frac{P}{\Omega} \frac{G(\Omega) \omega_l^2}{\Omega^2 + \omega_l^2}, \quad (5.33)$$

and $\omega_l \equiv 2\pi l / \beta$, $l \in \mathbf{N}$.

CHAPTER 6

APPLICATION FOR REAL MATERIALS

What is the meaning of life?

—John Doe, *Thoughts*, 1971

This is the introduction paragraph.

6.1 Methylammonium Lead Halide Perovskites

I have produced a Julia Pluto.jl notebook that uses the multiple phonon theory to evaluate the decomposed Fröhlich α_j components associated with 15 modes of Methylammonium lead iodide (MAPbI_3). The frequencies and infrared activities associated with these modes are listed in Table 1. The decomposed α_j parameters and phonon frequencies ω_j are then inserted into the variational principle for multiple phonons to obtain a v and w parameter that provide the lowest upper-bound to the exact free energy of the multi-modal polaron system. The two effective phonon frequencies schemes, labelled scheme A and B in [14] (c.f. section 3.6.5), evaluate the Fröhlich alpha for MAPbI_3 to be $\alpha = 2.52$ (towards zero temperature the A scheme gives a slightly different value of 2.44). In comparison, including the ionic contributions of each MAPbI_3 phonon mode explicitly produced the decomposed Fröhlich alpha α_j shown in Table 1. From there, I obtain an effective alpha for MAPbI_3 of $\alpha_{\text{eff}} = 2.66$ which is only slightly larger than the value predicted by the effective mode A and B schemes. The free energy approximated by the multiple phonon theory is compared to the Hellwarth and Biaggio effective mode

Phonon Frequencies (THz)	IR Activity	$\epsilon_j^{\text{ionic}}$	α_j
4.017	0.082	0.300	0.034
3.888	0.006	0.025	0.003
3.531	0.054	0.254	0.031
2.755	0.021	0.166	0.023
2.438	0.232	2.308	0.336
2.249	0.262	3.071	0.465
2.080	0.234	3.203	0.505
2.034	0.062	0.893	0.142
1.567	0.037	0.886	0.161
1.019	0.013	0.721	0.162
1.002	0.007	0.402	0.091
0.997	0.010	0.618	0.141
0.920	0.011	0.767	0.182
0.801	0.002	0.156	0.040
0.574	0.007	1.163	0.349

Table 6.1: Infrared activity, ionic dielectric contribution and decomposed Fröhlich alpha values associated with each of the phonon modes in MAPbI₃ taken from Ref [41]. The effective Fröhlich alpha $\alpha_{\text{eff}} = \sum_j \alpha_j$ is found to be 2.66 for MAPbI₃.

theory in Figure 6.1a. The two Hellwarth schemes agree for almost all temperatures except for a small deviation towards zero temperature, whereas the A scheme gives a slightly lower value. The multiple phonon theory clearly gives a lower estimate of the free energy of the polaron compared to the Hellwarth theory for all temperatures above roughly 100K but gives a higher value at lower temperatures and zero temperatures. Figure 6.1b compares the multiple phonon variational v and w parameters to the effective variational parameters from the Hellwarth and Biaggio effective mode theory. The two agree at zero temperature, but the multiple phonon theory predicts larger polaron frequencies at higher temperatures and a smaller difference in v and w , $v - w$, at all temperatures.

Figures 6.2 (contour plots) and 6.3 (ridge-line plots) compare the complex conductivity obtained from the multiple phonon model (left column) to the complex conductivity obtained from the Hellwarth and Biaggio B scheme (right column). The top rows show the real part of the conductivity (i.e. the AC mobility), the middle rows show the imaginary part, and the bottom rows show the absolute value. I chose the B scheme over the A scheme because it matches an effective frequency to the full extent of Ōsaka's finite temperature variational principle, arguably more accurate. On the other hand, the A scheme produces a temperature-dependent Fröhlich alpha parameter and effective phonon frequency. This is unlike the original Fröhlich alpha and phonon frequency, which are independent

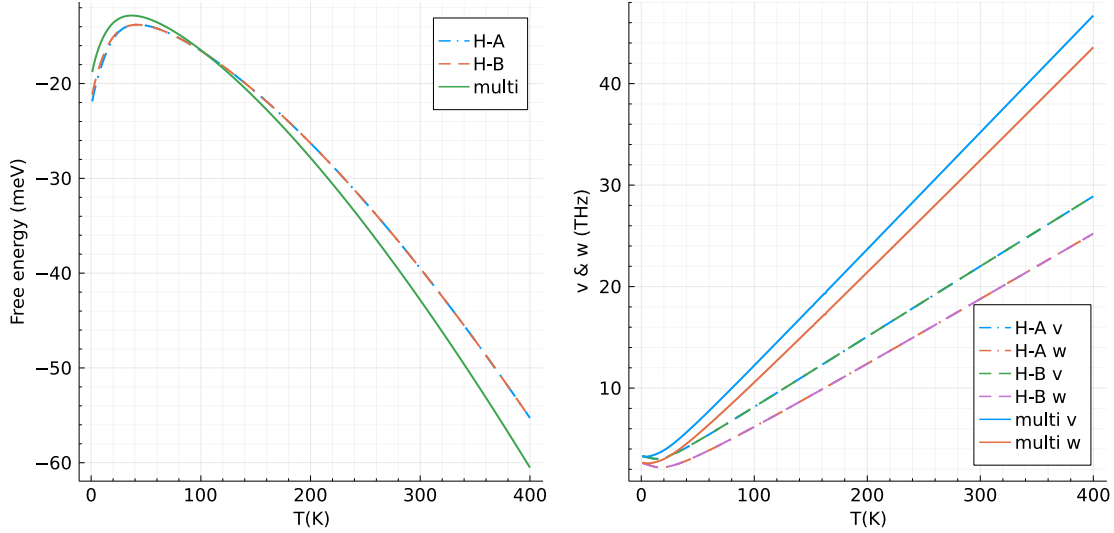


Figure 6.1: (left): The free energy of the Hellwarth and Biaggio effective mode A & B schemes and for the multiple phonon model between 1K and 400K. The two Hellwarth schemes agree almost exactly, except for a small deviation at low temperatures. The multiple phonon model gives a lower free energy estimate for temperatures above 100K. (right): The variational parameters v & w from the Hellwarth and Biaggio effective mode A & B schemes and the multiple phonon model. The effective mode schemes agree, whereas the multiple phonon model gives values larger than the Hellwarth schemes but approaches their values towards zero temperature.

of temperature. Nonetheless, the two schemes do produce near-identical results for most temperatures anyway, except for a slight deviation at very low temperatures. So, many comparisons with the B scheme will also be comparable to those of the A scheme.

Both the multiple phonon theory and the Hellwarth and Biaggio effective mode theory have similar DC mobilities and high-temperature complex conductivities. Likewise, they both possess a broad peak starting around a frequency of 2.03 THz, which is the effective phonon frequency derived from the B scheme. (At zero temperature, the A scheme gives an effective phonon frequency of 2.17 THz). The start of the main peak then shifts up in frequency as the temperature increases whilst primarily broadening and flattening. The theories differ in their frequency dependence. Whilst both possess the same main peak starting around 2 THz, the multiple phonon theory possesses extra peaks below 2 THz, particularly two fairly sharp peaks starting around 0.50 THz and 1.00 THz. All of these extra details are washed out at higher temperatures to leave one main broad peak with a maximum located at a slightly lower frequency than Hellwarth's and Biaggio's theory.

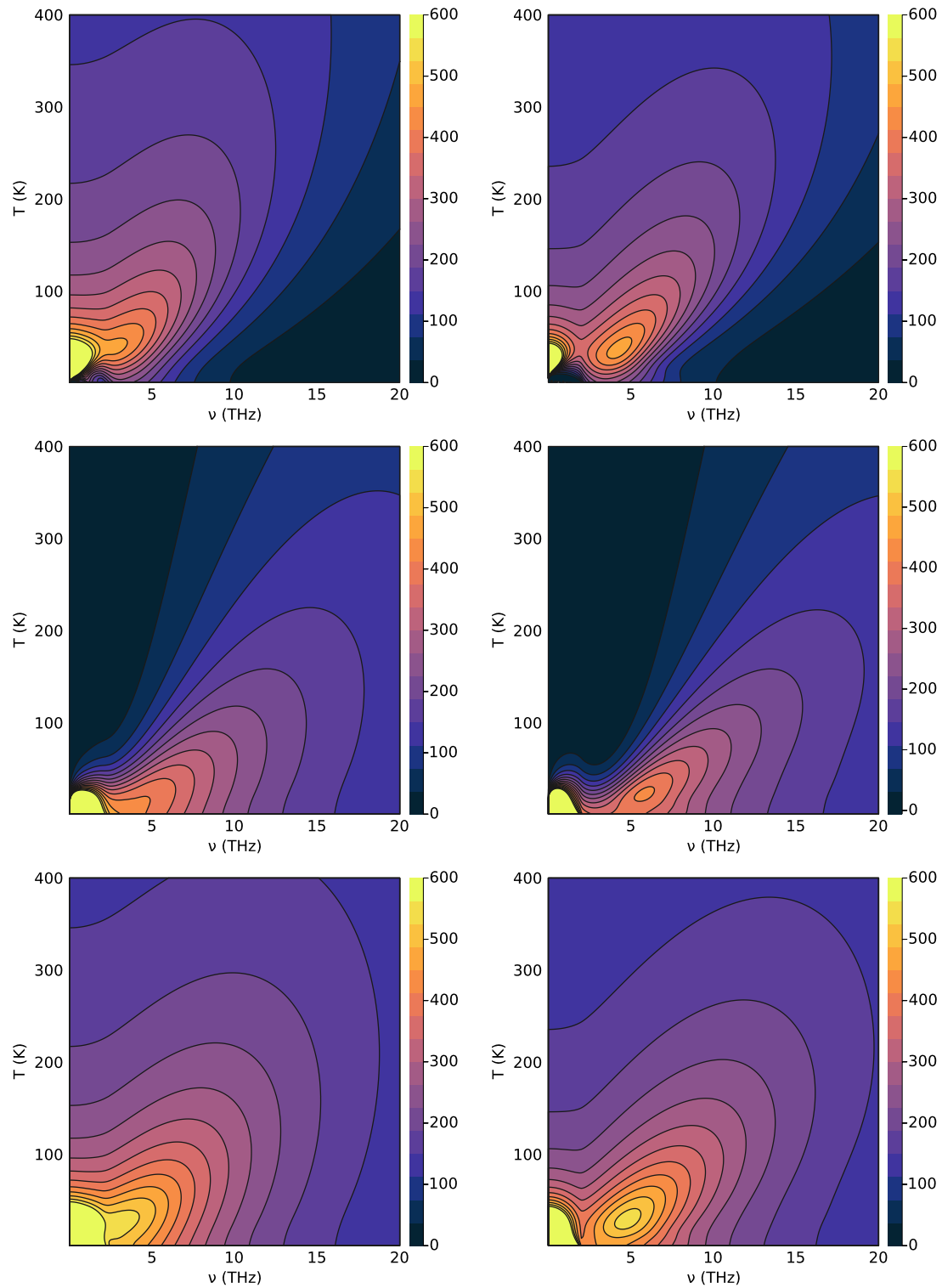


Figure 6.2: Left: Multiple phonon scheme (a) real conductivity, (c) imaginary conductivity, (e) absolute conductivity. Right: Hellwarth 'B' scheme: (b) real conductivity, (d) imaginary conductivity, (f) absolute conductivity.

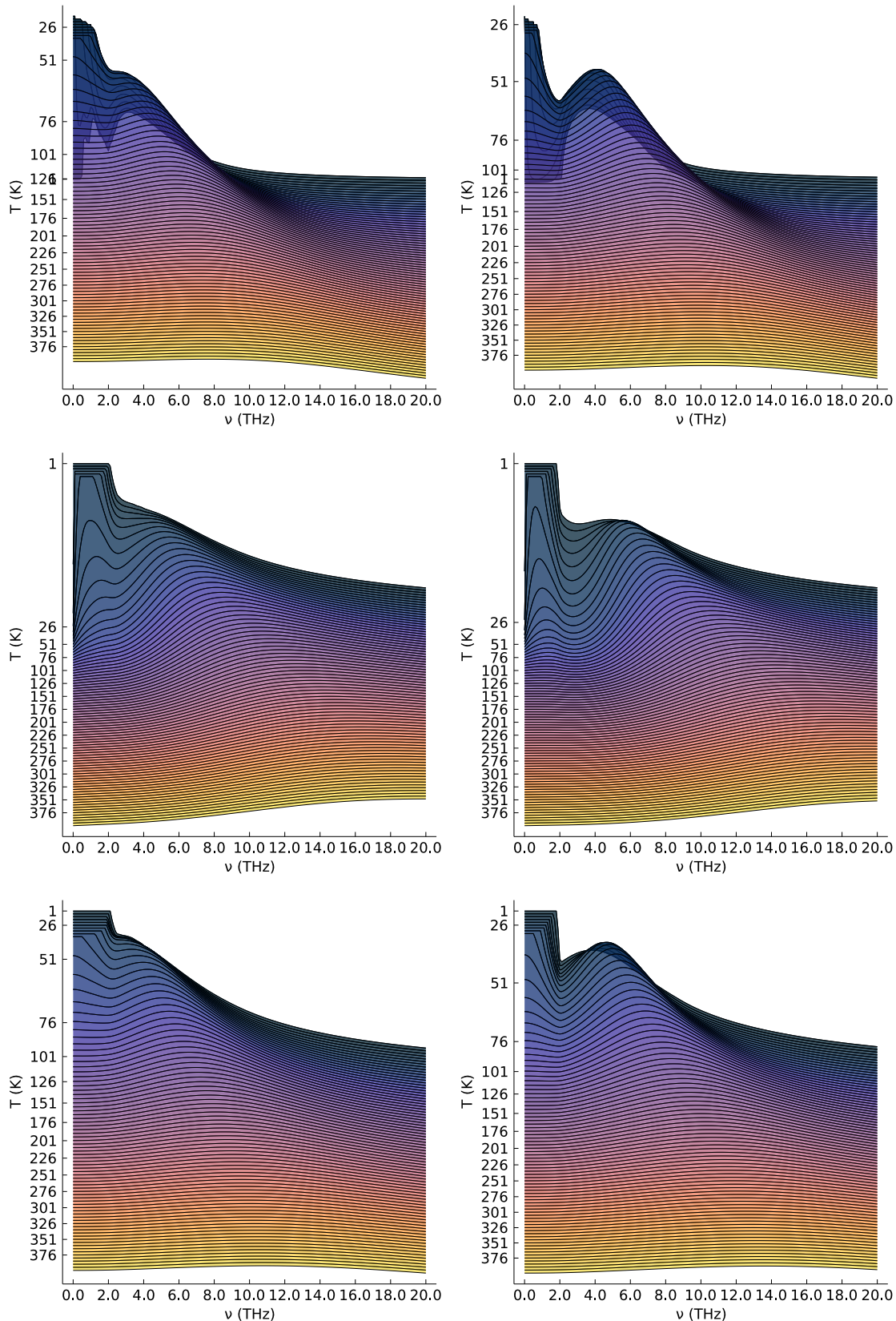


Figure 6.3: Left: Multiple phonon scheme (a) real conductivity, (c) imaginary conductivity, (e) absolute conductivity. Right: Hellwarth 'B' scheme: (b) real conductivity, (d) imaginary conductivity, (f) absolute conductivity. At lower temperatures, the conductivity has been cut off at 600 to enable us to see the main features.

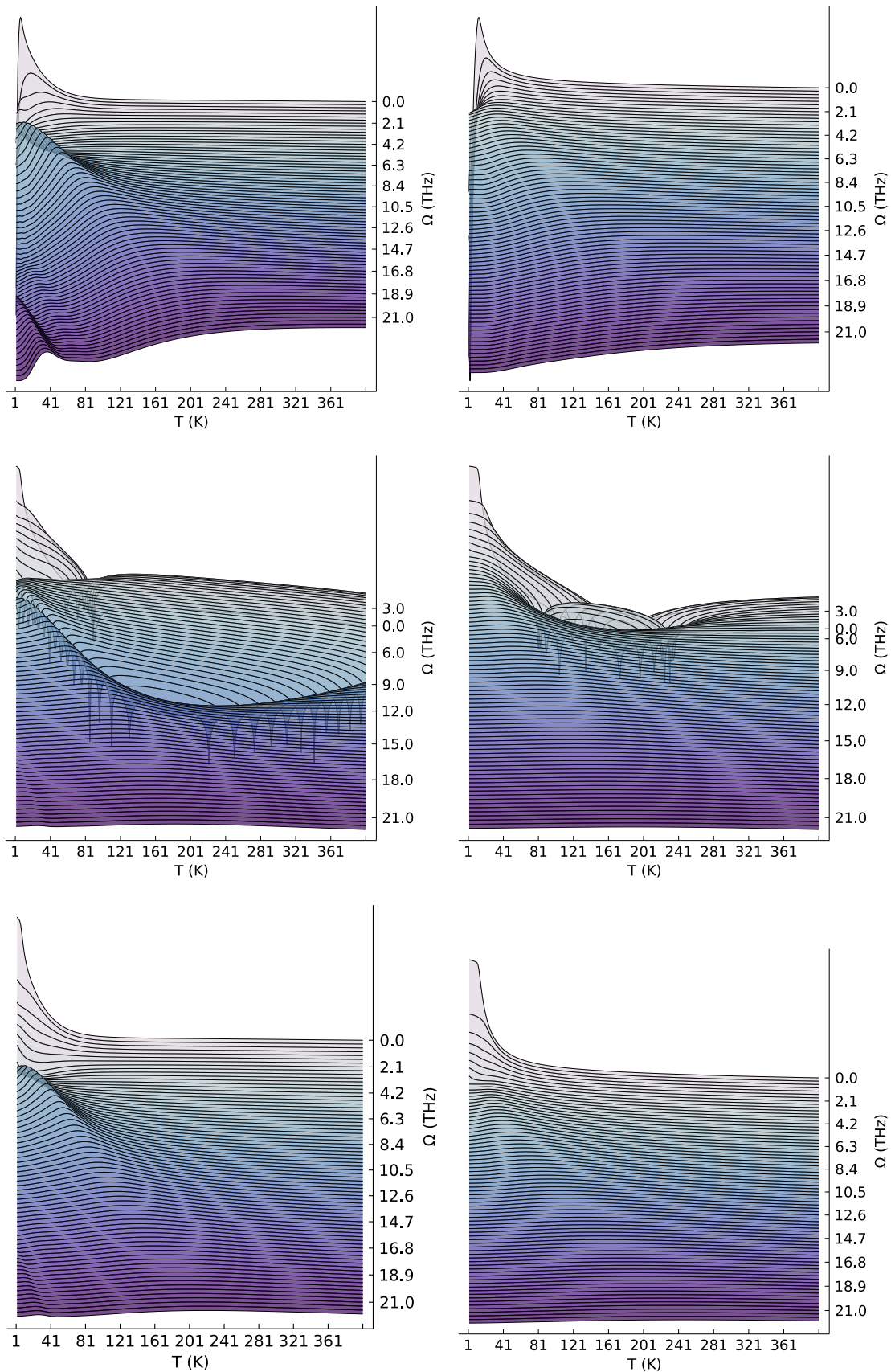


Figure 6.4: (a) Multiple phonon real conductivity. (b) A scheme of real conductivity. (c) Multiple phonon imaginary conductivity. (d) A scheme of imaginary conductivity. (e) Multiple phonon absolute conductivity. (f) A scheme of absolute conductivity.

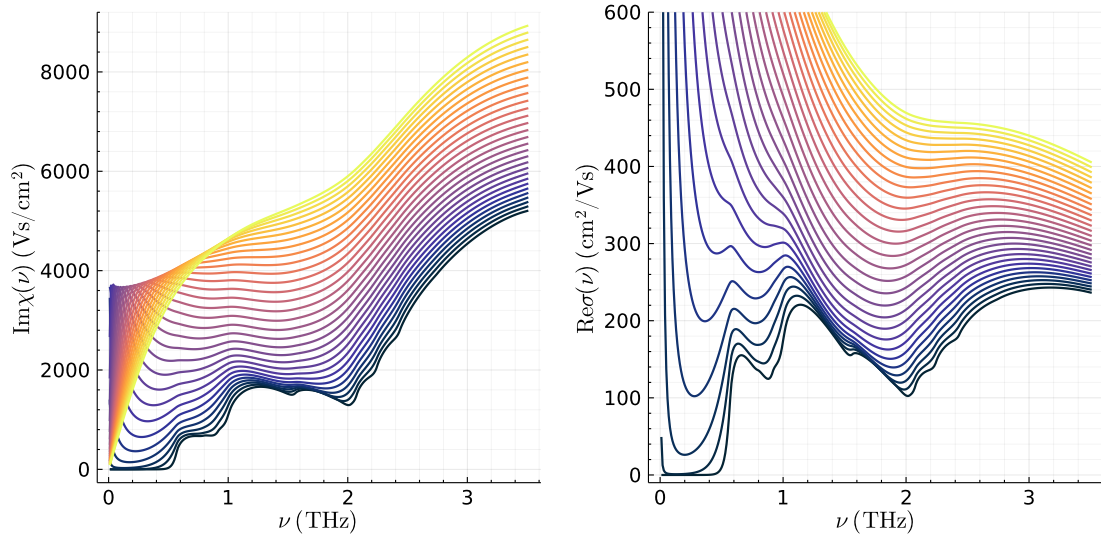


Figure 6.5: (left): The imaginary part of the multiple phonon mode memory function in Eq. (5.17) evaluated for MAPbI_3 . (right): The real part of the multiple phonon mode complex conductivity (i.e. mobility) in Eq. (5.20) evaluated for MAPbI_3 . These are calculated for the phonon modes listed in Table 1. The reduced thermodynamic beta $\beta_j = \hbar\omega_j/(k_B T)$ is evaluated for temperatures $T = 1 \text{ K}$ (black curves) to $T = 30 \text{ K}$ (yellow curves).

6.1.1 Modelling terahertz spectroscopy unveiled polaron photo-conductivity dynamics in Metal-Halide Perovskites

Recently, we used ultrafast visible pump-infrared push-terahertz probe spectroscopy to measure the real-time photo-conductivity of methyl-ammonium lead iodide in [42]. In this paper, I provided my multiple phonon mode mobility, applied to the 15 modes of MAPbI_3 in Table 1, to model the complex conductivity and compare the results to the photo-conductivity measurements.

In Figure 6.5, I provide the low-temperature ($T = 1 \text{ K}$ to $T = 30 \text{ K}$) results of the imaginary component of the memory function $\text{Im}\chi(\nu)$ (left) and the real part of the complex conductivity $\text{Re}\sigma(\nu)$ (right). These have peaks that occur around the frequencies 0.60 THz, 1.25 THz and 1.75 THz, as well as a very broad peak that starts around 2.00 THz that seems to have extra peaks underlying it to give the appearance of oscillations around 2.15 THz and 2.25 THz.

Figures 6.2 and 6.3 show that the broad peak is the last feature that decays away at higher frequencies. The broad peak has a maximum of around 3.00 THz at $T = 1$, which flattens and shifts to higher frequencies at higher temperatures, where it becomes the only remaining feature. This is to be compared to the photo-conductivity measurements shown in Figure 6.6, where the real component maxima occur around the frequencies 1.25 THz and 2.25 THz, with a shoulder occurring on the side of the 1.25 THz peak around 0.60 THz. The shoulder and

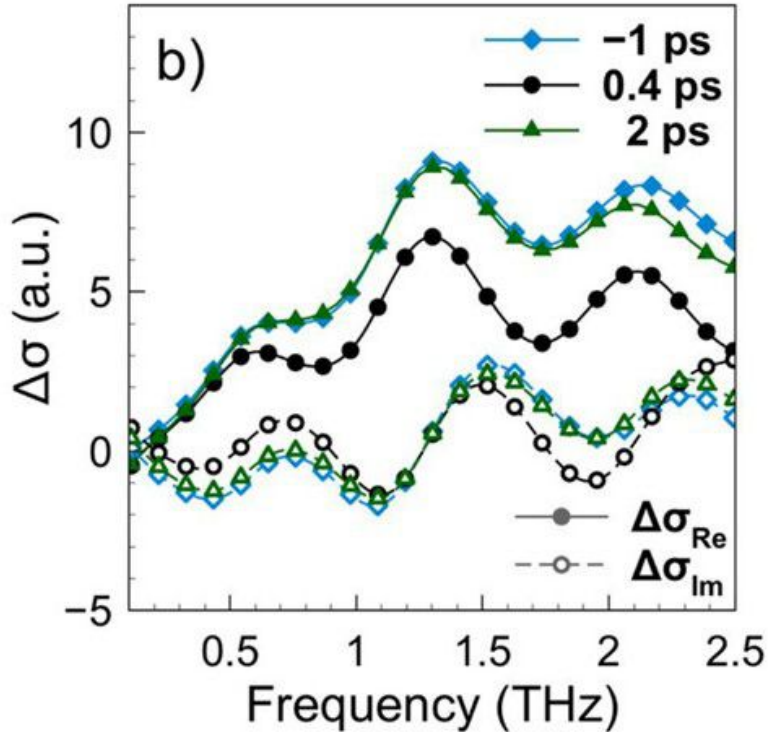


Figure 6.6: Terahertz photo-conductivity spectra obtained from a visible pump-IR push-THz probe measurement in [42]. The plot shows the complex conductivity's real (solid markers) and imaginary (hollow markers) parts in MAPbI_3 . The blue, black and green dashed lines show before, at and after the arrival of the push pulse, respectively.

1.25 THz peak seems to be in agreement with the multiple phonon model; however, the broader peak, whilst roughly around the right frequency of 2.25 THz, is far broader and prominent in the theoretical model compared to the photo-conductivity measurements.

One thing to note is the apparent temperature differences between the multiple phonon model and the experiment. In the multiple phonon model, the one-phonon peaks associated with each phonon mode only appear at very low temperatures and are quickly washed out as the temperature increases until at around $T > 10$ K, only the broad peak around 3.00 Thz remains. The multiple phonon theory assumes that the electron and phonon thermal bath are at thermal equilibrium. However, in the experiment, the electron(s) is definitely not at thermal equilibrium and is very hot.

6.2 Rubrene & Organic Crystals

In organic electronic materials, it is understood that the charge-carrier state is a small polaron. This is often modelled with semi-classical transfer rate theories

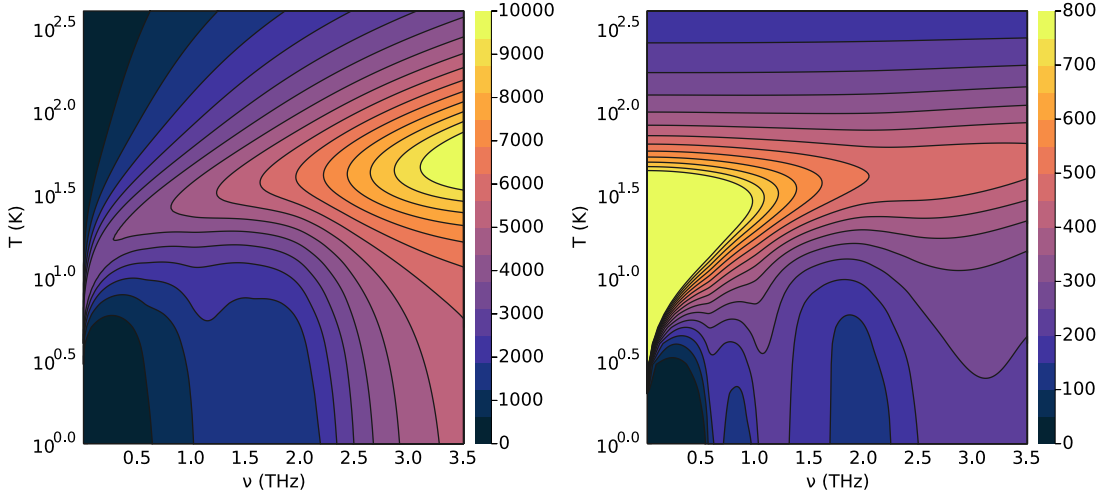


Figure 6.7: Contour plots for (left): The imaginary part of the multiple phonon mode memory function (5.17) evaluated for MAPbI_3 . (right): The real part of the multiple phonon mode complex conductivity (5.20) evaluated for MAPbI_3 . Here the temperature axis is log-scaled and ranges from $T = 1 \text{ K}$ to $T = 400 \text{ K}$ and frequency zoomed in onto the range $\nu = 0 \text{ THz}$ to $\nu = 3.5 \text{ THz}$.

as a classical object hopping from site to site. The matrix elements which parameterise these rate equations can be calculated, within certain approximations, from electronic-structure calculations, but it is a challenge (and often input to the simulation and calculations) to define the sites on which the charge carriers are localised.

One of the prototypical materials studied frequently to investigate electron-phonon coupling is Rubrene (5,6,11,12-tetraphenyltetracene), which has one of the highest carrier mobilities and can reach a few tens of cm^2/Vs for holes. This is a good test for applying our newly derived variational Holstein model to predict its charge-carrier mobility in bulk. I take parameters for Rubrene from Ordejon et al. [43] where they derived Peierls (off-site) and Holstein (on-site) contributions by fitting the generalise Holstein-Peirels model with Density Functional Theory (DFT) calculations performed using SEISTA code. Here, I use their Holstein parameter coupling, which I have listed in Table 1, and use these parameters within our newly derived variational Holstein method. For simplicity, I consider a single effective phonon frequency, though the method presented here could be extended to multiple phonon modes, as I have demonstrated for the Fröhlich Hamiltonian [44].

The results for ground-state Holstein and Fröhlich polarons for Rubrene are shown in Table 2. Likewise, Table 3 gives the result for $T = 300 \text{ K}$, including the finite temperature DC mobility, which I calculate to be $\mu_{\text{Rubrene}}^{(H)} = 11.55 \text{ cm}^2\text{V}^{-1}\text{s}^{-1}$ for the Holstein polaron and $\mu_{\text{Rubrene}}^{(F)} = 89.76 \text{ cm}^2\text{V}^{-1}\text{s}^{-1}$ for the Fröhlich polaron. Immediately, the Holstein prediction is inline with what's observed in

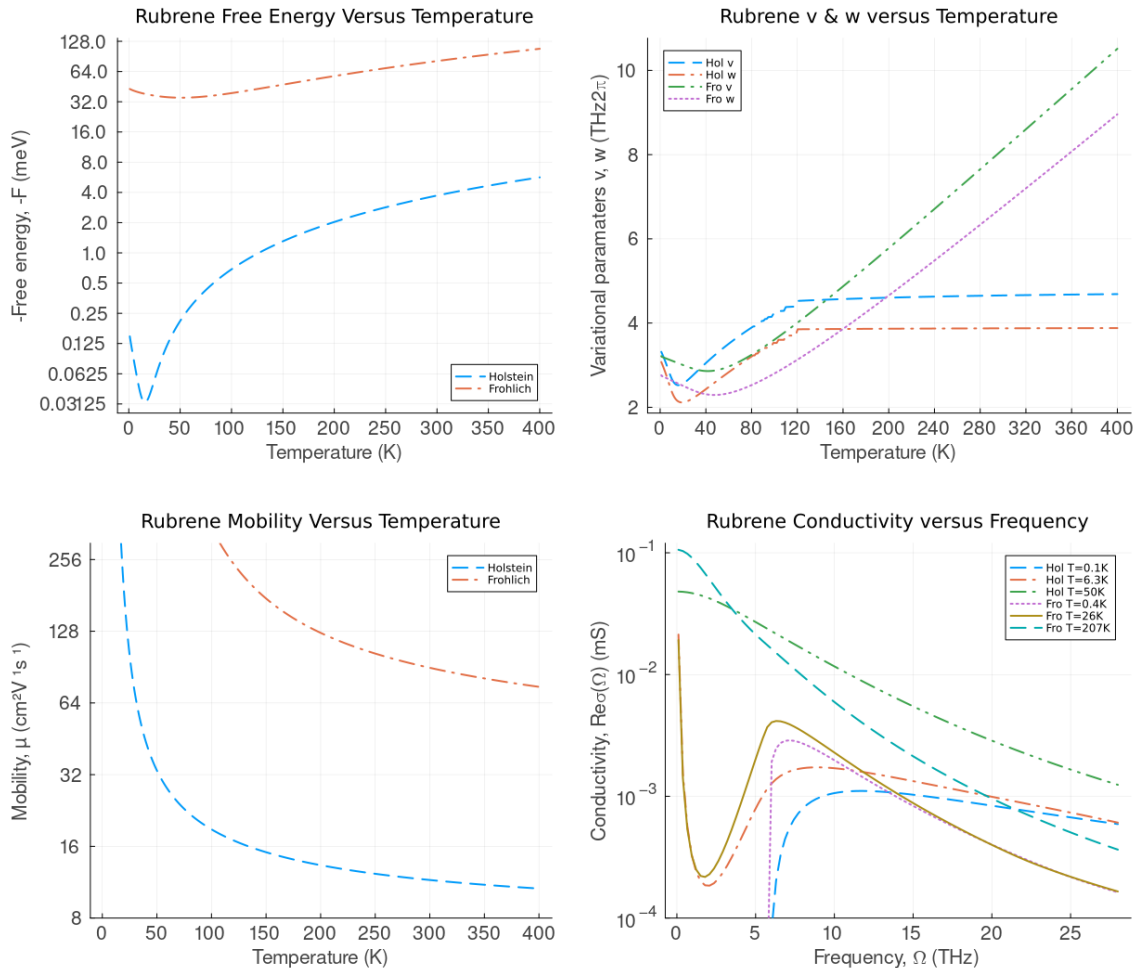


Figure 6.8: Polaron properties of the variational Holstein model for a bulk 3D Rubrene organic crystal. **Top-left:** The polaron free energy F (meV) in Rubrene as a function of temperature (K). **Top-right:** Optimal variational parameters v and w (THz 2π) as a function of temperature (K). There appears to be some possible numerical artefact manifesting as the step-like increments. **Bottom-left:** The DC polaron mobility $\mu(T)$ ($\text{cm}^2 \text{V}^{-1} \text{s}^{-1}$) as a function of temperature T (K). **Bottom-right:** The real component of the conductivity $\text{Re}\sigma(\Omega)$ (mS) as a function of frequency Ω (THz) for temperatures $T = 0.1 \text{ K}, 0.8 \text{ K}, 6.3 \text{ K}$ and 50 K .

g (meV)	ω_0 (THz)	J (meV)	a (Å)	γ	m_b (m_e)	λ^2	α
106.8	5.768	134.0	14.06	0.178	0.144	20.04	0.595

Table 6.2: 3D Rubrene Bulk crystal data. Here g is the Holstein hole-phonon coupling element, ω_0 is the single-mode effective phonon frequency, J is the electron transfer/hopping integral, a is the geometric-meaned crystal lattice constant, γ is the Holstein adiabaticity unitless parameter, m_b is the effective hole band-mass, $\lambda^2 = (g/\hbar\omega_0)^2$ is the unitless squared hole-phonon coupling element and $\alpha = \lambda^2\gamma/6$ is the 3D unitless Holstein electron-phonon parameter.

	v_0 (THz 2π)	w_0 (THz 2π)	M_0 (m_e)	κ_0 (mN m $^{-1}$)	R_0 (Å)	F_0 (meV)
Holstein	3.376	3.139	0.157	24.71	0.828	-0.178
Fröhlich	3.213	2.758	0.357	3.250	48.33	-43.60

Table 6.3: Ground-state polaron properties for a Rubrene Bulk crystal calculated using the variational Holstein and Fröhlich models.

experiments whereas the Fröhlich greatly overestimates. Note that for the Fröhlich model, I have used an approximate comparative unitless coupling value of $\alpha^{(F)} \approx 3.0 \times \alpha^{(H)} = 1.785$.

At zero temperature, the Holstein polaron radius R_0 is 0.058 times the lattice constant and so is definitely a *small* polaron. Compare this to the Fröhlich model where the polaron radius is 3.436 times the lattice constant and so is a *large* polaron. The Holstein polaron mass M_0 is only slightly large at 1.08 times the hole band mass, whereas the Fröhlich polaron mass is already 2.48 times heavier than the valence-band hole. Notably, the spring-constant κ_0 for the Holstein polaron is over 7 times stronger than for the Fröhlich polaron, which may correspond to an increased likelihood for the Holstein polaron to stay local to its current lattice site compared to the Fröhlich polaron which is more delocalised and likely to move around. This is certainly reflected in the predicted room-temperature mobilities, as mentioned above.

At room temperature $T = 300$ K, both polarons have roughly doubled in size. The Holstein polaron radius is still only 0.1 times the lattice constant, whereas the Fröhlich polaron is now about 6 times larger than the lattice constant. Both polarons now have the same mass, around 3 times heavier than the valence-band

	v (THz 2π)	w (THz 2π)	M (m_e)	κ (mN m $^{-1}$)	R (Å)	F (meV)	μ (cm 2 V $^{-1}$ s $^{-1}$)
Holstein	4.656	3.875	0.444	106.8	1.465	-3.735	11.55
Fröhlich	8.143	6.780	0.442	24.33	83.07	-81.58	89.76

Table 6.4: Room temperature (300 K) polaron properties for a Rubrene Bulk crystal calculated using the variational Holstein and Fröhlich models.

hole. The spring constant for the Holstein polaron is now only 4 times greater than the Fröhlich polaron.

In Figs. (6.8) I give the temperature-dependent properties for the Rubrene polaron: polaron-free energy and mobility. I also provide the optimal variational parameters v and w with respect to temperature. Additionally, I provide the frequency-response of the optical conductivity at temperatures $T = 0.1$ K, 6.3 K and 50 K for the Holstein polaron and $T = 0.4$ K, 26 K and 207 K for the Fröhlich polaron. The difference in temperatures is because the two models are within the same temperature regime for their respective inverse thermodynamics temperatures. For the Holstein polaron, $T^{(H)} = 1$ in polaron units is about $T = 11.6$ K, whereas in the Fröhlich polaron units $T^{(F)} = 1$ is about $T = 48$ K. In the top-left figure, we have the polaron free energies for Rubrene, which has a maximum of $T = 1$ in polaron units (note that the figure shows the negative of the free energy). The Holstein polaron free energy is significantly smaller than the Fröhlich polaron since it only ever couples to one lattice site, whereas the Fröhlich polaron (in principle) couples to many lattice sites over an extent of multiple lattice constants. The Holstein polaron seems to have a sharper dependence on temperature at lower temperatures, but both polarons have a similar dependence above the Debye temperature $T_D \sim 120$ K corresponding to the energy of the Rubrene effective phonon mode. The top-right figure shows the temperature dependence of the v and w variational parameters. For both polarons, these take a minimum at $T = 1$ in the respective polaron units, but whilst above the Debye temperature v and w increase linearly with temperature for the Fröhlich polaron, they reach a sudden plateau for the Holstein polaron. In the bottom-right figure, we see the temperature dependence of the polaron charge-carrier mobility. The Holstein polaron mobility descends far more quickly than for the Fröhlich polaron and reaches what will eventually become a constant value around $\mu \sim 9.0 \text{ cm}^2\text{V}^{-1}\text{s}^{-1}$ towards higher temperatures, whereas the Fröhlich mobility will continue to decrease at a rate proportional to $\mu \sim T^{-1/2}$. Finally, the bottom-right figure shows the frequency dependence of the real component of the complex conductivity for both polarons. At low temperatures, both polarons see a response peak beginning at the phonon frequency $\omega_0 = 5.768$ THz, but then the Fröhlich polaron response decays far more rapidly with frequency than the Holstein polaron. As we increase the temperature, this trend continues, except that for both polarons, we begin to see some response below the phonon frequency due to the presence of thermally excited phonons that generate an extra background response. This results in a local minimum in the conductivity around the effective polaron frequency v as energy is lost to internal phonons that make up the polaron state. At much higher temperatures,

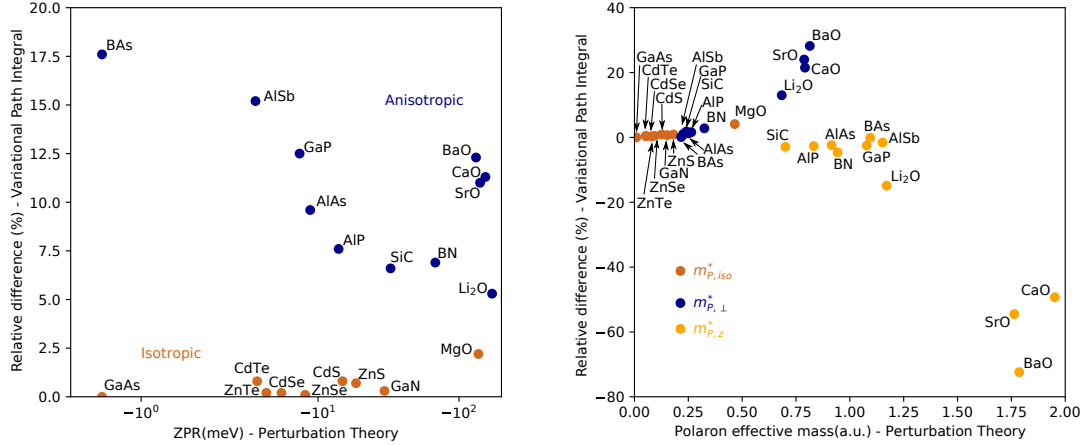


Figure 6.9: Both figures are taken from [45]. (left): The relative differences between the ground-state energy of the polaron determined using perturbation theory (which fully accounts for any anisotropy) and the Feynman variational approach (using my approximate treatment of anisotropy). (right): The relative difference between the effective masses was determined using perturbation theory and the Feynman variational approach (again, only approximately accounting for anisotropy). $m_{p,iso}^*$ is the isotropic effective mass, $m_{p,\perp}^*$ and $m_{p,z}^*$ are the in-plane and out-of-plane polaron effective masses.

the thermally excited phonon response now drowns out any polaronic response, and we are left with a typical Drude-like conductivity for both polarons, again with the Holstein polaron decaying more slowly than the Fröhlich polaron with increasing frequency.

By applying both polaron models to Rubrene, we can more clearly see that the physics described by either model is very different. However, the predictions of the Holstein model seem to better align with the experimentally observed charge-carrier mobility.

6.3 Cubic & Anisotropic Materials

In [45], we investigate the polaron effective mass, radius and ground-state energy that arise from a generalised Fröhlich Hamiltonian that incorporates degenerate bands with anisotropy and multiple phonon branches. These polaron properties are calculated for 20 cubic materials (including II-VI compounds: CdS, CdSe, CdTe, ZnS, ZnSe, ZnTe; III-V compounds: AlAs, AlSb, AlP, BAs, BN, GaAs, GaN, GaP; oxides: BaO, CaO, Li₂O, MgO, SrO; and SiC) using the lowest order of perturbation theory and the strong coupling limit.

In the non-degenerate case, I provide a naïve extension of Feynman’s path integral approach to include anisotropic effective band masses, which is used as a point of comparison with the full perturbative treatment for characterising the polaron in the weak-coupling limit (c.f. section IIb in [45] and subsection 3.8 of this chapter). From Figure 6.9 (left), we see that the variational approach gives a lower estimate for the ground-state compared to the perturbative result for both isotropic (up to 2.5% lower) and anisotropic (up to 17.5% lower) materials. In Figure 6.9 (right), we have the relative difference in polaron effective mass between the two approaches. The largest difference is found in materials that, within the Fröhlich approach, are found in [45] to be at the continuum limit breakdown where the discrete nature of the lattice cannot be ignored. These materials include BaO, CaO, SrO and, to a lesser extent, Li₂O. In both the anisotropic and isotropic cases, the relative difference increases with polaron effective mass, and the in-plane and out-of-plane effective mass differences seem to diverge. This sudden increase in the relative difference is associated with a breakdown limit around $\alpha = 6$ in the perturbative approach for determining the polaron effective mass.

6.4 High-Throughput Material Classification

CHAPTER 7

CONCLUSION & OUTLOOK

What is the meaning of life?

—John Doe, *Thoughts*, 1971

This is the introduction paragraph.

Path integration is a powerful tool for finding accurate approximate solutions to the free energy of the polaron model and for describing the response of the polaron. The main result of my project so far has been the extension of the path integral approach to the polaron to include multiple phonon modes explicitly and using the previously established techniques to make predictions of the complex conductivity. I will discuss my interpretation of the results of my new multiple phonon model and the comparisons to Hellwarth's effective frequency model here. Additionally, I will discuss the result of applying my model to terahertz conductivity measurements of MAPbI_3 and the result of modelling anisotropy in materials in two recent papers.

7.0.1 Predictions from FHIP and DSG for the complex mobility

The first thing to discuss is what one might expect to get from including multiple phonon modes, given the result of a single mode. In [2] and [13], the predicted imaginary component of the memory function $\text{Im}\chi(\nu)$ and real component of the complex conductivity $\text{Re}\sigma(\nu)$ always included an initial peak starting sharply at the phonon mode frequency when at zero temperature. This is the only peak present for lower values of the electron-phonon coupling with $\alpha < 4.5$. It is only at couplings stronger than this that extra oscillatory peaks arise at multiples of

the phonon mode frequency multiplied by the value of the variational parameter $\omega_{LO} \times v$.

This new frequency, $\omega_{LO} \times v$, can be considered the polaron frequency, so these extra peaks would be identified as polaron excitations. The first peak also develops a bit of an initial shoulder, followed by a tall, sharp peak. DSG identified these peaks as an initial one-phonon peak at $\Omega = \omega_{LO}$ at lower α s. As α increases, extra oscillator strength is added due to transitions to final states where lattice adaption to excited electronic configurations (Relaxed Excited States or RES) has occurred. A further increase in coupling produces a separation of the one-phonon and RES states. Eventually, a side-band structure forms, which leads to a broad Frank-Condon (FC) peak that is a superposition of multiphonon sidebands and is less pronounced than the RES peak.

The conductivity becomes very ‘structured’ at strong coupling, and it is hard to identify clear features. The extra ‘structure’ is likely due to the breakdown of the Fröhlich model in the strong-coupling limit, where the linewidth of the FC peak becomes smaller than ω_{LO} . This violates the lifetime of $1/\omega_{LO}$ derived from uncertainty relations and signals the breakdown of the Fröhlich model at strong coupling due to the continuum approximation; the breakdown is not due to the FHIP approximation.

Devreese has used an operator-based theory [Devreese2001] for the strong coupling limit that agrees well with Diagrammatic Monte Carlo data. This would explain the apparent breakdown of the conductivity in the $\alpha = 9$ plots.

7.0.2 Comparison of the multiple phonon and effective frequency mobilities

I found that regardless of coupling strength, all peaks broaden, flatten and blue-shift to high frequencies as the temperature increases. Eventually, we recover a Drude-like response for temperatures greater than 100 K with all the oscillations damped away.

Including multiple phonon modes would superimpose multiple peaks in the memory function $\chi(\nu)$ (Eq. (5.17)), each starting at each of the respective phonon mode frequencies. The magnitude of these peaks would depend on the relative contributions of the modes to the overall electron-phonon coupling. The coupling would be proportional to the infrared activity of each respective mode.

Comparing the memory function and the complex conductivity in DSG, we expect that the complex conductivity would possess a similar structure to the memory

function, with peaks starting at each phonon mode frequency. However, the overall structure does not result from a straightforward superposition and instead involves the reciprocal of the sum over phonon modes as seen from Eq. (5.20). Since most real materials have Fröhlich α values less than 4.5, we would not expect to see any additional oscillations at higher frequencies corresponding to polaron excitations. Any extra peaks would be due to some combination of the many one-phonon peaks from each mode.

Figure 9 shows that the multiple phonon mode mobility $9a$ has a very similar form to the single effective mode mobility $9b$, with one primarily broad peak starting around the Hellwarth and Biaggio effective frequency 2.03 THz. This broad peak in the multiple phonon mobility is likely a result of the combined contributions from the 2.080 THz, 2.249 THz and 2.438 THz modes, which, from Table 1, we can see have the first, second and fourth largest contributions to the decomposed α_j parameter. Due to the combination of these three modes to form the broad peak, the multiple phonon mobility shows extra detail in the broad peak. The extra detail appears as a small initial oscillation at the start of the peak, as seen in Figure 10.

Below 2 THz in Figure 9, the multiple phonon mobility possesses three main extra peaks that do not appear in the effective frequency mobility. These peaks are sharper than the broad peak and begin around 0.60 THz, 1.00 THz and 1.50 THz. Table 1 shows that the 0.574 THz mode has the third largest contribution to the decomposed alpha parameter α_j and is likely the source of the first sharp peak around 0.60 THz. The cluster of modes ranging from 0.801 THz to 1.019 THz is probably the source of the peak that starts around 1.00 THz. Finally, the 1.567 THz mode has a comparatively intermediate contribution to α_j and is likely the source of the small peak around 1.50 THz, which appears more like a shoulder off the back of the 1.00 THz peak.

7.0.3 Comparison of the multiple phonon mobility with THz photo-conductivity data

From the photo-conductivity measurements, the two strong resonances around 1.25 THz and 2.25 THz are attributed to two groups of optical phonon modes associated with the bending and stretching of the Pb-I bond in MAPbI_3 .

In [42], we conclude that the origin of the non-Drude-like spectral response cannot be explained primarily by non-polaronic free carriers alone and will likely require further investigation with non-equilibrium response theories. Nonetheless, the

dominant effect of reducing the conductivity is attributed to the excitation of the electronic states and an interplay between the polaron and surrounding lattice that results in peaks in the conductivity. The scenario described is one where the underlying phonons, which are strongly coupled to the charge carriers and are a part of polaron formation, are heated by the carriers as the carriers cool. This occurs before the heat can be dissipated from these strongly coupled phonon modes scattering into non-coupled phonons (that are not involved in the polaron formation).

Comparison with the multiple mode conductivity in Figure (6.5) leads to reasonable qualitative agreements where the main resonances in the predicted response seem to align with the observed response. The 2.25 THz peak is far broader in theory, but it should be noted that the form the predicted response takes is sensitive to the modes provided, so alternative measured/predicted values of phonon mode frequencies and infrared activities would alter the predicted spectral response.

The best agreement with the measurements occurs when the system's effective temperature is near zero. This suggests that the sub-picosecond time scale of the THz probe measurement corresponds to a pre-thermal equilibrium mobility regime. However, it is unclear how this can be established qualitatively, and further investigations will be required.

The multiple phonon mode models can involve more than two v and w variational parameters, corresponding to having more fictitious harmonic oscillators coupled to the charge carrier in the model system. Investigating how including more harmonic oscillators changes the predicted response would be interesting. It may be that matching the number of fictitious oscillators to the number of strongly coupled phonon modes would make more accurate predictions. However, I have not been able to investigate this yet due to issues with computational convergence of the variational expression in Eq. (4.6).

7.0.4 Comparison of the variational and full perturbative approaches for modelling anisotropy

From [45] and shown in Figure (6.9), we find reasonable agreement in the weak-coupling regime between the proper perturbative treatment of anisotropy in the Fröhlich model and the naive inclusion of anisotropy in the athermal Feynman path integral model. The best agreement is clearly for the inherently isotropic materials, with a poorer agreement for the more anisotropic materials, although the difference is minor. The Feynman approach seems to overestimate the in-plane

effective masses for the anisotropic materials compared to the full perturbative approach. This is likely due to improperly treating the anisotropic mass in the variational principle when determining the variational parameters corresponding to in- and out-of-plane directions. This would explain the underestimation of the ground-state energy by the Feynman approach, too, although it should be noted that the Feynman approach will always be expected to predict a lower ground-state energy than the perturbative approach.

I recently found a 1982 paper by Peeters and Devreese [Devreese1982] where they extend Feynman's polaron theory to account for anisotropy of the effective electron-phonon interaction under the influence of a perturbing magnetic field. The extended free energy variational principle in [Devreese1982] would give the foundation for proper treatment of anisotropic in the path integral approach to obtaining polaron effective masses. When comparing the Feynman and perturbative approaches, we found that defining a polaron radius can be quite ambiguous. Finding a formal definition for the polaron radius would be useful in comparing different theoretical approaches. One way to do this may be to look at the maxima of the dynamic structure factor, which may help define an effective polaron radius. In terms of the path integral model, the dynamic structure factor is found by evaluating $\langle \exp(i\mathbf{k} \cdot [\mathbf{r}_{el}(t) - \mathbf{r}_{el}(0)]) \rangle_{S_0}$ Eq. ((2.184)) as indicated in [Devreese2001] and [Devreesetwo].

– B I B L I O G R A P H Y –

- [1] R. P. Feynman Slow Electrons in a Polar Crystal. *Physical Review*. 97 (3) (February 1955). Publisher: American Physical Society, 660–665. DOI: [10.1103/PhysRev.97.660](https://doi.org/10.1103/PhysRev.97.660). Available from: URL: <https://link.aps.org/doi/10.1103/PhysRev.97.660> [Accessed 9 January 2024].
- [2] R. P. Feynman, R. W. Hellwarth, C. K. Iddings & P. M. Platzman Mobility of Slow Electrons in a Polar Crystal. *Physical Review*. 127 (4) (August 1962). Publisher: American Physical Society, 1004–1017. DOI: [10.1103/PhysRev.127.1004](https://doi.org/10.1103/PhysRev.127.1004). Available from: URL: <https://link.aps.org/doi/10.1103/PhysRev.127.1004> [Accessed 9 January 2024].
- [3] L. D. Landau The motion of electrons in a crystal lattice. *Physikalische Zeitschrift der Sowjetunion*. 3 (1933), 664–665. ISSN: 0369-9811. Available from: URL: <https://cds.cern.ch/record/444288>.
- [4] S. I. Pekar Local quantum states of electrons in an ideal ion crystal. *Zhurnal Eksperimentalnoi I Teoreticheskoi Fiziki*. 16 (4) (1946), 341–348. ISSN: 0044-4510.
- [5] S. I. Pekar. *J. Phys. USSR*. 10 (1946), 341.
- [6] S. I. Pekar. *Zhurnal Eksperimentalnoi I Teoreticheskoi Fiziki*. 17 (1947), 868.
- [7] S. I. Pekar & L. D. Landau Effective Mass of a Polaron. *Zh. Eksp. Teor. Fiz.* 18 (5) (1948), 419–423. Available from: URL: <http://archive.ujp.bitp.kiev.ua/files/journals/53/si/53SI15p.pdf>.
- [8] H. Fröhlich Electrons in lattice fields. en. *Advances in Physics*. 3 (11) (July 1954), 325–361. ISSN: 0001-8732, 1460-6976. DOI: [10.1080/00018735400101213](https://doi.org/10.1080/00018735400101213). Available from: URL: <http://www.tandfonline.com/doi/abs/10.1080/00018735400101213> [Accessed 30 September 2020].

- [9] T. Holstein Studies of polaron motion: Part I. The molecular-crystal model. *Annals of Physics*. 8 (3) (November 1959), 325–342. ISSN: 0003-4916. DOI: [10.1016/0003-4916\(59\)90002-8](https://doi.org/10.1016/0003-4916(59)90002-8). Available from: URL: <https://www.sciencedirect.com/science/article/pii/0003491659900028> [Accessed 9 January 2024].
- [10] T. Holstein Studies of polaron motion: Part II. The “small” polaron. *Annals of Physics*. 8 (3) (November 1959), 343–389. ISSN: 0003-4916. DOI: [10.1016/0003-4916\(59\)90003-X](https://doi.org/10.1016/0003-4916(59)90003-X). Available from: URL: <https://www.sciencedirect.com/science/article/pii/000349165990003X> [Accessed 9 January 2024].
- [11] Y. Ōsaka Polaron State at a Finite Temperature. *Progress of Theoretical Physics*. 22 (3) (September 1959), 437–446. ISSN: 0033-068X. DOI: [10.1143/PTP.22.437](https://doi.org/10.1143/PTP.22.437). Available from: URL: <https://doi.org/10.1143/PTP.22.437> [Accessed 9 January 2024].
- [12] Y. Ōsaka Theory of Polaron Mobility: *Progress of Theoretical Physics*. 25 (4) (April 1961), 517–536. ISSN: 0033-068X. DOI: [10.1143/PTP.25.517](https://doi.org/10.1143/PTP.25.517). Available from: URL: <https://doi.org/10.1143/PTP.25.517> [Accessed 9 January 2024].
- [13] J. Devreese, J. De Sitter & M. Goovaerts Optical Absorption of Polarons in the Feynman-Hellwarth-Iddings-Platzman Approximation. *Physical Review B*. 5 (6) (March 1972). Publisher: American Physical Society, 2367–2381. DOI: [10.1103/PhysRevB.5.2367](https://doi.org/10.1103/PhysRevB.5.2367). Available from: URL: <https://link.aps.org/doi/10.1103/PhysRevB.5.2367> [Accessed 9 January 2024].
- [14] R. W. Hellwarth & I. Biaggio Mobility of an electron in a multimode polar lattice. *Physical Review B*. 60 (1) (July 1999). Publisher: American Physical Society, 299–307. DOI: [10.1103/PhysRevB.60.299](https://doi.org/10.1103/PhysRevB.60.299). Available from: URL: <https://link.aps.org/doi/10.1103/PhysRevB.60.299> [Accessed 9 January 2024].
- [15] N. V. Prokof'ev & B. V. Svistunov Polaron Problem by Diagrammatic Quantum Monte Carlo. *Physical Review Letters*. 81 (12) (September 1998). Publisher: American Physical Society, 2514–2517. DOI: [10.1103/PhysRevLett.81.2514](https://doi.org/10.1103/PhysRevLett.81.2514). Available from: URL: <https://link.aps.org/doi/10.1103/PhysRevLett.81.2514> [Accessed 9 January 2024].
- [16] A. S. Mishchenko, N. V. Prokof'ev, A. Sakamoto & B. V. Svistunov Diagrammatic quantum Monte Carlo study of the Fröhlich polaron. *Physical Review B*. 62 (10) (September 2000). Publisher: American Physical Society, 6317–6336. DOI: [10.1103/PhysRevB.62.6317](https://doi.org/10.1103/PhysRevB.62.6317). Available from: URL: <https://link.aps.org/doi/10.1103/PhysRevB.62.6317> [Accessed 9 January 2024].

- [17] F. M. Peeters & J. T. Devreese Theory of Polaron Mobility. In: H. Ehrenreich, D. Turnbull & F. Seitz (eds.), *Solid State Physics*. Vol. 38. Academic Press, January 1984, pp. 81–133. DOI: [10.1016/S0081-1947\(08\)60312-4](https://doi.org/10.1016/S0081-1947(08)60312-4). Available from: URL: <https://www.sciencedirect.com/science/article/pii/S0081194708603124> [Accessed 9 January 2024].
- [18] T. D. Schultz Slow Electrons in Polar Crystals: Self-Energy, Mass, and Mobility. *Physical Review*. 116 (3) (November 1959). Publisher: American Physical Society, 526–543. DOI: [10.1103/PhysRev.116.526](https://doi.org/10.1103/PhysRev.116.526). Available from: URL: <https://link.aps.org/doi/10.1103/PhysRev.116.526> [Accessed 9 January 2024].
- [19] K. K. Thornber & R. P. Feynman Velocity Acquired by an Electron in a Finite Electric Field in a Polar Crystal. *Physical Review B*. 1 (10) (May 1970). Publisher: American Physical Society, 4099–4114. DOI: [10.1103/PhysRevB.1.4099](https://doi.org/10.1103/PhysRevB.1.4099). Available from: URL: <https://link.aps.org/doi/10.1103/PhysRevB.1.4099> [Accessed 9 January 2024].
- [20] X. Gonze & C. Lee Dynamical matrices, Born effective charges, dielectric permittivity tensors, and interatomic force constants from density-functional perturbation theory. *Physical Review B*. 55 (16) (April 1997). Publisher: American Physical Society, 10355–10368. DOI: [10.1103/PhysRevB.55.10355](https://doi.org/10.1103/PhysRevB.55.10355). Available from: URL: <https://link.aps.org/doi/10.1103/PhysRevB.55.10355> [Accessed 9 January 2024].
- [21] G. Verbist, F. M. Peeters & J. T. Devreese Extended stability region for large bipolarons through interaction with multiple phonon branches. *Ferroelectrics*. 130 (1) (May 1992). Publisher: Taylor & Francis _eprint: <https://doi.org/10.1080/001500150199208019532>. Available from: URL: <https://doi.org/10.1080/001500150199208019532> [Accessed 9 January 2024].
- [22] J. T. Devreese, S. N. Klimin, J. L. M. van Mechelen & D. van der Marel Many-body large polaron optical conductivity in $\text{SrTi}_{x}\text{Nb}_{3-x}\text{O}_3$. *Physical Review B*. 81 (12) (March 2010). Publisher: American Physical Society, 125119. DOI: [10.1103/PhysRevB.81.125119](https://doi.org/10.1103/PhysRevB.81.125119). Available from: URL: <https://link.aps.org/doi/10.1103/PhysRevB.81.125119> [Accessed 9 January 2024].
- [23] J. Poulter & V. Sa-yakanit A complete expression for the propagator corresponding to a model quadratic action. en. *Journal of Physics A: Mathematical and General*. 25 (6) (March 1992), 1539. ISSN: 0305-4470. DOI: [10.1088/0305-4470/25/6/018](https://doi.org/10.1088/0305-4470/25/6/018)

- 4470/25/6/015. Available from: URL: <https://dx.doi.org/10.1088/0305-4470/25/6/015> [Accessed 9 January 2024].
- [24] H. De Raedt & A. Lagendijk Numerical calculation of path integrals: The small-polaron model. *Physical Review B*. 27 (10) (May 1983). Publisher: American Physical Society, 6097–6109. DOI: [10.1103/PhysRevB.27.6097](https://doi.org/10.1103/PhysRevB.27.6097). Available from: URL: <https://link.aps.org/doi/10.1103/PhysRevB.27.6097> [Accessed 9 January 2024].
- [25] H. De Raedt & A. Lagendijk Monte Carlo simulation of quantum statistical lattice models. *Physics Reports*. 127 (4) (October 1985), 233–307. ISSN: 0370-1573. DOI: [10.1016/0370-1573\(85\)90044-4](https://doi.org/10.1016/0370-1573(85)90044-4). Available from: URL: <https://www.sciencedirect.com/science/article/pii/0370157385900444> [Accessed 9 January 2024].
- [26] P.E. Kornilovitch & E.R. Pike Polaron effective mass from Monte Carlo simulations. *Physical Review B*. 55 (14) (April 1997). Publisher: American Physical Society, R8634–R8637. DOI: [10.1103/PhysRevB.55.R8634](https://doi.org/10.1103/PhysRevB.55.R8634). Available from: URL: <https://link.aps.org/doi/10.1103/PhysRevB.55.R8634> [Accessed 9 January 2024].
- [27] P.E. Kornilovitch Continuous-Time Quantum Monte Carlo Algorithm for the Lattice Polaron. *Physical Review Letters*. 81 (24) (December 1998). Publisher: American Physical Society, 5382–5385. DOI: [10.1103/PhysRevLett.81.5382](https://doi.org/10.1103/PhysRevLett.81.5382). Available from: URL: <https://link.aps.org/doi/10.1103/PhysRevLett.81.5382> [Accessed 9 January 2024].
- [28] P.E. Kornilovitch Ground-state dispersion and density of states from path-integral Monte Carlo: Application to the lattice polaron. *Physical Review B*. 60 (5) (August 1999). Publisher: American Physical Society, 3237–3243. DOI: [10.1103/PhysRevB.60.3237](https://doi.org/10.1103/PhysRevB.60.3237). Available from: URL: <https://link.aps.org/doi/10.1103/PhysRevB.60.3237> [Accessed 12 June 2024].
- [29] P.E. Kornilovitch Giant enhancement of anisotropy by electron-phonon interaction. *Physical Review B*. 59 (21) (June 1999). Publisher: American Physical Society, 13531–13534. DOI: [10.1103/PhysRevB.59.13531](https://doi.org/10.1103/PhysRevB.59.13531). Available from: URL: <https://link.aps.org/doi/10.1103/PhysRevB.59.13531> [Accessed 12 June 2024].
- [30] P.E. Kornilovitch Band Structure of the Jahn-Teller Polaron from Quantum Monte Carlo. *Physical Review Letters*. 84 (7) (February 2000). Publisher: American Physical Society, 1551–1554. DOI: [10.1103/PhysRevLett.84.1551](https://doi.org/10.1103/PhysRevLett.84.1551).

Available from: URL: <https://link.aps.org/doi/10.1103/PhysRevLett.84.1551> [Accessed 12 June 2024].

- [31] P. E. Kornilovitch *On Feynman's calculation of the Froehlich polaron mass*. arXiv:cond-mat/0404121. April 2004. DOI: [10.48550/arXiv.cond-mat/0404121](https://doi.org/10.48550/arXiv.cond-mat/0404121). Available from: URL: <http://arxiv.org/abs/cond-mat/0404121> [Accessed 9 January 2024].
- [32] P. Kornilovitch Path Integrals in the Physics of Lattice Polarons. en. In: A. S. Alexandrov (ed.), *Polarons in Advanced Materials*. Springer Series in Materials Science. Dordrecht, Springer Netherlands, 2007, pp. 192–230. ISBN: 978-1-4020-6348-0. DOI: [10.1007/978-1-4020-6348-0_5](https://doi.org/10.1007/978-1-4020-6348-0_5). Available from: URL: https://doi.org/10.1007/978-1-4020-6348-0_5 [Accessed 9 January 2024].
- [33] H. F. Trotter On the Product of Semi-Groups of Operators. *Proceedings of the American Mathematical Society*. 10 (4) (1959). Publisher: American Mathematical Society, 545–551. ISSN: 0002-9939. DOI: [10.2307/2033649](https://doi.org/10.2307/2033649). Available from: URL: <https://www.jstor.org/stable/2033649> [Accessed 9 January 2024].
- [34] N. Hatano & M. Suzuki Finding Exponential Product Formulas of Higher Orders. en. In: A. Das & B. K. Chakrabarti (eds.), *Quantum Annealing and Other Optimization Methods*. Lecture Notes in Physics. Berlin, Heidelberg, Springer, 2005, pp. 37–68. ISBN: 978-3-540-31515-5. DOI: [10.1007/11526216_2](https://doi.org/10.1007/11526216_2). Available from: URL: https://doi.org/10.1007/11526216_2 [Accessed 9 January 2024].
- [35] A. S. Alexandrov & J. T. Devreese *Advances in Polaron Physics*. en. Vol. 159. Springer Series in Solid-State Sciences. Berlin, Heidelberg, Springer, 2010. ISBN: 978-3-642-01895-4 978-3-642-01896-1. DOI: [10.1007/978-3-642-01896-1](https://doi.org/10.1007/978-3-642-01896-1). Available from: URL: <https://link.springer.com/10.1007/978-3-642-01896-1> [Accessed 9 January 2024].
- [36] R. Abe & K. Okamoto An Improvement of the Feynman Action in the Theory of Polaron. I. *Journal of the Physical Society of Japan*. 31 (5) (November 1971). Publisher: The Physical Society of Japan, 1337–1343. ISSN: 0031-9015. DOI: [10.1143/JPSJ.31.1337](https://doi.org/10.1143/JPSJ.31.1337). Available from: URL: <https://journals.jps.jp/doi/10.1143/JPSJ.31.1337> [Accessed 9 January 2024].
- [37] R. Rosenfelder & A. W. Schreiber On the best quadratic approximation in Feynman's path integral treatment of the polaron. *Physics Letters A*. 284 (2) (June 2001), 63–71. ISSN: 0375-9601. DOI: [10.1016/S0375-9601\(01\)00287-0](https://doi.org/10.1016/S0375-9601(01)00287-0).

Available from: URL: <https://www.sciencedirect.com/science/article/pii/S0375960101002870> [Accessed 9 January 2024].

- [38] D. Sels *Dynamic polaron response from variational imaginary time evolution*. arXiv:1605.04998 [cond-mat]. May 2016. DOI: [10.48550/arXiv.1605.04998](https://doi.org/10.48550/arXiv.1605.04998). Available from: URL: <http://arxiv.org/abs/1605.04998> [Accessed 9 January 2024].
- [39] J. M. Luttinger & J. C. Ward Ground-State Energy of a Many-Fermion System. II. *Physical Review*. 118 (5) (June 1960). Publisher: American Physical Society, 1417–1427. DOI: [10.1103/PhysRev.118.1417](https://doi.org/10.1103/PhysRev.118.1417). Available from: URL: <https://link.aps.org/doi/10.1103/PhysRev.118.1417> [Accessed 9 January 2024].
- [40] A. S. Mishchenko, L. Pollet, N. V. Prokof'ev, A. Kumar, D. L. Maslov & N. Nagaosa Polaron Mobility in the “Beyond Quasiparticles” Regime. *Physical Review Letters*. 123 (7) (August 2019). Publisher: American Physical Society, 076601. DOI: [10.1103/PhysRevLett.123.076601](https://doi.org/10.1103/PhysRevLett.123.076601). Available from: URL: <https://link.aps.org/doi/10.1103/PhysRevLett.123.076601> [Accessed 9 January 2024].
- [41] F. Brivio, J. M. Frost, J. M. Skelton, A. J. Jackson, O. J. Weber, M. T. Weller, A. R. Goñi, A. M. A. Leguy, P. R. F. Barnes & A. Walsh Lattice dynamics and vibrational spectra of the orthorhombic, tetragonal, and cubic phases of methylammonium lead iodide. *Physical Review B*. 92 (14) (October 2015). Publisher: American Physical Society, 144308. DOI: [10.1103/PhysRevB.92.144308](https://doi.org/10.1103/PhysRevB.92.144308). Available from: URL: <https://link.aps.org/doi/10.1103/PhysRevB.92.144308> [Accessed 9 January 2024].
- [42] X. Zheng, T. R. Hopper, A. Gorodetsky, M. Maimaris, W. Xu, B. A. A. Martin, J. M. Frost & A. A. Bakulin Multipulse Terahertz Spectroscopy Unveils Hot Polaron Photoconductivity Dynamics in Metal-Halide Perovskites. *The Journal of Physical Chemistry Letters*. 12 (36) (September 2021). Publisher: American Chemical Society, 8732–8739. DOI: [10.1021/acs.jpcllett.1c02102](https://doi.org/10.1021/acs.jpcllett.1c02102). Available from: URL: <https://doi.org/10.1021/acs.jpcllett.1c02102> [Accessed 9 January 2024].
- [43] P. Ordejón, D. Boskovic, M. Panhans & F. Ortmann Ab initio study of electron-phonon coupling in rubrene. *Physical Review B*. 96 (3) (July 2017). Publisher: American Physical Society, 035202. DOI: [10.1103/PhysRevB.96.035202](https://doi.org/10.1103/PhysRevB.96.035202). Available from: URL: <https://link.aps.org/doi/10.1103/PhysRevB.96.035202> [Accessed 9 January 2024].

- [44] B. A. A. Martin & J. M. Frost Multiple phonon modes in Feynman path-integral variational polaron mobility. *Physical Review B*. 107 (11) (March 2023). Publisher: American Physical Society, 115203. DOI: [10.1103/PhysRevB.107.115203](https://doi.org/10.1103/PhysRevB.107.115203). Available from: URL: <https://link.aps.org/doi/10.1103/PhysRevB.107.115203> [Accessed 8 January 2024].
- [45] B. Guster, P. Melo, B. A. A. Martin, V. Brousseau-Couture, J. C. de Abreu, A. Miglio, M. Giantomassi, M. Côté, J. M. Frost, M. J. Verstraete & X. Gonze Fröhlich polaron effective mass and localization length in cubic materials: Degenerate and anisotropic electronic bands. *Physical Review B*. 104 (23) (December 2021). Publisher: American Physical Society, 235123. DOI: [10.1103/PhysRevB.104.235123](https://doi.org/10.1103/PhysRevB.104.235123). Available from: URL: <https://link.aps.org/doi/10.1103/PhysRevB.104.235123> [Accessed 9 January 2024].

APPENDIX A



FIRST APPENDIX

Write supplementary material here.